

UNIVERSITY
OF TWENTE.

Deltares

Numerical Assessment of Floating Breakwater Effects at Intertidal Flats

Hydro-morphodynamic study using Delft3D

MSc Thesis

Afif Taufiiqul Hakim - S2698129

Numerical Assessment of Floating Breakwater Effects at Intertidal Flats

Hydro-morphodynamic study using Delft3D

A Master's Thesis

by

Afif Taufiiqul Hakim

to obtain the degree of Master of Science
at the University of Twente
to be defended publicly on August 31, 2023

cover: Aerial view of the Roggenplaat, intertidal flat in the Eastern Scheldt basin, The Netherlands,
with the storm surge barrier in the background taken by Edwin Paree

**UNIVERSITY
OF TWENTE.**

Deltares

Colophone

This document is a Master's Thesis to obtain the degree of Master of Science (MSc) in Civil Engineering and Management, with a River and Coastal Engineering specialization, from the University of Twente.

Title	Numerical Assessment of Floating Breakwater Effects at Intertidal Flats
Author	Afif Taufiiqul Hakim
Student number	S2698129
Student e-mail	afiftaufiiqulhakim@student.utwente.nl
Personal e-mail	avfhakim@gmail.com
Version	Final
Date	31 August 2023
Educational Institute	University of Twente - Faculty of Engineering Technology Civil Engineering and Management Department of Water Engineering and Management River and Coastal Engineering Track
External Institute	Deltares Applied Morphodynamics (AMO) Department
Supervising Committee	
Head of Committee	dr.ir. J.J. van der Werf (Jebbe) <i>University of Twente</i>
Internal Daily Supervisor	dr.ir. P.W.J.M. Willemsen (Pim) <i>University of Twente</i> dr.ir. B.W. Borsje (Bas) <i>University of Twente</i>
External Daily Supervisor	dr. Anouk De Bakker (Anouk) <i>Deltares</i>
Location	Delft, The Netherlands

Preface

In front of you, you can see my thesis as a representation of the final part of my journey in my Master's in Civil Engineering and Management program at the University of Twente.

First, I would like to express my gratitude to Nuffic Neso Indonesia, which is now known as Nuffic South East Asia (Nuffic SEA). Without the funding from The Kingdom of the Netherlands facilitated by the Nuffic SEA through the StuNed scholarship batch 2021, I would never have achieved my dream of studying in the Netherlands and learning much with the great teachers in an esteemed campus, the University of Twente.

Furthermore, I would also like to thank the people behind this report, who helped me a lot before and during my internship. First, my daily supervisor from Deltares, Anouk de Bakker, for guiding me from the beginning when I arrived at Deltares, discussing the approach I could make in this research, and facilitating me to meet with the experts in Deltares. Apart from that, I would also like to thank the people in the Applied Morphodynamics (AMO) Department in Deltares, especially Lodewijk de Vet, Denzel Harlequin (ex-employee), Pieter Koen Tonnon, and Nienke Vermeer, who guided me in solving the problems I found in my research during my internship.

Next, from the University of Twente side, I would like to thank Pim Willemsen, who supported me from the beginning before I started the internship. Thank you for the brainstorming, ideas, and inspiration. Also, this Master's thesis would not have been completed without the support of Bas Borsje, who kindly took over Pim's role in the colloquium. Equally important, I would like to thank Jebbe van der Werf for ensuring this graduation process went as planned and always being open for discussion.

Moreover, special thanks to Joep van der Zanden from MARIN and Arne van der Hout from Deltares, who helped me gain insight into floating breakwaters relevant to my research.

To my family, I would like to thank my supportive parents, (Bapak) Sumardiyana and (Mama) Indrayati, who supported me and encouraged me to learn until I finished this thesis. Bapak and Mama always motivate and inspire me in life: their courage, strong ambitions, patience, and sincerity in doing anything.

Also, I would like to thank myself; the journey of living in the Netherlands for two years is a very pleasant one. I am happy because of able to survive in this new place that I already consider as my second home for now. I will always remember many pieces of memory I made in this country: early morning travel to Delft, a very late night to come to my house in Enschede, and many more experiences.

Finally, with deep gratitude for finishing this Master's thesis. I present you this report, I hope this report will provide valuable insights into the field of Coastal Engineering. Enjoy!

Afif Taufiiqul Hakim
31 August 2023

Summary

Intertidal flats in the Eastern Scheldt, a tidal basin in the southwest of the Netherlands, have been encountering severe erosion issues. One of the intertidal flats subject to erosion in the Eastern Scheldt is Roggenplaat. The erosion in Roggenplaat causes a decrease in the intertidal area. As a consequence, reduces the foraging for various species dependent on the habitats. Multiple measures are available to prevent erosion that could be applied in the Roggenplaat. For instance, nourishment that could be eroding and has a limited lifetime. Another option is conventional breakwaters. Yet, it is not economically attractive, especially in deep water and poor soil conditions.

Floating breakwater can potentially protect the intertidal area like Roggenplaat against erosion. This is foreseen based on the wind-generated waves in the Eastern Scheldt that can be handled by a floating breakwater and the availability of deeper water considering the channel-shoal interaction in the Eastern Scheldt. However, even though the floating breakwater has potential, the effects of the floating breakwater on hydrodynamic and morphodynamics under realistic conditions are still not fully understood. Therefore, the current study aims to assess the hydrodynamic and morphodynamic effects of a floating breakwater (FB) under varying wave conditions, FB positions, and slopes on the intertidal flats.

In this study, two research phases are undertaken. The first is to understand whether the Delft3D model can be used to reproduce the results of the laboratory experiment by Shimoda et al. (1991) that explored the effect of FB intervention. In the second research phase, various data parameters are derived, including wave conditions, water depths at FB position, channel slopes, and intertidal area slopes inspired by conditions in the Eastern Scheldt. A total of 180 unique combinations of these data parameters are created for the data input of Delft3D simulations. From these simulations, three hydrodynamic parameters, such as wave height, near-bed orbital velocity, and bed shear stress, and three morphodynamic parameters, such as bed load transport, suspended load transport, and cross-sectional erosion area, are used for the interpretation. FB is represented by the transmission coefficient feature (obstacle) in Delft3D for both the first and the second research phases.

Based on the results in the first research phase, it was found that Delft3D could not predict the erosion and sedimentation pattern of the three observed cross-sections in the laboratory. Nevertheless, Delft3D was able to reproduce the effects of FB in terms of reducing erosion and sedimentation in the lee side of FB for the three cross-sections. The result in the first research phase gave insight into the effect of using the transmission coefficient to represent FB, which was also used for the second research phase.

Furthermore, results in the second research phase showed that FB is less effective as the wave conditions became more extreme. Under mild wave conditions with incident wave height (H_0) = 0.40 m and peak wave period (T_p) = 1.7 s as well as H_0 = 0.70 and T_p = 2.3 s, hydrodynamic parameters, bed load and suspended load transport were effectively reduced. As a result, erosion could be fully diminished with a 100% reduction. Next, with slightly more extreme wave conditions, H_0 = 1.20 m and T_p = 3.0 s, erosion was reduced by 92.7% - 96.4%. Meanwhile, with more energetic wave: H_0 = 1.8 m and T_p = 3.8 s, erosion was reduced by 57.4% - 62.6%. The ranges emerged from different water depths at FB position, channel slopes, and intertidal area slopes.

The annual cross-sectional erosion that can be mitigated by FB was also predicted. Due to more frequent occurrences, the FB under wave condition with $H_0 = 0.40 \text{ m}$, $T_p = 1.7 \text{ s}$ could mitigate erosion by $\pm 4500 \text{ m}^2$. This is followed by a wave condition of $H_0 = 0.70 \text{ m}$, $T_p = 2.3 \text{ s}$, with the mitigated cross-sectional erosion of $\pm 2000 \text{ m}^2$. For the other two most extreme wave conditions, $H_0 = 1.20 \text{ m}$, $T_p = 3.0 \text{ s}$ and $H_0 = 1.80 \text{ m}$, $T_p = 3.8 \text{ s}$, due to less probability of occurrence compared to the two mentioned mild wave conditions, the mitigated erosion per year were $\pm 1200 \text{ m}^2$ and $\pm 400 \text{ m}^2$ respectively.

Lastly, the key findings of the current study are, first, wave conditions determine the effectiveness of FB in reducing erosion at the intertidal area. In this case, the FB is effective in reducing erosion under mild wave conditions like $H_0 = 0.40 \text{ m}$, $T_p = 1.7 \text{ s}$ as well as $H_0 = 0.70 \text{ m}$ and $T_p = 2.3 \text{ s}$ and less effective as the waves become more extreme. Second, the FB located in deeper water (10 m, 15 m, and 20 m) may reduce erosion more significantly than in shallower water (5 m). Third, with FB intervention, different channels (1:15, 1:25, 1:55) and intertidal area slopes (1:200, 1:400, 1:600) do not affect the erosion much.

Keywords: Floating breakwater, hydro-morphodynamic, Delft3D, Eastern Scheldt

Contents

	Page
Preface	ii
Summary	iii
List of Figures	vii
List of Tables	xiv
List of Symbols	xvii
1 Introduction	1
1.1 Background	1
1.2 Problem statement	2
1.3 Research objective	3
1.4 Research questions	3
1.5 General approach	4
1.6 Scope	4
1.7 Structure of the report	5
2 Theoretical background	6
2.1 Floating breakwater	6
2.2 Wave attenuation due to floating breakwater	6
2.3 Morphodynamic effects of floating breakwater	9
2.4 Hydrodynamic parameters relevant to sediment transport	9
2.5 Morphodynamic parameters	11
3 Methodology	12
3.1 Numerical model Delft3D	13
3.2 First research phase: reproduce the FB effects observed in the laboratory experiment by Shimoda	14
3.2.1 Laboratory experiment reported by Shimoda et al. (1991)	14
3.2.2 Data of laboratory experiment for Delft3D modelling in the first research phase	15
3.2.3 Delft3D settings in the first research phase	17
3.2.4 Post-processing and interpretation of Delft3D outcomes in the first research phase	22
3.3 Second research phase: floating breakwater's effects at intertidal flats	24
3.3.1 Data insight: The Eastern Scheldt	24
3.3.2 Data derivation for the second research phase	25
3.3.3 Derived data for Delft3D input in the second research phase	29
3.3.4 Delft3D settings in the second research phase	32
3.3.5 Post-processing and interpretation in the second research phase	34
4 Results: comparison of experiment and numerical model Delft3D	37
4.1 Comparison of the cross-shore profiles from the experiment and numerical model Delft3D	37
4.1.1 Cross-shore profile without FB	39
4.1.2 Cross-shore profile with landward FB	43

4.1.3	Cross-shore profile with seaward FB	46
4.2	Wave height under FB interventions	48
4.3	Sediment transport under FB interventions	50
4.4	Reflection on the first research phase	52
5	Results: hydrodynamics and morphodynamic effects of a floating breakwater at intertidal flats (Delft3D output)	53
5.1	Transmission coefficients of the floating breakwater at intertidal flats	53
5.2	Hydrodynamic effects of floating breakwater at intertidal flats	55
5.2.1	Effects of FB on wave height	55
5.2.2	Effects of FB on near-bed orbital velocity	60
5.2.3	Effects of FB on bed shear stress	65
5.3	Morphodynamic effects of the floating breakwater at intertidal flats	70
5.3.1	Effects of FB on bed load and suspended load transport	70
5.3.2	Effects of FB on the cross-sectional area of erosion at intertidal area	77
6	Discussion	82
6.1	Limitations of the current study	82
6.1.1	Model dimension	82
6.1.2	Excluded process and condition in the second research phase	82
6.1.3	Schematized bathymetry	83
6.1.4	FB specifications and Macagno relation for the second research phase	84
6.2	Evaluation based on relevant previous studies	84
6.2.1	Shimoda experiment vs Delft3D model	84
6.2.2	Applicability of Macagno relation	85
6.2.3	Channel-shoal (intertidal area) interaction	86
6.3	Implication of the results	86
6.3.1	Effect of FB placement against erosion	86
6.3.2	Intertidal area and near shoal edge erosion	87
6.3.3	Protecting the intertidal flats in the Eastern Scheldt	88
6.4	Extra outlook	89
6.4.1	Estimation of mitigated annual erosion by FB in the intertidal area	89
6.4.2	Effects of tide variation on erosion	91
6.4.3	LIVING breakwater	92
7	Conclusions and Recommendations	94
7.1	Conclusions	94
7.2	Recommendations	100
	References	101
	Appendix A - Physical and Numerical Aspects of Delft3D	105
	Appendix B - Data Derivation	108
	Appendix C - Calibration in Delft3D	121
	Appendix D - Complementing information for research phase 1 and 2	123

List of Figures

1.1	The morphological evolution of a cross-section of the Roggenplaat (intertidal flats) from 1988 to 2014, retrieved from van der Werf et al. (2019).	1
2.1	Interaction between wave and floating breakwater, retrieved from Biesheuvel (2013)	7
2.2	Box type floating breakwater, representing the type of FB that defines the Macagno formula	7
2.3	Transmission coefficient with different FB width and FB draft, calculated with a wave period $T = 3.0$ s and a water depth at FB position = 10 m	8
2.4	Results of experimental study of floating breakwater effects on bed level changes in an eroded-type beach, adapted from Shimoda et al. (1991)	9
2.5	Different modes of sediment transport (a) bed load at small shear stresses (b) bed load at relatively higher shear stresses (sheet flow) (c) suspended load, retrieved from Bosboom and Stive (2021)	11
3.1	Steps of the first research phase and second research phase	12
3.2	Settings in Shimoda experiment, D = height of FB, B_f = width of FB, D_f = draft of FB, h = water depth, l_x = distance from the coast to the FB, adapted from Shimoda et al. (1991)	14
3.3	Evolution of nearshore bed level (a) without SMFB (b) with more shallow SMFB (solid black box) from the water surface, located landward (c) with deeper SMFB from the water surface located seaward; H_0/L_0 represents the wave steepness applied for the experiments; adapted from Shimoda et al. (1991)	15
3.4	Evolution of nearshore bed level (a) without SMFB (b) with more shallow SMFB from the water surface, located landward (c) with deeper SMFB from the water surface located seaward; adapted from Shimoda et al. (1991)	16
3.5	Plan view of the grids with the FLOW grid (dark blue) and WAVE grid (light blue) for hydro-morphodynamic simulation of Shimoda experiment in Delft3D. Blue arrows represent the incoming waves (open boundary), and the brown dashed line represents the coast (closed boundary)	18
3.6	Bathymetry and positions of SMFB for Delft3D simulations in the first research phase, the waves come from the open boundary ($x=50$ m)	19
3.7	Bathymetry of the Eastern Scheldt, the land with the red dashed line above indicates the location of Roggenplaat. Another land on the lower right indicates the location of the Galgeplaat; <i>Vaklodingen</i> data set by Rijkswaterstaat	24
3.8	Slope of the Roggenplaat based on the elevation between -1.5 to 1.5 m, derived using QGIS from <i>Vaklodingen</i> data set by Rijkswaterstaat	25
3.9	Example of cross-section of the Roggenplaat, taken according to the red dashed line presented in Figure 3.7.	26
3.10	Determined dimension of the FB to calculate the transmission coefficients as input of Delft3D in the second research phase	28
3.11	FLOW and WAVE grid for the second research phase; the alongshore green line in WAVE-grid visualizes the position of the specified transmission coefficients which can vary depending on the water depth below FB; a red dot with the X, Y coordinates represent the position and values of the reference point	30
3.12	Schematized bathymetry of the intertidal flats; point A200, A400, and A600 indicate the channel edge for different intertidal area slope. These points are used for the observation points in the results phase	31
3.13	Post-processing for hydrodynamic parameters	35

3.14 Post-processing for morphodynamic parameters	36
4.1 Derived bed evolution with the calculated $H_0 = 0.30$ m and $L_0 = 5.05$ m using linear wave theory equation; (a) the evolved bed profile without SMFB (b) the evolved bed profile with landward SMFB (c) the evolved bed profile with seaward SMFB; adapted from Shimoda et al. (1991)	38
4.2 Cross-section derived from Delft3D model and laboratory experiment; The cross-section from Delft3D model is derived from the simulation with model setting 4 (see Table 3.4) .	39
4.3 Cumulative erosion and sedimentation without SMFB from the Delft3D outcome and experiment, derived from the simulation with model setting 4 (see Table 3.4)	39
4.4 Area of erosion and sedimentation of experiment and model with different basic settings of Delft3D revealed in Table 3.4. The area of erosion/sedimentation for model setting 4 represents the area for cross-section in Figure 4.2	42
4.5 Comparison between the evolved cross-sections affected by landward FB from the experiment and Delft3D model; complemented with the cross-sections without FB from the experiment and the Delft3D model; C_t represents the transmission coefficient of FB applied in D3D; SMFB means submerged-moored floating breakwater (the FB type applied in the experiment); model results using model setting 4, which is the best model setting	43
4.6 Normalized bed level with landward FB based on model and experiment; normalized means the initial bed level subtracts the bed level of the evolved cross-sections	44
4.7 Area of erosion and sedimentation of experiment and model with landward FB ($x=6.5$ m) using different input of transmission coefficients from 0.1 to 0.9	45
4.8 Comparison between the evolved cross-sections affected by seaward FB from the experiment and Delft3D model; complemented with the cross-sections without FB from the experiment and the Delft3D model; C_t represents the transmission coefficient of FB applied in D3D; SMFB means submerged-moored floating breakwater (the FB type applied in the experiment); model results using model setting 4 (best model setting) . .	46
4.9 Normalized bed level with landward FB based on model and experiment; normalized means the initial bed level subtracts the bed level of the evolved cross-sections	47
4.10 Area of erosion and sedimentation of experiment and model with seaward FB ($x=8.0$ m) using different input of transmission coefficients from 0.1 to 0.9; no FB means experiment or simulations without FB	48
4.11 Effect of the presence of landward (cross-shore distance = 6.5 m) and seaward FB (cross-shore distance = 8 m) with different transmission coefficient on wave height . .	49
4.12 Direction of bed load and suspended load without FB; cross-section = 0 m indicates the shoreline; the bigger arrows indicate the higher magnitude of the bed load or suspended load	50
4.13 Direction of bed load and suspended load based on Delft3D model with FB ($C_t = 0.1$); cross-section = 0 m indicates the shoreline; the bigger arrows indicate the higher magnitude of the bed load or suspended load; FB position is landward (cross-shore distance = 6.5 m)	50
4.14 Mean bed load and suspended load transport without and with FB ($C_t = 0.1$); C_t means transmission coefficient; the bed load transport is predominantly onshore-directed and suspended load transport is predominantly offshore-directed	51

5.1	Potential transmission coefficient (C_t) of the floating breakwater at the Eastern Scheldt. The transmission coefficient indicates the transmitted wave height over the incident wave height. The transmission coefficients are calculated using Macagno relation with the data of FB's widths: 8.00 m; FB's drafts: 2.20 m.	53
5.2	Floating breakwater effects under different wave height conditions with different floating breakwater positions; simulations with an intertidal area slope 1:200 and a channel slope 1:15; h_{fb} means water depth at FB position	55
5.3	Transmitted wave height H_1 on the shoal edge (points A200, A400, A600) with different water depths at FB positions; Derived from the simulations with FB in different FB positions (h_{fb}), shoal slopes (S_s), and channel slopes (S_c); grouped based on FB positions (h_{fb})	57
5.4	Transmitted wave height H_1 on the shoal edge (points A200, A400, A600) with different channel slopes; Derived from the simulations with FB in different FB positions (h_{fb}), shoal slopes (S_s), and channel slopes (S_c); grouped based on channel slopes (S_c)	58
5.5	Effects of the intertidal area slope on wave height, derived from the simulations with FB ($h_{fb} = 20m$) on the same channel slope (S_c) 1:15 with different intertidal area slopes (S_s) = [1:200 1:400 1:600]	59
5.6	Near bed orbital velocity under different incident wave heights without and with floating breakwater in different positions (water depth at FB position), derived from the simulations with an intertidal area slope of 1:200 and a channel slope of 1:15	60
5.7	Near-bed orbital velocity with different water depths at FB positions; Derived from the simulations with FB in different FB positions (h_{fb}), shoal slopes (S_s), and channel slopes (S_c); grouped based on FB positions (h_{fb})	62
5.8	Mean near-bed orbital velocity with different channel slopes; Derived from the simulations with FB in different FB positions (h_{fb}), shoal slopes (S_s), and channel slopes (S_c); grouped based on channel slopes (S_c)	63
5.9	Mean near-bed orbital velocity with different intertidal area slopes; Derived from the simulations with FB in different FB positions (h_{fb}), intertidal area slopes (S_s), and channel slopes (S_c); grouped based on intertidal area slopes (S_s)	64
5.10	Bed shear stress under different wave conditions without and with floating breakwater in different positions (water depth at FB position); derived from the simulations with an intertidal area slope 1:200 and channel slope 1:15	65
5.11	Mean bed shear stress with different water depths at FB positions; Derived from the simulations with FB in different FB positions (h_{fb}), shoal slopes (S_s), and channel slopes (S_c); grouped based on FB positions (h_{fb})	67
5.12	Mean bed shear stress with different channel slopes; Derived from the simulations with FB in different FB positions (h_{fb}), shoal slopes (S_s), and channel slopes (S_c); grouped based on channel slopes (S_c)	68
5.13	Mean bed shear stress with different intertidal area slopes; Derived from the simulations with FB in different FB positions (h_{fb}), shoal slopes (S_s), and channel slopes (S_c); grouped based on intertidal area slopes (S_s)	69
5.14	Bed load and suspended load transport under different wave conditions without and with floating breakwater in different water depths at FB position); derived from the simulations with an intertidal area slope 1:200 and channel slope 1:15	70
5.15	Direction of bed load and suspended load transport under different wave conditions without FB; derived from the simulation with an intertidal area slope 1:200 and channel slope 1:15	71

5.16	Direction of bed load and suspended load transport under different wave conditions with FB, $h_{fb} = 20$ m; derived from the simulation with an intertidal area slope 1:200 and channel slope 1:15	72
5.17	Mean bed load and suspended load transport with different water depths at FB positions; Derived from the simulations with FB in different FB positions (h_{fb}), shoal slopes (S_s), and channel slopes (S_c); grouped based on FB positions (h_{fb})	74
5.18	Mean bed load and suspended load transport with different channel slopes; Derived from the simulations with FB in different FB positions (h_{fb}), shoal slopes (S_s), and channel slopes (S_c); grouped based on channel slopes (S_c)	75
5.19	Mean bed load and suspended load transport with different intertidal area slopes; Derived from the simulations with FB in different FB positions (h_{fb}), shoal slopes (S_s), and channel slopes (S_c); grouped based on intertidal area slopes (S_s)	76
5.20	Cumulative erosion and sedimentation under different wave conditions without and with floating breakwater in different water depths at FB position; derived from the simulations with an intertidal area slope 1:200 and channel slope 1:15; A200 represents shoal edge for this specific intertidal area slope (see Figure 3.12)	77
5.21	Cross-sectional erosion with different water depths at FB positions; Derived from the simulations with FB in different FB positions (h_{fb}), shoal slopes (S_s), and channel slopes (S_c); grouped based on FB positions (h_{fb})	79
5.22	Cross-sectional erosion with different channel slopes; Derived from the simulations with FB in different FB positions (h_{fb}), shoal slopes (S_s), and channel slopes (S_c); grouped based on channel slopes (S_c)	80
5.23	Cross-sectional erosion with different intertidal area slopes; Derived from the simulations with FB in different FB positions (h_{fb}), shoal slopes (S_s), and channel slopes (S_c); grouped based on intertidal area slopes (S_s)	81
6.1	Behaviour of the wave height without and with wind input in Delft3D, simulated with $H_0 = 0.40$ m and $T_p = 1.7$ s, the case with wind process is imposed with a wind velocity of 5 m/s	83
6.2	Illustration of multiple protections to tackle intertidal area erosion during mild wave conditions (upper panel) and near-edge erosion during more extreme wave conditions (lower panel)	88
6.3	Area to locate FB according to the desired depth of 10 m; the water depth below FB is based on the results of current research; the intertidal flats on the upper left are Roggenplaat, and the lower right is Galgeplaat, adapted from EcoShape (2020)	89
6.4	Estimated erosion per year that can be mitigated by FB; mitigated cross-sectional erosion by the FB (upper panel); mitigated volumetric erosion by the FB, assuming the length of the intertidal flat is 6000 m, which is approximately the length of Roggenplaat (lower panel); errors depicted in both panels are due to different water depth at FB positions, channel slopes and intertidal area slopes	90
6.5	Cumulative erosion and sedimentation with different tide levels; simulations without FB on the channel slope 1:25 and intertidal area slope 1:400	91
6.6	Annual erosion that could be mitigated by FB ($h_{fb} = 10$ m) with different tide level under different wave conditions, simulated with a channel slope 1:25 and intertidal area slope 1:400	92

6.7	Novel floating (LIVING) breakwater (left) and the transmission coefficient of LIVING breakwater, represented by dots and square marks (right); L_f represents length of the floater, which is width (B_f) in this study, K_t is transmission coefficient (C_t) in the current study; retrieved from Zanden et al. (2022)	92
6.8	Erosion on different transmission coefficients; simulated using bathymetry with an intertidal area slope of 1:400 and channel slope of 1:25 (average); under wave condition 4: $H_0 = 1.8$ m, $T_p = 3.8$ s; box-type FB is the type of FB used in the current study; the simulations for this figure were derived by 12 hours simulation (morphology)	93
A.1	Incident and transmitted wave with the application of the transmission coefficient in Delft3D; Bigger arrow/curve represents the greater wave height and smaller for the smaller wave height, retrieved from Mojabi et al. (2018)	107
B.1	Slope of Galgeplaat as another reference of shoreface slope derivation	109
B.2	Plan view of Roggenplaat representing the cross-sections to derive channel slopes	110
B.3	Cross-sections of Roggenplaat 1-4	110
B.4	Cross-sections of Roggenplaat 5-8	111
B.5	Cross-sections of Roggenplaat 9-12	111
B.6	Cross-sections of Roggenplaat 13-14	112
B.7	Location of two wind stations: STAV and ZBWI in the Eastern Scheldt, the upper right panel shows the overview position where the stations are located	113
B.8	Wind rose for STAV station, data recorded from 1990 to 2022	114
B.9	Wind rose for ZBWI station, data recorded from 2010 to 2022	114
B.10	Fetch distance measurement near the Roggenplaat and Galgeplaat in the Eastern Scheldt	115
B.11	Wave nomogram, retrieved from Breugem and Holthuijsen (2007)	116
B.12	Wave derivation with the wind speeds of 5, 7.5, 10, 12.5, 15, 17.5, and 20 m/s and fetch of 2 km	116
B.13	Wave rose for the wave height recorded from 01 January 2015 to 31 December 2022	117
B.14	Wave rose for the wave period recorded from 01 January 2015 to 31 December 2022	117
B.15	Probability of occurrence of the wind for deriving wave conditions in the second research phase, ES means Eastern Scheldt	119
C.1	Different wave grid size to avoid unexpected wave height decline across the boundary (cross-shore profile), simulated using wave condition phase 1 (Shimoda), $H_0 = 0.30$ m $T_p = 1.8$ s	121
C.2	Calibration runs to avoid unexpected wave height decline across the boundary (cross-shore profile), simulated using wave condition 1 (research phase 2): $H_0 = 0.40$ m $T_p = 1.7$ s, except for one case (orange line)	122
D.1	Cross-section and wave height based on model settings 1	123
D.2	Cross-section and wave height based on model settings 2	124
D.3	Cross-section and wave height based on model settings 3	125
D.4	Cross-section and wave height based on model settings 4	126
D.5	Cross-section and wave height based on model settings 5	127
D.6	Cross-section and wave height based on model settings 6	128
D.7	Near bed orbital velocity without and with FB, see the peak and reduced peaks near the shoreline for seeing the FB effects	129
D.8	Bed shear stress without and with FB, see the peak and reduced peaks near the shoreline for seeing the FB effects	129

D.9	Depth averaged velocity without submerged moored floating breakwater (SMFB) in the first research phase	129
D.10	Depth averaged velocity with submerged moored floating breakwater (SMFB), $C_t = 0.1$, in the first research phase, white dashed line represents FB	129
D.11	Shoaling effects with different positions of FB, derived from the simulations with a shoreface slope of 1:200 and channel slope of 1:55	130
D.12	Wave dissipation due to bottom friction (bfric) on different channel slopes; the same intertidal area slopes = 1:200; incident wave $H_0 = 1.80$ m and $T_p = 3.80$ s; simulations without FB	130
D.13	Effects of different channel slopes on near bed-orbital velocity (u_b) without FB; derived from the simulations with shoreface slopes of 1:200, different channel slopes: 1:15, 1:25 and 1:55	131
D.14	Effects of different channel slopes on near bed-orbital velocity (u_b) with FB ($h_{fb} = 20$ m); derived from the simulations with shoreface slopes of 1:200, different channel slopes: 1:15, 1:25 and 1:55 under wave condition 3 (left panel) and 4 (right panel)	131
D.15	Effects of different intertidal area slopes on near bed-orbital velocity (u_b) without FB under all wave conditions; A200, A400, A600 represent the locations of the edges separating the intertidal flats and channel (shoal edge)	132
D.16	Effects of different intertidal area slopes on near bed-orbital velocity (u_b) with FB ($h_{fb} = 20$ m); derived from the simulations with channel slopes of 1:15, under wave condition 3 (left panel) and 4 (right panel)	132
D.17	Effects of different channel slopes on bed shear stress without FB; derived from the simulations with intertidal area slopes of 1:200, different channel slopes: 1:15, 1:25 and 1:55	133
D.18	Effects of different channel slopes on bed shear stress with FB ($h_{fb} = 20$ m), wave conditions 3 (left panel) and 4 (right panel); derived from the simulations with intertidal area slopes of 1:200, different channel slopes: 1:15, 1:25 and 1:55	133
D.19	Effects of different intertidal area slopes on bed shear stress without FB; derived from the simulations with channel slopes of 1:15, different intertidal area slopes: 1:200, 1:400 and 1:600	134
D.20	Effects of different intertidal area slopes on bed shear stress with FB ($h_{fb} = 20$ m); derived from the simulations with channel slopes of 1:15, different intertidal area slopes: 1:200, 1:400 and 1:600; wave condition 3 (left panel) and wave condition 4 (right panel)	134
D.21	Effects of different channel area slopes on bed load transport without FB; derived from the simulations with intertidal area slopes of 1:200, different channel slopes: 1:15, 1:25 and 1:55	135
D.22	Effects of different channel slopes on bed load transport with FB ($h_{fb} = 20$ m), wave conditions 3 (left panel) and 4 (right panel); derived from the simulations with intertidal area slopes of 1:200, different channel slopes: 1:15, 1:25 and 1:55	135
D.23	Effects of different channel slopes on suspended load transport without FB; derived from the simulations with intertidal area slopes of 1:200, different channel slopes: 1:15, 1:25 and 1:55	136
D.24	Effects of different channel slopes on suspended load transport with FB ($h_{fb} = 20$ m), wave conditions 3 (left panel) and 4 (right panel); derived from the simulations with intertidal area slopes of 1:200, different channel slopes: 1:15, 1:25 and 1:55	136

D.25 Effects of different intertidal area slopes on bed load transport without FB; derived from the simulations with channel slopes of 1:15, different intertidal area slopes: 1:200, 1:400, and 1:600	137
D.26 Effects of different intertidal area slopes on bed load transport with FB ($h_{fb} = 20$ m), wave conditions 3 (left panel) and 4 (right panel); derived from the simulations with channel slopes of 1:15, different intertidal area slopes: 1:200, 1:400, and 1:600	137
D.27 Effects of different intertidal area slopes on suspended load transport without FB; derived from the simulations with channel slopes of 1:15, different intertidal area slopes: 1:200, 1:400, and 1:600	138
D.28 Effects of different intertidal area slopes on suspended load transport with FB ($h_{fb} = 20$ m), wave conditions 3 (left panel) and 4 (right panel); derived from the simulations with channel slopes of 1:15, different intertidal area slopes: 1:200, 1:400, and 1:600	138
D.29 Erosion on different channel slope without FB; derived from the simulations with channel slopes of 1:15, 1:25 and 1:55 with an intertidal area slope of 1:200	139
D.30 Erosion on different channel slope with FB ($h_{fb} = 20$ m); wave conditions 3 (left panel) and 4 (right panel); derived from the simulations with intertidal area slopes of 1:200, different channel slopes: 1:15, 1:25 and 1:55	139
D.31 Erosion profile on different intertidal area slope without FB; derived from the simulations with the intertidal area slopes of 1:200, 1:400, and 1:600 with a channel slope of 1:15	140
D.32 Erosion on different intertidal area slope with FB ($h_{fb} = 20$ m); wave conditions 3 (left panel) and 4 (right panel); derived from the simulations with the intertidal area slopes of 1:200, 1:400, 1:600 with a channel slope of 1:15	140

List of Tables

3.1	Data of the laboratory experiment by Shimoda et al. (1991) that will be used for Delft3D modeling in the first research phase	17
3.2	Basic input for Delft3D-WAVE and Delft3D-FLOW in the first research phase	20
3.3	Simulations for the first research phase	21
3.4	Different model settings in the first research phase for Delft3D-FLOW and Delft3D-WAVE	21
3.5	Data/information from the experiment and numerical model used to answer the research questions in the first phase, identity number of a simulation can be seen in Table 3.3	23
3.6	Data for undertaking the second research phase	28
3.7	Placement of FB at the schematized intertidal flats bathymetry in Figure 3.12; the position of the FB in this table is relative to the reference specified in WAVE grid, see Figure 3.11	31
3.8	Basic input for Delft3D-WAVE and Delft3D-FLOW in the second phase	33
4.1	Error statistics of the bed profile generated by Delft3D for simulation without FB under different model setting model settings provided in Table 3.4	41
4.2	Error statistics of the cross-shore profile generated by Delft3D for simulation with landward FB under different transmission coefficients	44
4.3	Error statistics of the cross-shore profile generated by Delft3D for simulation with seaward FB under different transmission coefficients	47
5.1	Calculated transmission coefficients for different water depth at FB positions (h_{fb}) under different wave conditions, width of FB = 8.00 m and draft of FB = 2.20 m	54
5.2	Ranges of the transmitted wave height H_1 on the shoal edge (points A200, A400, A600) yielded from the simulations without FB and with FB in different FB positions (h_{fb}), shoal slopes (S_s), and channel slopes (S_c); and reduction of incident wave height H_0	56
5.3	Ranges and reduction percentage of the mean near-bed orbital velocity (\bar{u}_b) yielded from the simulations without FB and with FB in different water depth at FB positions (h_{fb}), intertidal area slopes (S_s), and channel slopes (S_c)	61
5.4	Ranges and reduction percentage of the mean bed shear stress (τ_b) yielded from the simulations without FB and with FB in different water depth at FB positions (h_{fb}), intertidal area slopes (S_s), and channel slopes (S_c); τ_{cr} is critical bed shear stress	66
5.5	Ranges and reduction percentage of the mean bed load transport yielded from the simulations without FB and with FB in different water depths at FB positions (h_{fb}), intertidal area slopes (S_s), and channel slopes (S_c)	73
5.6	Ranges and reduction percentage of the mean suspended load transport yielded from the simulations without FB and with FB in different water depths at FB positions (h_{fb}), intertidal area slopes (S_s), and channel slopes (S_c)	73
5.7	Ranges and reduction of erosion yielded from the simulations without FB and with FB in different water depths at FB positions (h_{fb}), intertidal area slopes (S_s), and channel slopes (S_c)	78
6.1	Evaluation of the data being used in the second research phase for checking the applicability of Macagno relation; text in <i>italic</i> means it does not comply with the criteria; criteria one and two depend on water depth at FB positions h_{fb} ; criteria three dependant on wave period T_p ; $B_f = 8.00\ m$ and $D_f = 2.20\ m$	85
6.2	Mean of transmitted wave height (H_1), near-bed orbital velocity (u_b) and bed shear stress (τ_b) with different water depths at FB position (h_{fb})	87
6.3	Mean of suspended load transport and erosion	87

B.1	Qualification of error ranges of process parameters (brier skill score) based on van Rijn et al. (2003)	108
B.2	Derived wave conditions from different fetch length and wind velocity, derived data in bold is the used wave conditions for the second research phase	117

List of Symbols

Symbol	Description	Unit
θ_w	Wave direction	°
θ_{cr}	Dimensionless critical shear stress	—
B_f	Width of floating breakwater	m
$\tilde{\beta}$	Gumbel parameter	—
D_f	Draft of floating breakwater	m
D_*	Dimensionless sediment diameter	—
D_{50}	Median sediment particle size	μm
C_t	Transmission coefficient, (H_1/H_0)	—
f_c	Current-related friction factor	—
f_w	Wave friction factor	—
g	Acceleration of gravity	m/s^2
h	Water depth	m
h_{fb}	Water depth at floating breakwater position	m
H	Wave Height	m
H_0	Incident wave height/wave height at open boundary	m
H_1	Transmitted wave height	m
H_s	Significant wave height	m
k	Wave number	m
L	Wavelength	m
L_0	Wavelength in the deep water	m
P	Probability of occurrence	-
ρ_w	Water density	kg/m^3
ρ_s	Mass of sediment per unit volume	kg/m^3
q_b	Bed load transport	$\text{m}^3/\text{s}/\text{m}$
q_s	Suspended load transport	$\text{m}^3/\text{s}/\text{m}$
R_2	Determination coefficient	—
S_s	Slope of the intertidal flats (shoal)	m/m
S_c	Slope of the channel	m/m
τ_b	Bed shear stress	N/m^2
$\tau_{b,w}$	Bed shear stress due to wave	N/m^2
$\tau_{b,c}$	Bed shear stress due to current	N/m^2
τ_{cr}	Critical bed shear stress	N/m^2
T	Wave period	s
T_p	Peak wave period	s
u_{10}	Wind speed	m/s
u_b	Near-bed orbital velocity	m/s
\bar{u}_b	Averaged near-bed orbital velocity	m/s
u_c	Current velocity	m/s

Symbol	Description	Unit
U_w	Orbital velocity	m/s
$\tilde{\mu}$	Gumbel parameter	—
ν	Kinematic viscosity coefficient	m^2/s
$x_{lowershoreface}$	A cross-shore distance of the intertidal area below the waterline (0 MSL)	m
$X_{lowershoreface}$	A total cross-shore distance of the intertidal area below the waterline (0 MSL)	m

1 Introduction

1.1 Background

The Eastern Scheldt is a tidal basin in the southwest of the Netherlands with intertidal flats that have been encountering a serious erosion issue, known as "Sand demand" or "*Zandhonger*" in Dutch (Bosboom & Stive, 2021; van der Werf et al., 2019; Maas, 2020). This erosion was caused by the storm surge barrier and the closure of the upstream branches in 1986, leading to a decline in tidal velocity. This condition resulted in less sediment transport from the channels onto the intertidal flats, making the wave-induced erosion dominate the net sediment transport process (van der Werf et al., 2019). To justify, Figure 1.1 illustrates the observed bed level changes of Roggenplaat (the largest intertidal flat in Eastern Scheldt) from 1988 to 2014. The figure reveals the erosion and flattening of the Roggenplaat, which is expected to continue in the upcoming years (Beiboer, 2020; Maas, 2020). The decrease in intertidal areas like the Roggenplaat consequently reduces the foraging area for various species dependent on these habitats. For example, the approximately 20,000 waders that feed in this area at low tide during winter and migration periods are at risk due to this reduction (van der Werf et al., 2019). Considering this consequence, protection of the intertidal areas against erosion is needed.

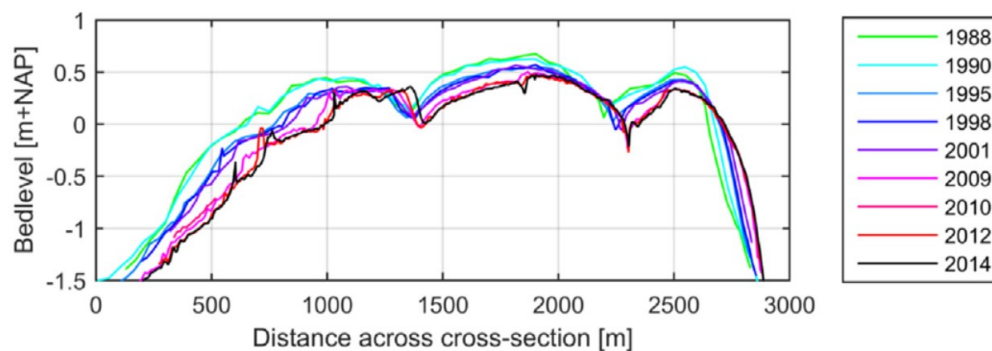


Figure 1.1. The morphological evolution of a cross-section of the Roggenplaat (intertidal flats) from 1988 to 2014, retrieved from van der Werf et al. (2019).

Soft and hard constructions are used to protect the coast (also intertidal areas) against erosion (Brand et al., 2022). An example of a soft construction is sand nourishment, which is usually applied at the beach or shoreface (Brand et al., 2022). In the Eastern Scheldt, especially Galgeplaat, Rijkswaterstaat has been investigating the effectiveness and impact of the nourishment (van der Werf et al., 2015). Monitoring showed that intertidal flat nourishments are relatively stable (van der Werf et al., 2019) and have the potential to effectively restrain the negative consequence of erosion in terms of ecology (van der Werf et al., 2015). However, the effectiveness of the nourishment also depends on its lifetime. Severe storms are expected to significantly shorten the nourishment's lifespan due to their impact on nourishment morphology (van der Werf et al., 2015). Thus, the nourishment needs to be renewed periodically to maintain the intertidal flat area and its exposure time for birds foraging. This would require an increase in the nourishment budget for the future.

Hard measures, like conventional breakwaters, can also be used to counteract erosion (Ranasinghe et al., 2010; Vlijm, 2011; Biesheuvel, 2013). In this case, conventional breakwater refers to a structure that reflects incoming waves and is mounted on the bottom of the coastal bed (Biesheuvel, 2013). Studies have proven that conventional breakwaters can control wave transmission and erosion. For

example, [Vieira et al. \(2020\)](#) demonstrated that conventional breakwaters yielded a substantial decrease in wave heights for different wave directions. They also verified that the presence of conventional breakwaters could induce accretion near the shoreline. These two previous statements agree with the studies by [Vona et al. \(2020\)](#) and [Vlijm \(2011\)](#). From the studies mentioned earlier, conventional breakwaters can be effective to counteract erosion. Nevertheless, this breakwater type is not economically attractive in deep water, is not favorable in poor soil conditions, and is not easily adapted after construction ([Biesheuvel, 2013](#)). Therefore, the use of conventional breakwaters might be not feasible for protecting the intertidal flats in the Eastern Scheldt.

Considering the limitations of the mentioned hard and soft constructions, floating breakwaters, nonetheless, could potentially provide a long-lasting solution for the erosion of intertidal flats in the Eastern Scheldt. This potential is foreseen based on the erosion in the Eastern Scheldt driven by wind-generated waves ([Eelkema, 2013](#)), this kind of wave potentially can be handled by the floating breakwater ([Biesheuvel, 2013](#)). Another reason because the Eastern Scheldt has a channel-shoal (intertidal area) interaction ([Eelkema, 2013](#)). Therefore, the channels near the shoals (intertidal flats) are presumably deeper. The availability of deeper water makes floating breakwater more effective to be implemented ([Biesheuvel, 2013](#)). This reasoning is also strengthened by [Zanuttigh and Nicholls \(2015\)](#) stating that in deep water depths greater than 6 m, traditional breakwaters are often more expensive than floating ones. Given the reasons mentioned earlier, it is intriguing to identify how floating breakwaters impact the reduction of erosion at intertidal flats like in the Eastern Scheldt.

Regarding the floating breakwater, ReShore and MARIN are two institutes that have been researching the impacts of a floating breakwater. ReShore is a Wageningen-based startup that is developing a floating breakwater, which is a so-called "LIVING breakwater". Next, MARIN is a research institute that was involved in laboratory experiments for the floating breakwater. Their recent study developed a novel floating breakwater with basin testing and numerical calculations ([Zanden et al., 2022](#)). From their study, the breakwater's hydrodynamic and wave attenuation performance were known. This is also similar to other studies, for example, [Zhang et al. \(2019\)](#); [Li et al. \(2021\)](#); [Liang et al. \(2022\)](#), which only focused on the hydrodynamic effects of floating breakwater. With the focus of floating breakwater studies on hydrodynamic, the effect of the floating breakwater on morphodynamics in sheltered areas like intertidal flats and estuaries remains questionable. This is essential for the practicality of the floating breakwater.

1.2 Problem statement

Until now, studies about floating breakwaters have been heavily concerned with attenuation performance in regular wave conditions, i.e., hydrodynamics ([Zanden et al., 2022](#)). In other words, those studies merely focused on how well the floating breakwater can dissipate wave energy under controlled laboratory conditions. Hence, there is still a limited understanding of the floating breakwater effects under realistic conditions (e.g., varying bed slopes and extreme wave height) and how the floating breakwater affects morphodynamics.

While there is a study by [Shimoda et al. \(1991\)](#) on the effects of floating breakwaters on coastal erosion, it only examines the impact of a few conditions, such as different distances from the coast and floating breakwater's draft. In addition, the study did not thoroughly explore the effects of various wave parameters (e.g., storm wave height and wave period), water depth below the floating breakwater, the floating breakwater's dimensions, and beach slope toward various hydrodynamic and morphodynamics parameters like near-bed orbital velocity and bed level change.

1.3 Research objective

Given the limitations of studies mentioned in Section 1.2, it would be beneficial to study the effects of floating breakwaters on hydrodynamic and morphodynamics under more realistic and varying parameters (wave conditions, water depths below floating breakwater, and slopes), which could have practical implications for their use.

Therefore, based on the interests mentioned, the aim of this research is to:

Assess the hydrodynamic and morphodynamic effects of a floating breakwater (FB) under varying wave conditions, FB positions, and slopes on the intertidal flats

1.4 Research questions

Two research questions were formulated to achieve the main research objective. The first research question identifies whether the numerical model Delft3D can reproduce the evolved cross-shore profile and its hydrodynamic and morphodynamic behavior when floating breakwater (FB) interventions are present, based on the laboratory study conducted by Shimoda et al. (1991). The first research question with its sub-research questions can be read below:

1. How well does a numerical model Delft3D reproduce the FB effects yielded from the laboratory experiment of Shimoda et al. (1991)?
 - (a) How well does the numerical model Delft3D reproduce the cross-shore profiles observed in the laboratory experiment conducted by Shimoda et al. (1991)?
 - (b) How does the presence of FB impact the wave height based on the experiment and Delft3D model?
 - (c) How does the presence of FB impact the sediment transport according to the experiment and Delft3D model?

Next, the second research question unravels how FB impacts the hydrodynamic and morphodynamics in simplified tidal flat environments. The study focuses on the wave and seabed slopes in the Eastern Scheldt area. By varying these conditions (waves, seabed slopes, and the locations of the FB), we aim to comprehend how the hydrodynamic and sediment-related characteristics are influenced. The second research question, followed by sub-research questions, is as follows:

2. What are the hydrodynamic and morphodynamic effects of a floating breakwater (FB) under varying wave conditions, FB positions, and slopes representing the intertidal flats in the Eastern Scheldt?
 - (a) How do the transmission coefficients of the selected FB vary under different wave conditions and water depths below FB (FB positions)?
 - (b) How do the hydrodynamic parameters (wave height, near-bed orbital velocity, and bed shear stress) vary under different wave conditions, floating breakwater (FB) positions, and slopes representing the intertidal flats environment?
 - (c) How does the presence of a floating breakwater (FB) in the intertidal flats environment, under varying wave conditions, FB positions, and slopes, impact the amount of sediment transported (bed load and suspended load) and cross-sectional erosion area?

- (d) What inferences can be made from the hydrodynamic and morphodynamic effects of floating breakwaters under different wave conditions, floating breakwater positions, and slopes, particularly with regard to erosion?

1.5 General approach

Following the structure of the research questions, this research is structured in two phases. In the first phase, the FB effects in the experiment reported by Shimoda et al. (1991) are compared to the FB effects derived from a numerical model. The experiment of Shimoda et al. (1991) is considered because it exhibited the cross-sectional evolution of the beach (in laboratory settings) due to FB. This was complemented with explanations regarding the effects of FB on wave height and sediment transport in the laboratory. To be able to compare the results from the laboratory, the hydrodynamic and morphodynamic modelings are performed using Delft3D. The numerical model Delft3D is used because it provides a feature called "transmission coefficient" that can be used to represent the FB's function to attenuate waves. The outcomes of Delft3D in the first research phase, which comprise cross-sections, wave height, and sediment transport, are compared with the results of the experiment by Shimoda et al. (1991). Data visualization for comparing the laboratory and numerical model results is executed using the programming language MATLAB. The comparison gives information on whether Delft3D can replicate the effects of FB according to the experiment.

Next, in the second research phase, the hydrodynamic and morphodynamics effects of FB on intertidal flats are identified using Delft3D. Variations of wave conditions, FB positions (water depth below FB), and linear slopes (representing bathymetry and topography) at intertidal flats are derived based on the corresponding situations in the Eastern Scheldt. These variations were established to generate multiple unique combinations (simulations) for Delft3D modeling inputs. Before running the simulations, the transmission coefficients corresponding to wave conditions and determined FB specifications are computed. This is done to understand the FB effectiveness in attenuating waves on different wave conditions and FB positions and have the inputs representing FB in Delft3D. Using the calculated transmission coefficients and variations of derived data, multiple Delft3D simulations are performed. All simulations resulting in hydrodynamic and morphodynamic parameters are then processed in MATLAB for interpretation. The FB effects on hydrodynamic and morphodynamics parameters are interpreted by visualizing and comparing their magnitudes for different wave conditions, FB positions, and slopes. Lastly, implications are elaborated based on the integrated knowledge of the FB effects on both hydrodynamic and morphodynamics.

1.6 Scope

Due to the time limit, these constraints are introduced:

1. A wave height reduction capacity of an FB is only based on the transmission coefficient. Thus, the motion effects of the FB will not be assessed.
2. There are many types of FB, for instance, single-pontoon, double-pontoon, and A-frame (Biesheuvel, 2013); Nonetheless, only a box type FB will be widely assessed.
3. The research will use a numerical model with simplified and uniform bed levels along the intertidal flats, focusing on the effects of the floating breakwater, specifically in the cross-shore direction.

1.7 Structure of the report

The report of this research is structured as follows: In Chapter 2, the description of the floating breakwater and its hydro-morphodynamic effects will be theoretically explained, followed by the explanation of the hydrodynamic and morphodynamic parameters relevant to this research. Then, Chapter 3 describes the data and the methodology that will be applied for research phase 1 and phase 2. Chapter 4 and Chapter 5 present the results of the research phase 1 and 2, respectively. This is then followed by discussion in Chapter 6 and finally, the conclusions and recommendations in Chapter 7.

2 Theoretical background

2.1 Floating breakwater

A floating breakwater is one of the alternatives to the conventional breakwater. This breakwater is a moored structure that attenuates waves through a combination of reflection and dissipation (Zanden et al., 2022). Commonly, the reasons for implementing this type of floating breakwater are:

- economically attractive in deep water (Biesheuvel, 2013),
- applicable in poor soil conditions (Biesheuvel, 2013),
- flexible in terms of placement, for instance, it can be removed during summer (Biesheuvel, 2013; Drieman, 2011),
- good for seawater exchange between the onshore and offshore side of the breakwater (Shimoda et al., 1991),
- relatively easy for obtaining permission compared to a construction permit for conventional breakwater (Drieman, 2011).

Multiple studies about floating breakwaters have been carried out. For instance, Zanden et al. (2022), Biesheuvel (2013), and Guo et al. (2022) studied the attenuating performance of different floating breakwaters under the different hydrodynamic conditions. Furthermore, Drieman (2011) investigated the technical feasibility of a floating breakwater to protect the beach in Balchik, Bulgaria. In that study, Drieman (2011) explored the floating breakwater design to achieve a required transmission coefficient for attaining a desired wave height (maximum allowed wave height) behind the floating breakwater. In terms of morphodynamics, Shimoda et al. (1991) performed laboratory experiments to evaluate the capability of a floating breakwater to reduce erosion.

2.2 Wave attenuation due to floating breakwater

As the preceding section mentions, floating breakwater attenuates waves by reflecting the incoming waves, which also causes a reflected waves. Furthermore, the remainder of wave energy is transmitted, yielding a reduced wave height behind the floating breakwater or on the lee side (protected area). The transmitted wave height is an accumulation of the transmitted wave energy under the breakwater, water over-topping, and radiated waves due to the motions of the floating breakwater. Furthermore, due to turbulence, energy dissipation occurs at the edges of the floating breakwater (Biesheuvel, 2013). For a more understandable explanation, see an illustration of the floating breakwater in Figure 2.1.

Wave attenuation is the hydrodynamic effect promoted by a floating breakwater. The amount of wave attenuation is defined as an incoming wave energy minus reflected and dissipated wave energy. Due to the wave being attenuated, there is a reduction in the wave height from the seaward to the shoreward side of the floating breakwater (see Figure 2.1) (Biesheuvel, 2013).

Transmission coefficient

A transmission coefficient describes the effectiveness of floating breakwaters in attenuating waves (reducing the wave height). This coefficient can be calculated by Equation 1, which depends on the incident wave height and transmitted wave heights. Here, C_t represents transmission coefficient, H_t the transmitted wave height, H_i incident wave height (Biesheuvel, 2013).

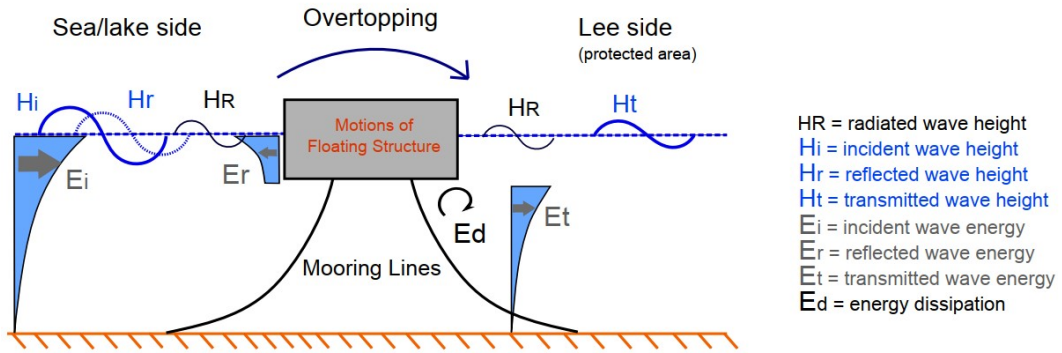


Figure 2.1. Interaction between wave and floating breakwater, retrieved from Biesheuvel (2013)

$$C_t = \frac{H_t}{H_i} \quad (1)$$

It can be interpreted from Equation 1 that a lower transmission coefficient means that a floating breakwater can effectively attenuate waves or effectively reduce an incident wave height. Furthermore, for a common floating breakwater, box-type, the transmission coefficient can be described by the Macagno relation, formulated by a researcher, namely Macagno, in 1954, (Bouwmeester & Breggen, 1984; Biesheuvel, 2013; Zanden et al., 2022) in Equation 2. The illustration of box-type FB, can be viewed below:

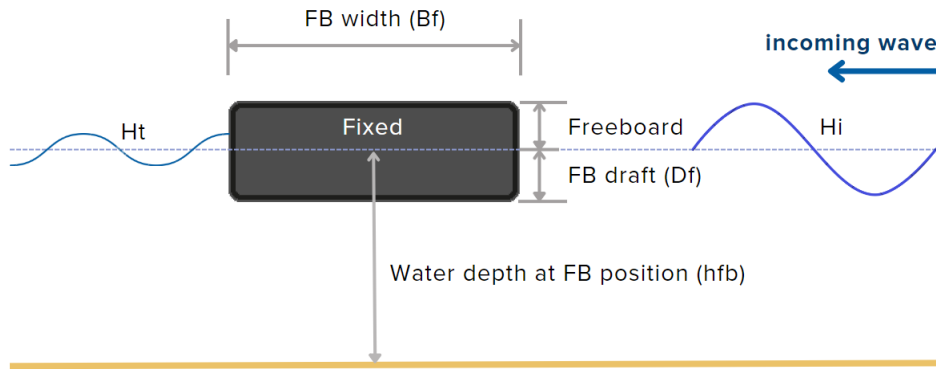


Figure 2.2. Box type floating breakwater, representing the type of FB that defines the Macagno formula

Furthermore, the parameters employed for the Macagno relation are the wave number (k), the water depth (h_{fb}), the FB width (B_f), and the FB draft (D_f) as seen in Equation 2 (Macagno relation)

$$C_t = \frac{1}{\sqrt{1 + \left[\frac{kB_f \sinh(kh_{fb})}{2 \cosh(kh_{fb} - kD_f)} \right]^2}} \quad (2)$$

With different water depths at FB positions and different FB drafts, the transmission coefficient varies as depicted by Figure 2.3 below.

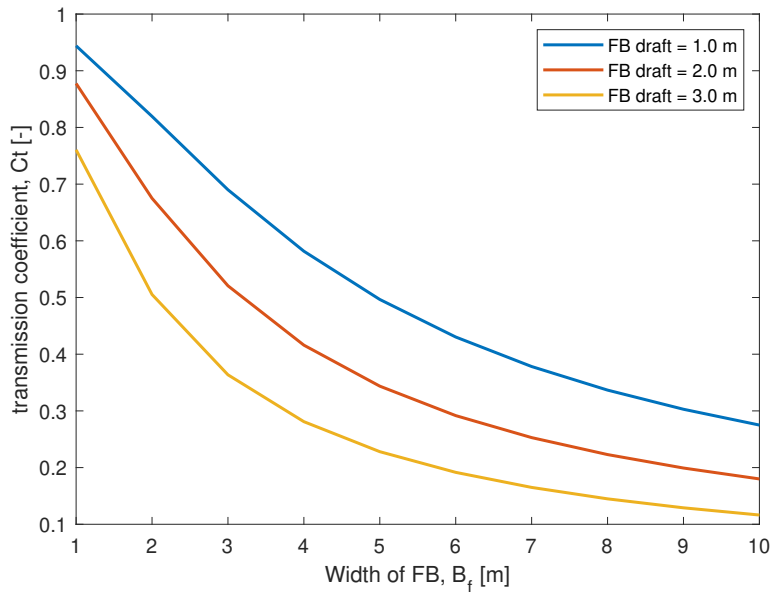


Figure 2.3. Transmission coefficient with different FB width and FB draft, calculated with a wave period $T = 3.0$ s and a water depth at FB position = 10 m

Furthermore, this equation employed the following assumptions (Biesheuvel, 2013):

- Rigid structures, the shape does not change;
- Fixed structures, the position does not change;
- Finite width of FB;
- Deep water (linear wave theory);
- No overtopping.

There are limitations of the Macagno relations such as:

- it is not expected to predict accurate results in presence of movements (Ruol et al., 2012),
- it overestimates the transmission coefficient under irregular waves (Biesheuvel, 2013),
- when the draft of floating breakwater (D_f) is equal to water depth (h), the formula predicts some transmission. Yet, in reality, no transmission is expected (Ruol et al., 2013).

Here, wave number (k) in Equation 2 can be related to wavelength (L) and wave period (T). Equations 3, 4 and 5 (Bosboom & Stive, 2021; van der Werf, 2021) present the relationship between these three parameters (k , L , T) for clarifying wave number (k) in Equation 2, with g represents gravitational acceleration and L_0 the wavelength in deep water.

$$k = \frac{2\pi}{L} \quad (3)$$

$$L = L_0 \tanh\left(\frac{2\pi h}{L}\right) \quad (4)$$

$$L_0 = \frac{gT^2}{2\pi} \quad (5)$$

2.3 Morphodynamic effects of floating breakwater

As the floating breakwater alters the hydrodynamics involving sediment transport, coastal morphodynamic can be affected. The effect on coastal morphodynamic continues until a new situation is reached (Bosboom & Stive, 2021). In this case, Bosboom and Stive (2021) described that when a breakwater attenuates the waves, there will be a reduction in wave activity (wave energy), denoted by a decline of incident wave height. Since reduced wave activity occurs, the sediment transport capacity is also less, causing the sediment to be deposited in the shadow zone (a tranquil area behind the breakwater).

In the case of a floating breakwater, Shimoda et al. (1991) performed laboratory experiments to assess the effects of a submerged moored floating breakwater on coastal erosion. They explained that this floating breakwater could attenuate waves, and the attenuated waves mean the reduction of hydrodynamic activity that could entrain sediment. The reduction of hydrodynamic activity near the shore leads to smaller erosion or even nearshore accretion.

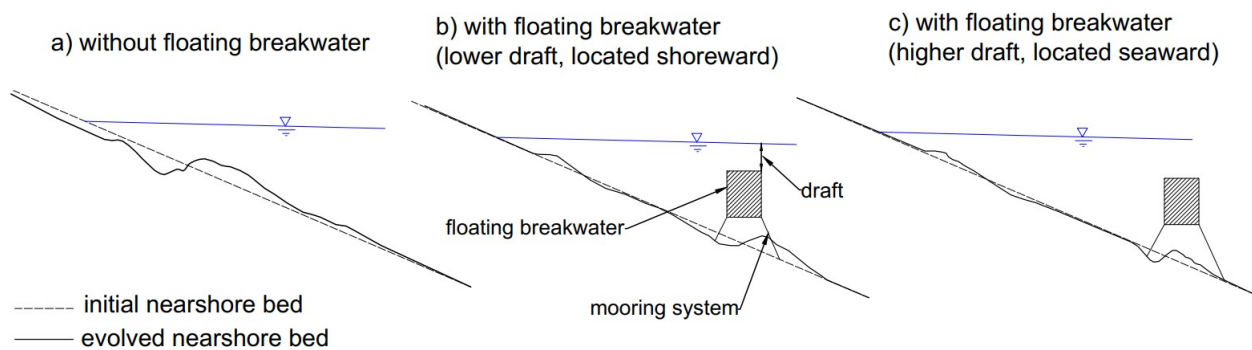


Figure 2.4. Results of experimental study of floating breakwater effects on bed level changes in an eroded-type beach, adapted from Shimoda et al. (1991)

To elaborate, Figure 2.4 describes three tests of the laboratory experiments by Shimoda et al. (1991). One was without a floating breakwater; the others had a floating breakwater located near the shore and slightly further from the shore. From their experiment presented in Figure 2.4a, relatively more erosion near the shore and sedimentation at more seaward occurred when the floating breakwater was not applied. Conversely, when the floating breakwater was applied, a small accretion was apparent near the shore with a scouring below the floating breakwater (Figure 2.4b,c). Furthermore, with a lower draft and more landward floating breakwater (Figure 2.4b), scouring below the floating breakwater was more significant than the seaward floating breakwater (Figure 2.4c). Nevertheless, accretion near shore was still apparent. This confirms that the floating breakwater could reduce erosion or even induce sedimentation near the shoreline.

2.4 Hydrodynamic parameters relevant to sediment transport

Because the final interest in this thesis is the morphodynamic effects of FBs, important hydrodynamic parameters that are relevant to sediment transport are explained. In relation to this, Xiong et al. (2018) and Wiberg and Sherwood (2008) explained that hydrodynamic parameters, e.g., wave height, near-bed wave orbital velocity, and wave-induced shear stresses are important hydrodynamic parameters for sediment transport. Considering the previous statement, three hydrodynamic parameters such as wave height, near-bed orbital velocity, and bed shear stress are elaborated in this section.

Wave height (H)

The wave height is linkable to the rates of movement of sediment onto and off beaches because, for instance, when the waves get higher, these changes lead to an increase in the maximum orbital velocity of the wave. The shear stress at the sea bed thus increases, and so does the potential for sediment movement (Wright et al., 2008). It is also important to mention that the wave height does not control so much the sediment transport direction, but it does have a large impact on the magnitude. In this context, higher waves can mobilize more sediment.

Near-bed orbital velocity (u_b)

As mentioned before, the movement of sediment is also related to near-bed orbital velocity. The term "orbital velocity" is the time it takes for a water particle to complete a full orbit in a water column, going from crest to trough, and back to the crest of the next wave as it passes (Wright et al., 2008). Again, the orbital velocity related to sediment transport is near-bed orbital velocity. When waves occur in water depths that are greater than $L/20$ but less than $L/2$, the maximum horizontal near-bed orbital velocity (u_b) is linkable to the wave height (H), water depth (h), wavelength (L), and wave period (T), described by the equation below (Wright et al., 2008; Bosboom & Stive, 2021; van der Werf, 2021):

$$u_b = \frac{\pi H}{T \sinh\left(\frac{2\pi h}{L}\right)} \quad (6)$$

The equation shows that when waves have the same period and if the wave height increases, the speed of water near the bed (horizontal velocity), u_b also increases (Wright et al., 2008). Next to that, when waves have the same height, the water speed near the bed (u_b) is higher for waves with shorter periods than waves with longer periods. In other words, there is a reverse relationship between (u_b) and the wave period (T) (Wright et al., 2008).

Bed shear stress (τ_b)

Waves and currents affect sediment movement on the seabed mainly by creating friction with the seabed. This friction is called "bed shear stress" (τ_b), and it represents the force that the flow applies to the bed per unit area (van der Werf, 2021). The way we calculate the strength of the bed shear stress from waves is similar to how we calculate it for currents, which is described in this equation below for waves:

$$\tau_{b,w} = \frac{1}{2} \rho_w f_w u_b^2 \quad (7)$$

where f_w is the wave friction factor and u_b is near-bed orbital velocity, ρ_w density of water. Meanwhile, for the current-related bed shear stress, we can compute using a similar equation below:

$$\tau_{b,c} = \frac{1}{2} \rho_w f_c u_c^2 \quad (8)$$

where f_c is current-related friction coefficient and u_c is current-related velocity.

From Equation 8 and Equation 7, it is seen that both equations are computed with squared velocity. Nevertheless, it is important to mention that a thin wave boundary layer in wave orbital velocity produces a much larger velocity shear and bed shear stress for a given orbital velocity than a current with an equal speed (van der Werf, 2021; Bosboom & Stive, 2021).

2.5 Morphodynamic parameters

Coastal morphodynamic is the mutual adjustment of morphology and hydrodynamic processes involving sediment transport (Bosboom & Stive, 2021). Since we already discussed the hydrodynamic parameters relating to sediment transport. In this section, we now delve into the sediment transport itself. We can distinguish between bed load and suspended load transport in this case. This distinction was also considered by Van Rijn (1993) for the formulation in numerical model Delft3D (Deltares, 2022). Regarding this, Van Rijn (1993) distinguishes the sediment transport below and above a reference level. Below the reference level, it is treated as bed load; above, it is treated as suspended load.

Bed load and suspended load transport

Bed load transport is the transport of sediment particles in a thin layer close to the bed. The sediment particles are continuously in contact with the bed. Figure 2.5a shows bed load transport at low shear stresses. When the shear stress is higher, an entire layer of sediment moves on a plane bed; this is the so-called sheet flow 2.5b. Still, this is considered as bed load since grain-grain interaction plays an important role (Bosboom & Stive, 2021).

Next, suspended load transport is the movement of sediment particles suspended in the water column without direct contact with the bed (see Figure 2.5). Turbulent diffusive forces in the water flow carry and support these particles to stay in the water column (Bosboom & Stive, 2021).

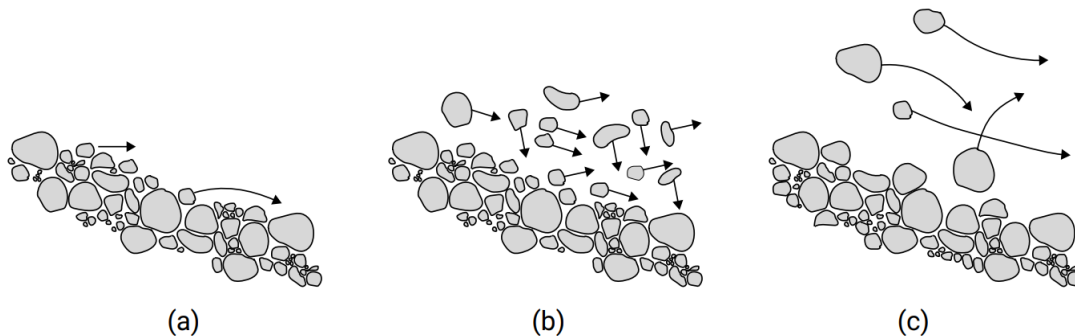


Figure 2.5. Different modes of sediment transport (a) bed load at small shear stresses (b) bed load at relatively higher shear stresses (sheet flow) (c) suspended load, retrieved from Bosboom and Stive (2021)

The sum of the bed load and suspended load equals the total load, which can be rewritten as follows:

$$q_{total} = q_b + q_s \quad (9)$$

All of these parameters, q_{total} , q_b , q_s , have a unit of $kg/m^3/m$.

The numerical model implements transport formulas to compute bed and suspended load. For instance, Deltares (2022) described multiple formulations that can be implemented in the numerical model Delft3D for calculating bed load and suspended load transport. Nevertheless, by default, the Delft3D numerical model uses van Rijn (1993) as the formulation for calculating bed load and suspended load transport (Deltares, 2022; van de Wardt, 2018).

3 Methodology

The research in this thesis will be undertaken by performing two research phases corresponding to the research questions (see Section 1.4). As briefly explained in Section 1.5, the first research phase attempts to reproduce the outcomes of the experiment of Shimoda et al. (1991) by running hydro-morphodynamic numerical modeling in Delft3D (D3D). In the first research part, to better understand the experiments that were carried out by Shimoda et al. (1991), we first explain their experiment, which can be read in Section 3.2.1. Subsequently, we organize and utilize the pertinent data from the experiment to create input for the Delft3D model, which will be discussed in detail in Section 3.2.2. As the relevant data for the modeling are obtained, Delft3D modeling preparation for the first research phase is explained in Section 3.2.3. This is followed by explaining the post-processing techniques applied to the Delft3D results to accurately address the first research question (see Section 3.2.4).

Furthermore, the second research phase explores the floating breakwater's hydrodynamic and morphodynamic effects under varying conditions. We first need to derive the data necessary for having the intended variations: topography and bathymetry of the Eastern Scheldt, wave conditions, and FB positions. The data derivation is explained in Section 3.3.2. Afterward, we also explain how some pieces of derived raw data are prepared and converted into a suitable format for inputting into Delft3D in Section 3.3.3. The prepared data are then assigned to carry out multiple unique simulations according to the variations mentioned. The basic setting of Delft3D for undertaking the multiple unique simulations is explained in Section 3.3.4. Finally, the post-processing steps required to answer the second research question are explained in Section 3.3.5

To better understand the whole concept in methodology, the explained steps of the research phases are illustrated in Figure 3.1 below.

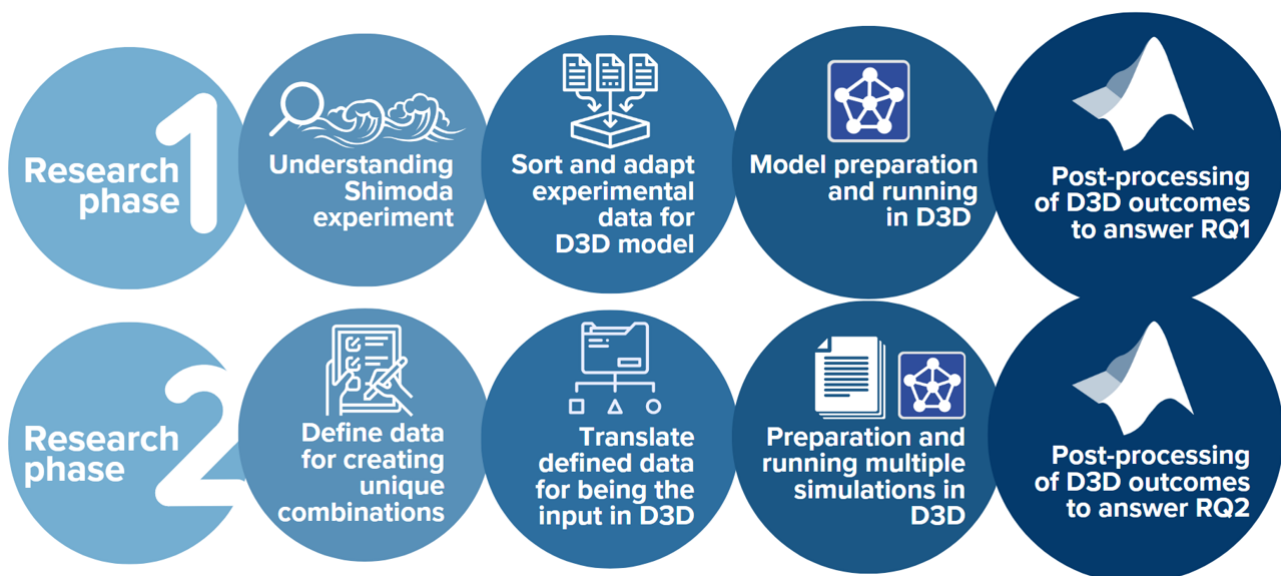


Figure 3.1. Steps of the first research phase and second research phase

3.1 Numerical model Delft3D

A numerical model can be a powerful tool for performing hydrodynamic and morphodynamic analyses (Giardino et al., 2010; Vlijm, 2011). The advantages of using a numerical model are that it is relatively cheap compared to performing field observations or physical model tests (scaled model) and allows studying the effect of individual design parameters (Vlijm, 2011). Examples of studies that were conducted by the numerical model are by Lesser et al. (2004), Vlijm (2011), Pezij (2015), Vona et al. (2020), Vieira et al. (2020) and Sabrina and Karjadi (2022). In general, they studied the hydrodynamic and morphodynamic effects of different types of obstacles (conventional breakwaters, coastal reefs, floating cages) in the nearshore by using Delft3D-FLOW and Delft3D-WAVE.

There are benefits in utilizing Delft3D for hydrodynamic and morphodynamic analyses such as:

- Delft3D is capable of representing all the important hydrodynamic and morphologic processes accurately in a limited amount of computational time for longer (morphological) time scales (Vlijm, 2011),
- It has proven that Delft3D could perform well to do the hydrodynamic and morphodynamic analysis in several theoretical, laboratory, and real-life situations (Lesser et al., 2004),
- Delft3D provides an obstacle feature to specify a value of transmission coefficient representing the breakwater performance (Mojabi et al., 2018).

With the aforementioned relevant examples of the research that uses Delft3D and the advantages of using Delft3D, we also use Delft3D in this study.

Delft3D for modelling the FB

In the hydrodynamic study of the floating breakwater (also conventional breakwater), researchers commonly report the value of the transmission coefficient, which describes the effectiveness of floating breakwaters in attenuating waves (read Section 2.2 for more explanation). In light of the previous statement, Zanden et al. (2022) and Biesheuvel (2013) also discussed the transmission coefficient of the floating breakwater. In Delft3D, Sabrina and Karjadi (2022) used the transmission coefficient feature in Delft3D as an input to model the hydrodynamic and morphodynamic effects of floating cages. Inspired by the studies that discussed the transmission coefficient and used it to represent a floating structure, this study also uses the transmission coefficient as input to represent a floating breakwater in Delft3D. As input in Delft3D, the transmission coefficient serves as an obstacle, causing waves to be blocked between neighboring points on the grid as they move from one point to the next in the computational grid. This occurs wherever the obstacle line, which is represented by the transmission coefficient, is positioned between two nearby grid points (Deltares, 2023a). Further explanation is available in Appendix A.

To obtain the value of the transmission coefficient, the derived data (wave conditions and FB specifications) is used as input of Macagno relation (Equation 2). The calculated transmission coefficients are then used as inputs in Delft3D. In addition, using the Macagno relation to estimate the transmission coefficient means that we will assume the FB implemented in the model is a box-type FB (read Section 2.2). As a notice, the calculation of the transmission coefficient using the Macagno relation is only applied to the second research phase. The Macagno relation is not used to calculate the transmission coefficient in the first research phase because the type of FB experimented by Shimoda et al. (1991) was submerged moored floating breakwater (SMFB), which is different than box-type FB. Therefore, instead of using the Macagno relation, we define a range of transmission coefficients (sensitivity) that represent the SMFB in the first research phase.

3.2 First research phase: reproduce the FB effects observed in the laboratory experiment by Shimoda

3.2.1 Laboratory experiment reported by Shimoda et al. (1991)

Explanation about Shimoda experiment

The experiments by Shimoda et al. (1991) were carried out in a wave tank. This wave tank has a 1.0 m width, 1.5 m height, and 50.0 m length. As an initial condition of these experiments, a beach slope of 1:10 was built of sand with a $D_{50} = 0.380$ mm. Furthermore, different wave steepness i.e., H_0/L_0 was imposed for these experiments, such as 0.01, 0.03, and 0.06. These three wave steepness are intended to establish accreted-type, intermediate-type, and eroded-type beaches before placing the submerged moored floating breakwater (SMFB). This SMFB was represented by a fixed-moored model with four stainless wires. The dimension of this SMFB was 10 cm in height, 30 cm in width (cross-shore), and 99 cm in length (alongshore). The waves in the flume were generated for about 4 hours. Afterward, the beach profiles were measured and drawn. To better understand the aforementioned laboratory settings, Figure 3.2 illustrates the settings used by Shimoda et al. (1991).

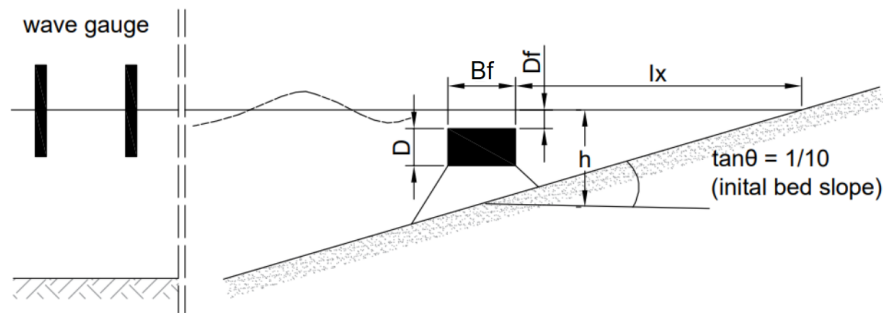


Figure 3.2. Settings in Shimoda experiment, D = height of FB, B_f = width of FB, D_f = draft of FB, h = water depth, l_x = distance from the coast to the FB, adapted from Shimoda et al. (1991)

Understanding the hydrodynamic and morphodynamic effects of SMFB

All relevant elaborations from Shimoda et al. (1991) are summarized to understand the hydrodynamic and morphodynamic effects of SMFB. For morphodynamic interpretation, apart from outlining the explanations from Shimoda et al. (1991), the evolving bed profiles presented in their report are digitized. This is done to obtain the data points that can be plotted for checking the maximum erosion and sedimentation, also computing the area of erosion and sedimentation. To calculate the maximum erosion and sedimentation, the digitized-evolved bed will be subtracted from the initial bed. Furthermore, the area above and below the zero line will be computed to know the area of erosion and sedimentation. These processes are performed using the data of bed profile (Figure 3.3) that are digitized (Figure 3.4). In this case, the values of the x-axis and y-axis in Figure 3.4 are adjusted by using the calculated H_0 and L_0 . The values of H_0 and L_0 are calculated in Section 3.2.2 under discussion about wave height, wave period, and wave direction.

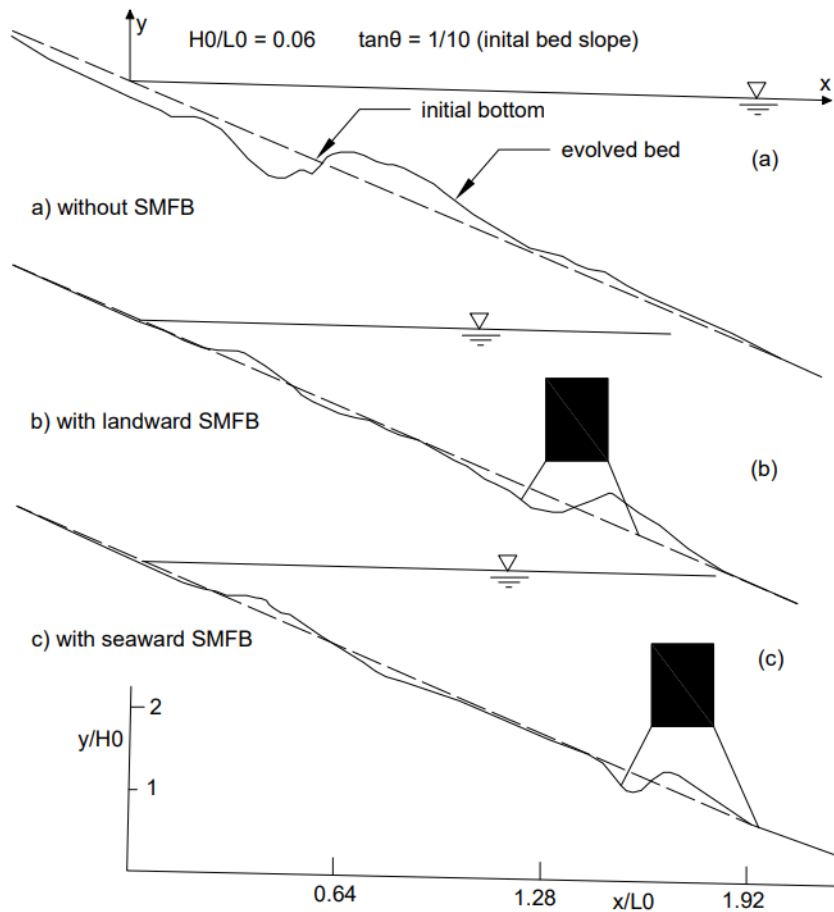


Figure 3.3. Evolution of nearshore bed level (a) without SMFB (b) with more shallow SMFB (solid black box) from the water surface, located landward (c) with deeper SMFB from the water surface located seaward; H_0/L_0 represents the wave steepness applied for the experiments; adapted from Shimoda et al. (1991)

3.2.2 Data of laboratory experiment for Delft3D modelling in the first research phase

The previous section explains the data that were used for the experiment by Shimoda et al. (1991) and how we will process the laboratory data for the comparison with Delft3D modeling outcomes. To reproduce the results of the laboratory experiment observed by Shimoda et al. (1991) using Delft3D, the data from their paper are sorted and used for the Delft3D model input.

Wave height, wave period and wave direction

Wave height is derived using linear wave theory (with H_0/L_0 and Equation 5). With the wave period (T) in Shimoda et al. (1991) = 1.8 s, the wavelength in deep water (L_0) can be calculated with Equation 5. This results in wavelength in deep water (L_0) = 5.05 m. Considering the wave steepness (H_0/L_0) = 0.06 in Shimoda’s experiment, the wave height (H_0) was calculated by multiplying the wavelength in deep water (L_0) with wave steepness. This operation yields a wave height H_0 of 0.303 m \approx 0.30 m, which is then used for the simulation in the first research phase. Important to mention that the wave steepness used for the previous calculation is only $(H_0/L_0) = 0.06$ instead of all wave steepness: $(H_0/L_0) = [0.01 \ 0.03 \ 0.06]$. This is because Shimoda et al. (1991) reported the evolved bathymetry

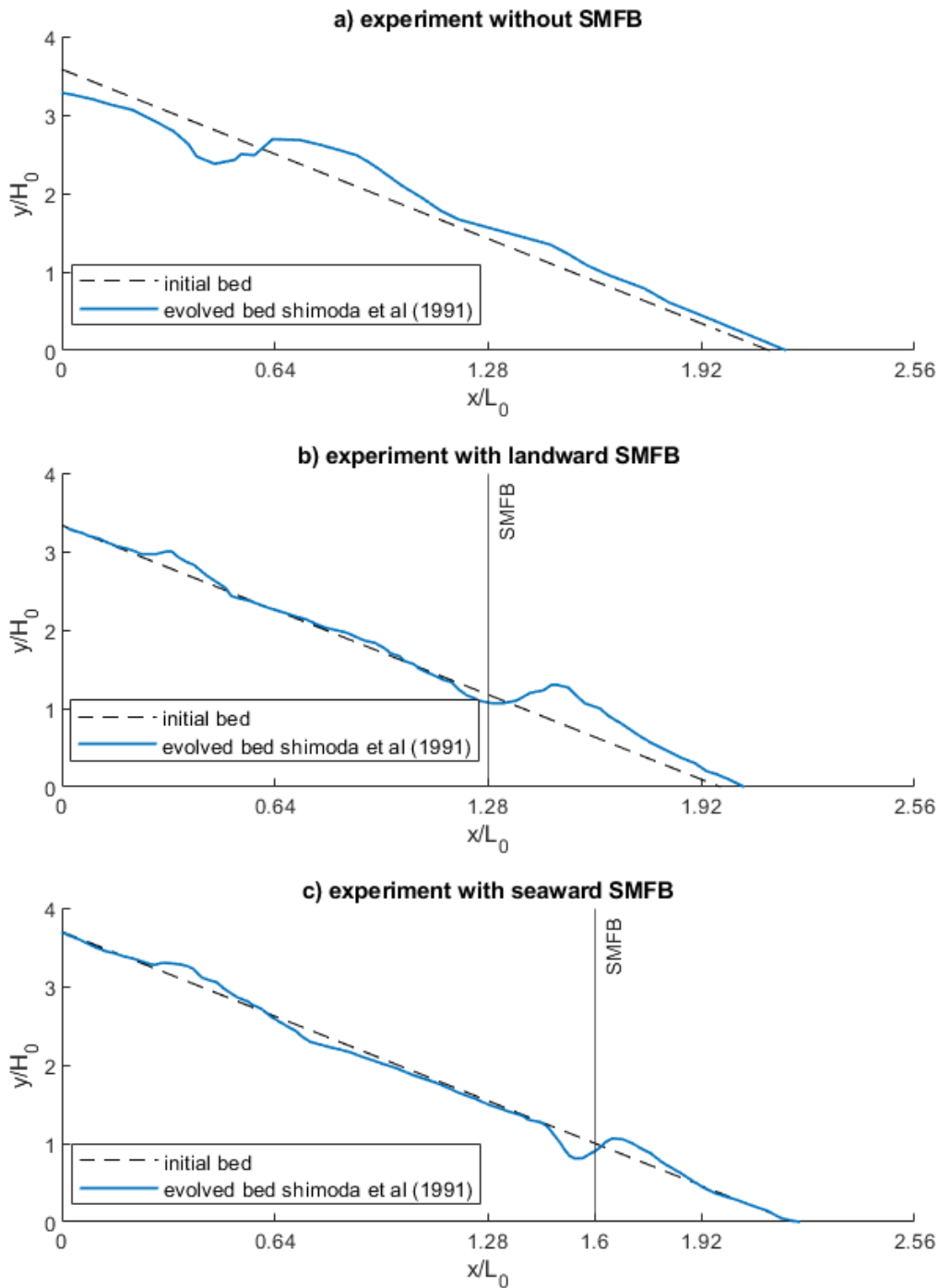


Figure 3.4. Evolution of nearshore bed level (a) without SMFB (b) with more shallow SMFB from the water surface, located landward (c) with deeper SMFB from the water surface located seaward; adapted from Shimoda et al. (1991)

only with a wave steepness (H_0/L_0) of 0.06 (see Figure 3.3). Next, for the wave direction, Shimoda et al. (1991) only simulated the conditions with a normal-directed wave to the shore.

Table 3.1. Data of the laboratory experiment by Shimoda et al. (1991) that will be used for Delft3D modeling in the first research phase

Parameter	Value	Unit
Length of the wave tank	50	<i>m</i>
Beach slope	1/10	-
Wave height (H_0)	0.30	<i>m</i>
Wave period (T)	1.8	<i>s</i>
Wave direction	normal to shore	-
Sediment diameter (D_{50})	0.380	<i>mm</i>

3.2.3 Delft3D settings in the first research phase

Grid and bathymetry

Grid and bathymetry are established according to the specification of the wave flume and the bathymetry (bed profile) used in the laboratory experiment by Shimoda et al. (1991). In the current study, we specify a depth-averaged 1D model. This is established by having a uniform alongshore bathymetry associated with the grid.

For the grid, it is set to have a length of 50 m, following the length of the wave tank in Shimoda's experiment (see Table 3.1). Two separate grids (for Delft3D-FLOW and WAVE) are created using RGFGRID, an integrated tool within Delft3D, to facilitate the modeling process in Delft3D-FLOW and Delft3D-WAVE. For Delft3D-FLOW, a grid of 6 m width times 50 m length was created. The resolution of this grid ranges from 0.75 m to 2.26 m (x-directed, right to left in Figure 3.5), which is coarser offshore and becomes finer as it reaches onshore. This is done because it is intended to capture finer detail of the computed parameters (e.g., bed level changes), especially in the onshore part where the changes presumably occur. In the alongshore direction (bottom to top in Figure 3.5), the FLOW grid has a resolution of 1.0 m. This is considered because we are only interested in the change of cross-shore.

Next, for the grid in Delft3D-WAVE, a wider grid is used with a length of 50 m and a width of 166 m. Initially, attempts are made to use a smaller width for the WAVE grid. Nevertheless, the smaller WAVE grid led to boundary effects, indicated by the sudden drop in wave height. We also report the attempts to use different widths of the WAVE grid in Chapter 6. Regarding the resolution of the WAVE grid, it has a coarser size offshore and a finer size nearshore with a value of 1.12 - 3.35 (x-directed, right to left in Figure 3.5). This is considered because it is aimed to capture the changes in wave height in a finer resolution, especially near the shoreline. In the alongshore direction, the grid has a size of 1.0 m for each cell. The FLOW and WAVE grids can be viewed in Figure 3.5.

After the FLOW and WAVE grids are established, the bathymetry associated with each grid is generated with a slope corresponding to the slope experimented by Shimoda et al. (1991). With the grid length of 50 m for both FLOW and WAVE, the highest part of the model domain is 1 m, with the deepest part being -4 m. These elevations are determined to have an area of the beach above the water line. In this case, we consider the water level at 0 MSL. These elevations also ensure that the

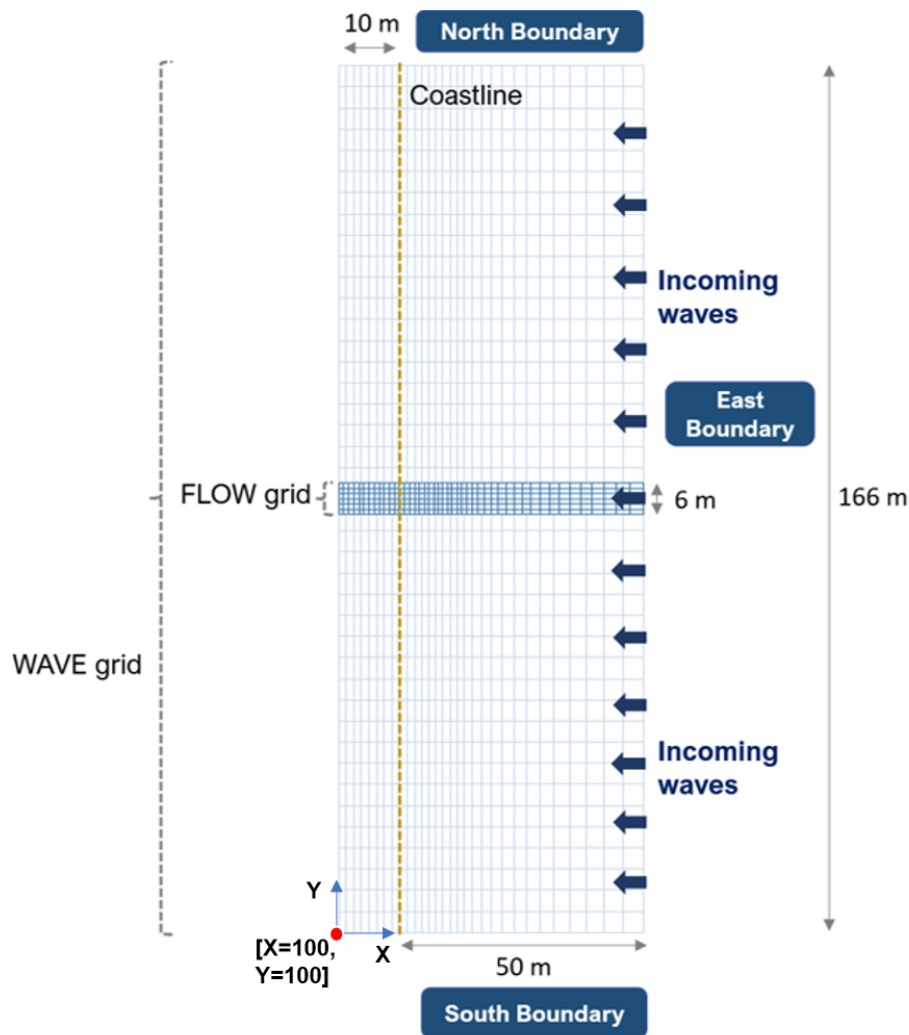


Figure 3.5. Plan view of the grids with the FLOW grid (dark blue) and WAVE grid (light blue) for hydro-morphodynamic simulation of Shimoda experiment in Delft3D. Blue arrows represent the incoming waves (open boundary), and the brown dashed line represents the coast (closed boundary)

slope corresponds to that used by Shimoda et al. (1991). To generate this bathymetry, QUICKIN, a built-in feature within Delft3D, is employed. Figure 3.6 is provided to see the bathymetry used for the research phase one.

Input for Delft3D-FLOW and Delft3D WAVE

In Delft3D-FLOW, considerations about the time step, sediment diameter, sediment layer thickness, also boundary are made. Before, the generated grids and bathymetry were imported to Delft3D-FLOW. Then, the time step is prescribed to be 0.0125 minutes, ensuring that the Courant Number is below the maximum prerequisite value of Courant Numbers of 10 to achieve the model stability (Deltares, 2022). In addition, the sediment diameter is set to be similar to the D_{50} used by Shimoda et al. (1991), which was 380 micrometers. Furthermore, the sediment layer thickness (erodible layer) is set to be 30 m. This value of the erodible layer is chosen to keep the availability of sediment that can be eroded (as the erodible beach). The open boundary for this simulation is only one located east of the domain, with a constant water level of 0 m above the mean sea level. This constant water level persists throughout the simulation time. The simulation consists of 12 hours of spin-up time and 4 hours of simulation with



Figure 3.6. Bathymetry and positions of SMFB for Delft3D simulations in the first research phase, the waves come from the open boundary ($x=50$ m)

morphology (16 hours). A duration of 4 hours after the spin-up time in Delft3D was chosen because 4 hours was the duration of the laboratory experiment executed by Shimoda et al. (1991).

In Delft3D-WAVE, grid, bathymetry, boundaries, transmission coefficient, and position of SMFB (see Figure 3.6) are prescribed. The created WAVE grid associated with its bathymetry is defined. The boundaries, such as wave height, wave period, wave direction, and directional spreading, are determined following the condition of the Shimoda experiment (see Table 3.1). As reported by Shimoda et al. (1991), wave direction was normally directed to the shore; under the nautical mode, the angle where the waves come is set to 90° (waves normally propagate to the shore). Next, the directional spreading and Gaussian spreading are defined to the smallest possible values, 1×10^{-2} . This is done to represent the wave propagation in the Shimoda experiment (stationary wave condition). With a small value of directional spreading and Gaussian spreading, it is assumed that the waves propagate in a stationary condition. It is worth mentioning that the boundaries for wave conditions (significant wave height, peak period, wave direction, directional spreading, spectral space) are defined at three boundary orientations: North, East, and South (see Figure 3.5). This is done to mitigate the presence of attenuated waves near the southern and northern boundaries of the model domain where wave conditions are not explicitly specified.

Still, in Delft3D WAVE, the SMFB is represented by a value of transmission coefficient that can be inputted. Because there is no information regarding the transmission coefficient of the SMFB from Shimoda et al. (1991), different transmission coefficients ranging from 0.10 - 0.90 with an increment of 0.10 are considered. According to the experiment, there are two different FB positions, landward and seaward (see Figure 3.6). To obtain the value of the cross-shore distance of the FB, we multiply the positions of the SMFB in the experiment (x/L_0) by the calculated wavelength in deep water ($L_0 = 5.05$ m). This factor adjusts the position on the scaled axis, which is represented as x/L_0 in Figure 3.4. By unscaling the position of SMFB, we obtain the cross-shore distance of the SMFB, which gives landward FB position = 16.5 m (in the x-axis) and seaward FB position = 18.0 m (in the x-axis). The grids we use for Delft3D-FLOW and Delft3D-WAVE start at $(X, Y) = [100, 100]$ m (see Figure 3.5) to avoid a warning message in Delft3D computation. Hence, we need to add the value of landward and seaward FB positions (x-axis) with a value of the starting point ($x = 100$ m). This gives us the coordinate positions of landward FB (X start - X end) = 116.5 m and seaward FB (X start - X end) = 118.0 m. The position of FB in the Y axis follows the width of the FLOW grid. Additionally, for the case

without SMFB, no transmission coefficient is required.

To summarize all the inputs for Delft3D-FLOW and Delft3D-WAVE, the table below presents the inputs for both modules. All parameters that are not described in the explanation and Table 3.2 remain default.

Table 3.2. Basic input for Delft3D-WAVE and Delft3D-FLOW in the first research phase

D3D	Parameter	Value	Unit
Flow	Simulation time	16	hrs
	Time step	0.0125	min
	Initial Water level	0	m
	Specific density	2650	kg/m ³
	Dry bed density	1600	kg/m ³
	Median sediment diameter (D_{50})	380	μm
	Initial sediment layer thickness	30	m
	Wave-related susp. load transport factor ($SusW$)	1.0	-
	Wave-related bed load transport factor ($BedW$)	1.0	-
	Sediment transport formulation	van Rijn (1993)	-
Wave	Significant wave height (H_s)	0.3	m
	Peak period (T_p)	1.8	s
	Direction (nautical)	90	°
	Directional spreading	0.01	-
	Spectral space: Gaussian (spreading)	0.01	-
	Transmission coefficient (represents FB)	0.10 - 0.90	
	Obstacle, landward FB (X start - X end)	[116.5 116.5]	m
	Obstacle, seaward FB (X start - X end)	[118.0 118.0]	m
Obstacle (Y start - Y end)	[100 106]	m	

Number of simulations in Delft3D

Following the experiment of Shimoda et al. (1991), one simulation without FB is performed (see Table 3.6 number 1). Hence, the model defines only wave conditions (wave height, wave period, and frequency) without transmission coefficient as a representation of an SMFB.

For the simulations with SMFB, 18 simulations are done. nine simulations are for analyzing the effects of landward SMFB, and the other nine are for seaward SMFB (see Figure 3.6). To clarify, numbers 2-10 in Table 3.6 are the simulations of the landward FB with different transmission coefficients from 0.1 to 0.9. Next, numbers 11-18 are the simulations with the seaward FB with different transmission coefficients ranging from 0.1 to 0.9.

Changing the model settings

In Delft3D, we do sensitivity analyses of the simulations presented in Table 3.3 by changing the basic input in Table 3.2. Changing the basic input is intended to avoid the sudden drop in the incident wave height and to obtain the best results of Delft3D in reproducing the cross-section observed in the laboratory. The adjustment of the basic settings is done by changing the value of several parameters presented in Table 3.2: directional spreading, Gaussian (spreading) in Delft3D-WAVE; wave-related suspended load transport factor ($SusW$), wave-related bed load transport factor ($BedW$), and sediment transport formulation in Delft3D-FLOW.

Table 3.3. Simulations for the first research phase

No	Simulations
1	Without SMFB, no transmission coefficient
2	With landward SMFB, transmission coefficient = 0.1
3	With landward SMFB, transmission coefficient = 0.2
4	With landward SMFB, transmission coefficient = 0.3
5	With landward SMFB, transmission coefficient = 0.4
6	With landward SMFB, transmission coefficient = 0.5
7	With landward SMFB, transmission coefficient = 0.6
8	With landward SMFB, transmission coefficient = 0.7
9	With landward SMFB, transmission coefficient = 0.8
10	With landward SMFB, transmission coefficient = 0.9
11	With seaward SMFB, transmission coefficient = 0.1
12	With seaward SMFB, transmission coefficient = 0.2
13	With seaward SMFB, transmission coefficient = 0.3
14	With seaward SMFB, transmission coefficient = 0.4
15	With seaward SMFB, transmission coefficient = 0.5
16	With seaward SMFB, transmission coefficient = 0.6
17	With seaward SMFB, transmission coefficient = 0.7
18	With seaward SMFB, transmission coefficient = 0.8
19	With seaward SMFB, transmission coefficient = 0.9

In Table 3.4, we see the adjustments of the basic settings. The first row in this table presents the initial setting that was introduced in Table 3.2. The next five model settings (settings 2 - 6) are considered to also perform the simulation no 1 (without SMFB) in Table 3.3. We only consider simulation no. 1 because it is first planned to compare the cross-section without SMFB with different model settings for obtaining the best-reproduced cross-section. Afterward, a preferred model setting is used for other simulations (no. 2 to 19 in Table 3.3).

Table 3.4. Different model settings in the first research phase for Delft3D-FLOW and Delft3D-WAVE

Model settings	Delft3D-WAVE			Delft3D-FLOW	
	Directional spreading	Gaussian (spreading)	SusW	BedW	Sediment formulation
1 (initial)	0.01	0.01	1.0	1.0	van Rijn (1993)
2	0.01	0.01	0.5	0.5	van Rijn (1993)
3	0.1	0.01	0.5	0.5	van Rijn (1993)
4	0.1	0.1	0.5	0.5	van Rijn (1993)
5	0.1	0.1	1.0	1.0	van Rijn (1993)
6	0.1	0.1	1.0	1.0	van Rijn (2007)

3.2.4 Post-processing and interpretation of Delft3D outcomes in the first research phase

After completing the simulations, the hydrodynamic and morphodynamic results are extracted and analyzed in relation to the research questions. MATLAB is utilized to export the results, offering flexibility in creating and customizing figures for result interpretation.

Post-processing and interpretation for research question 1A

In research question 1A, cross-sections without and with FB are extracted. The steps that are involved in answering research question 1A are:

1. From Delft3D results, extract the cross-shore profile without FB in different model settings presented in Table 3.4;
2. Compare the derived cross-shore profile from the previous step with the digitized cross-shore profile from the laboratory experiment (without FB) based on visual, error statistics (R^2 , Scatter Index (SCI), Relative Bias, Brier Skill Score), and area of erosion and sedimentation. See the second row of Table 3.5;
3. Consider the best-reproduced cross-section derived from Delft3D according to the comparison;
4. Use the model setting that results in the best cross-section to perform the simulations with SMFB (see simulation 2-19 in Table 3.3);
5. Repeat step 2 for the simulations with SMFB (see third and fourth rows in Table 3.5).

It is important to note that the explanations about the mentioned error statistics like formula and criteria which determines good or bad modelling outcomes are available in Appendix B.

Post-processing and interpretation for research question 1B

Research question 2B is answered by comparing the effects of FB on wave height explained by Shimoda et al. (1991) with the results retrieved from the simulations in Delft3D. Since Shimoda et al. (1991) only reported that:

- Steep incident wave was attenuated by the FB,
- With increasing FB dimension and decreasing draft (distance of the water surface to the top of the submerged FB), the wave attenuating capacity of FB became larger.

Thus, we assess whether the transmission coefficient attenuates the wave height. Furthermore, we also check different transmission coefficients to understand how they affect the attenuating capacity. The post-processing for the comparison is executed by extracting the wave height without FB (simulation no. 1 in Table 3.3), also the wave height with landward FB and seaward FB. For the wave height with landward and seaward FB, only the simulations with the transmission coefficient of 0.1, 0.5, and 0.9 are extracted. This is done because we assumed that it is not necessary to include all C_t to understand the effects of different C_t .

Post-processing and interpretation for research question 1C

In research question 1C we compare the sediment transport that occurred in the laboratory experiment with the results of the model. The key points that were elaborated by Shimoda et al. (1991) are:

- the attenuated wave due to FB encouraged onshore sediment transport,
- material landward of the FB was suspended by wave-breaking.

To confirm this statement based on the Delft3D results, the bed load and suspended load transport are extracted. The extracted bed and suspended load transport are from the simulations without FB intervention (see Table 3.3) with the preferred setting and those with FB interventions possessing the transmission coefficients of 0.10, 0.50, 0.90 also with the selected setting.

Table 3.5. Data/information from the experiment and numerical model used to answer the research questions in the first phase, identity number of a simulation can be seen in Table 3.3

RQ	Description	Lab. experiment (Shimoda)	Numerical model D3D
1A	Compare the cross-shore profile without SMFB	Digitized profile in Figure	Output of simulation 1 (bed level)
	Compare the cross-shore profile landward SMFB	Digitized profile in Figure	Output of simulation 2-10 (bed level)
	Compare the cross-shore profile seaward SMFB	Digitized profile in Figure	Output of simulation 11-19 (bed level)
1B	Compare the wave height	Explanation of effects of FB on wave height	Effect of Ct (represents FB) on wave height
1C	Compare the sediment transport	Explanation of effects of FB on sediment transport	Effect of Ct (represents FB) on sediment transport

3.3 Second research phase: floating breakwater's effects at intertidal flats

This section explains the methodology for undertaking the second research phase. For this phase, we do sensitivity analyses of the FB effects under different conditions: intertidal flat slopes-channel slopes, wave conditions (wave height and wave period), and FB locations (water depth below FB). Before delving into the specific method for conducting the second research phase, we provide an introduction in Section 3.3.1 that explains the location from which the data inspiration is derived, as well as the rationale behind selecting that particular location. Following that, the explanation regarding data derivation is elaborated in Section 3.3.2. After the data derivation, not all gathered data can be utilized directly as Delft3D input. Hence, Section 3.3.3 presents the explanations of the derived data that require pre-processing before they can be used as input in Delft3D. Then, the next section discusses the model settings in Delft3D for the second research phase (Section 3.3.4). Afterward, the post-processing of the modeling outcomes to address the second research phase is explained in Section 3.3.5.

3.3.1 Data insight: The Eastern Scheldt

As our aim is to analyze the FB effects at intertidal flats, the Eastern Scheldt is selected as a location to inspire data derivation. The motivation for choosing the Eastern Scheldt is due to erosion at the intertidal flats, which is driven by wind-generated waves (Eelkema, 2013), thus potentially can be protected by the FB (Biesheuvel, 2013). Another reason is that the Eastern Scheldt has a channel-shoal (intertidal area) interaction (Eelkema, 2013), which indicates that the locations near the shoal (intertidal flats) are presumably deeper, hence more effective for implementing the FB (Biesheuvel, 2013). Furthermore, to see the depth of the channel surrounding the intertidal flats in the Eastern Scheldt, Figure 3.7 is provided.

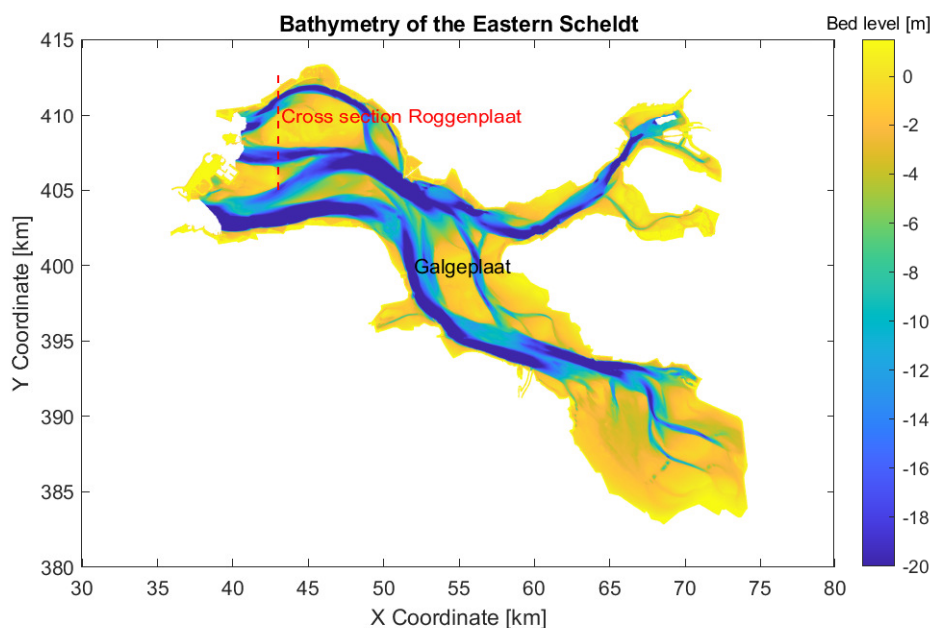


Figure 3.7. Bathymetry of the Eastern Scheldt, the land with the red dashed line above indicates the location of Roggenplaat. Another land on the lower right indicates the location of the Galgeplaat; *Vaklodingen* data set by Rijkswaterstaat

From Figure 3.7, it can be seen that the Eastern Scheldt has a bathymetry with a maximum depth of around -20 m around the Roggenplaat (see Figure 3.7). This again suggests that the floating breakwater could be applied. Regarding this, Zanuttigh and Nicholls (2015) stated that in deep water depths greater than 6 m, traditional breakwaters are often more expensive than floating ones. This highlights the suitability of the Eastern Scheldt as a potential location for implementing floating breakwaters and emphasizes that the Eastern Scheldt is suitable for obtaining relevant data insights. In addition, to represent the condition of intertidal flats in the Eastern Scheldt, we mostly use the Roggenplaat and Galgeplaat, the two largest intertidal shoal in the Eastern Scheldt.

3.3.2 Data derivation for the second research phase

To answer the second research question, we have gathered data that are used for Delft3D modeling. The data consist of intertidal area slope, channel slope, wave conditions, and specification of FB (depth below FB, width of FB, draft of FB). Before presenting the data, explanations of metadata are provided. The explanation of metadata relates to the measurement method, the unit of measurement, spatial resolution (if any), data sources, pre-processing steps that were done beforehand (how the data was created), and documentation (creation date, version, ownership).

Intertidal area slopes/shoal's slopes (S_s)

The intertidal area slopes are derived using *Vaklodigen* data containing the bathymetry of Roggenplaat and Galgeplaat, the intertidal flats in the Eastern Scheldt (de Vet et al., 2018). The information originates from Rijkswaterstaat and was made available in 2021. The dataset merges measurements taken along 100/200-meter transects using single beam technology with GPS Real-Time Kinematic (RTK) measurements performed on the tidal flats. Before the introduction of GPS RTK, less advanced leveling methods were used. Starting from 2001, the elevated sections of the intertidal area have been surveyed using the Light Detection and Ranging (LiDAR) method. (de Vet et al., 2017).

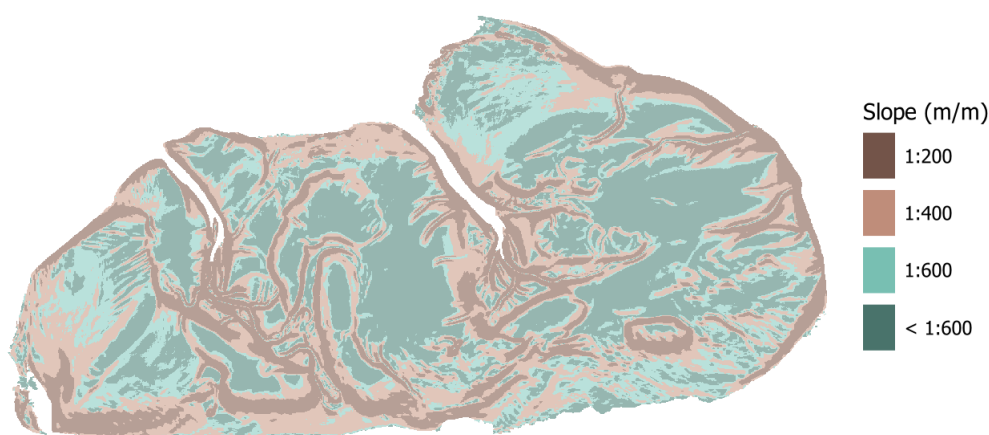


Figure 3.8. Slope of the Roggenplaat based on the elevation between -1.5 to 1.5 m, derived using QGIS from *Vaklodigen* data set by Rijkswaterstaat

To obtain the slopes of the intertidal flat, the raster data that contains topography/bathymetry was processed in a GIS software called QGIS. Before the QGIS processing, the gaps or missing values within the raster are filled using the internal diffusion feature in QUICKIN, a built-in feature in Delft3D. This was done to ensure that there was no gap in the raster data. Next, data smoothing was also done

after filling the gaps within the raster (topography). Finally, the analysis can be executed in QGIS by utilizing the Raster Terrain Analysis with a feature called slope to obtain intertidal flat/shoal's slope. To see the variations of slopes of Roggenplaat, Figure 3.8 is provided.

According to Figure 3.8, it is seen that the slopes on the Roggenplaat are distinguished from 1:200, 1:400, and 1:600. Those are the slopes that are used for the data analysis. In this case, we do not include a slope smaller than 1:600 for further steps. This is because, arguably, employing the 1:200, 1:400, and 1:600 slopes already covers most of the Roggenplaat and Galgeplaat (intertidal flats). For the slope map of the Galgeplaat, we presented it in Appendix B.

Channel slope (S_c)

The channel slope is derived using the same data described previously for deriving the intertidal area/shoal slope. The difference is that we take the cross-sections from this data (raster of *Vaklodingen*) to extract the channel slope. 14 cross-sections of Roggenplaat are taken to derive the channel slope by computing the gradient of two points from the surface of the flats to the bottom of the channel (see an example: red dashed line, in Figure 3.9). The channel slope data variation was generated by calculating the average slope of 14 cross-sections, the averaged slope minus standard deviation to obtain the smallest slope, and the average plus standard deviation to get the maximum slope. From these calculations, three slope variations are derived. The values of the slopes are provided in Table 3.6.

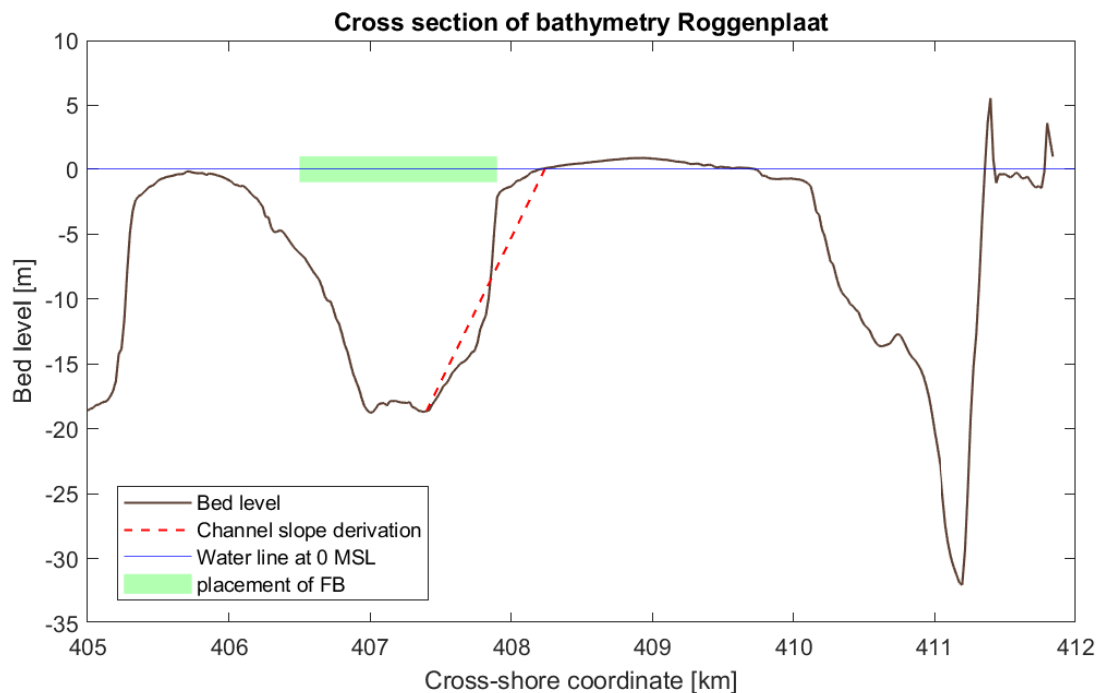


Figure 3.9. Example of cross-section of the Roggenplaat, taken according to the red dashed line presented in Figure 3.7.

Wave height (H_0), wave period (T_p) and wave direction (θ_w)

Wave height and wave period are derived using a wave growth nomogram by Breugem and Holthuijsen (2007); Anonymous (2020). This wave nomogram needs the fetch and wind speed to approximate the wave height and wave period. The fetch is calculated by measuring the distance from the edge of intertidal flats: Roggenplaat and Galgeplaat, to the edge of the land. The direction of the fetch follows

the dominant direction of the wind. When discussing wind speed, we consider the wind speed in the wind rose for the STAV and ZBWI stations (see Section B4 in [Appendix B](#)). Specifically, we focus on wind speeds of 5.0 m/s, 7.5 m/s, 10.0 m/s, 12.5 m/s, 15 m/s, 17.5 m/s, and 20 m/s. These values were considered because they were depicted in the wind rose. Therefore, we use them for generating the values of wave height and wave period.

After determining the fetch and wind speed, the wave height and wave period are derived using the nomogram ([Breugem & Holthuijsen, 2007](#); [Anonymous, 2020](#)), see also [Appendix B](#). Based on the derivation of the wave height and wave period, we selected the wave heights and wave periods that were in the range of the wave roses showing the wave height and wave period in the Eastern Scheldt, near the Roggenplaat. These wave roses showed the variation of wave height and wave period magnitudes near the Roggenplaat from 1 January 2015 to 31 December 2022 (see Section B4 in [Appendix B](#)). By considering the magnitude of wave heights and wave periods shown in the wave roses, the wave heights and wave periods associated with wind speed (and fetch) of 10.0 m/s (2 km), 15.0 m/s (3 km), 17.5 m/s (6 km), and 20 m/s (10 km) were chosen for the data simulations. These wind speeds and fetch also correspond to wave conditions 1 to 4 in [Table 3.6](#). To add, the selected wind speeds are also associated with different probabilities of occurrence. The wind speed of 10 m/s has a probability of occurrence (P) of 5.5%, 15 m/s (P = 0.49%), 17.5 m/s (P = 0.15%), 20 m/s (P = 0.043%). Further explanation about the probabilities is available in [Appendix B](#).

Regarding wave angle, although the prevailing wind direction in the Eastern Scheldt is to the north-east ([van der Werf et al., 2019](#)), we are simplifying our analysis by concentrating on north-directed waves (normal incident waves) for better alignment with our chosen model (1D). Furthermore, the oblique incident wave might reduce the transmission coefficient of FB ([Biesheuvel, 2013](#)), making the calculated transmission coefficient in this research phase presumably inaccurate. Thereby, without adding the complexity (i.e., considering oblique waves), it is hoped that the essential physics and behavior of the results are still valuable to be understood. Also, this consideration reduces the complexity of the modeling process. Hence, we prescribe a wave angle of 90° in the current study.

For a more detailed explanation of wave data, [Appendix B](#) also provides more elaboration on wave data derivation, which relates to fetch measurement, the mentioned wind roses, reading nomogram, all derived and selected waves, and the mentioned wave roses.

Water depth at the location of FB (h_{fb})

The water depth at the location of FB is planned according to the possible depth of the water near the intertidal flats in the Eastern Scheldt. Therefore, the water depth at the location of FB can be planned around 5 to 20 meters relative to 0 NAP (Dutch vertical datum close to mean sea level). As seen in [Figure 3.7](#), a maximum depth of around 20 m can be reached based on *Vaklodingen* data set. To clarify the consideration about the water depth at the location FB, [Figure 3.9](#) presents the schematization of the FB position. Illustration of the FB is depicted in [Figure 3.10](#).

Width of FB (B_f) and Draft of FB (D_f)

For the width and draft of FB, we refer to a specification of pontoon FB from SF Marina possessing one of the biggest widths in the market ([SF-Marina, 2022](#)). This potentially could perform well (small transmission coefficient) in attenuating the incoming waves to the intertidal flats. The selected FB width and draft are based on the specification of the pontoon FB by SF Marina with the type of SFBW800/3,0 ([clickable link](#)). This FB has a width of 8.00 m, height of 3.00 m, and freeboard of 0.80 m. With the mentioned height and freeboard, the draft is 2.20 m (See [Figure 3.10](#) for illustration). It is important to note that the determined dimensions are used to calculate the transmission coefficient. In the

numerical model Delft3D, we only input a value representing the effectiveness of the FB (transmission coefficient).

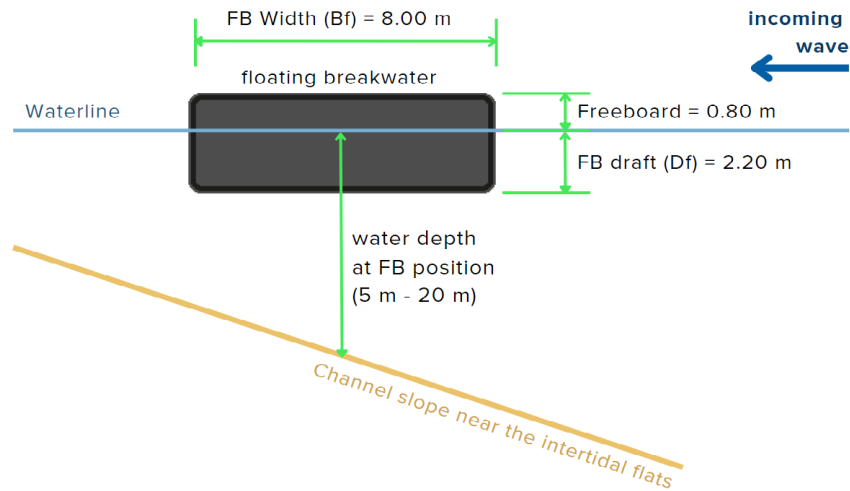


Figure 3.10. Determined dimension of the FB to calculate the transmission coefficients as input of Delft3D in the second research phase

Sediment diameter (D_{50})

Sediment diameter is also defined by referring to the median sediment diameter (D_{50}) that was reported by [Eelkema \(2013\)](#). In light of this, [Eelkema \(2013\)](#) reported that from data on sediment grain size diameters of the Dutch continental shelf (Geological Survey of the Netherlands, 2007), it is known that the median grain size has a spatial variability. For the shoal (intertidal flats), it is approximately $\approx 150 \mu m$.

After all data derivation is done, the derived data is presented in [Table 3.6](#). The variations for each data are also presented in that table. This number of variations for each data determines the number of unique combinations for the simulation in Delft3D.

Table 3.6. Data for undertaking the second research phase

No.	Data	Unit	Variation	No. of var.
1	Intertidal flats slope (S_s)	m/m	[1/200 1/400 1/600]	3
2	Channel slope (S_c)	m/m	[1/15 1/25 1/55]	3
3	<u>Wave conditions</u>		1) $H_0 = 0.40$; $T_p = 1.7$; $\theta_w = \text{normal (90)}$	4
	Wave height (H_0)	m	2) $H_0 = 0.60$; $T_p = 2.3$; $\theta_w = \text{normal (90)}$	
	Wave period (T_p)	s	3) $H_0 = 1.20$; $T_p = 3.0$; $\theta_w = \text{normal (90)}$	
	Wave angle (θ_w)	$^\circ$	4) $H_0 = 1.80$; $T_p = 3.8$; $\theta_w = \text{normal (90)}$	
4	Depth at FB loc. (h_{fb})	m	[5.00 10.00 15.00 20.00]	4
5	Width of FB (B_f)	m	[8.00]	1
6	Draft of FB (D_f)	m	[2.20]	1
7	Sediment diameter (D_{50})	μm	[150]	1
Total simulations with FB				144
Total simulations without FB (9 slopes x 4 wave conditions)				36
Total simulations				180

3.3.3 Derived data for Delft3D input in the second research phase

Not all derived data can be directly used as input in Delft3D. Hence, pre-processing is needed. This section discusses pre-processing for intertidal area slope, channel slope, and relevant parameters in Table 3.6 to calculate the transmission coefficient.

Intertidal flats/shoal slope and channel slope for grid and bathymetry input in Delft3D

Intertidal flats slope and channel slopes are used to establish bathymetry that schematizes the condition of intertidal flats. Considering the grid effects that we explain in Section 3.2.3 (Delft3D setting in the first research phase) under discussion about grid and bathymetry, the WAVE grid should be sufficiently wide. Therefore, we generate the WAVE grid with a width 3 times greater than the length. So, for instance, the WAVE grid with a length of 1400 m ($S_s = 1:200$, $S_c = 1:15$) is considered to have a WAVE grid with a width of 4200 m. Important to note, the grid lengths are different with different S_s and S_c . We can calculate by using the formula below (applicable to both FLOW and WAVE grid):

$$Grid\ length\ (L_g) = \left(3 \times \frac{1}{S_s}\right) + \left(20 \times \frac{1}{S_c}\right) + 500 \quad (10)$$

S_s is the intertidal flat slope, S_c is the channel slope, 3 (in meter) represents the differences of elevation at intertidal flats in m, 20 (in meter) represents the differences between the shoal's edge and bottom of the channel, and 500 represents the additional length in m.

Next, for the grid resolution, we make the grid coarser close to the open boundary or near incoming waves and finer near the intertidal flats (see Figure 3.11). Furthermore, with different channel and intertidal area slope combinations, the WAVE and FLOW grids have different resolutions. The grid sizes range from 2.7 to 66.7 m for the WAVE grid and from 3.6 to 47.5 m for the FLOW grid, covering a range of sizes from small to large. These grids were considered to obtain the balance between the permissible Courant Number < 10, (with the defined time step, 0.05 minutes) and finer grid resolution, especially near the intertidal flats.

Regarding bathymetry, as stated by Eelkema (2013), the Eastern Scheldt consists of channel-shoal interaction, which was also visualized in Figure 3.9. Regarding this, nine bathymetries that resemble channel-shoal interaction are made using the derived channel slopes and intertidal area (shoal) slopes. Nine bathymetries are considered from the channel slopes and intertidal area slope variation (see Table 3.6, which gives 9 possible combinations). Three different elevations are considered for this establishment: +1.5 m NAP (*Normaal Amsterdams Peil*) as the maximum, -1.5 m NAP as the minimum elevation of the Roggenplaats, and -21.5 NAP for the maximum depth of the channel. Figure 3.12 presents the generated bathymetries from the nine slopes. These bathymetries are used for the input in Delft3D. Important to mention that in Figure 3.12, we visualize the bathymetry only in cross-sectional view because we also consider a uniform alongshore bathymetry associated with the grid (see Figure 3.11). Related to this, we consider only extracting all results in a cross-sectional view instead of a plan view.

Water depth at the FB location

In addition to specifying the water depth below the floating breakwater (FB) provided in Table 3.6, it is necessary to determine the cross-shore distance of the FB. This distance corresponds to the planned water depth at FB position (h_{fb}) and varies depending on the channel slopes and intertidal area (shoal) slopes. It is important to mention that 100 m is added to the calculated distance considering the starting

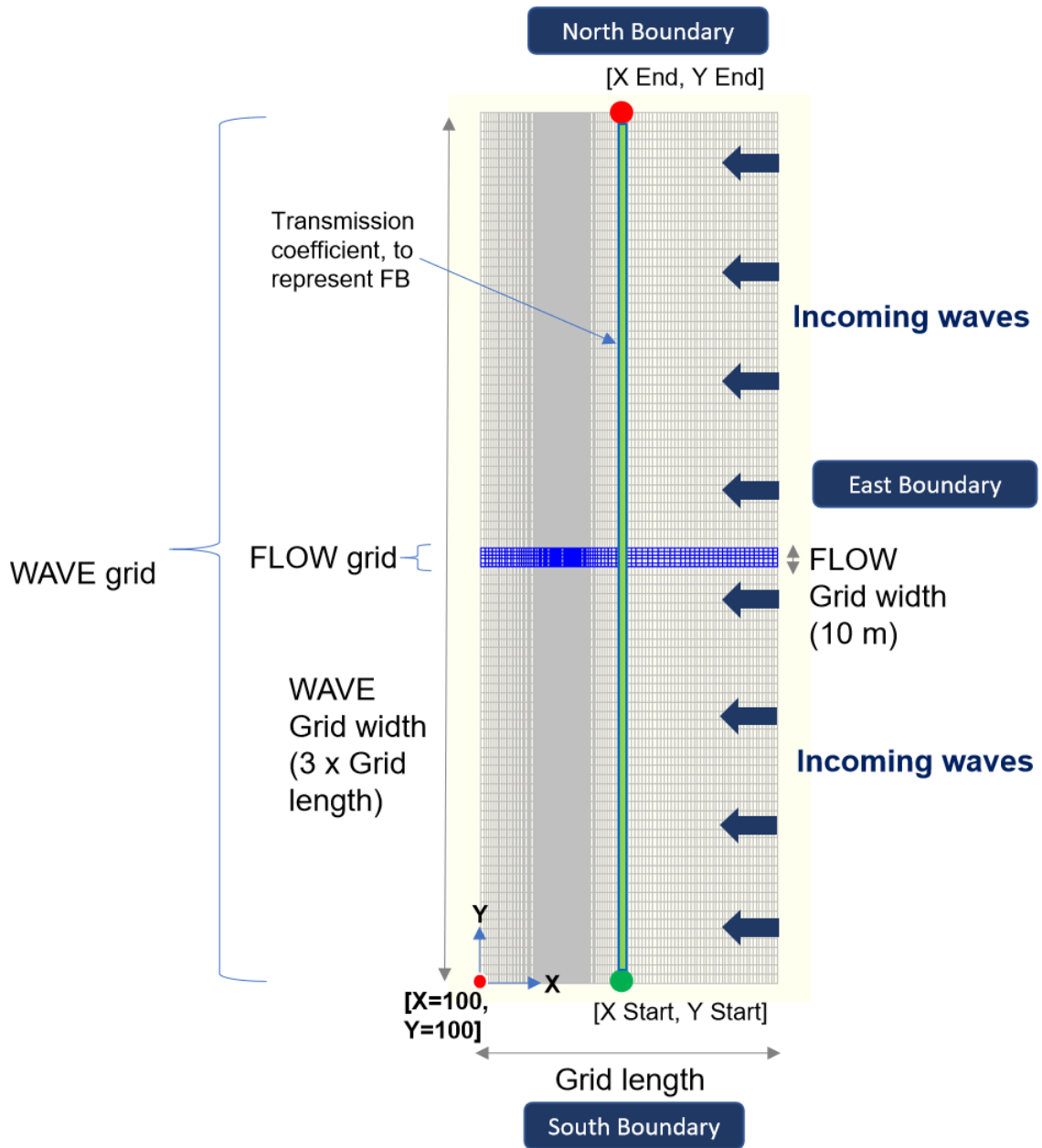


Figure 3.11. FLOW and WAVE grid for the second research phase; the alongshore green line in WAVE-grid visualizes the position of the specified transmission coefficients which can vary depending on the water depth below FB; a red dot with the X, Y coordinates represent the position and values of the reference point

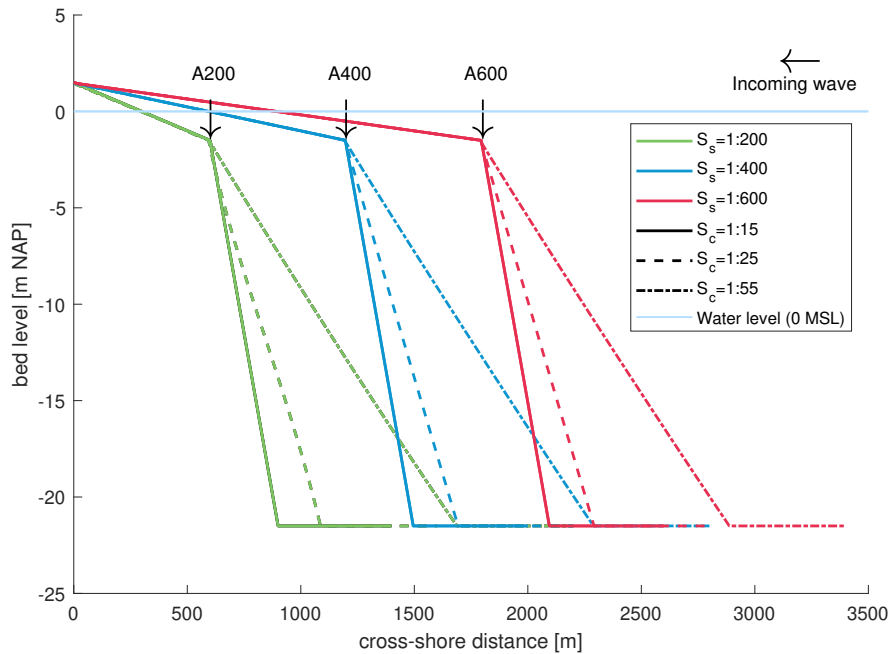


Figure 3.12. Schematized bathymetry of the intertidal flats; point A200, A400, and A600 indicate the channel edge for different intertidal area slope. These points are used for the observation points in the results phase

point of the reference coordinate in the WAVE grid (see Figure 3.11). To see the cross-shore distance at which the FB is located, Table 3.7 is provided. When seeing Figure 3.12, the distance provided in Table 3.7 should be subtracted by 100 m (to normalize/remove the reference distance prescribed in WAVE grid). Moreover, It is important to mention that the cross-shore distances of FB provided in Table 3.7 are actually the inputs of X Start and X End in Delft3D represented by Figure 3.11.

Table 3.7. Placement of FB at the schematized intertidal flats bathymetry in Figure 3.12; the position of the FB in this table is relative to the reference specified in WAVE grid, see Figure 3.11

Slope variations	Cross-shore distance FB + WAVE grid reference (100 m)			
	[m]			
	$h_{fb}=5\text{ m}$	$h_{fb}=10\text{ m}$	$h_{fb}=15\text{ m}$	$h_{fb}=20\text{ m}$
$S_s = 1:200\ S_c = 1:15$	752.5	827.5	902.5	977.5
$S_s = 1:200\ S_c = 1:25$	787.5	912.5	1037.5	1162.5
$S_s = 1:200\ S_c = 1:55$	892.5	1167.5	1442.5	1717.5
$S_s = 1:400\ S_c = 1:15$	1352.5	1427.5	1502.5	1577.5
$S_s = 1:400\ S_c = 1:25$	1387.5	1512.5	1637.5	1762.5
$S_s = 1:400\ S_c = 1:55$	1492.5	1767.5	2042.5	2317.5
$S_s = 1:600\ S_c = 1:15$	1952.5	2027.5	2102.5	2177.5
$S_s = 1:600\ S_c = 1:25$	1987.5	2112.5	2237.5	2362.5
$S_s = 1:600\ S_c = 1:55$	2092.5	2367.5	2642.5	2917.5

Data to calculate the transmission coefficient of FB

The transmission coefficient (C_t) input in Delft3D represents the floating breakwater. The input of C_t is obtained by calculating the value of the transmission coefficient using Equation 2 (Macagno relation), with the data provided in Table 3.6. The calculation of the transmission coefficient employs the following steps:

1. Calculation of wavelength in the deep water (L_0) with an input of wave period (T_p) for all wave conditions in Table 3.6 using Equation 5. With 4 wave conditions, we have 4 wavelengths in the deep water (L_0)
2. Calculation of wavelength (L) with the inputs from the calculated wavelengths in the deep water (L_0) and four different water depths at FB location (h_{fb}) using Equation 4. Here, we have 16 different wavelengths (L) due to 4 different wave conditions and 4 water different water depths below FB.
3. Calculation of wave number (k) with the inputs from 16 different wavelengths (L) using Equation 3.
4. Calculation of the transmission coefficient (C_t) with the inputs of four parameters such as the calculated wave number (k), the width of FB (B_f), water depth (h): represented by the corresponding water depth below FB (h_{fb}) and the draft of FB (D_f). The C_t calculation is performed using the Macagno relation, which is revisited below.

$$C_t = \frac{1}{\sqrt{1 + \left[\frac{kB_f \sinh(kh)}{2 \cosh(kh - kD_f)} \right]^2}} \quad (2 \text{ revisited})$$

By knowing the transmission coefficient for different wave conditions and water depth below FB, we can already answer research question 2A (read Section 1.4) and use the transmission coefficients as the inputs in Delft3D to represent FB.

3.3.4 Delft3D settings in the second research phase

Delft3D-FLOW

In Delft3D-FLOW, parameters are specified, including grid properties, bathymetry, simulation duration, time step, water level, sediment diameter (D_{50}), and sediment thickness. The FLOW grid has a smaller width, in this case, 10 m, with the grid length adaptable following the combination of intertidal area slope and channel slope. The simulation duration is specified as 24 hours with 12 hours of spin-up time and 12 hours running with morphology. The specified duration of 12 hours is intended to be roughly double the length of the typical storm period, which is 6-8 hours (Bosboom & Stive, 2021). A time step of 0.05 minutes is defined for all simulations to have a Courant Number below 10 for model stability (Deltares, 2022). Next, there is no variation in water level, so it is specified at 0 m MSL (see Figure 3.7). The sediment thickness is defined as 30 m to ensure a sufficiently large erodible layer.

Delft3D-WAVE

The wave conditions are applied on three different boundary orientations: East, North, and South. A Gaussian shape is employed with a spreading factor of 0.1 for the wave spectral space to minimize variations in wave conditions during a storm. This approach considers the relatively constant mean wind speeds that occur during storms (Bosboom & Stive, 2021). Next, we set the white capping to

be off; this is done to ensure that the wave height does not decline once it propagates from the open boundary (further explanation about this is available in [Appendix C](#)). Then, for the FB, the calculated transmission coefficients resulting from the steps explained in Section 3.3.3 are used. The positions of the FB (corresponding to water depths) are defined based on Table 3.7. The explanation of how the FB is located in the grid can be viewed in Figure 3.11.

Next, Table 3.8 is provided to summarize the settings in Delft3D-FLOW and Delft3D-WAVE. This basic setting is applied for running all 180 unique simulations in the second research phase. Furthermore, FB position and transmission coefficient are not inputted in the simulation when running the simulations without FB.

Table 3.8. Basic input for Delft3D-WAVE and Delft3D-FLOW in the second phase

D3D	Parameter	Value	Unit
Flow	Simulation time	24	hrs
	Time step	0.05	min
	Water level	0	m
	Specific density	2650	kg/m ³
	Dry bed density	1600	kg/m ³
	Median sedimen diameter (D_{50})	150	μm
	Initial sediment layer thickness	30	m
	Multiplication factor for susp. sed. (Sus)	1.0	-
	Multiplication factor for bed load (Bed)	1.0	-
	Wave-related susp. load transport factor ($SusW$)	1.0	-
	Wave-related bed load transport factor ($BedW$)	1.0	-
	Sediment transport formulation	van Rijn (1993)	-
	Wave	Significant wave height (H_s)	see Table 3.6
Peak period (T_p)		see Table 3.6	s
Direction (nautical)		see Table 3.6	°
Directional spreading		0.1	-
Spectral space: gauss (spreading)		0.1	-
Whitecapping		off	-
Transmission coefficient (represents FB)		from calculation	
FB position (X start - X end), the same X values		see Table 3.7	m
FB position (Y start- Y end)	[100, $3L_g+100$]	m	

3.3.5 Post-processing and interpretation in the second research phase

Research question 2A

The goal of this sub-research is to compare transmission coefficients under various wave conditions and water depths at FB points. To achieve this, the results of the calculation of transmission coefficient outlined in Section 3.3.3 are organized and grouped based on two main factors: the water depths at the FB positions and the specific wave conditions.

Based on the categorized transmission coefficients, a figure and a table exhibit the transmission coefficients associated with different wave conditions within varying water depths at the FB positions are established. The established figure visualizes how the transmission coefficients change in those varying conditions. Meanwhile, the table emphasizes how the transmission coefficients vary in more detail.

By answering the sub-research question 2A, we could draw a hypothesis about how FB affects hydrodynamic parameters (especially wave height) in different wave conditions. Also, how different water depths at FB points influence the effectiveness of FB intervention in affecting these hydrodynamic parameters.

Research question 2B

In the figure below, we present the data used for interpretation (column 1), the calculation or the process carried out (column 2) before creating visualizations or tables (column 3), and the type of visualization or table (column 4). The icons on the header represent the software used for that step. Next, small circles on the third column indicate the data used based on the first column.












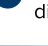









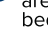





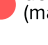

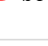



 Delft3D output or calculation	 Additional process	 Products for results chapter	Type
(D3D) Wave height	-	 Wave height propagation on one channel and intertidal area slopes	
(D3D) Initial bed level	Take H1 based on shoal edge points and sort based on initial wave conditions, FB/ no FB	 Effects of FB under different wave conditions on the transmitted wave height H1	
	Take H1 (with FB) based on shoal edge points and sort based water depths at FB, FB/no FB	 Effects of FB with different water depths at FB positions on the transmitted wave height H1	
	Take H1 based on shoal edge points and sort based on channel slopes and FB/no FB	 Effects of FB with different channel slopes on the transmitted wave height H1	
	-	 Propagation of wave height on different intertidal area slopes	
(D3D) Near-bed orbital vel		 Profile of near-bed orbital velocity on one channel and intertidal area slopes	
(D3D)Initial bed level	Calculate mean near-ned orbital velocity and sort based on wave conditions, FB/no FB	 Effects of FB under different wave conditions on the averaged near-bed orbital velocity	
	Calculate mean near-ned orbital velocity and sort based on H0 & water depths at FB positions	 Effects of FB with different water depths at FB positions on the averaged near-bed orbital velocity	
	Calculate mean near-ned orbital velocity and sort based on H0 & channel slopes	 Effects of FB with different channel slopes on the averaged near-bed orbital velocity	
	Calculate mean near-ned orbital velocity and sort based on H0 & intertidal area slopes	 Effects of FB with different intertidal area slopes on the averaged near-bed orbital velocity	
(D3D) Max. bed shear s.		 Profile of (maximum) bed shear stress on one channel and intertidal area slopes	
(D3D) Initial bed level	Calculate mean bed sher stress and sort based on wave conditions, FB/no FB	 Effects of FB under different wave conditions on the averaged (maximum) bed shear stress	
(Cal) Critical bed shear s.	Calculate mean bed shear stress and sort based on H0 & water depths at FB positions	 Effects of FB with different water depths at FB positions on the mean (maximum) bed shear stress	
	Calculate mean bed shear stress and sort based on H0 & channel slopes	 Effects of FB with different channel slopes on on the mean (maximum) bed shear stress	
	Calculate mean bed shear stress and sort based on H0 & intertidal area slopes	 Effects of FB with different intertidal area slopes on the mean (maximum) bed shear stress	

Figure 3.13. Post-processing for hydrodynamic parameters

Research question 2C

The process for post-processing of morphodynamic parameters is more or less the same as hydrodynamic parameters. Outputs from Delft3D (first column) are imported into MATLAB, then depending on the interpretation, additional processes are carried out (second column). The processes result in the products to be presented in the results chapter (third column) with the corresponding data type (fourth column).


























 Delft3D output	 Additional process	 Products for results chapter	Type
Bed load transport	-	 Bed load and suspended load transport on one channel and one intertidal area slopes	
Suspended load transport	-	 Direction of bed load and suspended load transport without and with FB on one channel and shoal slope	
Initial bed level			
Direction of bed load	Calculate mean bed /suspended load and sort based on initial wave conditions, FB/ no FB	 Effects of FB under different wave conditions on bed load and suspended load transport	
Direction of suspended load	Calculate mean bed /suspended load and sort based on H0 & water depths at FB positions	 Effects of FB with different water depths at FB positions on bed load and suspended load transport	
	Calculate mean bed load /suspended load and sort based on H0 & channel slopes	 Effects of FB with different channel slopes on bed load and suspended load transport	
	Calculate mean bed load /suspended load and sort based on H0 & intertidal area slopes	 Effects of FB with different intertidal area slopes on bed load and suspended load transport	
Cumulative erosion/sedimentation	-	 Cumulative erosion and sedimentation on one channel and intertidal area slopes	
Initial bed level	Calculate area of erosion and sort based on initial wave conditions, FB/ no FB	 Effects of FB under different wave conditions on the cross-sectional area of erosion	
	Calculate area of erosion and sort based on water depths at FB, FB/no FB	 Effects of FB with different water depths at FB positions on the cross-sectional area of erosion	
	Calculate area of erosion and sort based on channel slopes and FB/no FB	 Effects of FB with different channel slopes on the cross-sectional area of erosion	
	Calculate area of erosion and sort based on intertidal area slopes and FB/no FB	 Effects of FB with different intertidal area slopes on the cross-sectional area of erosion	

Figure 3.14. Post-processing for morphodynamic parameters

Research question 2D

To answer this sub-research question, no more data analysis is carried out. Answering this sub-research question is done by relating the results of sub-questions 2A, 2B and 2C. Relating the results helps to connect the dots between variations in transmission, hydrodynamic, and morphodynamics and how the FB influences this variation collectively based on the explorations that were done in the previous research steps. Hence, we directly put the answer to research question 2D in the conclusions.

4 Results: comparison of experiment and numerical model Delft3D

This section provides explanations regarding the results of Delft3D that are compared with the experiment. Here, the explanation of each section follows the order of the first research question. We first discuss the cross-section resulting from Delft3D outcomes and the experiment by Shimoda et al. (1991). After the cross-sections are compared, the hydrodynamic and morphodynamic parameters are discussed in the next sections. Corresponding to research question 1B, we intend to compare the hydrodynamic effects due to FB. We only refer to hydrodynamic parameters that were explained by Shimoda et al. (1991) for comparing the results with Delft3D outcomes (wave height and total wave energy). After that, research question 1C is explained in Section 4.3. This section (Section 4.3) provides explanations about the differences in terms of morphodynamic parameters explained by Shimoda et al. (1991) and results yielded from Delft3D.

4.1 Comparison of the cross-shore profiles from the experiment and numerical model Delft3D

To compare the cross-sections without and with FB resulting from the experiment and numerical model Delft3D, we derived the cross-sections from Shimoda by unscaling the cross-sections depicted in Figure 3.3. The cross-section from the experiment by Shimoda et al. (1991) can be seen in Figure 4.1.

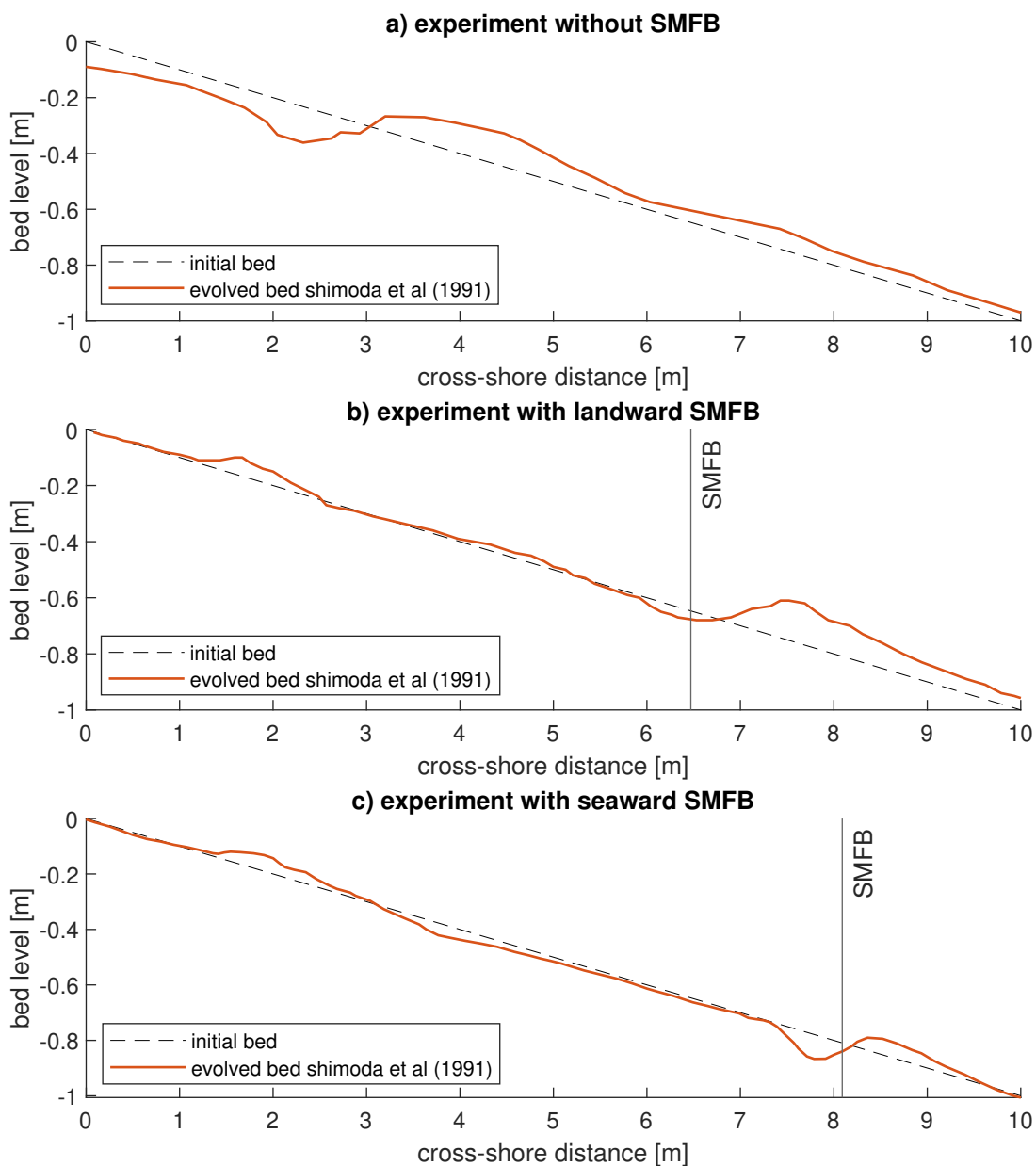


Figure 4.1. Derived bed evolution with the calculated $H_0 = 0.30$ m and $L_0 = 5.05$ m using linear wave theory equation; (a) the evolved bed profile without SMFB (b) the evolved bed profile with landward SMFB (c) the evolved bed profile with seaward SMFB; adapted from Shimoda et al. (1991)

4.1.1 Cross-shore profile without FB

Visual comparison

Figure 4.2 shows the evolved cross-section from the experiment under a condition of without SMFB together with the cross-section from Delft3D under the same condition (without SMFB). Here, we select the cross-shore profile derived from the simulation with the altered basic setting (see Table 3.2) according to model setting 4 (see Table 3.4). This is selected because this setting exhibits the best performance compared to other settings (see the explanation about model skill performance on the next page and see Table 4.1).

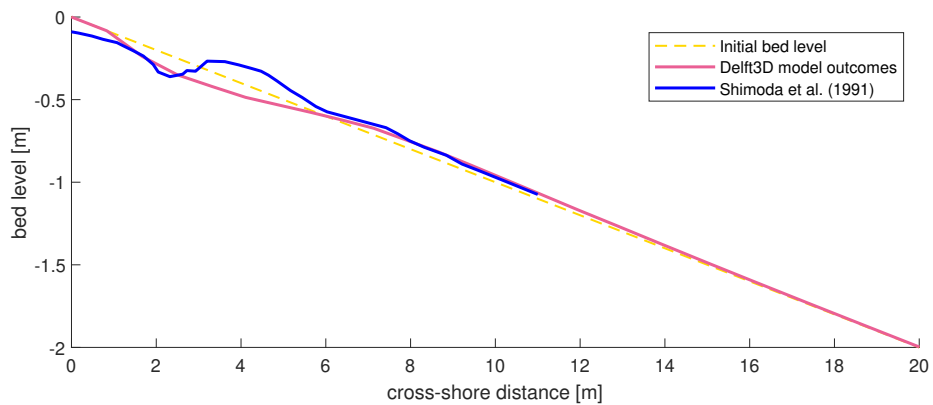


Figure 4.2. Cross-section derived from Delft3D model and laboratory experiment; The cross-section from Delft3D model is derived from the simulation with model setting 4 (see Table 3.4)

Figure 4.2 shows that erosion occurs at different ranges for the experiment and numerical model results. One from the experiment exhibits a smaller range of erosion, whereas the Delft3D outcome presents a greater range of erosion. Furthermore, to better see the differences where the erosion and sedimentation occurred for both simulations without SMFB in the experiment and Delft3D, we also provide a normalized bed level (cumulative erosion and sedimentation), where the initial bed level subtracts the evolved cross-shore profile from Delft3D outcome and the experiment.

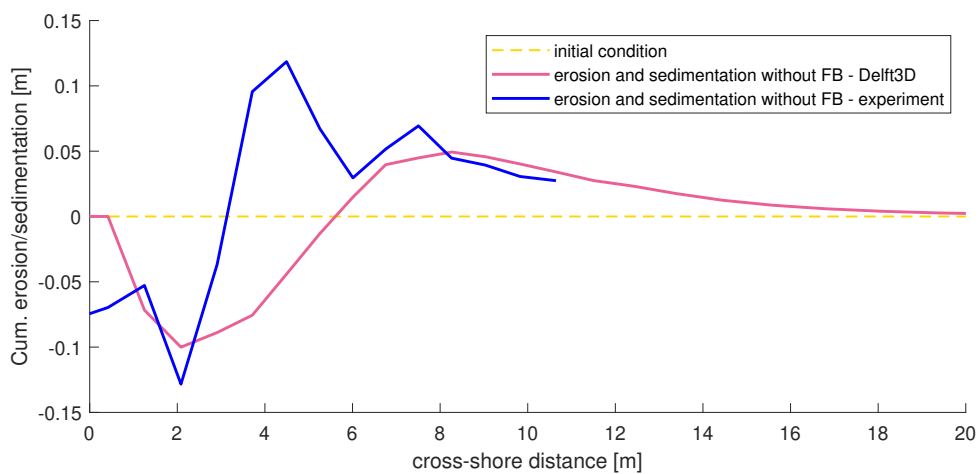


Figure 4.3. Cumulative erosion and sedimentation without SMFB from the Delft3D outcome and experiment, derived from the simulation with model setting 4 (see Table 3.4)

From Figure 4.3, it is noticeable that more or less the depths of erosion between the one exported from Delft3D and experiment are similar. Nevertheless, this figure emphasizes that the erosion from the experiment has a minimum range (0 to 3 m). This differs from the erosion resulting from the Delft3D result, which has a wider erosion range (around 0 to 5 m).

Regarding the reasons for the occurring erosion in those specific locations (for Delft3D result), it is caused by the wave height which induced the increase of near-bed orbital velocity near the shoreline, increasing the bed shear stress near the shoreline as well. Increasing bed shear stress led to increased sediment transport, moving the sediment via bed load and suspended load transport. The sediment in suspension is then transported seaward by the flow velocity. Thereby, the sediment particle is transported offshore. To check the near-bed orbital velocity, the bed shear stress, and the depth-averaged velocity related to this explanation check Figure D.7 to Figure D.10 in Appendix D. A figure visualizing bed load and suspended load transport is also provided in Figure 4.14.

Regarding sedimentation, from the experiment, it appears closer to the shoreline (see Figure 4.3, cross-shore distance from 3 to 10 m). Meanwhile, sedimentation from the Delft3D model is further offshore (cross-shore distance from 6 to 18 m). This condition highlights that Delft3D could not generate the same pattern as that observed in the laboratory. Furthermore, sedimentation occurred between 6 to 18 m because the flow velocity started decreasing when the water depth got deeper (see Figure D.9). This weakened flow velocity declined suspended sediment transport (see Figure 4.14). Thereby, the deposition occurred.

Model skill performance

Apart from visually comparing the results, we also evaluate the similarity of the cross-shore profile for the scenario without SMFB by calculating the model skills by using four error statistic parameters. The values of each parameter represent the skills of the Delft3D model to reproduce the cross-shore profile in the experiment. The score below is based on the simulation with model setting 4 (Figure 4.2):

- Determination coefficient (R^2) = 0.87
- Relative Bias (relbias) = -0.11
- Scatter Index (sci) = 0.28
- Brier Skill Score (bss) = 0.74

Here, we have a BSS above 0.70 for the cross-shore profile in Figure 4.2, so we can state that this morphodynamic model is good. Regarding this, van Rijn et al. (2003) revealed a table that informs: the morphological model, which results in a BSS with a range between 0.6 to 0.8, can be considered as a good model. To better understand how to interpret the results based on error statistics, read Appendix B.

Since we also run the other simulations with model settings on basic settings (see Table 3.4 and Table 3.2), we summarize the model skills with different model setting on the basic setting. The model skills and remarks related to the results are presented in Table 4.1. By viewing this table, we can compare the skills of the model in reproducing the cross-section from the experiment by Shimoda et al. (1991) under a condition without FB. model settings 1-3 give a significant drop in wave height due to the settings regarding the wave spreading and gauss spreading in Delft3D, which results in less erosion and sedimentation. Next, model setting 5 created bigger erosion and sedimentation since we used default values (1.0) for the calibration factors (bed load and suspended load factors). With model setting 6, we had a visually different profile, denoted by sedimentation nearshore then erosion offshore, which is not similar to the profile in the experiment (see Figure 4.2 for the experiment, erosion

then sedimentation). Finally, by having lower calibration factors in model setting 4 (bed load and suspended load factors = 0.5), we obtained acceptably good results according to error statistics (see Table 4.1) without any significant drop in wave height though visually the cross-shore profile/pattern is not perfectly similar (see Figure 4.2). We consider **model setting 4** to be the best model setting to reproduce the cross-shore profile of the experiment without FB in the current study.

Table 4.1. Error statistics of the bed profile generated by Delft3D for simulation without FB under different model setting model settings provided in Table 3.4

model settings	R2	relbias	sci	bss	remarks
1 (initial)	0.89	-0.03	0.19	0.86	big drop in wave height
2	0.89	-0.02	0.19	0.85	big drop in wave height
3	0.89	-0.02	0.20	0.85	big drop in wave height
4	0.87	-0.11	0.28	0.74	cross-section Figure 4.2
5	0.86	-0.17	0.35	0.65	
6	0.87	-0.02	0.28	0.68	visually different profile

Additionally, to complement this Table 4.1, we also provide the corresponding cross-sections in different model settings. Next to that, the plots of the wave height propagation based on different model settings are also provided. This information can be seen in Section D1, Appendix D.

Area of erosion and sedimentation

We also compare the results of the cross-sections from the experiment and the Delft3D model by calculating the area of erosion and sedimentation. Here, the area of erosion means the area covering the region below 0 m bed level change in Figure 4.3 and above 0 m in the same figure for sedimentation. We also include the area of sedimentation erosion for different basic model setting model settings according to the explained method (see Table 3.4).

From Figure 4.4, it can be seen that the area of erosion and sedimentation vary with different model settings. Comparing the area of erosion and sedimentation, model setting 4 and model setting 5 are the settings that could result in the closer area of erosion and sedimentation to the experiment. Nevertheless, the closer area of erosion and sedimentation does not mean that the pattern of erosion and sedimentation is similar (as shown in Figure 4.2).

Furthermore, the erosion and sedimentation of model settings 1, 2, and 3 are less than erosion resulting from model settings 4 and 5 because model settings 1, 2, and 3 decrease the incoming wave height from the open boundary. If we revisit the model settings 1, 2, and 3 in Table 3.4, model settings were related to wave spreading and Gaussian spreading. Because these two parameters are set to below 0.1 (for model settings 1, 2, and 3), the wave height declines significantly after propagating from the open boundary. This leads to a smaller erosion and sedimentation. Therefore, with significantly reduced wave height near the open boundary and a bigger difference in the area of erosion/sedimentation, using this setting to reproduce the cross-shore profile is not favorable.

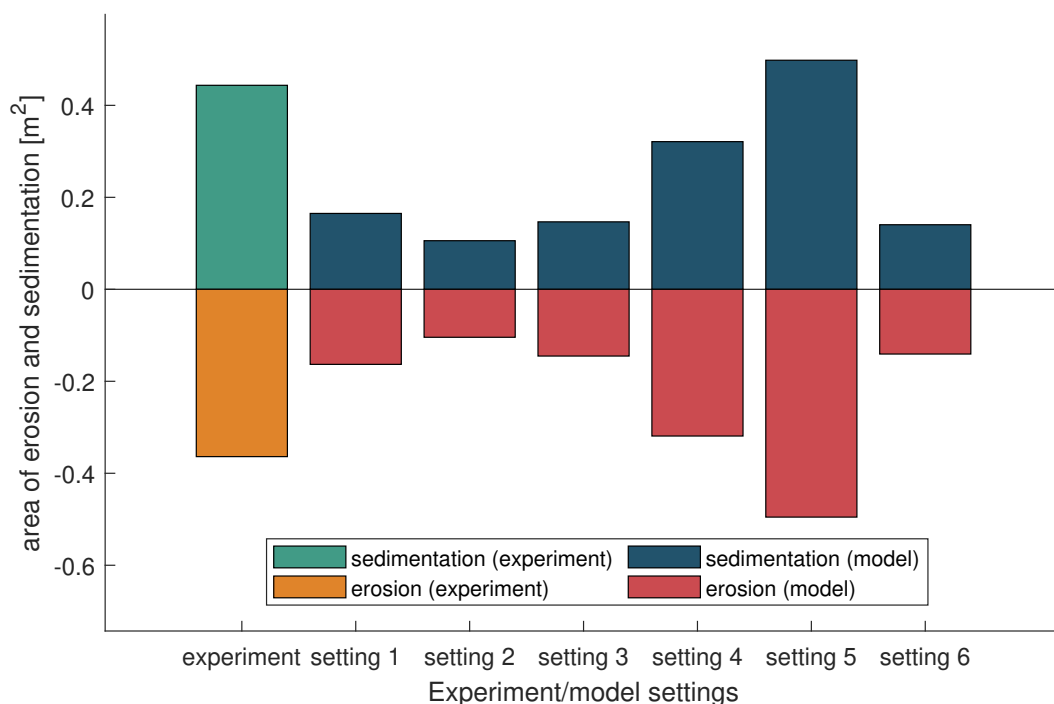


Figure 4.4. Area of erosion and sedimentation of experiment and model with different basic settings of Delft3D revealed in Table 3.4. The area of erosion/sedimentation for model setting 4 represents the area for cross-section in Figure 4.2

Next, it is also visible that model setting 6 has a smaller erosion compared to model settings 4, 5, and the experiment. We used a different sediment formulation for model setting 6, which is van Rijn (2007) instead of van Rijn (1993), a default and commonly used sediment formulation in Delft3D. We obtain a smaller erosion and sedimentation with a different sediment formulation than the experiment. Hence, we also did not proceed with this setting for further simulations.

Even though visually, the profile reproduced by Delft3D with model setting 4 is not perfectly similar to the experiment, the model's performance is deemed acceptable when considering error statistics, stable wave height in the model (no significant drop), and an almost similar area of erosion/sedimentation.

4.1.2 Cross-shore profile with landward FB

Visual comparison

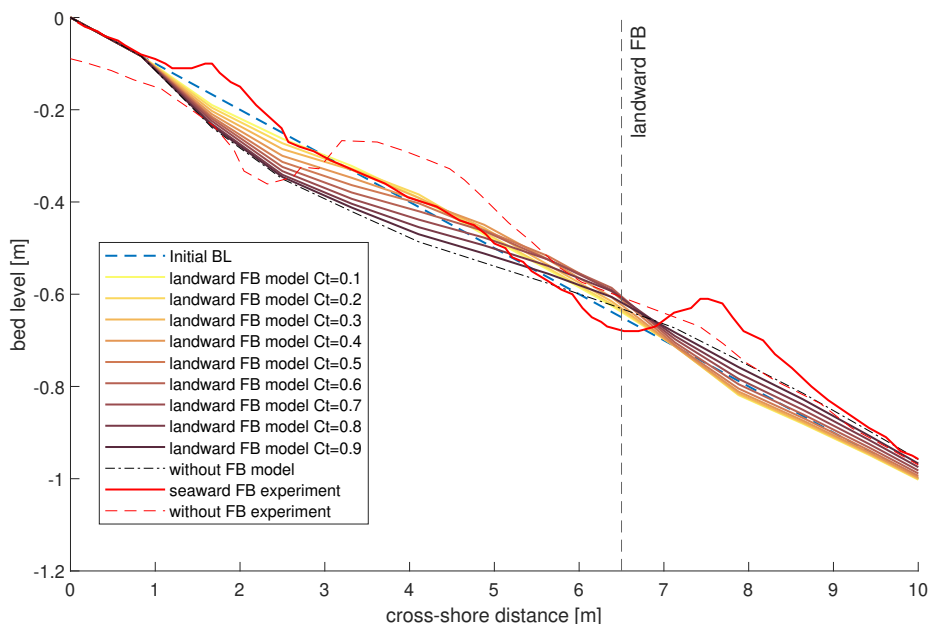


Figure 4.5. Comparison between the evolved cross-sections affected by landward FB from the experiment and Delft3D model; complemented with the cross-sections without FB from the experiment and the Delft3D model; Ct represents the transmission coefficient of FB applied in D3D; SMFB means submerged-moored floating breakwater (the FB type applied in the experiment); model results using model setting 4, which is the best model setting

From Figure 4.5, it can be viewed that the erosion and sedimentation patterns of landward SMFB according to the experiment and model are different. After landward SMFB was applied in the experiment, sedimentation near the shore appeared (cross-shore distance 1 - 2 m). Meanwhile, when landward SMFB was applied in D3D using transmission coefficient, no sedimentation appeared near the shore (cross-shore distance 1 - 2 m). Next, scouring or small erosion occurred when seeing the location near FB (cross-shore distance = 6.5 m) based on the experiment. Conversely, the model predicted sedimentation occurred at that location (cross-shore distance = 6.5 m). The deposition that occurred near the location of FB is because the depth-averaged velocity declined when passing the FB positions, see Figure D.10. This presumably reduced the magnitude of sediment transport that was directed to offshore (see Figure 4.13).

Even though the model could not predict the pattern of erosion and sedimentation very well, we could notice that the presence of FB in the model and experiment could reduce the amount of erosion (see Figure 4.5). Under a smaller transmission coefficient (Ct), it is visible that bigger erosion changes into less erosion. Almost similar, as shown by the experiment with FB, erosion near the shore became a little accreted nearshore. In short, the presence of FB reduces erosion near the shore, according to both the experiment and the model (with a lower transmission coefficient). The normalized bed level can also emphasize the previous statement, the evolved bed minus the initial bed level, depicted by Figure 4.6

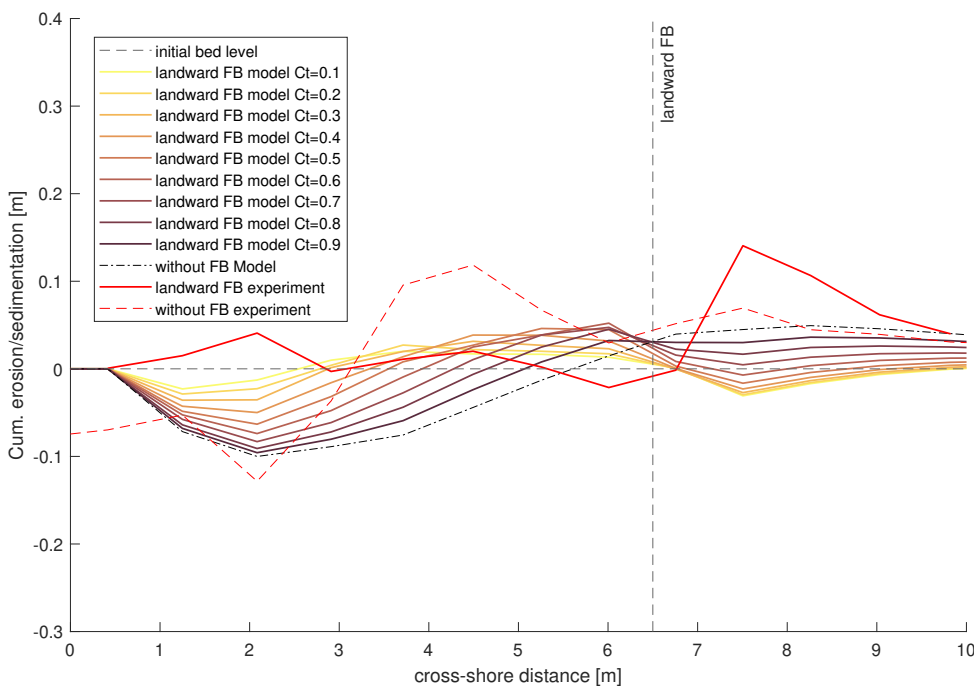


Figure 4.6. Normalized bed level with landward FB based on model and experiment; normalized means the initial bed level subtracts the bed level of the evolved cross-sections

Model skill performance

In this part, we aim to see the model skill performance to reproduce the cross-shore profile of the experiment with landward FB. Different FB transmission coefficients (Ct) are evaluated to see which one can result in statistically best cross-section in the condition with landward FB compared to the same condition in the experiment.

Table 4.2. Error statistics of the cross-shore profile generated by Delft3D for simulation with landward FB under different transmission coefficients

Ct	R2	relbias	sci	bss
0.1	0.92	-0.01	0.08	0.97
0.2	0.91	-0.01	0.09	0.97
0.3	0.91	-0.01	0.10	0.96
0.4	0.91	-0.02	0.12	0.94
0.5	0.90	-0.03	0.14	0.93
0.6	0.89	-0.04	0.15	0.92
0.7	0.89	-0.06	0.16	0.91
0.8	0.89	-0.08	0.17	0.91
0.9	0.88	-0.11	0.18	0.91

In Table 4.2, we can see that the higher transmission coefficient yields a lower brier skill score (bss),

lower R^2 , far relative bias from 0 and greater sci index. Hence, choosing the smallest C_t is more advisable since the higher BSS, the bigger R^2 , and the least relbias and sci are more desired. Also, when we look at the criteria by van Rijn et al. (2003), it is obvious that the transmission coefficient = 0.1 results in a value of bss of almost 1, which indicates that the model performs excellently. This shows that according to the Delft3D model perspective, the FB had a very effective attenuation ($C_t = 0.1$).

Area of erosion and sedimentation

We calculate the area of erosion and sedimentation behind the landward FB (see Figure 4.6 from 0 m to 6.5 m). According to the calculation of the area of erosion and sedimentation, it is visible in Figure 4.7 that the smaller the transmission coefficient (which represents FB), the closer the area of erosion and sedimentation to the experiment with landward FB. This finding confirms the previous discussion which indicated that the smallest transmission coefficient ($C_t = 0.1$) statistically performed well to reproduce the cross-section from the experiment with landward FB.

Furthermore, in the figure below, we also see that the higher the transmission coefficient, the greater the erosion area. This can be explained by the wave height behind Fb that was not effectively reduced when the transmission coefficient was big, e.g., $C_t = 0.9$ (see Figure 4.11). As a result, the peaks of near-bed orbital velocity (see Figure D.7) and bed shear stress (see Figure D.8) were more significant compared to the resulting peaks of the same parameters with lower transmission coefficients. Thereby, a greater magnitude of sediment transport occurred, resulting in a greater area of erosion, which can be seen in the figure below.

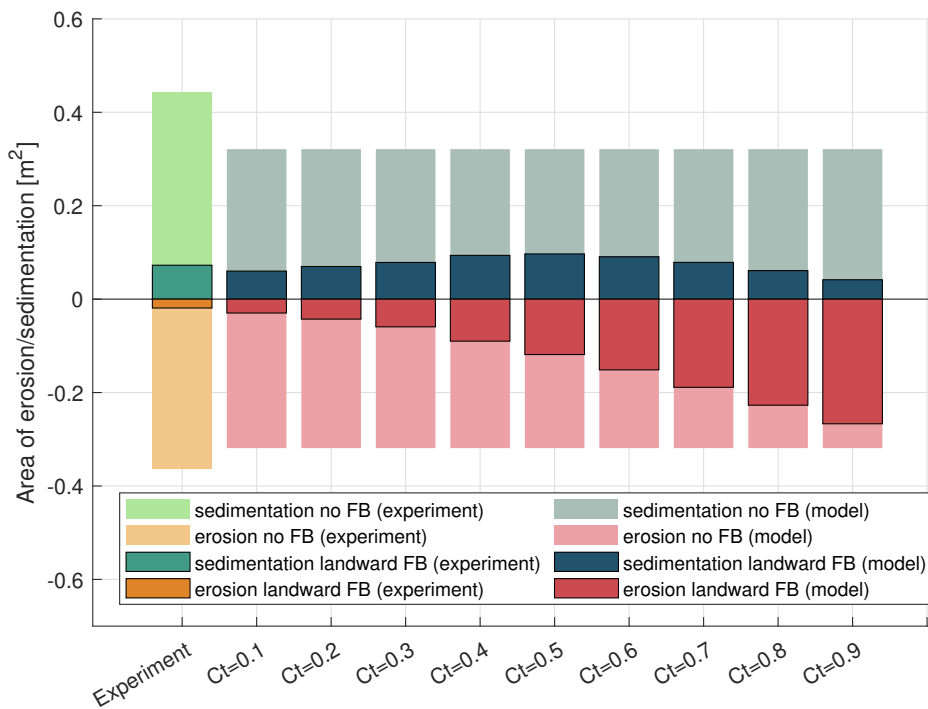


Figure 4.7. Area of erosion and sedimentation of experiment and model with landward FB ($x=6.5$ m) using different input of transmission coefficients from 0.1 to 0.9

4.1.3 Cross-shore profile with seaward FB

Visual comparison

Using the Delft3D model, a cross-shore profile with seaward FB from the experiment (see Figure 4.1c) is also reproduced. For the seaward FB, the transmission coefficient was prescribed a bit further offshore (cross-shore distance = 8.5 m, see Figure 4.1c) compared to landward FB. To see the evolved cross-shore profile due to seaward FB based on experiment and Delft3D model, Figure 4.8 is provided

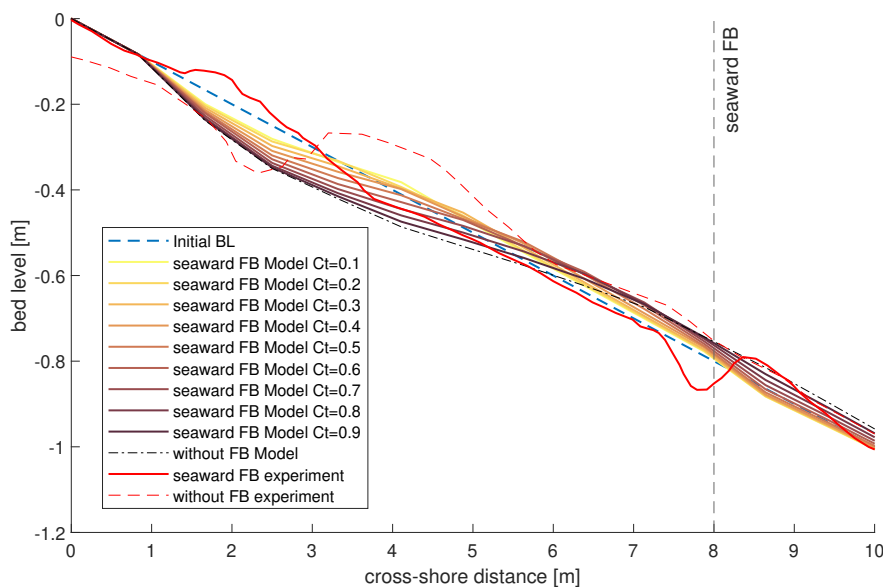


Figure 4.8. Comparison between the evolved cross-sections affected by seaward FB from the experiment and Delft3D model; complemented with the cross-sections without FB from the experiment and the Delft3D model; Ct represents the transmission coefficient of FB applied in D3D; SMFB means submerged-moored floating breakwater (the FB type applied in the experiment); model results using model setting 4 (best model setting)

As seen in Figure 4.8, due to the presence of FB at cross-shore distance = 8.0 m, the eroded area near the shoreline changes into the accreted shoreline in the experiment. Meanwhile, when Delft3D is used to reproduce the evolved cross-shore with the presence of seaward FB, we only see the eroded area near the shoreline become less. In light of this, the smaller the transmission coefficient assigned to the FB, the less erosion occurred near the shoreline.

When we compare the pattern of erosion and sedimentation due to the presence of FB in the experiment and model, we see that the model could not generate erosion near the shoreline, not similar to the experiment's result (see Figure 4.8, cross-shore distance 0 - 3 m). Next to that, the result of the experiment exhibits a slight erosion from a cross-shore distance of 3 m - 7 m. Accretion can be viewed according to the model in the same range, especially with a small transmission coefficient. Getting close to the location of FB (cross-shore distance = 8 m), we can see a scouring, which the model could not generate. In this case, the model result depicts erosion seaward from the FB position (around 8.5 m - 10 m), when the transmission coefficient is small.

From the previous explanation, which refers to Figure 4.8, it is acknowledged that Delft3D could not accurately replicate the erosion and sedimentation pattern. This is proven by the condition that when the experiment yielded accretion in a specific cross-shore length, the model resulted in (small)

erosion, and vice versa. We also provide the accumulated erosion and sedimentation, which shows the normalized cross-shore, evolved bed profile minus the initial bed profile. This can be viewed in Figure 4.9.

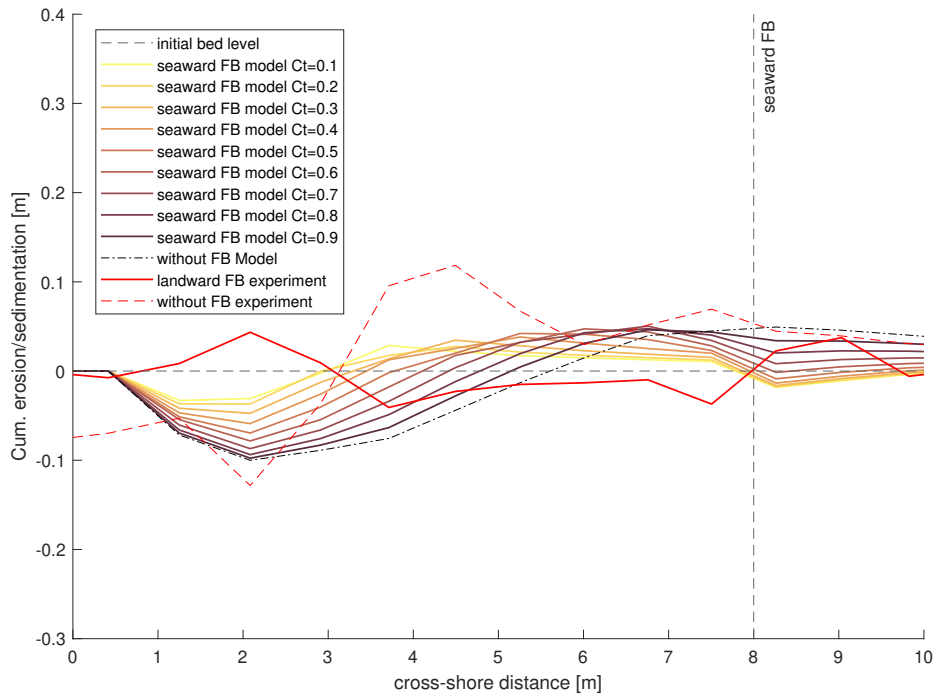


Figure 4.9. Normalized bed level with landward FB based on model and experiment; normalized means the initial bed level subtracts the bed level of the evolved cross-sections

Model skill performance

Model skill performance is also evaluated for the cross-shore profile with the presence of a seaward FB. To see the performance of the FB according to the previously discussed error statistic parameters, see Table 4.3.

Table 4.3. Error statistics of the cross-shore profile generated by Delft3D for simulation with seaward FB under different transmission coefficients

Ct	R2	relbias	sci	bss
0.1	0.91	0.01	0.11	0.96
0.2	0.91	0.01	0.11	0.96
0.3	0.91	0.00	0.12	0.95
0.4	0.91	-0.01	0.14	0.94
0.5	0.90	-0.01	0.14	0.93
0.6	0.90	-0.03	0.15	0.93
0.7	0.89	-0.05	0.15	0.93
0.8	0.89	-0.06	0.16	0.93
0.9	0.89	-0.08	0.17	0.93

According to Table 4.3, it is seen that with a smaller value of transmission coefficient, the generated cross-section with seaward FB in the model could resemble the cross-section observed in the experiment. This is proven by seeing the transmission coefficient = 0.1, which has the highest determination coefficient (R^2), minimum relative bias, minimum sci index, and maximum brier skill score (almost 1). With the bss approximately equal to 1, we can deem that the model with seaward FB (Ct = 0.1) performed excellent according to the criteria by van Rijn et al. (2003) (see also the criteria in Appendix B).

Area of erosion and sedimentation

Next, we again calculate the erosion and sedimentation area according to the simulations that include the seaward FB. From Figure 4.10, we see that the presence of FB could reduce erosion and sedimentation based on both experiment and model. Furthermore, it is noticeable that the erosion decreases until approaching the erosion area in the experiment when we lower the transmission coefficient. Noticeably, the seaward FB having a transmission coefficient of 0.1, 0.2, or 0.3 exhibits an almost equal amount of erosion and sedimentation like the experiment. Nevertheless, when we reflect on the error statistics discussed before, the evolved cross-section affected by seaward FB with a transmission coefficient of 0.1 is the closest to the experiment. It is important to mention that the area of erosion and sedimentation was calculated from a cross-section of 0 m to 8.0 m (behind seaward FB).

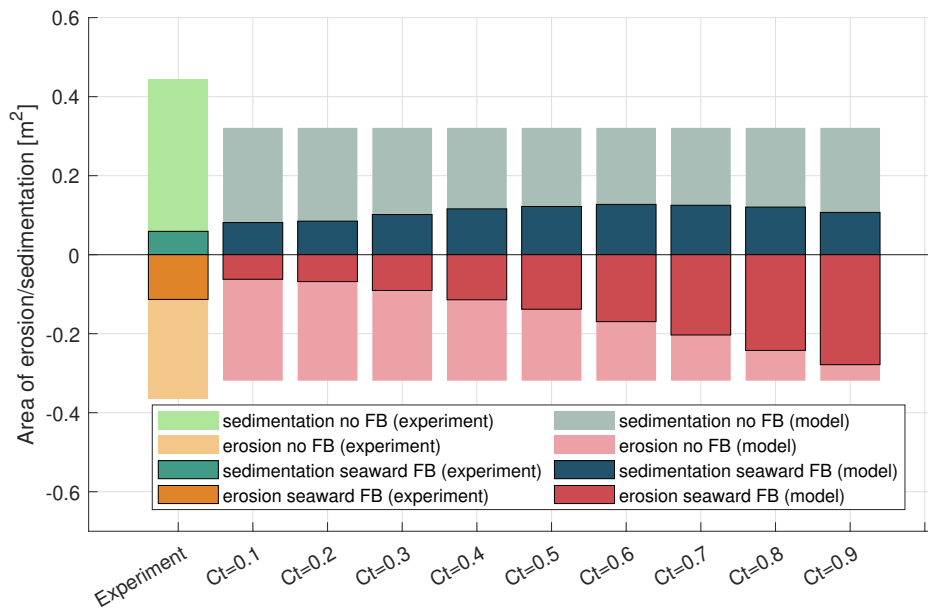


Figure 4.10. Area of erosion and sedimentation of experiment and model with seaward FB (x=8.0 m) using different input of transmission coefficients from 0.1 to 0.9; no FB means experiment or simulations without FB

4.2 Wave height under FB interventions

This section aims to see the effects of the FB transmission coefficient implemented in the Delft3D model on the hydrodynamic parameters: wave height. This parameter is chosen because Shimoda et al. (1991) explained about the wave attenuation in their report. Thereby, it is intended to relate the findings from the laboratory with Delft3D based on their explanations.

In Figure 4.11, it is seen that when there was no FB applied, the wave height declined slightly as the waves approached the shore but when the waves reached the breaking point around 1 m, the wave height decreased rapidly. Furthermore, when the FB was applied, we can see that the wave height declined differently depending on the transmission coefficient. For example, with the transmission coefficient of 0.1, the wave height declined significantly from approximately 0.27 m to 0.05.

Apart from the effect of FB, it is also seen that the wave height increased again after being dissipated by the FB. This is due to contact between the wave and the seabed, which increases the wave in height (shoaling). Apart from that, with seaward FB, it is seen in Figure 4.11 that the shoaling wave had a higher wave height compared to that with landward FB intervention. This is presumably because the wave had more opportunity to interact with the bed when the FB is located seaward, allowing waves to shoal and increase in height more than the simulation with landward FB.

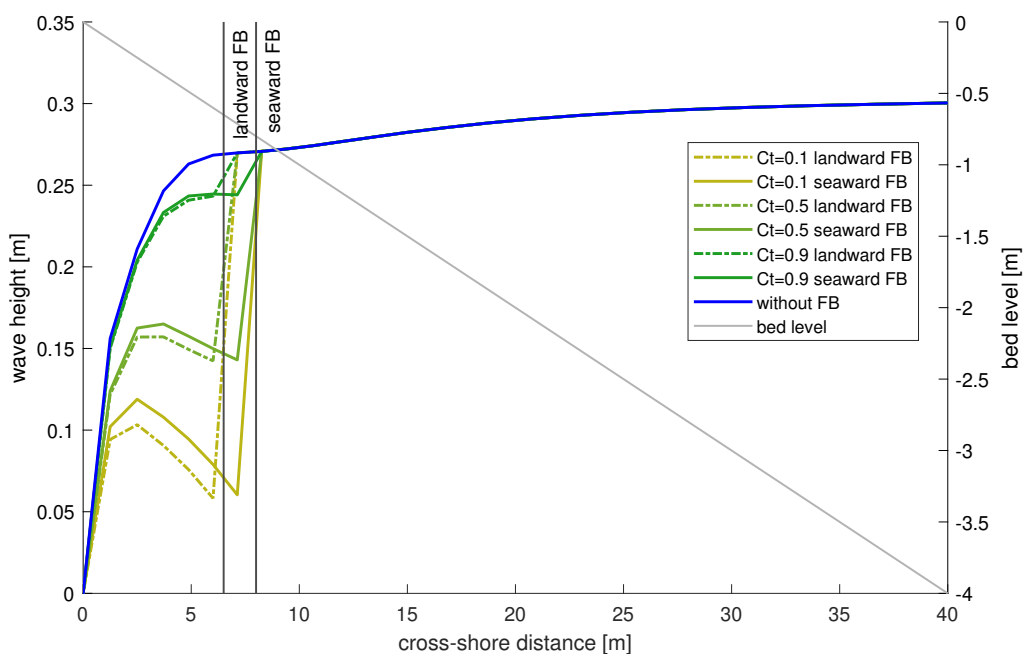


Figure 4.11. Effect of the presence of landward (cross-shore distance = 6.5 m) and seaward FB (cross-shore distance = 8 m) with different transmission coefficient on wave height

Relating the wave height modeled in Delft3D to the condition explained by Shimoda et al. (1991) when FB was present, from their explanation, the FB in the experiment breaks the incident wave. When we look at Figure 4.11, we can see that the presence of FB only reduced the incident wave, denoted by declined wave height between cross-shore distances 5 - 10 m. Since Shimoda et al. (1991) did not quantitatively observe the wave height for their experiment, it is hard to judge the similarity of the reduced wave height in their experiment and the simulations in the current study.

Furthermore, Shimoda et al. (1991) also explained that the incident wave attenuation could become larger as the FB’s height increases and the FB is more exposed to the water surface. Here, we can relate it to the difference in transmission coefficient. We could expect less wave attenuation as the transmission coefficient inputted in Delft3D is high. Meanwhile, the low transmission coefficient inputted in Delft3D could represent the condition when the FB has a bigger draft and is more exposed to the water surface, leading to bigger wave attenuation.

4.3 Sediment transport under FB interventions

Direction of bed load and suspended load transport

Figure 4.12 presents the direction of bed load and suspended load without FB. With alongshore uniform bathymetry, we can see that the bed load transport was directed onshore and suspended load transport was directed offshore. This condition matches the cross-shore sediment transport behavior, in which the bed load transport will generally be directed onshore (due to short wave skewness) and the suspended transport offshore due to the undertow (Bosboom & Stive, 2021), see Figure D.10.

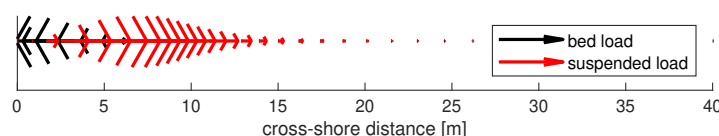


Figure 4.12. Direction of bed load and suspended load without FB; cross-section = 0 m indicates the shoreline; the bigger arrows indicate the higher magnitude of the bed load or suspended load

When the FB is applied (see Figure 4.13), the direction of bed load transport and suspended load transport remains slightly the same (bed load onshore-directed and suspended load offshore-directed). The presence of FB had apparently reduced the magnitude of the suspended load transport. This is confirmed by the magnitude of depth-averaged velocity that became small when it passed the FB toward the offshore direction (see Figure D.10). This also implies that the depth-averaged velocity (seaward-directed) and suspended load transport are related. Moreover, this finding answers why the deposition occurred near the FB location (see Figure 4.5 at cross-shore distance = 6.5 m). After erosion around cross-shore distance = 6.5 m, suspended sediment transport increased again. This was depicted by the depth-averaged velocity as well. Erosion after the FB position (see Figure 4.5, the cross-shore distance from 9 m to 15 m) was confirmed by the increased in depth-averaged velocity and suspended load transport in Figure 4.13 (cross-shore distance 10 - 15 m).

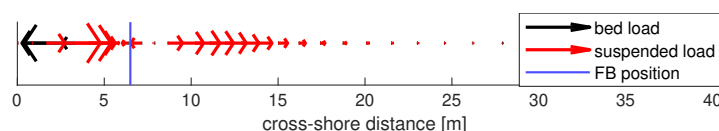


Figure 4.13. Direction of bed load and suspended load based on Delft3D model with FB ($C_t = 0.1$); cross-section = 0 m indicates the shoreline; the bigger arrows indicate the higher magnitude of the bed load or suspended load; FB position is landward (cross-shore distance = 6.5 m)

Comparing the direction of the suspended load transport with the laboratory experiment, Shimoda et al. (1991) remarked that due to wave-breaking, sediment particle onshore of the FB is suspended and is washed away mainly toward the offshore direction by the return flow. The Delft3D model also captured the behavior of the suspended sediment that was transported offshore. The return flow described in the laboratory was in the same direction of depth-averaged velocity in the Delft3D model, which is offshore-directed (see Figure D.9 and Figure D.10). Nevertheless, both parameters are not the same: return flow typically associated with velocity that is offshore-directed in the lower part of the water column and onshore-directed in the upper part (van der Werf, 2021), while depth averaged velocity is an average measure of the flow velocity across the entire depth of the cross-shore profile.

Magnitude of bed load and suspended load transport

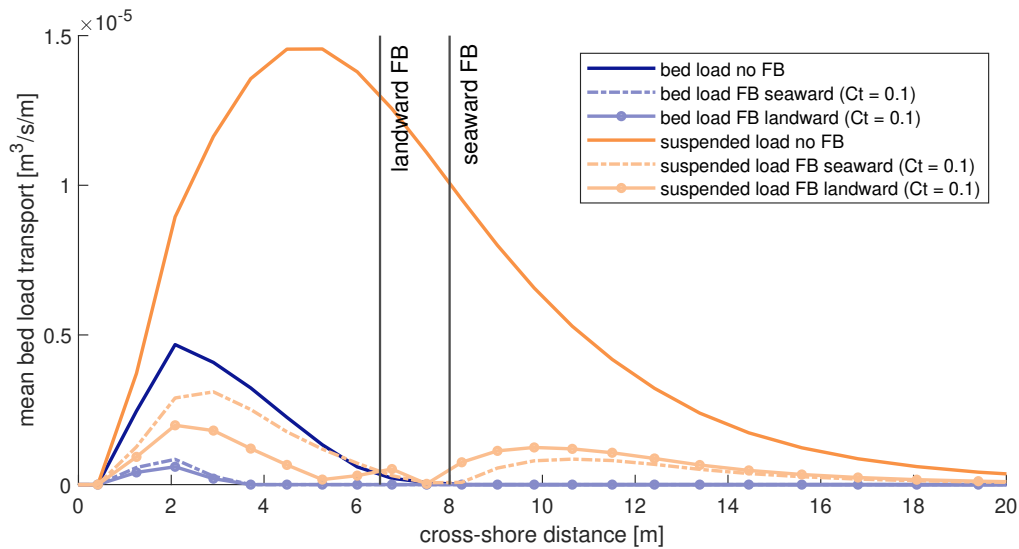


Figure 4.14. Mean bed load and suspended load transport without and with FB ($C_t = 0.1$); C_t means transmission coefficient; the bed load transport is predominantly onshore-directed and suspended load transport is predominantly offshore-directed

Figure 4.14 shows the differences between bed load and suspended load transport when the FB is prescribed and not prescribed. It is noticeable that the bed load transport declined when the FB is applied. Furthermore, the difference in the location of the FB affects the sediment transport. With landward FB, the peak of bed load transport is smaller than the peak with the seaward FB. This is relatable to higher (shoaling) waves when the FB was imposed (see Figure 4.11).

Regarding suspended load transport, we can see that the suspended transport rate is more significant compared to the bed load transport. This can be seen when we notice the order of magnitude for the suspended load transport (without FB intervention), which is 10^{-5} , while bed load transport was in the order of magnitude 10^{-6} (see Figure 4.14). When the FB was imposed, the suspended sediment transports decreased. Similar to the bed load transport, the magnitudes of suspended load transport with landward FB were smaller than the magnitudes of suspended load transport with seaward FB, which might be relatable to the wave height as well: lower (shoaling) wave with landward FB and higher with seaward FB (see Figure 4.11)

Next, if we relate to the experiment described by Shimoda et al. (1991): the sediment particle onshore of the FB is suspended due to wave breaking. In Figure 4.14, we see that even though the FB was not imposed, the suspended load transport was apparent. Hence, we could not draw a strong conclusion that the suspended sediment is caused by the wave breaking.

4.4 Reflection on the first research phase

In this research phase, we use the transmission coefficient to represent FB. By using this feature, erosion and sedimentation near the shoreline is reduced. The decrease in erosion and sedimentation was also reported in the laboratory experiment by Shimoda et al. (1991). Based on error statistics, the model performed well in reproducing the cross-shore profiles in the laboratory. Also, the area of erosion and sedimentation for all cross-sections was more or less close to the laboratory experiment. However, the erosion and sedimentation patterns in all cross-sections were not fit to the Delft3D results.

Apart from the cross-sections, the transmission coefficient feature was able to reduce the incident wave height. This was also the effect of FB reported in the experiment. Nevertheless, no strong conclusion can be drawn since the comparison of the wave height was not carried out by comparing the profile of wave height observed in the laboratory and derived from Delft3D simulations. Next, bed load and suspended load transport were discussed. In this context, we only found the similarity that the suspended load transport is transported to offshore direction. Yet, this is not because of the presence of FB since without FB the suspended transport was also offshore directed in the model.

Building upon the results in this first research phase, the transmission coefficient feature in Delft3D could be representative of FB in terms of its capability to reduce erosion and sedimentation also attenuate waves with its limitations. After this, we move on to the second research phase. Hydrodynamic and morphodynamic parameters are analyzed when the FBs are imposed under varying conditions in the intertidal flats. Using the knowledge in the first research phase, we already have the expectation of how the transmission coefficient could represent FB. Furthermore, regardless of the limitations of the transmission coefficient feature in Delft3D, the results of the next research phase were obtained by also using this feature to represent FB.

5 Results: hydrodynamics and morphodynamic effects of a floating breakwater at intertidal flats (Delft3D output)

5.1 Transmission coefficients of the floating breakwater at intertidal flats

In this research phase, we first discuss the possible transmission coefficients that the FB can possess in the intertidal flats environment. The transmission coefficient is calculated using the data provided in Table 3.6. This includes water depth at FB positions, the FB width, the FB draft, and the wave period. All mentioned data is used as the input in Macagno relation, Equation 2. For seeing the potential transmission coefficients of a floating breakwater at intertidal flats, Figure 5.1 is provided.

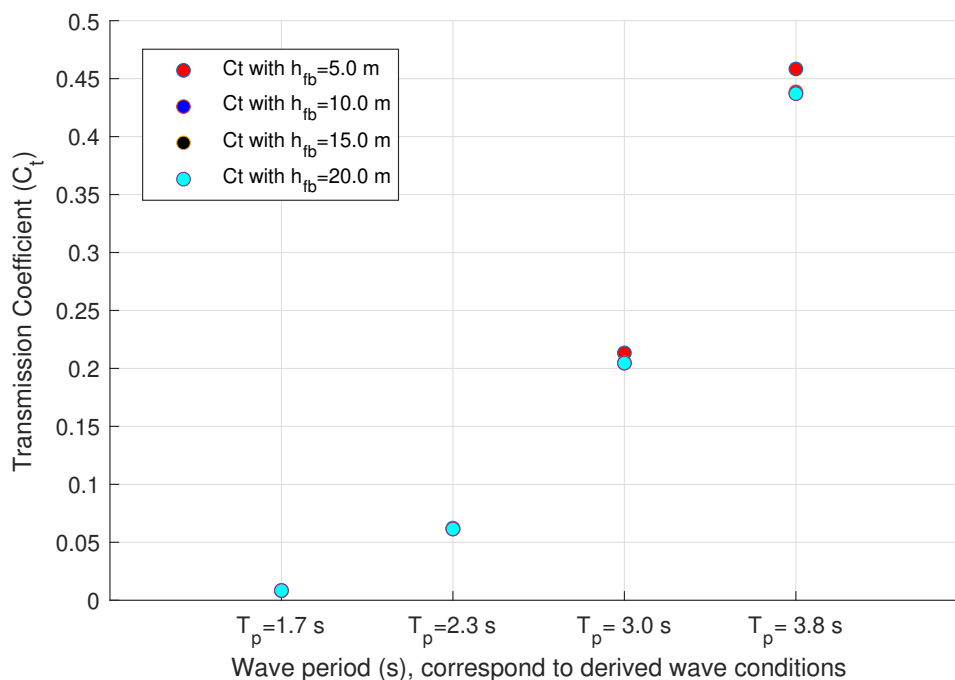


Figure 5.1. Potential transmission coefficient (Ct) of the floating breakwater at the Eastern Scheldt. The transmission coefficient indicates the transmitted wave height over the incident wave height. The transmission coefficients are calculated using Macagno relation with the data of FB’s widths: 8.00 m; FB’s drafts: 2.20 m.

Figure 5.1 shows the variation of transmission coefficients for different wave periods at the Eastern Scheldt location. It is observed that higher wave periods result in higher transmission coefficients, indicating that the floating breakwater becomes less effective in dissipating waves. On the other hand, lower wave periods lead to lower transmission coefficients, suggesting that the floating breakwater can attenuate waves more effectively. In light of this, Biesheuvel (2013); Zanden et al. (2022) confirmed that the floating breakwater is more effective in the region with short waves.

Furthermore, when we varied the water depth at FB positions (different h_{fb}) between 5, 10, 15, or 20 m, it is apparent in Figure 5.1 that there is no significant difference in the transmission coefficient. To be able to see the difference in more detail, Table 5.1 is provided.

Table 5.1. Calculated transmission coefficients for different water depth at FB positions (h_{fb}) under different wave conditions, width of FB = 8.00 m and draft of FB = 2.20 m

Wave conditions	Transmission coefficients (C_t)			
	$h_{fb}=5$ m	$h_{fb} = 10$ m	$h_{fb} = 15$ m	$h_{fb} = 20$ m
1) $H_0 = 0.40$ m $T_p = 1.7$ s	0.0084	0.0084	0.0084	0.0084
2) $H_0 = 0.70$ m $T_p = 2.3$ s	0.0623	0.0615	0.0615	0.0615
3) $H_0 = 1.20$ m $T_p = 3.0$ s	0.2134	0.2047	0.2046	0.2046
4) $H_0 = 1.80$ m $T_p = 3.8$ s	0.4584	0.4386	0.4371	0.4370

Based on Table 5.1, there are differences in the calculated transmission coefficients with different water depths at FB positions. Under more extreme wave conditions, the shallower water depth resulted in a slightly higher transmission coefficient compared to the FB located in deeper water. For example, for wave conditions 2, 3, and 4 (see Table 5.1), the transmission coefficients with $h_{fb} = 5$ m exhibited slightly higher values compared to those with deeper h_{fb} . This indicates that the FB is slightly ineffective when it is placed near the shoreline i.e., in shallower water.

Overall, it can be inferred that the wave period significantly affected the effectiveness of the floating breakwater. With a higher wave period, the transmission coefficient became high, implying that the effectiveness of FB declined. Meanwhile, a lower wave period led to more effective FB, denoted by a lower transmission coefficient. Furthermore, the water depth at FB positions slightly affected the transmission coefficient. FB located in shallower water led to slightly ineffective FB. This is denoted by the small increase in transmission coefficient compared to the FB located in deeper water. It is important to note that under mild wave conditions i.e., wave conditions 1 and 2, the transmission coefficient is very slightly or even not influenced by different FB positions (water depths).

5.2 Hydrodynamic effects of floating breakwater at intertidal flats

Three hydrodynamic parameters are discussed in this section: wave height, near-bed orbital velocity, and bed shear stress. The wave height is closely related to the near-bed orbital velocity (see Equation 6). Furthermore, the orbital velocity and bed shear stress (wave-induced) are also interrelated and essential for coastal engineering, especially in sediment transport (Xiong et al., 2018).

5.2.1 Effects of FB on wave height

Overview of wave height propagation with and without FB

Figure 5.2 depicts the propagation of wave height under different wave conditions without and with FB interventions. In general, without FB (blue line in Figure 5.2), the wave height remains at the same magnitude until the waves reach the intertidal flats edge (before cross-section = 600 m). On the shoal edge (transition of the intertidal area and channel), we see that the wave height declined rapidly (all wave conditions, more obvious on wave condition 1, the upper left panel in Figure 5.2). This presumably occurred due to the sudden changes in bathymetry. A sudden change in bathymetry presumably induced wave breaking, resulting in the sudden drops in wave height. Afterward, the wave heights appeared to gradually lower as they went further entering the intertidal flats (cross-shore = 600 m to 300 m). This could be due to waves crossing the shallow area on intertidal flats, increasing the influence of bed friction in dissipating waves.

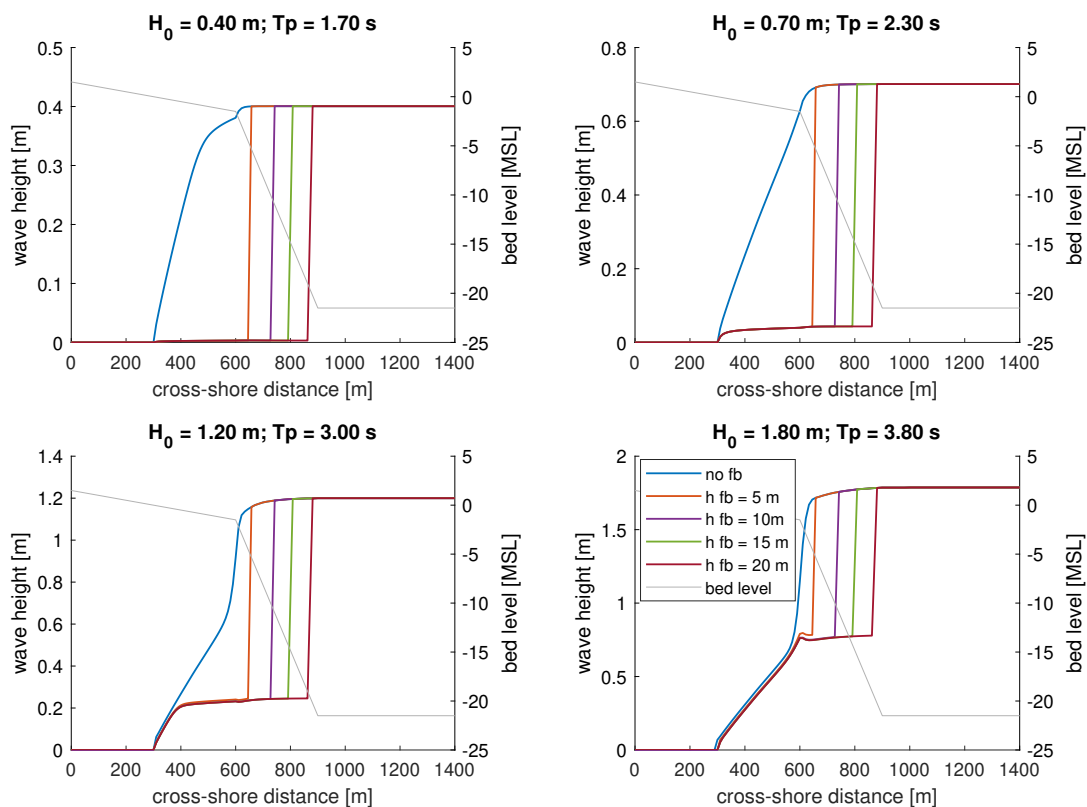


Figure 5.2. Floating breakwater effects under different wave height conditions with different floating breakwater positions; simulations with an intertidal area slope 1:200 and a channel slope 1:15; h fb means water depth at FB position

When the FB is implemented, it is seen that the wave heights declined before it reached the intertidal flats depending on the FB positions. Nevertheless, the transmitted wave heights on the lee side of FB did not exhibit a huge discrepancy under all incident wave conditions. This corresponds to the previous finding where the water depth below FB only slightly affected the transmission coefficients (read Section 5.1), implying that different FB positions did not reduce its effectiveness much.

With FB interventions and under different wave conditions, we can also see in Figure 5.2 that the waves were declined in different magnitude. When mild wave conditions like wave conditions 1 or 2 were imposed (see the upper left panel in Figure 5.2), the FB could dissipate wave effectively, denoted by the wave height with the magnitudes of almost 0 m and around 0.2 m, respectively. Furthermore, as the wave height and wave period increased, the transmitted wave height behind FB remained (relatively) high, which is presumably due to FB becoming ineffective (Biesheuvel, 2013). In this case, higher transmission coefficients (ineffective FB) in more extreme wave conditions.

Effects of FB under different wave conditions on the transmitted wave height (H_1)

Under different wave conditions, we summarized the transmitted wave height without and with FB complemented with the corresponding wave height reduction in percent, presented in Table 5.3. All of the transmitted wave heights reported in this table were observed on the shoal edge (transition between the intertidal area and channel, see Figure 3.12).

According to Table 5.3, it is seen that FB increases the capacity of wave height reduction before the waves enter the intertidal area. For example, under wave condition 1, without FB, the transmitted wave height is still almost similar to the incident wave height, with a value of 0.38 m. With the FB implementation, the transmitted wave height became 0 m (reduction capacity 99%), indicating that the FB was effective.

Furthermore, as the wave conditions became more extreme, the FB was still able to reduce the wave height on the shoal edge, adding the capacity for wave height reduction. Nevertheless, under more extreme conditions (like wave conditions 4), the capacity for wave height reduction with FB decreased (57.4% - 60.7%), almost the same as the capacity for wave height reduction without FB intervention (36.1% - 51.1%). This emphasized that the FB is ineffective when the wave condition is extreme. This is also relatable to the explanation that the transmission coefficient became high under more extreme conditions like wave condition 4.

Table 5.2. Ranges of the transmitted wave height H_1 on the shoal edge (points A200, A400, A600) yielded from the simulations without FB and with FB in different FB positions (h_{fb}), shoal slopes (S_s), and channel slopes (S_c); and reduction of incident wave height H_0

Wave conditions	Transmitted wave height H_1 [m]		reduction of H_0 (%)	
	without FB	with FB	without FB	with FB
1) $H_0 = 0.40$ m $T_p = 1.7$ s	0.38	0	4.7 - 5.3	99
2) $H_0 = 0.70$ m $T_p = 2.3$ s	0.60 - 0.63	0.04	10.0 - 14.0	94.3 - 94.4
3) $H_0 = 1.20$ m $T_p = 3.0$ s	0.78 - 0.92	0.22 - 0.23	23.2 - 35.2	80.7 - 81.2
4) $H_0 = 1.80$ m $T_p = 3.8$ s	0.88 - 1.15	0.71 - 0.77	36.1 - 51.1	57.4 - 60.7

Effects of different water depths at FB position on the transmitted wave height (H_1)

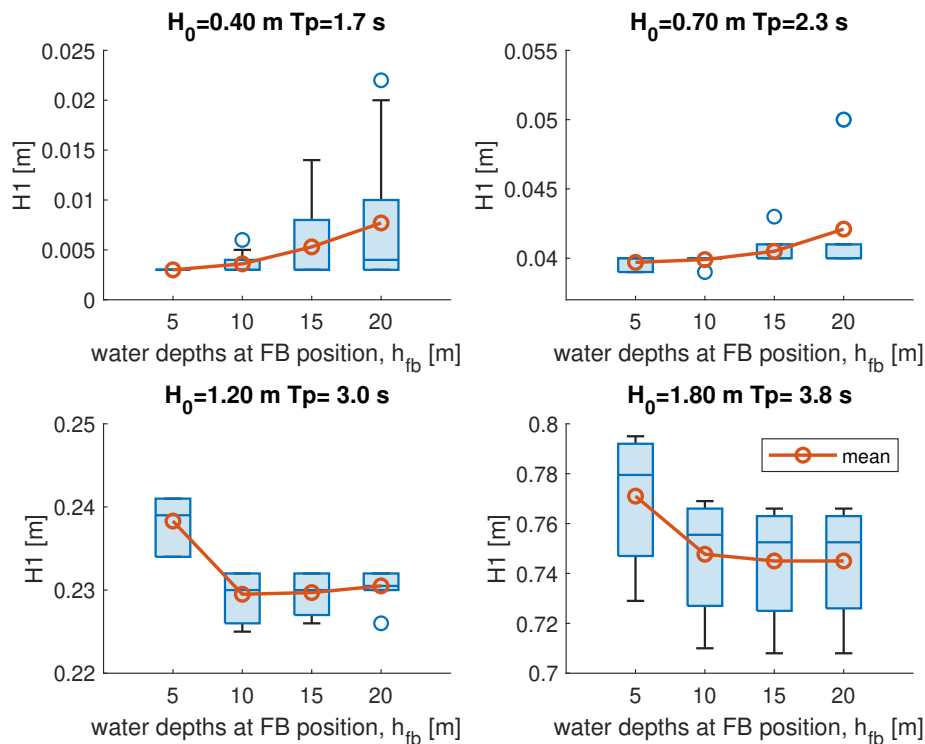


Figure 5.3. Transmitted wave height H_1 on the shoal edge (points A200, A400, A600) with different water depths at FB positions; Derived from the simulations with FB in different FB positions (h_{fb}), shoal slopes (S_s), and channel slopes (S_c); grouped based on FB positions (h_{fb})

Based on Figure 5.3, it can be seen that the transmitted wave height (H_1) varies depending on the water depths at the FB position. Under two low incident wave conditions (upper panels), the greater water depths at the FB position resulted in higher transmitted wave height (H_1) compared to H_1 with the FB at shallower water depth. This occurred because of shoaling, in which the wave height transforms (in this case, slightly increased, then decreased) due to the reduced water depth (van der Werf, 2021; Bosboom & Stive, 2021). Because the transmission coefficients for low wave conditions are more or less similar (see Table 5.1), there is no significant difference in the reduced wave height due to FB. Thereby, the waves with the FB at more offshore positions most likely encounter shoaling as they propagate to the intertidal flats (shoreface). Meanwhile, the waves with the landward FB were less likely to shoal; thus, the wave height did not change much after being attenuated. To see the shoaling phenomenon, see Figure D.11.

Furthermore, for more severe wave conditions (lower panels in Figure 5.3), when the water depth at FB position (h_{fb}) is low (for instance $h_{fb} = 5$ m), the transmitted wave height (H_1) was slightly bigger compared to H_1 with FB located in deeper water. For example, H_1 in wave condition 3 ($H_0 = 1.20$ and $T_p = 3.0$ s) and $h_{fb} = 5$ m had a slightly high (mean) transmitted wave height (0.24 m) compared to (H_1) with FB in deeper water ($h_{fb} = 10$ m), which was 0.23 m. From the presented results, the differences of H_1 are very small (for wave conditions 3 and 4, lower panels in Figure 5.3). Therefore, we still need to see the effects on other hydrodynamic parameters and morphodynamic parameters for drawing a conclusion on whether placing FB seaward or landward is an essential consideration.

Effect of FB with different channel slopes on the transmitted wave height (H_1)

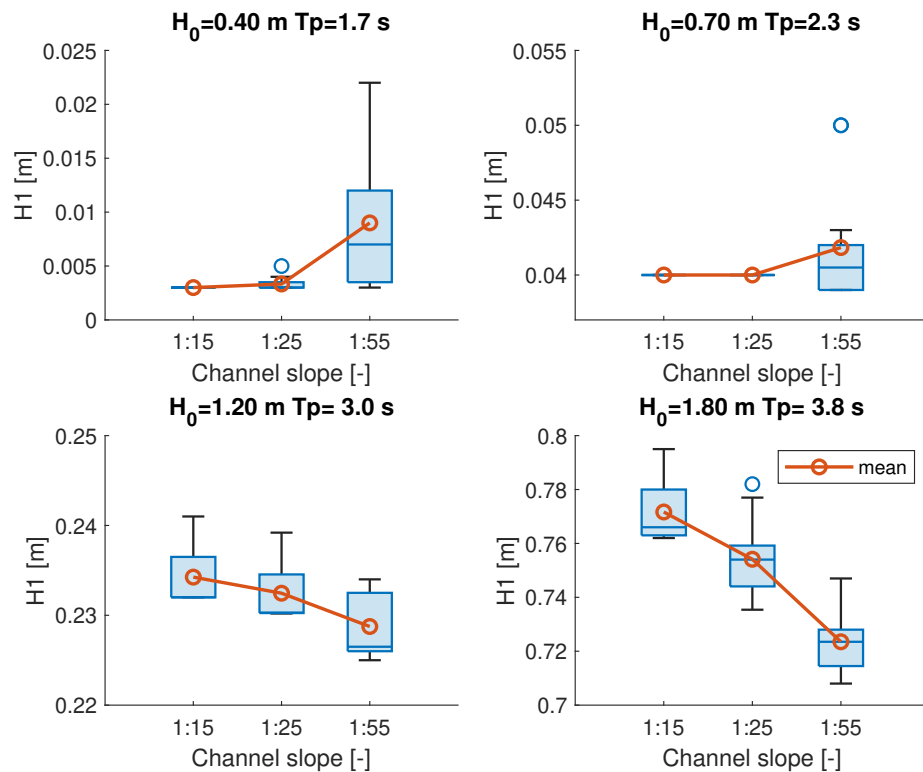


Figure 5.4. Transmitted wave height H_1 on the shoal edge (points A200, A400, A600) with different channel slopes; Derived from the simulations with FB in different FB positions (h_{fb}), shoal slopes (S_s), and channel slopes (S_c); grouped based on channel slopes (S_c)

Based on Figure 5.4, it can be understood that the channel slopes also contributed to diminishing the wave height together with the FB. Under mild wave conditions (upper panel), we see that the gentler slope, especially 1:55, exhibited a bigger transmitted wave height compared to H_1 with the steeper slope. This is due to shoaling, which is more pronounced when the seabed slope is gentler (see Figure D.11). In which the wave quickly starts to 'feel the seabed.' Thus, the waves coming onto a beach increase in height and steepness before breaking (Wright et al., 2008).

Furthermore, two bottom panels in Figure 5.4 show a trend that the gentler the channel slopes, the lower the transmitted wave height (with FB intervention). The trend shown by the lower panels in Figure 5.4 is presumably due to wave breaking. In this case, the gentle slope led to a bigger decrease in wave height compared to the wave height propagation on the steeper channel slope. However, regardless of the trend, the figure denotes that differences in the transmitted wave height on different channel slopes were not significant. This emphasizes that there is no significant impact on different channel slopes. Also, the effect of the bed friction is not much in this context, see Figure D.12.

Effects of different intertidal area slopes (S_s) on the wave height propagation

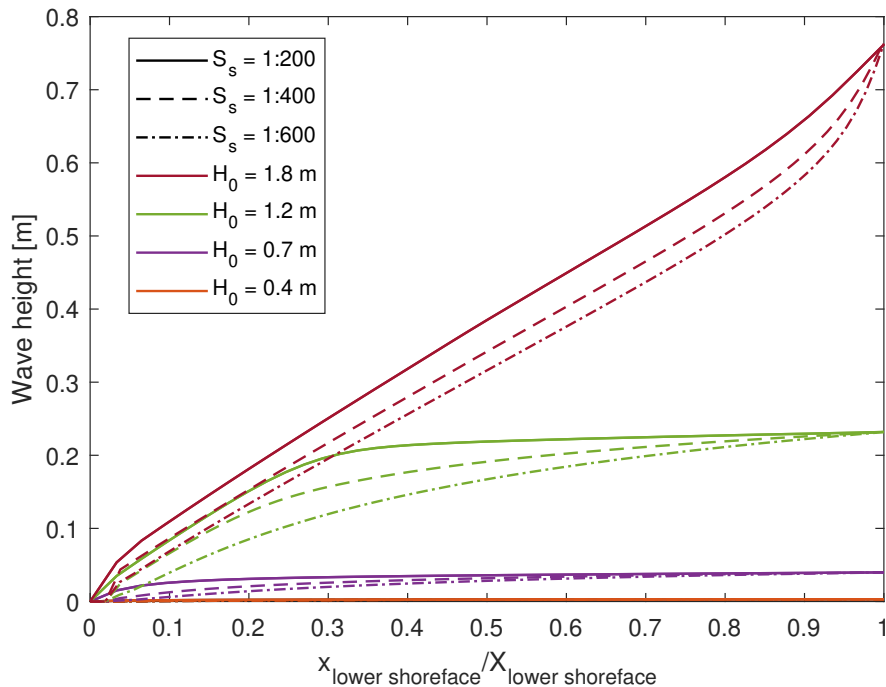


Figure 5.5. Effects of the intertidal area slope on wave height, derived from the simulations with FB ($h_{fb} = 20m$) on the same channel slope (S_c) 1:15 with different intertidal area slopes (S_s) = [1:200 1:400 1:600]

After the waves pass the shoal edges (point A200, A400, A600, see Figure 3.12), the waves propagate on the intertidal flats (intertidal area slope). In Figure 5.5, we present the effect of different intertidal area slopes. Remarkably by Tsai et al. (2005), the gentler slopes lead to increased energy dissipation, which in turn causes a reduction in wave height. Relating to Figure 5.5, it can be seen that the waves on the gentler intertidal area slopes had a wave height below the waves which propagated on the steeper slopes. For instance, when considering an incident wave height of 1.8 meters, the intertidal area slope of 1:600 yielded the smallest propagated wave height compared to intertidal area slopes of 1:200 and 1:400.

5.2.2 Effects of FB on near-bed orbital velocity

Overview of near-bed orbital velocity with and without FB

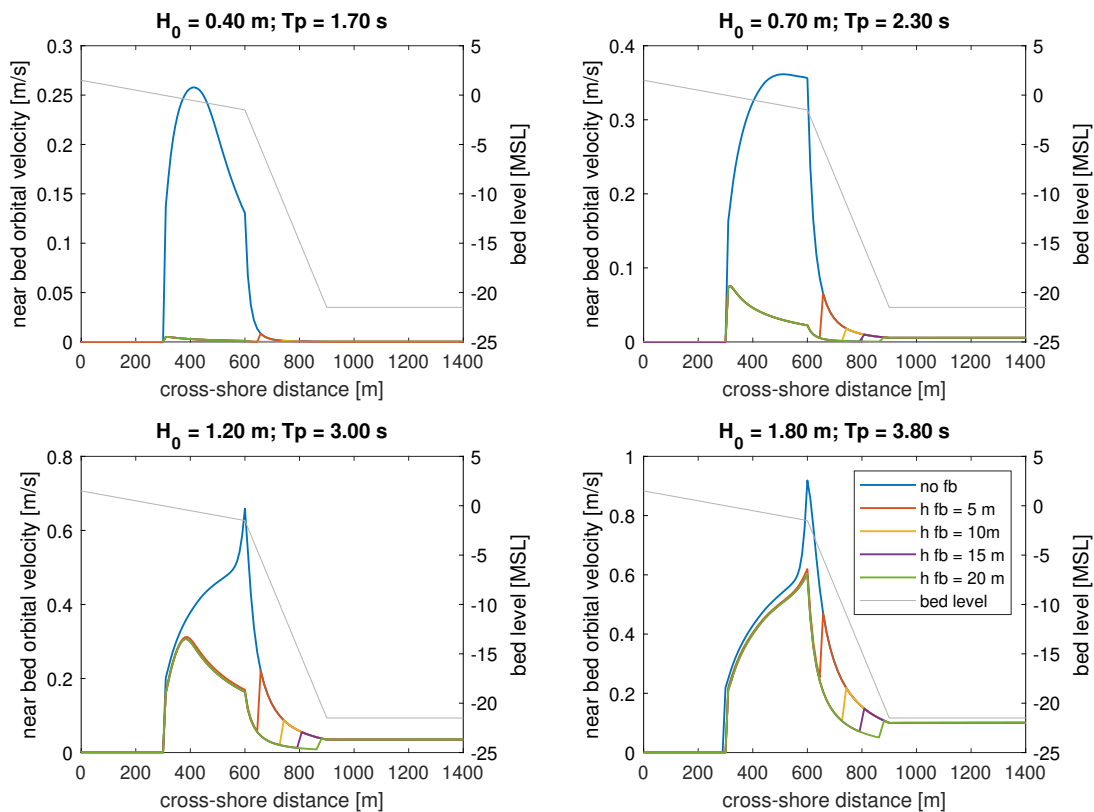


Figure 5.6. Near bed orbital velocity under different incident wave heights without and with floating breakwater in different positions (water depth at FB position), derived from the simulations with an intertidal area slope of 1:200 and a channel slope of 1:15

Figure 5.6 presents the magnitude of the near-bed orbital velocity across the intertidal flats. Under different wave conditions, it can be witnessed that the near-bed orbital velocity magnitude increased with the incident wave height increased. Furthermore, with different wave conditions, it is apparent that the peaks of near-bed orbital velocity differed. For example, without FB, for wave condition 1 (upper left panel), the peak of near-bed orbital velocity appeared on the intertidal area. Meanwhile, as the imposed wave increased, the peak of the near-bed orbital velocity profile appeared near the edge of the shoal/intertidal area. The shifting peak due to more extreme wave conditions also coincides with an increase in the magnitude of the peak itself.

Furthermore, with the presence of FB, it is obvious that the magnitudes of near-bed orbital velocity on all wave conditions declined. Apart from that, it is apparent that different water depths at FB positions exhibited slightly different effects:

- positions where the near-bed orbital velocity started increasing (due to different FB positions),
- and peak that occurred near the shoal edge, for example, see orange line ($h_{fb} = 5 \text{ m}$) on the upper right, lower left, and lower right panels.

Regarding the peak that occurred near the shoal edge, this was presumably because when the waves approached the intertidal flats, the water depths in the channel were shallow enough to increase the near-bed orbital velocity, and the waves had not been declined by the FB, while the channel slope did not significantly reduce the wave height. This resulted in the condition of relatively high wave height with shallower water depth near the shoal edge. As a result, the peak near the edge emerged (see Equation 6). It is important to note that this condition also occurred even though the determined channel slope is different.

Focusing on the profile of near-bed orbital velocity on the intertidal flat, it is also apparent that the presence of FB is not only reducing wave height (and reduced near-bed orbital velocity). Yet, the presence of FB affected the position of the peak of near-bed orbital velocity. For example, without FB, under wave conditions 3 ($H_0 = 1.20$ m and $T_p = 3.00$ s), the peak initially appeared near the shoal edge. After FB was imposed, the (lower) peak (compared to the condition without FB) was apparent in the intertidal area (cross-shore = 400 m). This also occurred with different channel slopes (see Figure D.18). Presumably, this indicates that the peak of bed shear stress might occur on the intertidal area, increasing the possibility of erosion. Additionally, if the intertidal area is gentle, it may flatten the peak on the intertidal area (see Figure D.16).

Effects of FB under different wave conditions on near-bed orbital velocity (u_b)

When seeing Table 5.3, we can argue that the effects of FB on near-bed orbital velocity agree with the results for the wave height (see Table 5.2). This is proven by: first, the high capacity of reduction in near-bed orbital velocity under mild wave conditions (wave conditions 1 and 2). Second, the less reduction capacity of near-bed orbital velocity under more extreme wave conditions (wave conditions 3 and 4). As a consequence, the (mean) near-bed orbital velocity with the condition without FB and with FB is almost similar, especially for wave condition 4. Third, the ranges of the magnitude of near-bed orbital velocity correspond to the (dissipated) wave height. For example, the \bar{u}_b of wave condition 1 without FB (0.071 - 0.086 m/s) with the range of the \bar{u}_b for wave condition 3 with FB (0.084 - 0.111 m/s). Compared with H_1 , the values are also similar, wave condition 1 (without FB): 0.38 m and wave condition 3 (with FB): 0.22 - 0.23 m (see Table 5.2).

Even though the values of the (transmitted) wave height and near-bed orbital velocity are relatable, the reduction of both parameters is not necessarily close. For example, it was reported that wave height with $H_0 = 1.20$ m can be reduced by 80.7% to 81.2% (see Table 5.2). In terms of near-bed orbital velocity, under the same wave condition, it only exhibited a range of reduction of 45.2% - 50.3%.

Table 5.3. Ranges and reduction percentage of the mean near-bed orbital velocity (\bar{u}_b) yielded from the simulations without FB and with FB in different water depth at FB positions (h_{fb}), intertidal area slopes (S_s), and channel slopes (S_c)

Wave conditions	mean near-bed orbital velocity (\bar{u}_b) [m/s]		reduction (%)
	without FB	with FB	
1) $H_0 = 0.40$ m $T_p = 1.7$ s	0.071 - 0.086	0.001 - 0.003	96.1 - 98.9
2) $H_0 = 0.70$ m $T_p = 2.3$ s	0.117 - 0.141	0.013 - 0.019	86.2 - 89.0
3) $H_0 = 1.20$ m $T_p = 3.0$ s	0.168 - 0.203	0.084 - 0.111	45.2 - 50.3
4) $H_0 = 1.80$ m $T_p = 3.8$ s	0.231 - 0.279	0.198 - 0.233	14.4 - 16.3

Effects of different water depths at FB position on near-bed orbital velocity (u_b)

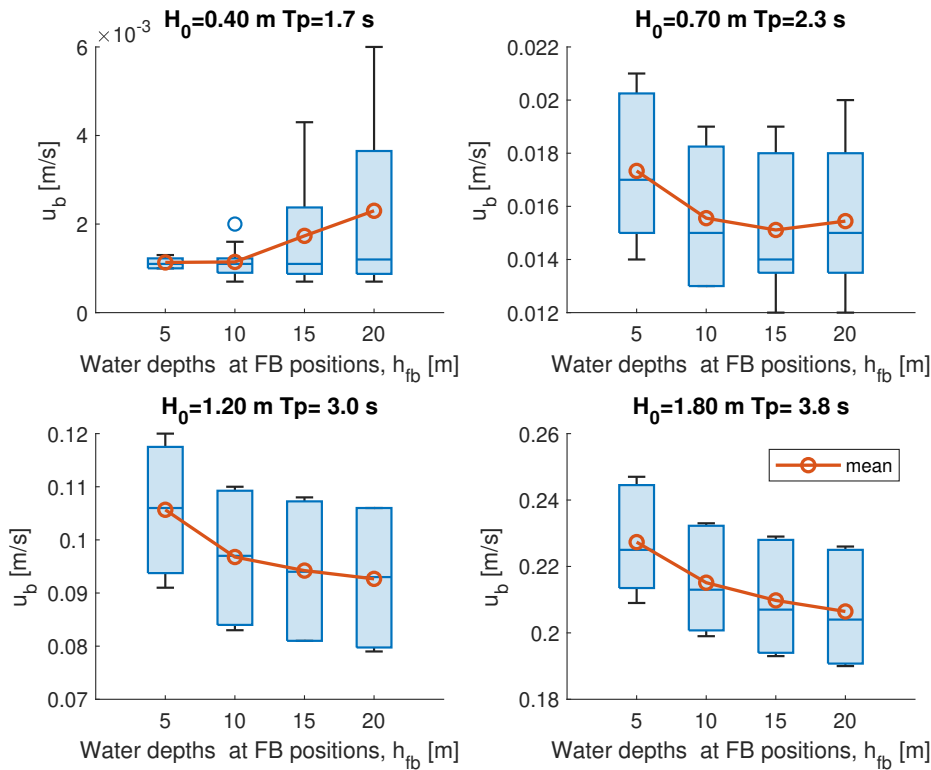


Figure 5.7. Near-bed orbital velocity with different water depths at FB positions; Derived from the simulations with FB in different FB positions (h_{fb}), shoal slopes (S_s), and channel slopes (S_c); grouped based on FB positions (h_{fb})

Figure 5.7 presents the near-bed orbital velocity magnitude when the FB is located at different water depths (FB positions). From this figure, it is understandable that under mild wave conditions (wave conditions 1 and 2, the top panels in Figure 5.7), magnitudes of near-bed orbital velocity were very low (below 0.1 m/s). Furthermore, for wave condition 2 (shallower water led to higher u_b), we see that the trend is different compared to wave condition 1 (shallower water led to lower u_b). Nevertheless, since the magnitudes of u_b are very small (for wave conditions 1 and 2), we could presume that there might be no effects on sediment transport under wave conditions 1 and 2 with FB intervention.

Moving on to the more severe wave conditions, lower panels in Figure 5.6 show a trend: high u_b on shallower water and low on deeper water. The reason behind the higher mean near-bed orbital velocity for landward FB is the peak near the shoal edge (see the orange line, $h_{fb} = 5$ m in Figure 5.6), which occurred as the wave heights had not declined by the FB and the water depth was already shallow, resulting in an increase in the (mean) near-bed orbital velocity. Therefore, the overall near-bed orbital velocity for the FB located in shallower water is high, as indicated by the top right, bottom left, and bottom right panels in Figure 5.7. The discrepancies of u_b on wave conditions 3 and 4 are quite small (± 0.02 m/s). Hence, we need to further see how these discrepancies affect the other parameters to draw a conclusion.

Effects of different channel slopes on near-bed orbital velocity (u_b)

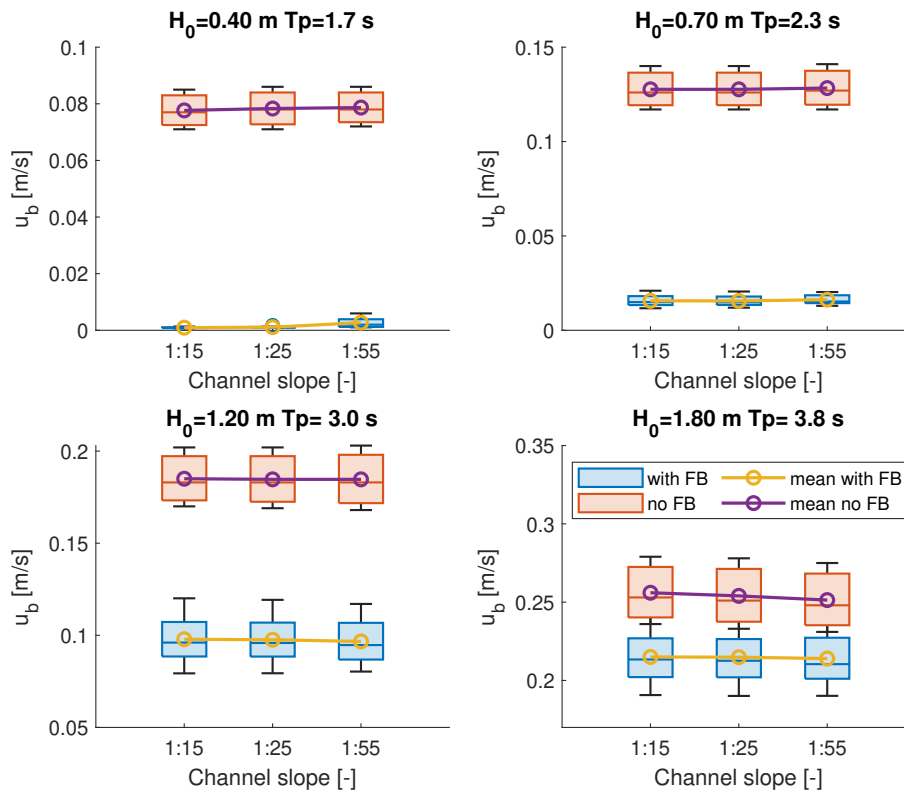


Figure 5.8. Mean near-bed orbital velocity with different channel slopes; Derived from the simulations with FB in different FB positions (h_{fb}), shoal slopes (S_s), and channel slopes (S_c); grouped based on channel slopes (S_c)

Figure 5.8 presents the magnitude of the near-bed orbital velocity when the FB is applied and not applied. It is clear that the near-bed orbital velocity decreased when the FB is applied. Furthermore, for both conditions, without and with FB, no specific channel slope is more prominent than the other channel slopes. This highlights that the channel slopes did not directly affect the overall near-bed orbital velocity.

Furthermore, the reason why there is no trend of u_b with different channel slopes is because the channel has sufficiently deeper water compared to the depths of the intertidal area. In this case, the increase in near-bed orbital velocity is not substantial when the water depth (in the channel) is sufficiently deep (Xiong et al., 2018). Hence, the limited increase in near-bed orbital velocity due to deep water in the channel is not expected to significantly affect the mean near-bed orbital velocity.

It is also important to mention that although there was little or no impact exhibited by different channel slopes on near-bed orbital velocity, the channel slopes (slightly) contributed to the reduction of the wave height along with FB. This also indirectly affects the overall near-bed orbital velocity.

Effects of different intertidal area slopes on near-bed orbital velocity (u_b)

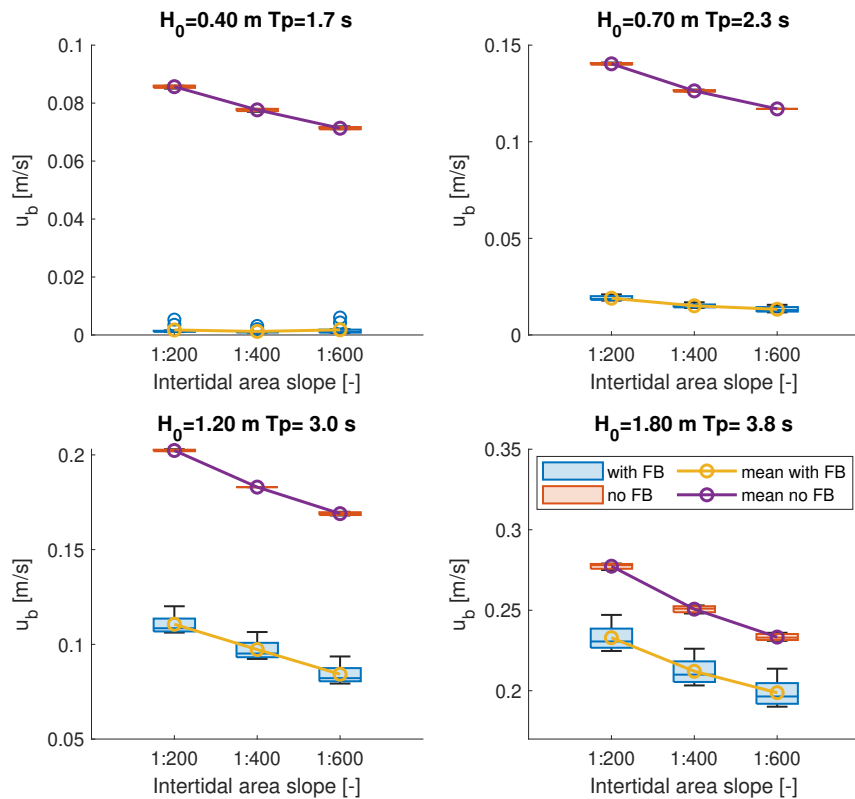


Figure 5.9. Mean near-bed orbital velocity with different intertidal area slopes; Derived from the simulations with FB in different FB positions (h_{fb}), intertidal area slopes (S_s), and channel slopes (S_c); grouped based on intertidal area slopes (S_s)

As mentioned in the previous part, the mean near-bed orbital velocity is noticeable in the intertidal area due to its shallower depth compared to the channel. Based on Figure 5.9, we can compare the magnitude of the near-bed orbital velocity on the intertidal area. In general, it is clear that the gentler intertidal area slope resulted in smaller magnitudes of mean near-bed orbital velocity compared to the near-bed orbital velocity on the steeper intertidal area slopes. This can be explained by revisiting Figure 5.5, where the transmitted wave height on the lee-side of FB is effectively reduced with the gentler intertidal area slope. Relating to the knowledge that the near-bed orbital velocity increases with the wave height (van der Werf et al., 2022), it does make sense if the near-bed orbital velocity is smaller on the gentler intertidal area slope. This is because of a more significant reduction of wave height on the gentler intertidal area slope compared to the steeper intertidal area slope.

Furthermore, with the presence of FB, under mild wave conditions (upper panels in Figure 5.9), the near-bed orbital velocity became very small (close to 0 m/s) and the "trend" (effect of steep or gentle intertidal area slope) is not prominent (see blue box charts on the upper panels in Figure 5.9). Under stronger wave conditions, the near-bed orbital velocity is still reduced with the presence of FB. However, the difference between the reduced near-bed orbital velocity due to FB and the near-bed orbital velocity without FB became smaller with increasing wave heights and wave periods. This was followed by the "trend" which appeared again (see blue box charts on the lower panels in Figure 5.9).

5.2.3 Effects of FB on bed shear stress

Overview of bed shear stress with and without FB

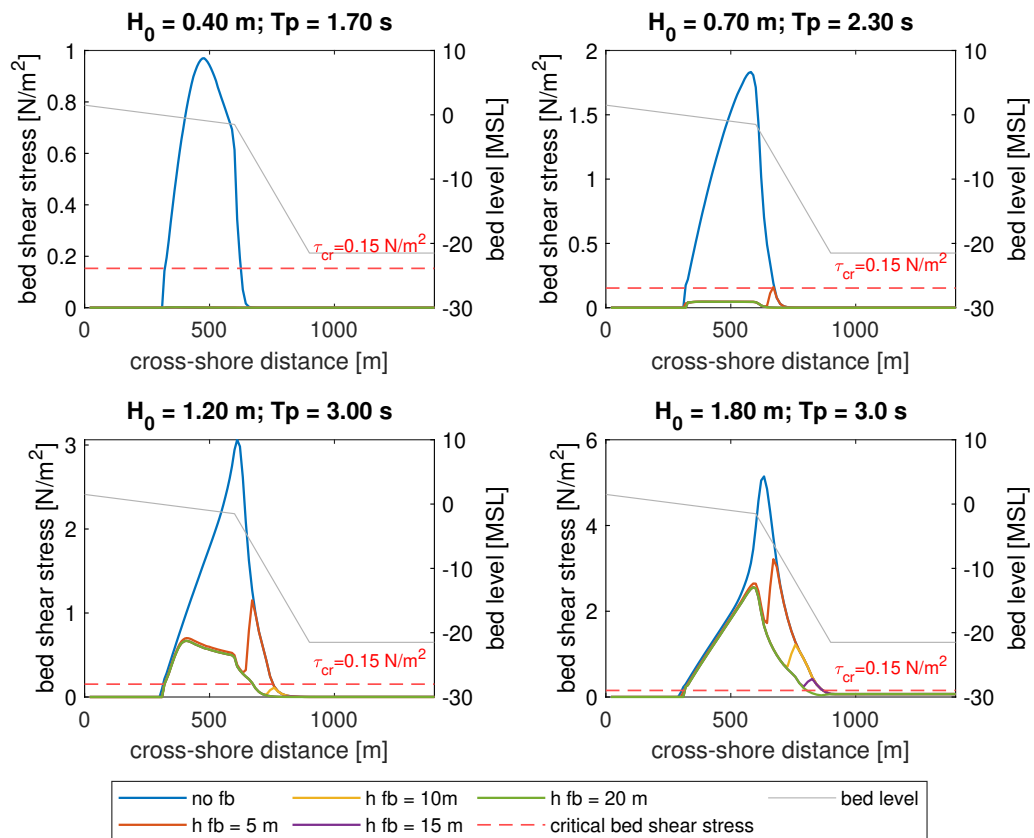


Figure 5.10. Bed shear stress under different wave conditions without and with floating breakwater in different positions (water depth at FB position); derived from the simulations with an intertidal area slope 1:200 and channel slope 1:15

By looking at Figure 5.10, it can be witnessed that the profile of magnitudes of bed shear stress exhibits similar behavior with the profile of near-bed orbital velocity (see Figure 5.6). The similarities that can be drawn are:

- Increase of magnitude (of bed shear stress) when the prescribed wave heights and wave periods increased;
- without FB, the peak (of the bed shear stress) is located on the intertidal area when the imposed wave condition is mild (wave condition 1, see blue line on the upper left panel in Figure 5.10, see Figure D.17 for the conditions with different channel slope);
- without FB, the peak (of bed shear stress) near the shoal edge when more extreme conditions were imposed (see blue line on wave conditions 2, 3, and 4: upper right, lower left, and right panels in Figure 5.10), see Figure D.17 for the conditions with different channel slope;
- with FB, the peak (of bed shear stress) is near the shoal edge when the FB is located in shallow water ($h_{fb} = 5$ m) for wave conditions 3 and 4 (see the orange line in lower panels).

Based on the previous information, and by realizing that the peaks of bed shear stress (without FB) were exceeding the critical bed shear stress, it can be interpreted that the sediment is entrained on the intertidal area when the incident wave conditions are mild (like wave condition 1, upper left panel 5.10). Meanwhile, under more extreme cases (wave conditions 2, 3, and 4), the entrainment of sediment mostly occurs near the shoal edge. The two previous statements are valid with different channel slopes and intertidal area slopes.

Next to that, with the presence of FB, there is no sediment entrainment for wave conditions 1 and 2 (due to bed shear stress below critical bed shear stress, see upper panels in Figure 5.10). Under more extreme situations (wave conditions 3 and 4), the FB could not mitigate the entrainment of sediment. For example, with the presence of FB in shallower depth at FB position (see the orange line, $h_{fb} = 5.00$ m), the bed shear stress is more significant compared to the bed shear stress with FB in deeper water. Since the exhibited bed shear stress with FB exceeds the critical, it can be argued that the presence of FB with $h_{fb} = 5.00$ m is less effective in mitigating sediment entrainment. Since the referred figure is based on one channel and intertidal area slope, a further check is provided in the upcoming part.

Effects of FB under different wave conditions on bed shear stress (τ_b)

In Table 5.4, it is seen that the bed shear stress exceeded the critical bed shear stress for all wave conditions. This observation indicates that the fluid motion (due to wave action) is generating enough force to exceed the threshold required to entrain sediment from the bed, leading to sediment transport in all wave conditions. Furthermore, when the FBs were applied, the bed shear stress for wave conditions 1 and 2 became very small, $0 - 0.025 \text{ N/m}^2$ and $0.013 - 0.019 \text{ N/m}^2$ respectively. The small bed shear stresses for these wave conditions were below the critical bed shear stress (0.152 N/m^2), indicating that no sediment would be entrained for wave conditions 1 and 2.

Under stronger wave conditions, with the FB being implemented (see lower panels in Figure 5.10), the bed shear stress decreased. However, unlike wave conditions 1 and 2, where the bed shear stresses were below critical bed shear stress, the bed shear stresses for wave conditions 3 and 4 exceeded critical bed shear stress, $0.164 - 0.241 \text{ N/m}^2$ and $0.620 - 0.779 \text{ N/m}^2$ respectively. This highlights that even though FB is present, the sediment is still entrained for wave conditions 3 and 4.

Table 5.4. Ranges and reduction percentage of the mean bed shear stress (τ_b) yielded from the simulations without FB and with FB in different water depth at FB positions (h_{fb}), intertidal area slopes (S_s), and channel slopes (S_c); τ_{cr} is critical bed shear stress

Wave conditions	τ_{cr} in N/m^2	τ_b in N/m^2		Reduction (%)
		without FB	with FB	
1) $H_0 = 0.40 \text{ m}$ $T_p = 1.7 \text{ s}$	0.152	0.245 - 0.305	0.000 - 0.025	99.1 - 99.9
2) $H_0 = 0.70 \text{ m}$ $T_p = 2.3 \text{ s}$		0.408 - 0.520	0.013 - 0.019	96.3 - 96.7
3) $H_0 = 1.20 \text{ m}$ $T_p = 3.0 \text{ s}$		0.572 - 0.751	0.164 - 0.241	67.8 - 71.3
4) $H_0 = 1.80 \text{ m}$ $T_p = 3.8 \text{ s}$		0.835 - 1.089	0.620 - 0.779	25.7 - 28.4

Effects of different water depths at FB position on bed shear stress (τ_b)

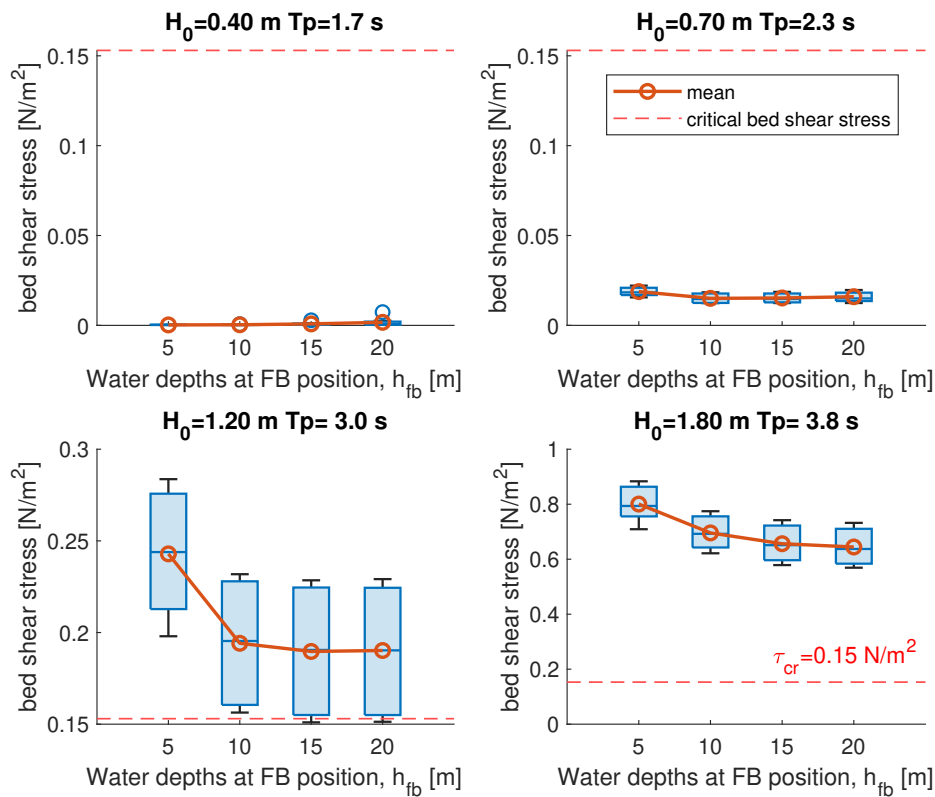


Figure 5.11. Mean bed shear stress with different water depths at FB positions; Derived from the simulations with FB in different FB positions (h_{fb}), shoal slopes (S_s), and channel slopes (S_c); grouped based on FB positions (h_{fb})

At a glance, the information in Figure 5.11 matches with the information provided in Table 5.4: FB successfully suppressed the bed shear stresses to below the critical bed shear stress (no sediment entrainment) under wave conditions 1 and 2 (upper panels). Conversely, under more energetic wave conditions 3 and 4, the mean bed shear stresses were still above the critical (sediment particle is entrained). Therefore, we do not discuss the difference in water depth at FB positions for wave conditions 1 and 2.

Furthermore, under more extreme conditions, when we compare the bed shear stress impacted by the FB in different water depths, it is seen that the FB located in deeper water exhibited higher bed shear stress. For example, under wave condition 3 ($H_0 = 1.20$ m, $T_p = 3.0$ s), magnitudes of bed shear stress with FB located in shallower (mean = ± 0.25 N/m^2) water were (on average) above the bed shear stress with the FB located in deeper water ((mean = ± 0.20 N/m^2). Nevertheless, the discrepancies of the bed shear stress with different water depths at FB positions were not significant. Morphodynamic parameters, especially erosion, will reveal whether this small discrepancies are essential or negligible.

Effects of different channel slopes on bed shear stress (τ_b)

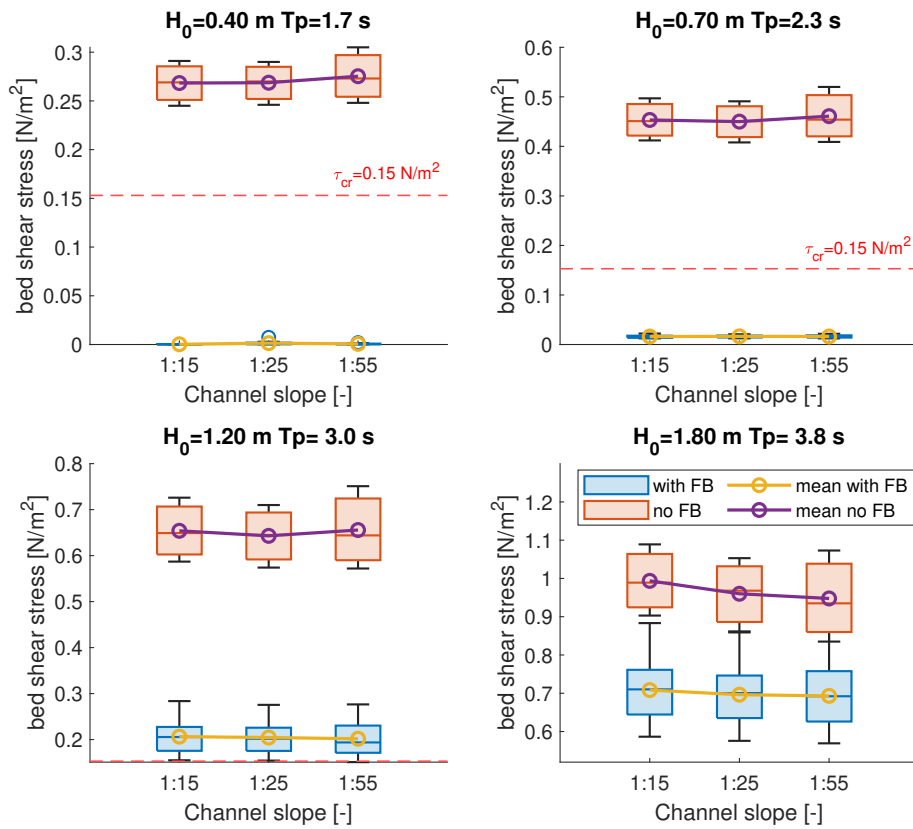


Figure 5.12. Mean bed shear stress with different channel slopes; Derived from the simulations with FB in different FB positions (h_{fb}), shoal slopes (S_s), and channel slopes (S_c); grouped based on channel slopes (S_c)

By briefly looking at Figure 5.8 (near-bed orbital velocity with different channel slopes) then Figure 5.12 (bed shear stress with different channel slopes), it can be understood that the trend of magnitude of the near-bed orbital velocity and bed shear stress are the same under different channel slopes. This confirms the relationship between these two variables.

Furthermore, the figure above shows no significant differences in bed shear stress with different channel slopes. This is because the bed shear is relatable to near-bed orbital velocity. Since the channels had deeper water than the intertidal area, there were not many discrepancies in (mean) near-bed orbital velocities with different channel slopes. This resulted in similar behavior for the bed shear stress with different channel slopes.

Effects of different intertidal area slopes on bed shear stress (τ_b)

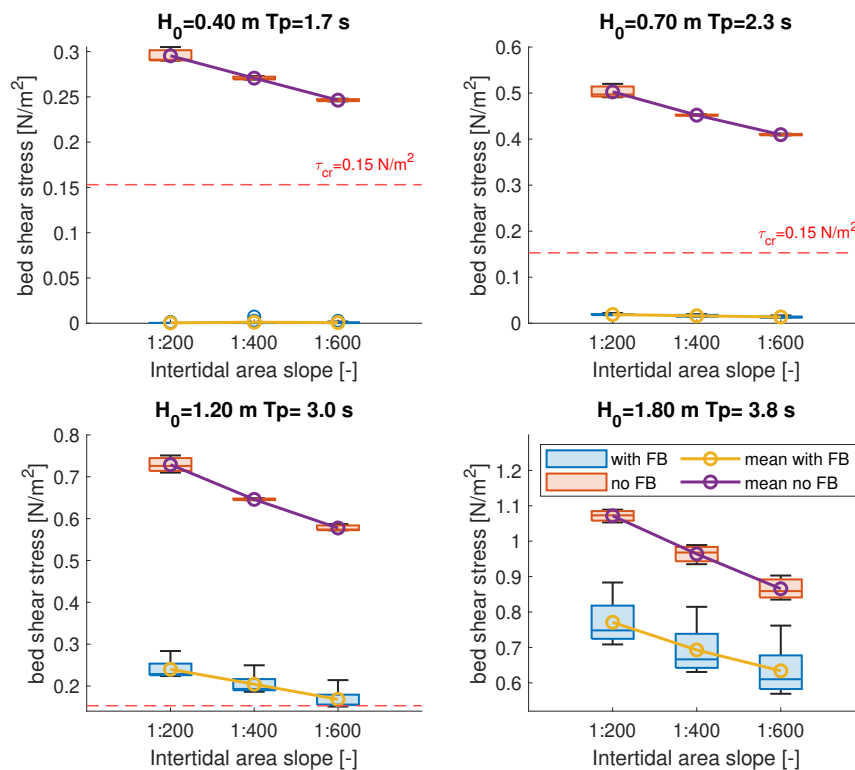


Figure 5.13. Mean bed shear stress with different intertidal area slopes; Derived from the simulations with FB in different FB positions (h_{fb}), shoal slopes (S_s), and channel slopes (S_c); grouped based on intertidal area slopes (S_s)

Figure 5.13 depicts the bed shear stress magnitudes with different intertidal area slopes. More or less, the trend shown by this figure is similar to that shown by Figure 5.9. This highlights the relationship between bed-shear stress and near-bed orbital velocity.

Furthermore, we also see that the bed shear stress is lesser on the gentler intertidal area slope compared to the bed shear stress with steeper intertidal area slope. For example, under wave condition 1 ($H_0 = 0.40$ m and $T_p = 1.7$ s), without FB, with an intertidal area slope of 1:200, the overall bed shear stress is approximately $0.3 N/m^2$. Meanwhile, the overall bed shear stress with an intertidal area slope of 1:200 is $\pm 0.25 N/m^2$. From the previous explanation, the gentler intertidal area slope could reduce the bed shear stress. Nevertheless, the difference in bed shear stress due to different intertidal area slopes is not prominent.

When the FB was imposed, significant reductions in bed shear stress were apparent, especially under mild wave conditions (upper panels in Figure 5.13). Meanwhile, under more extreme conditions, the FB reduced the bed shear stress but the magnitudes of bed shear stress were above the critical bed shear stress. Only on wave conditions 3 (bottom left panel in Figure 5.13), it seems that after FB was imposed with gentler intertidal area slope (1:600), the bed shear stress is approximately close to the critical bed shear stress. Hence, a minimal amount of sediment might have been picked upon that condition (wave condition 3 with FB intervention on intertidal area slope 1:600).

5.3 Morphodynamic effects of the floating breakwater at intertidal flats

5.3.1 Effects of FB on bed load and suspended load transport

Bed load and suspended load transport with and without FB

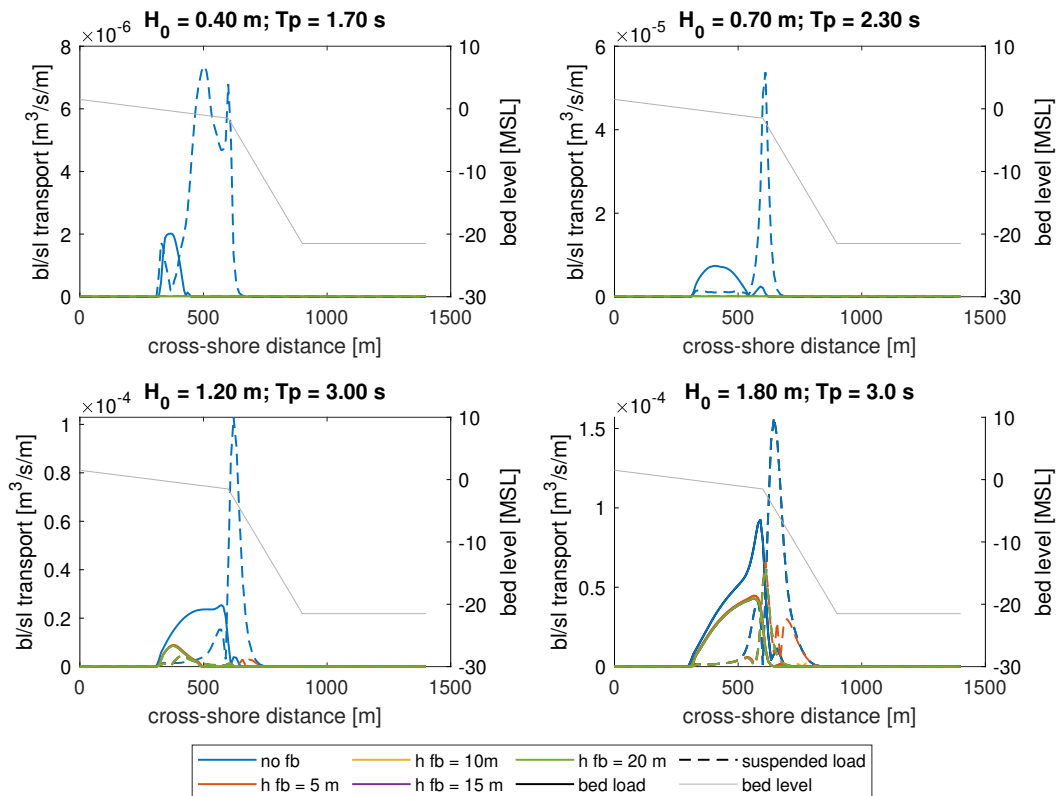


Figure 5.14. Bed load and suspended load transport under different wave conditions without and with floating breakwater in different water depths at FB position); derived from the simulations with an intertidal area slope 1:200 and channel slope 1:15

Figure 5.14 presents the bed load and suspended load transport under different wave conditions. It is seen that the more extreme wave conditions, the bigger the bed load/suspended load transport. Furthermore, when the FB is implemented, under wave conditions 1 and 2 (see upper panels Figure 5.14), it can be witnessed that there is no bed load or suspended load transport apparent. This finding is consistent with the previous observations of bed shear stress under mild wave conditions with FB intervention, where the bed shear stress remained below the critical value, which means that there is no entrainment of sediment particles.

Next, under wave conditions 3 and 4 (see lower panels in Figure 5.14 lower panels), the bed load and suspended load transport were suppressed to lower magnitudes with the presence of FB. However, the reduced bed load and suspended load transport (in wave conditions 3 and 4) were not entirely, like the reduced bed load and suspended load transport in wave conditions 1 and 2 (no sediment transport). Therefore, under wave conditions 3 and 4, we may expect erosion and sedimentation even when the FB is present.

Apart from identifying the reduced bed load and suspended load transport, in Figure 5.14, we can also see that the suspended load transport is more dominant compared to bed load transport. Putting the focus on suspended load transport, the shifting positions of the peak of suspended load transport under different wave conditions seem corroboratory with near-bed orbital velocity (see Section 5.2.2). In this case, we see in Figure 5.14 that:

- without FB, under wave condition 1 ($H_0 = 0.40$ m and $T_p = 1.70$ s), the peaks of suspended load transport (and bed load transport) are more significant on the intertidal area.
- without FB, under more extreme wave conditions 2, 3, 4 (upper right, two lower panels in Figure 5.14), the peaks of suspended load transport are apparent near the shoal edge.
- with FB, under wave condition 3 ($H_0 = 1.20$ m and $T_p = 3.00$ s), the peaks of the suspended load transport (and bed load transport) shifted to the intertidal area. For clarity, see the left panel in Figure D.24.
- with FB, under wave condition 4 ($H_0 = 1.80$ m and $T_p = 3.80$ s), the peak of the suspended load transport remained close the shoal edge. For clarity, see the right panel in Figure D.24.

The abovementioned conditions are valid for different channel slopes and intertidal area slopes. For a gentle slope of the intertidal area (1:400 and 1:600), the "peak" of suspended load transport that shifts to or on the intertidal area is of lower magnitude compared to the peak observed with a steeper intertidal area slope (1:200), see also Figure D.27.

Direction of bed load and suspended load transport

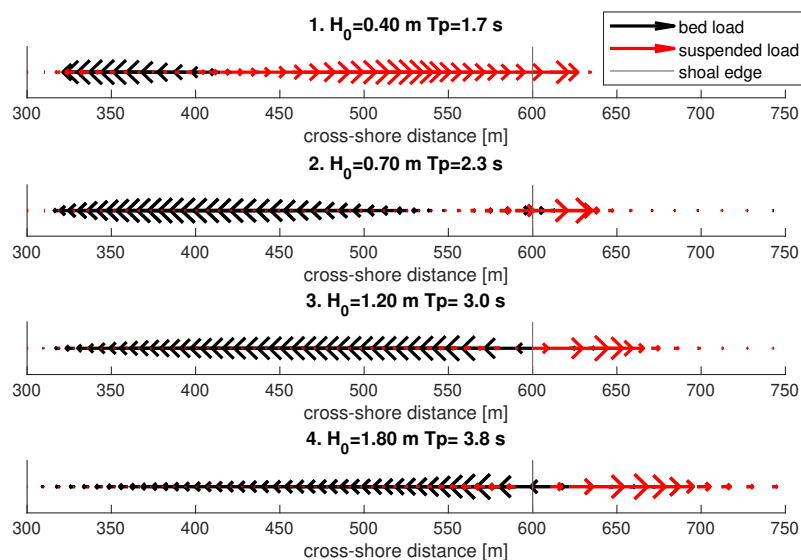


Figure 5.15. Direction of bed load and suspended load transport under different wave conditions without FB; derived from the simulation with an intertidal area slope 1:200 and channel slope 1:15

Previously, it was known that suspended load transport is more dominant than bed load transport. Based on Figure 5.15, the direction of bed load and suspended load differed. The bed load transport is toward the shoal (intertidal area). Meanwhile, the suspended load transport is toward the channel,

carrying the sediment particles outside of the intertidal area. With the dominant magnitude of suspended load transport, it can be inferred from Figure 5.15, under wave condition 1, that the material on shoal/intertidal area is transported. Meanwhile, under wave conditions 2, 3, and 4 in Figure 5.15, the suspended load transport is dominant near the shoal edge. This finding matches the explanation in the first two bullet points in the previous part: the peak of suspended load transport is more dominant on the intertidal area under mild wave conditions (wave condition 1) whereas under wave conditions 2,3,4, the peak of suspended load transport is near the shoal edge.

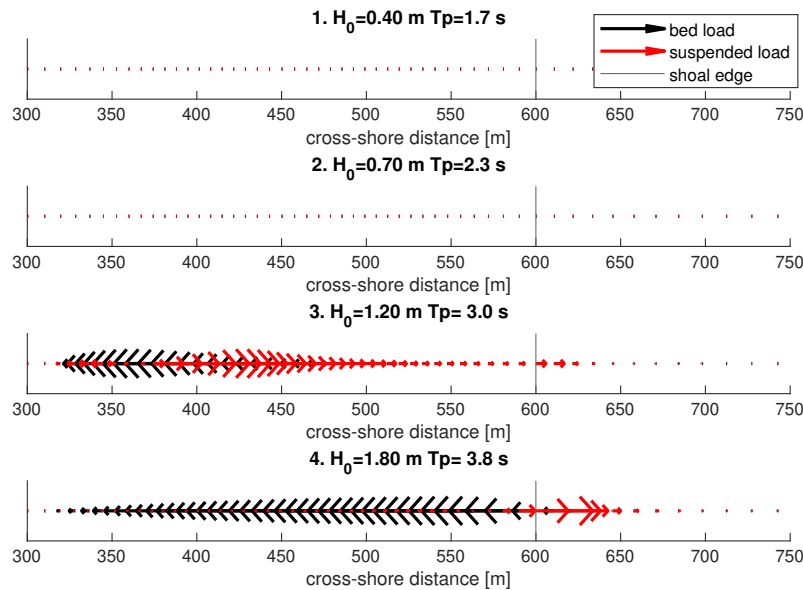


Figure 5.16. Direction of bed load and suspended load transport under different wave conditions with FB, $h_{fb} = 20$ m; derived from the simulation with an intertidal area slope 1:200 and channel slope 1:15

When the FB is applied, changes in magnitude sediment transport and where the suspended load transport starts occurring can be witnessed in Figure 5.16. With the imposed wave conditions 1 and 2, no bed load or suspended load transport was apparent (see two upper panels in Figure 5.16). Furthermore, by comparing Figure 5.16 and Figure 5.15 under wave condition 3 (the third panel from the top), we see that the starting point of suspended load transport shifted to the intertidal area. This finding matches with hydrodynamic parameters: the shifting peak of near-bed orbital velocity and bed shear stress from the shoal edge to the intertidal area when the FB was imposed with wave condition 3. From this finding, we can argue that when the wave height is low, whether because it is being transmitted by FB or a natural incident wave, suspended load transport predominantly occurs on the shoal/intertidal area. Under wave condition 4, the suspended load remains dominant near the shoal edge. This is presumably because the transmitted wave height (under FB intervention) is still high, resulting in high wave steepness. In this case, the high wave steepness most likely increases the probability of the waves breaking early near the shoal edge. The stronger effects of breaking waves near the shoal edge enhance the return velocity. Thereby, suspended load transport occurred near the edge and offshore directed.

Effects of FB under different wave conditions on bed load and suspended load transport

The previous part only discusses one intertidal area slope and one channel slope; now, mean bed load and suspended load transport with variations of water depths at FB position, intertidal area slopes, and channel slopes are summarized. Based on Table 5.5 and Table 5.6, it can be witnessed that bed load and suspended load transport entirely declined. This implies that regardless of variations in water depths at FB position, channel slopes, or intertidal area slopes, the FB can effectively reduce the wave height, eventually reducing sediment transport. For example, the presence of FB could reduce the bed load transport from a range of $8.51 \times 10^{-7} - 1.82 \times 10^{-6} \text{ m}^3/\text{s}/\text{m}$ to $0 \text{ m}^3/\text{s}/\text{m}$ and reduce suspended load transport from a range of $6.37 \times 10^{-7} - 2.43 \times 10^{-6} \text{ m}^3/\text{s}/\text{m}$ to $0 \text{ m}^3/\text{s}/\text{m}$.

We see that bed and suspended load transport were not entirely reduced under more energetic wave conditions (wave conditions 3 and 4). Based on Table 5.5 and Table 5.6, for wave condition 3, reduction of bed load and suspended load transport are in the range of 83.9% - 100% and 88.4% - 96.6%, respectively. Meanwhile, under wave condition 4, the presence of FB minimally reduces bed load and suspended load transport. In this context (wave condition 4), bed load can be reduced by around 33.6% to 34.9% and suspended load transport by 55.6% - 68.9%.

The results presented in Table 5.5 and Table 5.6 are corroboratory with the results of hydrodynamic parameters, where in general, the magnitudes of hydrodynamic parameters under milder wave conditions like wave conditions 1 and 2, can be reduced effectively. Yet, the reductions of the magnitudes under more extreme wave conditions (wave conditions 3 and 4) were ineffective.

Table 5.5. Ranges and reduction percentage of the mean bed load transport yielded from the simulations without FB and with FB in different water depths at FB positions (h_{fb}), intertidal area slopes (S_s), and channel slopes (S_c)

Wave conditions	Mean bed load transport [$\text{m}^3/\text{s}/\text{m}$]		mean BL reduction (%)
	without FB	with FB	
1) $H_0 = 0.40 \text{ m } T_p = 1.7 \text{ s}$	0 - 2.23E-07	0	100.0%
2) $H_0 = 0.70 \text{ m } T_p = 2.3 \text{ s}$	8.51E-07 - 1.82E-06	0	100.0%
3) $H_0 = 1.20 \text{ m } T_p = 3.0 \text{ s}$	4.26E-06 - 7.61E-06	0 - 1.22E-06	83.9% - 100.0%
4) $H_0 = 1.80 \text{ m } T_p = 3.8 \text{ s}$	1.01E-05 - 1.80E-05	6.70E-06 - 1.17E-05	33.6% - 34.9%

Table 5.6. Ranges and reduction percentage of the mean suspended load transport yielded from the simulations without FB and with FB in different water depths at FB positions (h_{fb}), intertidal area slopes (S_s), and channel slopes (S_c)

Wave conditions	Mean suspended load transport [$\text{m}^3/\text{s}/\text{m}$]		mean SL reduction (%)
	without FB	with FB	
1) $H_0 = 0.40 \text{ m } T_p = 1.7 \text{ s}$	3.61E-07 - 1.53E-06	0	100.0%
2) $H_0 = 0.70 \text{ m } T_p = 2.3 \text{ s}$	6.37E-07 - 2.43E-06	0	100.0%
3) $H_0 = 1.20 \text{ m } T_p = 3.0 \text{ s}$	1.62E-06 - 6.12E-06	5.53E-08 - 7.07E-07	88.4% - 96.6%
4) $H_0 = 1.80 \text{ m } T_p = 3.8 \text{ s}$	2.47E-06 - 1.20E-05	1.10E-06 - 3.73E-06	55.6% - 68.9%

Mean bed load and suspended load transport with different water depths at FB position

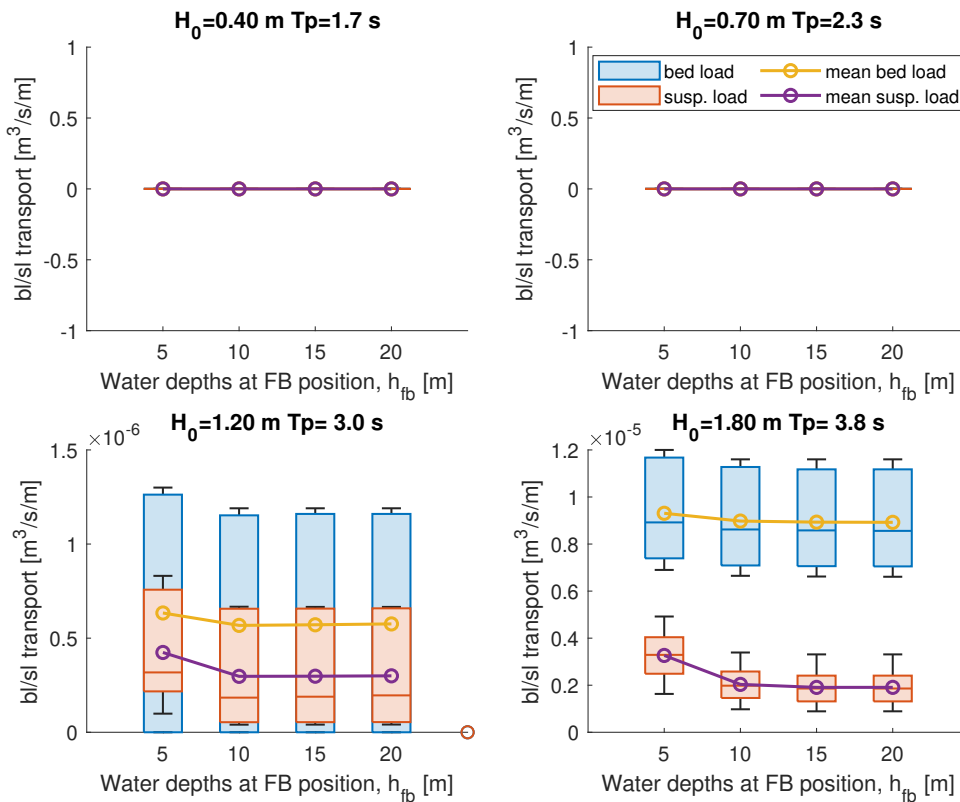


Figure 5.17. Mean bed load and suspended load transport with different water depths at FB positions; Derived from the simulations with FB in different FB positions (h_{fb}), shoal slopes (S_s), and channel slopes (S_c); grouped based on FB positions (h_{fb})

From upper panels in Figure 5.17, it is unsurprising that bed load and suspended load transport were fully reduced with the presence of FB since it was discussed previously.

Furthermore, under wave conditions 3 ($H_0 = 1.20$ m and $T_p = 3.00$ s) and 4 ($H_0 = 1.80$ m and $T_p = 3.80$ s), when the FB was located near the intertidal area ($h_{fb} = 5$ m), the reduced bed load and suspended load were insignificant compared to those with FB located offshore ($h_{fb} = [5, 10, 15]$ m). Yet, the differences in mean bed load and mean suspended load transport between different water depths at FB position were minimal, e.g., $\pm 2 \times 10^{-7}$ (suspended load, wave condition 3) and $\pm 2 \times 10^{-6}$ (suspended load wave condition 4). Hydrodynamic parameters (wave height, near-bed orbital velocity, and bed shear stress) also exhibited these minimal differences. We must clarify whether considering FB placement based on water depths is essential by checking the erosion impacted by different water depths at FB position. This is discussed in the next section.

Mean bed load and suspended load transport with different channel slopes

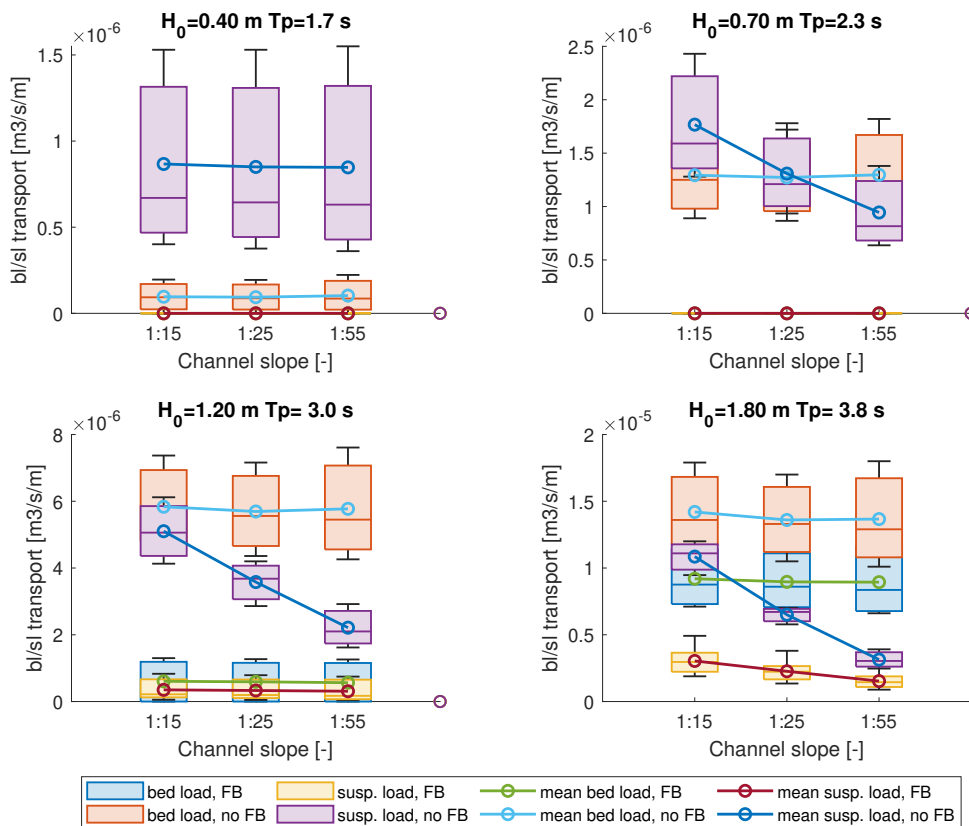


Figure 5.18. Mean bed load and suspended load transport with different channel slopes; Derived from the simulations with FB in different FB positions (h_{fb}), shoal slopes (S_s), and channel slopes (S_c); grouped based on channel slopes (S_c)

With different channel slopes imposed, it can be seen that there was no trend exhibited by bed load transport. This was also confirmed by two other hydrodynamic parameters: near-bed orbital velocity and bed shear stress, where there was no trend of magnitudes with different channel slopes. This can be explained by the bed load transport that is mostly occurring in intertidal areas (see Figure 5.15 and Figure 5.16). Thus, bed load transport is most likely impacted by different intertidal area slopes.

Furthermore, there is a difference in the trend of suspended load transport between wave condition 1 (upper left panel in Figure 5.18) and wave conditions 2, 3, and 4 (upper right, lower left, and lower right panels). In this context, the suspended load transport under wave condition 1 is not affected by different channel slopes, whereas wave conditions 2, 3, and 4 showed a 'trend': with a steeper channel slope (1:15), the suspended load transport is higher than those the suspended load transport with gentler channel slope, i.e., 1:15 and 1:55. This occurs because the suspended load transport under mild wave condition (wave condition 1) predominantly occurs on the shoal or intertidal area (see the first panel from the top in Figure 5.15). Regarding the 'trend,' this occurs since the steep slope intensifies wave breaking, subsequently leading to a higher suspended load transport (compared to the suspended load on gentler channel slope) (Knook, 2013).

Mean bed load and suspended load transport with different intertidal area slopes

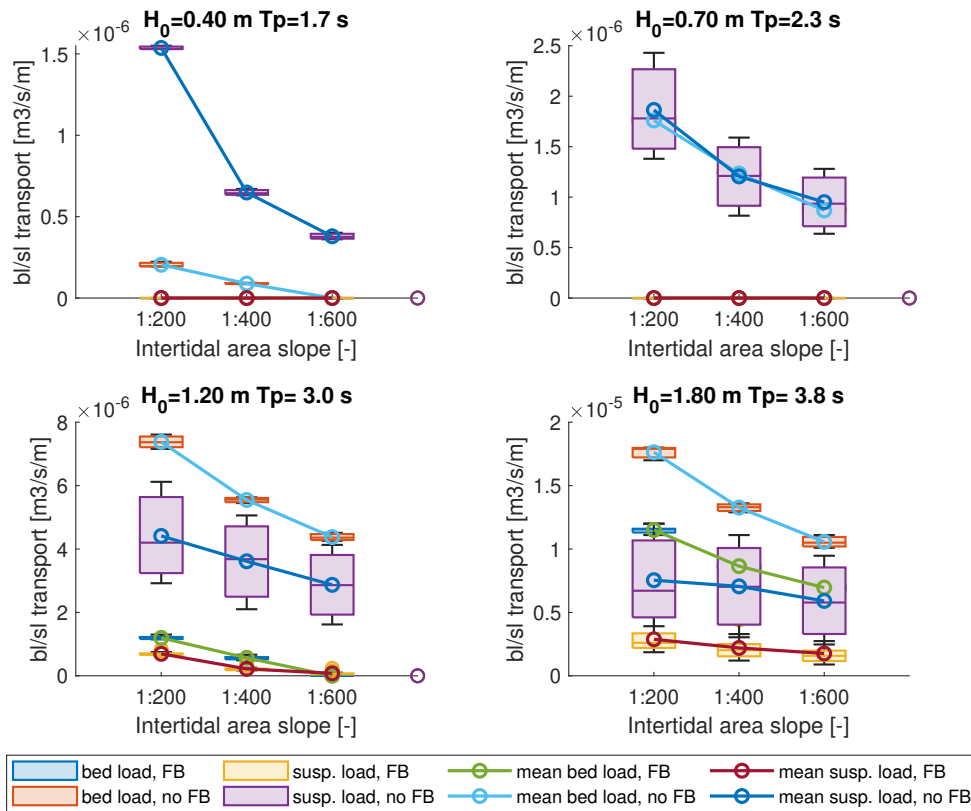


Figure 5.19. Mean bed load and suspended load transport with different intertidal area slopes; Derived from the simulations with FB in different FB positions (h_{fb}), shoal slopes (S_s), and channel slopes (S_c); grouped based on intertidal area slopes (S_s)

Figure 5.19 presents the effects of different intertidal area slopes on bed load and suspended load transport. Overall, we see a consistent bed load and suspended load transport trend on different intertidal area slopes. The trend shows that the magnitude of bed load and suspended load transport is higher with the steep intertidal area slope (1:200) than with the gentle intertidal area slope.

Regarding the effect of intertidal area slope, it is still difficult to judge whether Figure 5.19 shows a significant or small difference in bed load/suspended transport with different intertidal area slopes. The clear effect of the intertidal area can be seen in the upper left panel, where the bed load transport can be fully declined from around $0.2 \times 10^{-6} \text{ m}^3/\text{s}/\text{m}$ ($S_s = 1:200$) to $0 \text{ m}^3/\text{s}/\text{m}$ ($S_s = 1:600$). Another example is in the lower left panel, where with FB, bed load ($\pm 1 \times 10^{-6} \text{ m}^3/\text{s}/\text{m}$) and suspended load transport ($\pm 1 \times 10^{-6} \text{ m}^3/\text{s}/\text{m}$) can be reduced to $0 \text{ m}^3/\text{s}/\text{m}$ ($S_s = 1:600$). More clarity on how different intertidal area slopes affect erosion is further discussed in the next section.

5.3.2 Effects of FB on the cross-sectional area of erosion at intertidal area

Overview of erosion with and without FB

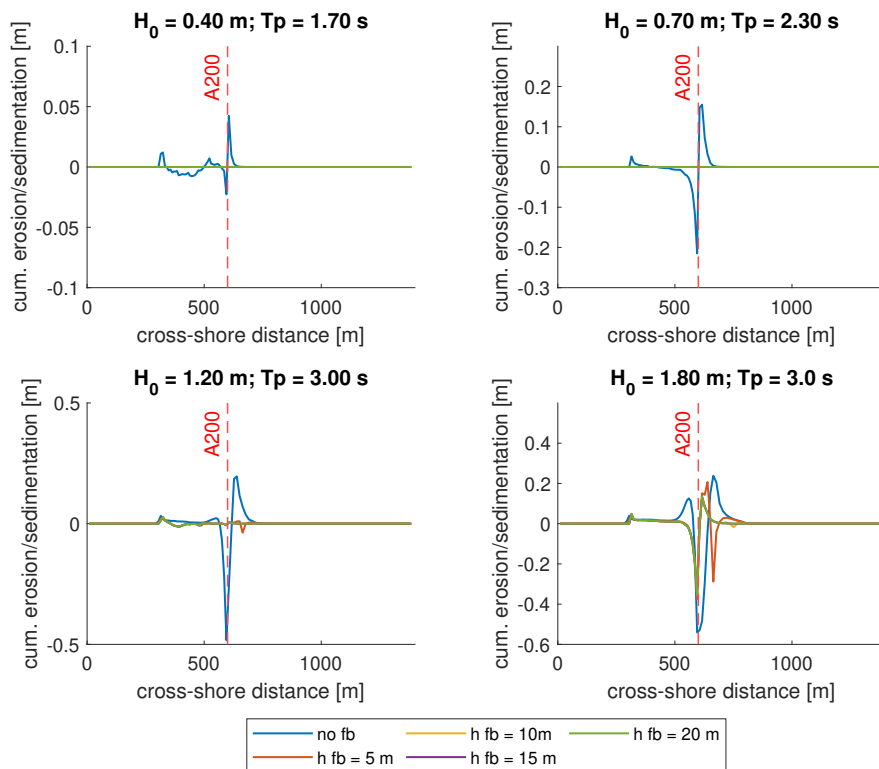


Figure 5.20. Cumulative erosion and sedimentation under different wave conditions without and with floating breakwater in different water depths at FB position; derived from the simulations with an intertidal area slope 1:200 and channel slope 1:15; A200 represents shoal edge for this specific intertidal area slope (see Figure 3.12)

In Figure 5.20, we see that different wave conditions resulted in different amounts of erosion and different erosion patterns. Under wave condition 1 (see Figure 5.20 upper left panel), (minimum) erosion occurred in the intertidal area with a slightly higher accretion near the shoal edge (A200). Under this wave condition, the eroded (and accreted) location turned into a non-eroded and -accreted location (see green line on the upper left panel in Figure 5.20. This finding also matches the peak of suspended load (also near-bed orbital velocity and bed shear stress) that peaked on the intertidal area when mild wave condition 1 was imposed.

Next, with a more powerful wave condition, wave condition 2, the erosion became deeper, especially near the edge (A200) (see Figure 5.20 upper right panel). Nonetheless, the presence of FB also mitigated the erosion, proven by the flat line, indicating that there was no erosion occurring.

Next, under the two biggest wave conditions (see Figure 5.20 lower panels), it is also seen that erosion is more concentrated near the intertidal area/shoal edge (A200). This corresponds to the peaks of near-bed orbital velocity/bed shear stress/suspended load transport shifting to the shoal edge's vicinity.

The presence of FB apparently reduced erosion for both wave conditions. To better see how impactful FB is in reducing erosion under varying conditions, see the results in the next part.

Effects of FB under different wave conditions

Based on Table 5.7, it can be seen that under mild wave conditions 1 and 2, the presence of FB could effectively prevent the intertidal area from erosion. With 12 hours of simulations in Delft3D, wave conditions 1 ($H_0 = 0.40$ m $T_p = 1.7$ s) without FB could result in erosion with a range of $0.50\ m^2$ to $1.01\ m^2$ while wave conditions 2 ($H_0 = 0.70$ m $T_p = 2.3$ s) with a range $2.52\ m^2$ to $5.29\ m^2$. The aforementioned erosion can be reduced to $0.00\ m^2$ with the presence of FB (100% reduction).

Furthermore, under more extreme wave conditions 3 and 4, erosion occurred more severely, and the presence of FB helps to reduce the erosion. In 12 hours, erosion due to $H_0 = 1.20$ m $T_p = 1.7$ s which ranges from $5.68\ m^2$ to $12.10\ m^2$ can be reduced to $0.21\ m^2 - 0.88\ m^2$ (92.7 - 96.4% reduction). Wave condition 4 is more severe, preventing the FB from effectively attenuating waves, resulting in (still) more intense wave height propagating to the intertidal area. Thereby, more significant erosion, $11.55\ m^2 - 24.08\ m^2$ can only be reduced to $4.92\ m^2 - 9.01\ m^2$ (57.4% - 62.6% reduction).

It is worth mentioning that two erosion events range from $0.50\ m^2 - 1.01\ m^2$ (wave condition 1 without FB) and $0.21\ m^2 - 0.88\ m^2$ (wave condition 3 with FB) were most likely took place on the intertidal area (see Figure 5.15 and Figure 5.16). This is because the mild (transmitted) wave height breaks further onshore (on the intertidal area) (EcoShape, 2020). This wave breaking made the sediment in suspension, and the return flow carried the sediment. As a result, erosion took place on the shoal/intertidal area.

Apart from that, more significant erosion due to wave conditions 2, 3, and 4 (without FB) would mostly occur near the shoal edge due to wave breaking that occurred before entering the intertidal area. Under FB intervention, only wave condition 4 encountered erosion near the shoal edge, accounting for $4.92 - 9.01\ m^2$.

Table 5.7. Ranges and reduction of erosion yielded from the simulations without FB and with FB in different water depths at FB positions (h_{fb}), intertidal area slopes (S_s), and channel slopes (S_c)

Wave conditions	Cross-sectional erosion area [m^2]		reduction of erosion (%)
	without FB	with FB	
1) $H_0 = 0.40$ m $T_p = 1.7$ s	0.50 - 1.01	0.000	100%
2) $H_0 = 0.70$ m $T_p = 2.3$ s	2.52 - 5.29	0.000	100%
3) $H_0 = 1.20$ m $T_p = 3.0$ s	5.68 - 12.10	0.21 - 0.88	92.7% - 96.4%
4) $H_0 = 1.80$ m $T_p = 3.8$ s	11.55 - 24.08	4.92 - 9.01	57.4% - 62.6%

Effects of FB in different water depths at FB positions

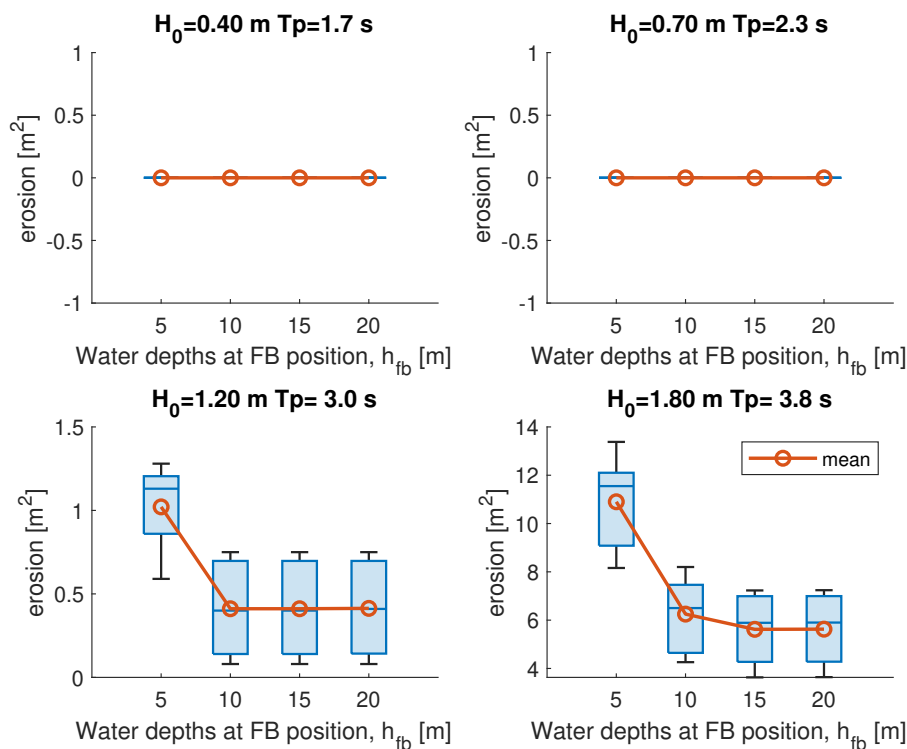


Figure 5.21. Cross-sectional erosion with different water depths at FB positions; Derived from the simulations with FB in different FB positions (h_{fb}), shoal slopes (S_s), and channel slopes (S_c); grouped based on FB positions (h_{fb})

According to Figure 5.21 on the upper panel, erosion did not occur with the presence of FB regardless of the water depths at the FB position.

Under stronger wave conditions (see lower panels in Figure 5.21), with FB intervention, the erosion still occurred. The trend shown by the lower panels is more or less the same as those shown by wave height, near-bed orbital velocity, bed shear stress, bed load, and suspended load transport for the effects of FB with different water depths at FB positions. Based on those results, it seemed that the difference between the magnitudes of those parameters with different water depths at FB position is minimal.

Furthermore, when seeing the mean of the area of erosion with different water depths in Figure 5.21 above, it can be seen that when we place the FB within 12 hours in shallow water ($h_{fb} = 5 m$), erosion is around $1 m^2$ (wave condition 3, lower left panel). Yet, when the FB is located more offshore, erosion is half of the mentioned value ($\pm 0.5 m^2$). This applies to wave condition 4, where erosion is almost $\pm 12 m^2$ with FB in shallower water ($h_{fb} = 5 m$), whereas the FB in deeper water could reduce erosion until reaching half of it ($6 m^2$).

Effects of FB with different channel slopes on erosion

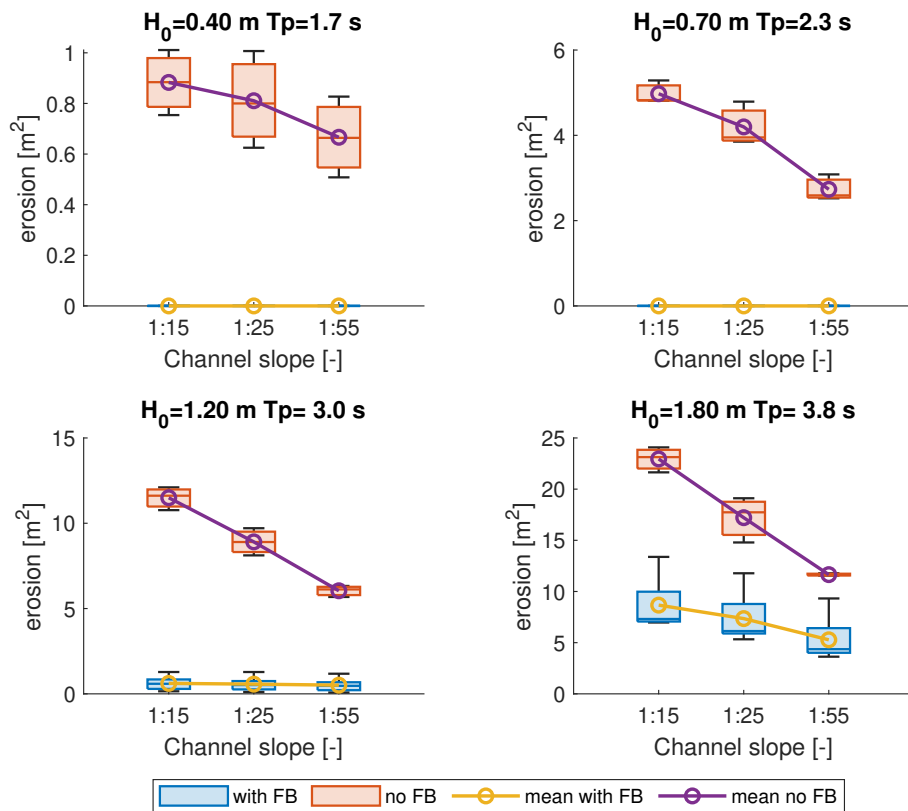


Figure 5.22. Cross-sectional erosion with different channel slopes; Derived from the simulations with FB in different FB positions (h_{fb}), shoal slopes (S_s), and channel slopes (S_c); grouped based on channel slopes (S_c)

On different channel slopes, the cross-sectional area of erosion varied. In this case, the trend in Figure 5.22 shows that erosion is more dominant with the steep channel slope. The difference in the cross-sectional erosion area with different channel slopes became clearer when the wave condition was more severe. For example, without FB and the incident wave height of $H_0 = 0.40$ and $T_p = 1.7$ s, the erosion varied in a range of $0.6 \text{ m}^2 - 0.9 \text{ m}^2$. Still without FB, under the most extreme case with $H_0 = 1.80$ and $T_p = 3.8$ s, the erosion area varied in a wider range than the previous case, $10 \text{ m}^2 - 24 \text{ m}^2$. This is because erosion occurred more near the shoal edge and channel with more severe wave conditions. Hence, a wide variation in erosion could be seen with different channel slopes in that condition.

With the FB intervention, it can be witnessed that mild wave conditions exhibit a full reduction of erosion (see upper panels in Figure 5.22). With a more energetic wave, $H_0 = 1.20$ and $T_p = 3.0$ s, under FB intervention, it is apparent that different channel slopes did not demonstrate any difference (no trend appeared). This is presumably due to the erosion that was happening in the intertidal area (see the third panel in Figure 5.16) in that wave condition. Finally, under $H_0 = 1.80$ and $T_p = 3.8$ s with FB intervention, the trend of more significant erosion on the steep slope persisted. This indicates that erosion was still occurring near the shoal edge. The amount of erosion was affected by different channel slopes.

Effects of FB with different intertidal area slopes on erosion

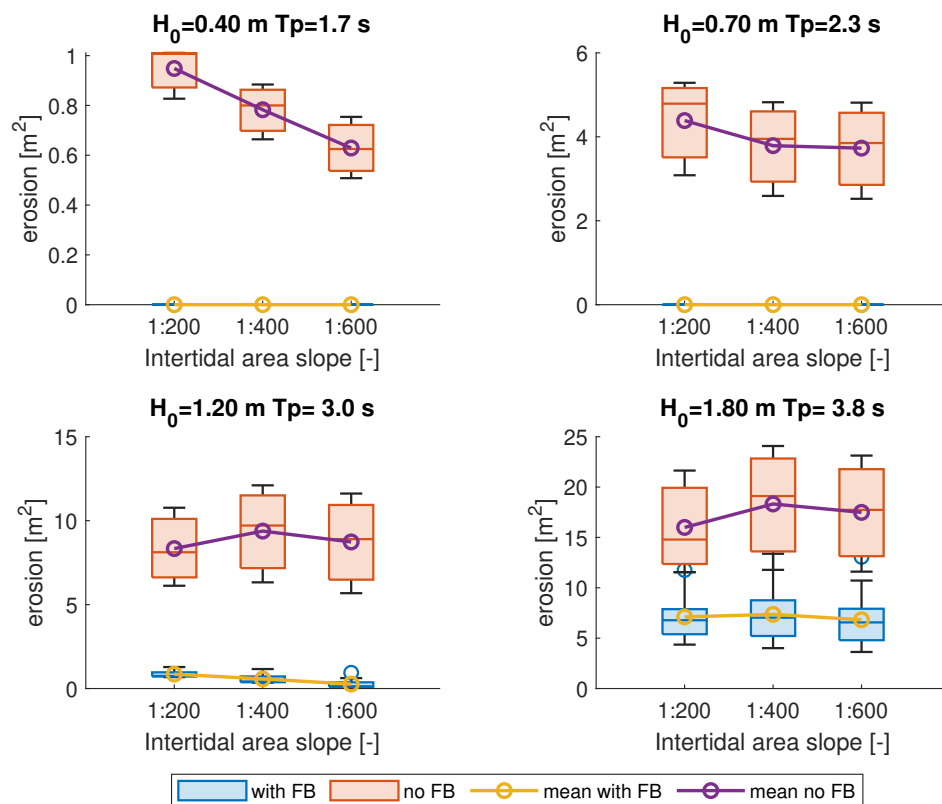


Figure 5.23. Cross-sectional erosion with different intertidal area slopes; Derived from the simulations with FB in different FB positions (h_{fb}), shoal slopes (S_s), and channel slopes (S_c); grouped based on intertidal area slopes (S_s)

On different intertidal area slopes, it is apparent that only under wave condition 1 ($H_0 = 0.40$ m $T_p = 1.7$ s) did the difference in the erosion area appear: trend showing that steep intertidal area slope resulted in more significant erosion compared to erosion with gentle intertidal area slope. With more extreme wave conditions, the trend did not appear anymore. This emphasized that there was no effect on erosion with different intertidal area slopes. This occurred due to erosion that took place near the shoal edge.

With FB intervention, no more erosion appeared for mild wave conditions shown in the upper panels in Figure 5.23. Next to that, under more extreme cases ($H_0 = 1.20$ m $T_p = 3.0$ s and $H_0 = 1.80$ m $T_p = 3.8$ s), with FB intervention, there were no significant differences of erosion with different intertidal area slopes. This highlights that the influence of intertidal area slope is insignificant after FB is implemented.

6 Discussion

6.1 Limitations of the current study

6.1.1 Model dimension

Even though Delft3D can resolve 2D (depth-averaged) or 3D computation (Deltares, 2023b), the current study uses uniform alongshore bathymetry similar to a one-dimensional (1D) cross-shore model. In this case, considering the 1D model is useful in conceptually understanding the effects of FB in varying conditions with less computation time. Therefore, with less computational time, various scenarios and the impact of different parameters can be assessed, like the simulations carried out in the second research phase. Regardless of the mentioned benefits, there are limitations of the 1D cross-shore model, such as:

- 1D model could not capture the velocity profile that may vary over the depth. Regarding this, Koftis et al. (2006) performed 2DV simulations to assess the hydrodynamic characteristics. Their study found a jet-type flow pattern at the seaward side of the FB. In the current study, with the FB represented by the transmission coefficient, the velocity that pass the transmission coefficient is reduced (see Figure D.10),
- 1D model could not model the oblique incident wave, including the important processes that may occur in the Eastern Scheldt, like wave refraction,
- 1D-models may not represent the sediment behavior, location of the accumulation, and sediment patterns since the sediments do not move in one direction with the flow (Theol, 2020). Reflecting on the sediment transport on the Roggenplaat (which is the intertidal area referred to in the current study), the sediment transport is mainly in the north-eastern direction (van der Werf et al., 2019). This sediment transport direction cannot be confirmed since a 1D model is used in the current study.

In the first research phase, the data used to validate the capability of Delft3D to model the FB effects was only based on the observed cross-section in the laboratory by Shimoda et al. (1991).

6.1.2 Excluded process and condition in the second research phase

Fundamentally, the model does not capture all the processes and details that occur in reality. To be able to generate the desired output while ensuring the reasonable time consumed to perform the model and undertake this study, some aspects or important parameters were simplified or not included in this study. Nevertheless, these aspects or parameters might be important in relation to the process occurring in the intertidal flats or channel-shoal system like what we simulated in our model.

Wind

In the second research phase, since the wave conditions (wave height and wave period) are generated using the wind data, the wind process in Delft3D is not included. Nevertheless, the wind may result in different wave height behavior when it is imposed in Delft3D separately from wave height. Figure 6.1 below explains how the wave height behavior may change due to the wind effect prescribed in Delft3D.

Based on Figure 6.1, it can be seen that the wave height increased when the wind process with a velocity of 5 m/s was included in the Delft3D model. Adding wind in the second research phase may add insights into the effectiveness of FB when different wind velocities are imposed.

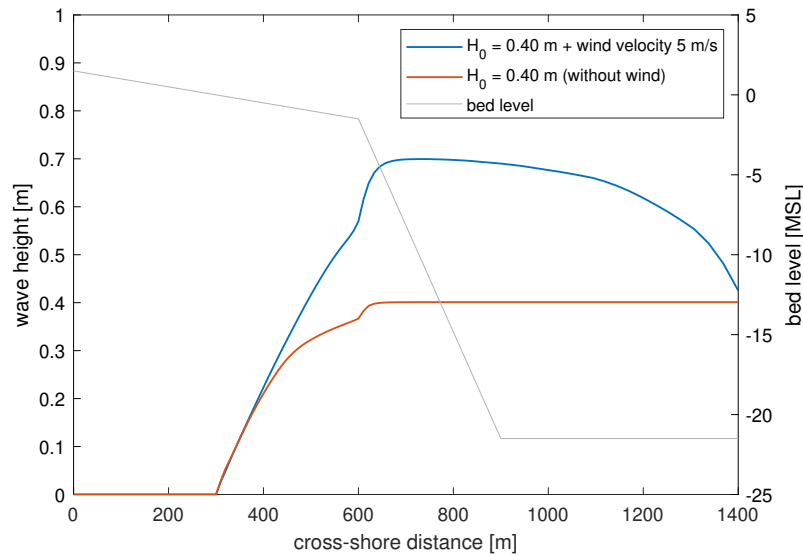


Figure 6.1. Behaviour of the wave height without and with wind input in Delft3D, simulated with $H_0 = 0.40$ m and $T_p = 1.7$ s, the case with wind process is imposed with a wind velocity of 5 m/s

Grain size

The grain size used for the simulations in the second research phase in the current study is $150 \mu\text{m}$. In this context, the sediment grain size refers to the information provided by [Eelkema \(2013\)](#). Nevertheless, there is different information in the sediment grain size representative of the sediment particle in the Eastern Scheldt reported by other researchers. For example, in citing [Kohsiek et al. \(1987\)](#), [de Vet et al. \(2017\)](#) informed that the intertidal areas near the mouth of the ES are characterized by a typical median grain size of around $200 \mu\text{m}$, whereas further from the mouth grain sizes in the order of $150 \mu\text{m}$ are more typical. In another study, [Pezij \(2015\)](#) used a median sediment grain size of $180 \mu\text{m}$. With discrepancies in sediment diameter being used in different studies, understanding the different effects of different median sediment diameters could be insightful. This is because there might be different erosion areas and different erosion patterns due to different prescribed median sediment grain size (D_{50}).

Tide level variation

[Beiboer \(2020\)](#) stated that some parts of the intertidal flat's erosion are related to large fetch, which influences the waves and morphological process. Our study also considered the fetch and wind speed to derive the wave conditions. However, other processes like tide level variations might be important for the intertidal flats. Regarding this, [Beiboer \(2020\)](#) stated that the average astronomic low water tide is -1.5 m NAP, and the average astronomic high tide is $+1.5$ m NAP in the Eastern Scheldt. With this information, we can reflect on the current study that the model would be more informative if we included the mentioned low and high tides. In this study, we only prescribed one water level for all simulations, which is 0 m NAP.

6.1.3 Schematized bathymetry

The bathymetry for the model input was established by referring to Roggenplaat's slope maps for the intertidal area slope and Roggenplaat's cross-sections for the channel slope. It is realized that the bathymetry is not similar to the derived bathymetry in this study. Hence, the detailed local evolution due

to the forcing in the intertidal flats would not be captured well in this study. For instance, [EcoShape \(2020\)](#) reported that during storm wave conditions, wave breaking could occur everywhere on the shoal, and no areas are sheltered; erosion is ubiquitous in the intertidal areas. Meanwhile, with the simplified bathymetry, this study found that the erosion occurred near the edge for more extreme wave conditions. The difference in bathymetry could be part of the cause of this discrepancy, in addition to storm surge or tidal variations in water levels.

6.1.4 FB specifications and Macagno relation for the second research phase

We only consider one FB specification for the second research phase—the FB with a width of 8.0 m and a draft of 2.2 m. This resulted in small transmission coefficients, especially under milder wave conditions (see [Table 5.1](#)). We realized that varying FB specifications, like different FB widths and drafts, could alter the transmission coefficient, adding more uncertainties in the hydrodynamic and morphodynamic analysis. This is also interesting for further research: variation of the draft and width of FB. Nevertheless, if we want to keep the FB performance as reported in this study, we could creatively explore the FB specification (width and draft) by knowing the transmission coefficient associated with the derived wave conditions in this study and using the Macagno relation (see [Equation 2](#)). Regarding the applicability of the Macagno relation, the theory of Macagno was compared by the laboratory experiment and numerical model by [Biesheuvel \(2013\)](#). This is further discussed in [Section 6.2.2](#).

6.2 Evaluation based on relevant previous studies

6.2.1 Shimoda experiment vs Delft3D model

In the first research question, three cross sections observed in the experiment by [Shimoda et al. \(1991\)](#) were reproduced. Based on the results, we found some similarities and differences. The similarities were related to the capability of the model to predict the cross-sections when evaluating the Delft3D performance according to the error statistics (see [Table 4.1](#), [Table 4.2](#), [Table 4.3](#)). Furthermore, the Delft3D model could also yield more or less similar areas of cross-sectional erosion (see [Figure 4.2](#), [Figure 4.5](#) and [Figure 4.8](#)). Nonetheless, Delft3D could not capture the pattern shown by the cross-sections from the laboratory experiment. This is presumably because of:

- The derivation of the cross-shore profile of the experiment is affected by a non-straight axis (see [Figure 3.3](#)), making it difficult to achieve accurate digitization. As a result, the derived cross-shore profile may be imprecise, leading to discrepancies between the experimentally obtained profile and the one simulated by the Delft3D model.
- The cross-shore profile reported by [Shimoda et al. \(1991\)](#) did not fully represent the evolved bed profile in the wave flume. This can be presumed when we see the unfinished cross-shore profile from the experiment in [Figure 4.3](#)—also the imbalance between the erosion and sedimentation span and area in the same figure (for the experiment).
- Only conducting sensitivity analysis for a few parameters, but not carrying out other relevant parameters. For example, by trying to vary parameters other than the model settings varied in the first research phase, like *Sus* (Multiplication factor for suspended sediment reference concentration) and *Bed* (Multiplication factor for bed-load transport vector magnitude).
- Simplifying the FB with transmission coefficient. This results in different behaviors. For example, by modeling FB using the transmission coefficient, the depth-averaged velocity

decreased, resulting in accretion in the vicinity of FB. However, in the laboratory experiment, scouring occurred beneath the FB, presumably due to increased flow velocity below the FB. In this context, the transmission coefficient as input in Delft3D could not capture this process.

- Limited data of hydrodynamics measurements. In this case, Shimoda et al. (1991) only reported the evolved cross-sections. The hydrodynamics measurements were not provided, for example, wave height, making it difficult to validate the model more thoroughly before replicating the observed cross-sections in Delft3D.

6.2.2 Applicability of Macagno relation

Biesheuvel (2013) undertook a study on the effectiveness of different FB types. Several formulas that can be used to compute the transmitted wave height, i.e., transmission coefficient, were compared with each other. Also, the formulas were compared with the results of laboratory experiments. The comparison results were used to draw conclusions regarding the applicability of the most appropriate formula, which can be used to compute the transmission coefficient. In this study, we also use a formula that was evaluated by Biesheuvel (2013), which is the so-called Macagno relation (read Section 2.2). For the Macagno relation (Equation 2), Biesheuvel (2013) described that the relation could be applicable if these criteria hold:

1. $0.4 < \frac{B_f}{h_{fb}} < 1.1$, where B_f is width of FB and h_{fb} is water depth (at FB position)
2. $\frac{D_f}{h_{fb}} < 0.2$, where D_f is draft of FB and h_{fb} is water depth (at FB position)
3. $0.60 < X < 1.20$, in this case, $X = \frac{T_p}{2\pi} \sqrt{\frac{g}{D_f + 0.35B_f}}$

According to Biesheuvel (2013), when a formula was implemented without complying with these criteria, the calculated transmission coefficient might be overestimated. To check the wave periods or the water depths at FB positions in the current study that comply with the criteria by Biesheuvel (2013), Table 6.1 is provided.

Table 6.1. Evaluation of the data being used in the second research phase for checking the applicability of Macagno relation; text in *italic* means it does not comply with the criteria; criteria one and two depend on water depth at FB positions h_{fb} ; criteria three dependant on wave period T_p ; $B_f = 8.00\text{ m}$ and $D_f = 2.20\text{ m}$

No	Criteria	$h_{fb}=5\text{ m}$	$h_{fb}=10\text{ m}$	$h_{fb}=15\text{ m}$	$h_{fb}=20\text{ m}$
1	$0.4 < B_f/h < 1.1$	1.60	0.80	0.53	0.40
2	$D_f/h < 0.2$	0.44	0.22	0.14	0.11
		Tp=1.7 s	Tp=2.1 s	Tp=3.0 s	Tp=3.8 s
3	$0.60 < X < 1.20$	0.38	0.46	0.67	0.85

Table 6.1 shows that $h_{fb} = 5\text{ m}$ did not comply with criteria 1 and 2, and $h_{fb} = 10\text{ m}$ did not comply with criteria 2. This suggests that the calculated transmission coefficient with $h_{fb} = 5\text{ m}$ and 10 m are presumably overestimated. Moreover, it can be noticed that $T_p = 1.7\text{ s}$ and $T_p = 2.1\text{ s}$ did not conform to criteria 3, implying that the calculated transmission coefficients under these wave periods were presumably overestimated. When the value of the transmission coefficient is overestimated, it is then presumed that the effectiveness of FB is slightly less than the real effectiveness possessed by

FB. As a result, the wave height reduction capacity of FB represented by the transmission coefficient does not accurately reflect the actual wave height reduction capacity. Nevertheless, for a preliminary design, this overestimation is not very relevant and a reasonable estimation is still obtained regarding the effectiveness of the floating breakwater without considering the mentioned criteria (Biesheuvel, 2013).

6.2.3 Channel-shoal (intertidal area) interaction

EcoShape (2020) reported that based on the process-based modeling, the process that caused the degradation of Galgeplaat (one of the intertidal flats in the Eastern Scheldt) is the combination of breaking waves and wave-induced current. During calm weather (weaker wave conditions), waves break on the shoal's upper part, influenced by wave height, local seabed configuration, and water level. As a result of these breaking waves, erosion is induced in the intertidal area (landward of the shoal edge). Presumably, erosion occurred due to the suspended sediment being carried by the wave-induced current, e.g., return flow.

The information in the previous paragraph implies that there is an agreement on the result of process-based modeling reported by EcoShape (2020) with the result of the current study. In this context, we could see that under calm wave conditions, the erosion occurred in the intertidal area (see the upper left panel in Figure 5.20 and wave condition 1 in Figure 5.15). Also, the erosion occurred in the intertidal area when the FB dissipated wave height to a sufficiently low wave height (see wave condition 3 in Figure 5.16). The erosion occurred in the intertidal area because of wave breaks on the upper part (shoal), stirring up the sediment into suspension, which is then transported by the return flow (see wave condition 1 in Figure 5.15).

Furthermore, EcoShape (2020) also reported that wave breaking is not only limited to the higher areas during storm events. Hence, erosion might be widely spreading on the intertidal flats environment. If we relate this information to our finding, it is not fully in line since more intense waves in the current study resulted in erosion near the shoal edge. The difference can be that this study did not include the rising water level for the storm event. Hence, the spread of erosion in the intertidal area (under more energetic wave conditions) was not found.

6.3 Implication of the results

Based on the results reported in this study, we can derive some implications that can be used for a broader context in the field of coastal engineering. In the implication, we focus on how the key findings and information from the results of the current study could be useful for real applications of FB or other relevant measures.

6.3.1 Effect of FB placement against erosion

We learned from the results obtained in the second research phase that the offshore FB could more effectively reduce wave height than the FB positioned onshore. This was also written in the report of Biesheuvel (2013), from 20 m deep, the FB starts to become economically attractive. In line with this statement, Zanuttigh and Nicholls (2015) stated that the conventional FB starts to become unattractive from depths greater than 6 m. They also added that the conventional breakwater is often more expensive than FB when the depth is greater than 6 m. From these two arguments, it can be implied that FB is more beneficial in deeper water.

Based on the results of this study, the magnitudes of hydrodynamic parameters (wave height, near-bed orbital velocity, and bed shear stress) were higher when the FB is located in shallower water. However, the differences in the magnitudes of those parameters when the FB was located in shallow or deep were apparently not much (see Table 6.2).

Table 6.2. Mean of transmitted wave height (H_1), near-bed orbital velocity (u_b) and bed shear stress (τ_b) with different water depths at FB position (h_{fb})

Wave conditions	H_1 [m]		u_b [m/s]		τ_b [N/m ²]	
	$h_{fb} = 5$ m	$h_{fb} = 20$ m	$h_{fb} = 5$ m	$h_{fb} = 20$ m	$h_{fb} = 5$ m	$h_{fb} = 20$ m
3) $H_0 = 1.20$ m $T_p = 3.0$ s	0.24	0.23	0.11	0.09	0.24	0.19
4) $H_0 = 1.80$ m $T_p = 3.8$ s	0.77	0.74	0.23	0.21	0.80	0.64

Even though the differences in magnitudes that are based on hydrodynamic parameters (wave height, near-bed orbital velocity, and bed shear stress) for different water depths at FB position were apparently not much, when considering erosion, there was a noticeable discrepancy. In this context, erosion may be reduced twice when FB is located in deep water than located in shallow water (see Table 6.3). For example, under wave condition 3, with $h_{fb} = 5$ m, it is apparent that erosion is 1.02 m². Next, by locating the FB further offshore (in deep water, $h_{fb} = 20$ m), erosion is reduced by more than 50%.

Table 6.3. Mean of suspended load transport and erosion

Wave conditions	suspended load transport [m ³ /s/m]		erosion [m ²]	
	$h_{fb} = 5$ m	$h_{fb} = 20$ m	$h_{fb} = 5$ m	$h_{fb} = 20$ m
3) $H_0 = 1.20$ m $T_p = 3.0$ s	1.42E-06	6.98E-07	1.02	0.41
4) $H_0 = 1.80$ m $T_p = 3.8$ s	8.14E-07	4.45E-07	10.90	5.63

This finding emphasizes that placing breakwater in deeper water is important since it can be effectively reducing erosion especially under more energetic wave conditions. Thereby, this study provides the insight about the benefit of FB in terms of its capability in reducing erosion in deep water, in addition to the economical perspective by Biesheuvel (2013) and Zanuttigh and Nicholls (2015). Apart from that, It is worth mentioning that under milder wave condition ($H_0 = 0.4$ m, $T_p = 1.7$ s; $H_0 = 0.7$ m $T_p = 2.3$ s), regardless of the water depths (5 m - 20 m), the FB could fully mitigate erosion.

6.3.2 Intertidal area and near shoal edge erosion

Based on the results, with FB intervention and under moderate wave condition ($H_0 = 1.2$ m, $T_p = 3.0$ s), erosion occurred on the intertidal area, whereas erosion occurred near the edge in more extreme wave conditions ($H_0 = 1.8$ m, $T_p = 3.8$ s). Nevertheless, low-wave conditions only resulted in small erosion on the intertidal area, and more extreme wave conditions resulted in more pronounced erosion near the shoal edge.

Based on the previous previous paragraph, it can be inferred that the wave still carries the remaining energy to the shore after being transmitted by FB. In this context, the destructive trait of the wave still inherently exists to erode the intertidal area. Therefore, multiple types of protection might be required to protect the intertidal flats fully. Under "moderate" wave conditions, brushwood dams can support floating breakwater, which can be used as an additional measure to reduce wave height and

flow velocity. Consequently, local bed shear stresses, thus, erosion rates are reduced (Siemes et al., 2020).

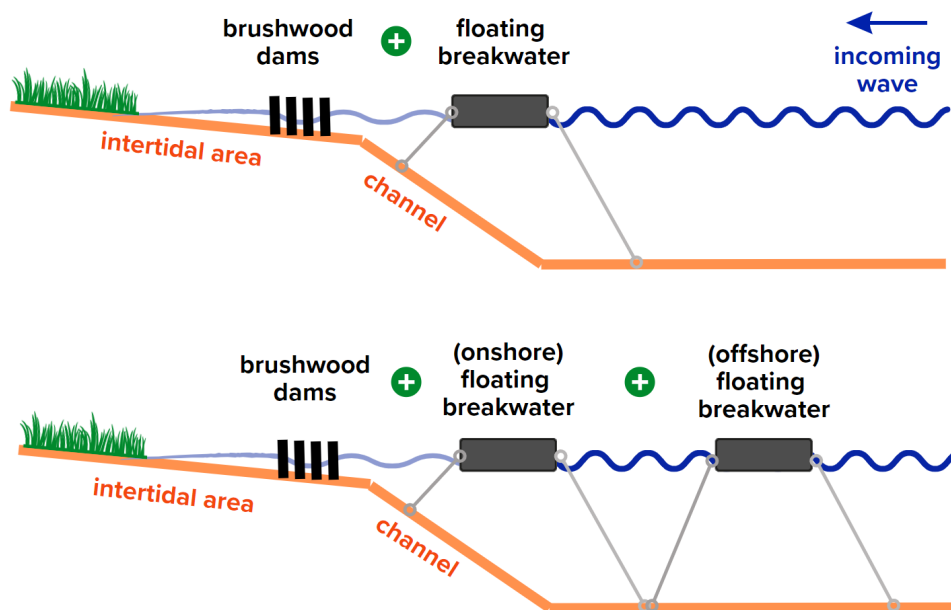


Figure 6.2. Illustration of multiple protections to tackle intertidal area erosion during mild wave conditions (upper panel) and near-edge erosion during more extreme wave conditions (lower panel)

Based on the results, the transmitted wave height under more extreme conditions was still quite significant (see Table 5.2). Hence, a parallel floating breakwater can be planned under more extreme wave conditions to have a double attenuating structure before the waves propagate to the intertidal area. Additionally, it is important to mention that this is only conceptual planning; further investigation regarding the reliability of this planning could be investigated in future research. In addition, replacing brushwood dams or adding support in the intertidal area (onshore of FB) with artificial reefs would also be interesting. This is because artificial reefs offer a positive and substantial significant wave height reduction and could be a better solution for morphodynamic (Vona et al., 2020).

6.3.3 Protecting the intertidal flats in the Eastern Scheldt

With the knowledge obtained in this study and because we undertook the schematized study from the Eastern Scheldt, we could arrange a measure using FB for protecting the intertidal flats in the Eastern Scheldt. Here, it is advised to place the FB not too close to the shore, or at least at the water depth of 10 m. The reason of selecting 10 m is because if FB is located in deeper than 10 m, it would be somewhere in the middle of the channel. In that case, FB may disturb the shipping access, one of the service in the Eastern Scheldt (van Noortwijk & Klatter, 1999). Next to that, the FB located in 10 m did not exhibit a significant difference compared to the effectiveness of the FB in deeper water e.g., 15 m or 20 m (see Figure 5.21). Hence, as a preliminary plan, the FB could be placed in front of eroding shoals (intertidal flats) like Roggenplaat and Galgeeplaat in the depth of 10 m. An illustration for the preliminary location where the FB could be located is available in Figure 6.3.

Regarding the channel and intertidal area slopes, since it was found that there was no significant difference in erosion with different channel and intertidal area slopes with the presence of FB (see Figure 5.22 and Figure 5.23, there is no specific preference on the planning of the FB position based

on the channel and intertidal area slopes. Next, since it is not easy to judge the slope on the real case with the real bathymetry (due to its complexity), the consideration of placing the FB based on channel or intertidal area slopes is not taken into account.

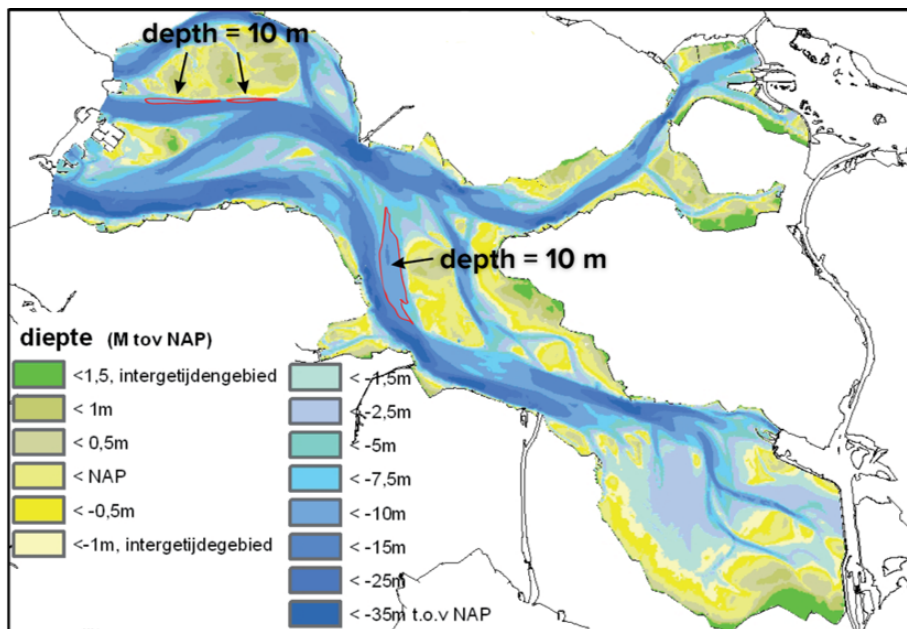


Figure 6.3. Area to locate FB according to the desired depth of 10 m; the water depth below FB is based on the results of current research; the intertidal flats on the upper left are Roggenplaat, and the lower right is Galgeplaat, adapted from [EcoShape \(2020\)](#)

Furthermore, with the proposed location to implement the FB, some challenges still need to be further investigated and solved. For example, the environmental impacts of FB, the effectiveness of FB when considering the flow in the channel near the intertidal flats, and the activity in the Eastern Scheldt that might be disturbed if the FB is present (even though it is already prevented by placing the FB near the shoal, $h_{fb} = 10$ m).

6.4 Extra outlook

6.4.1 Estimation of mitigated annual erosion by FB in the intertidal area

Based on the results of the simulations carried out in the second research phase, it was found that the presence of FB reduced the erosion in the intertidal area as presented in Table 5.7. Since the erosion was developed in 12 hours simulations, to obtain the erosion that may develop in a day, the obtained erosion in Table 5.7 is multiplied by 2. Furthermore, since the wave conditions (with their corresponding wind speeds) are not always occurring per day, the factor derived based on the probability of occurrence of the corresponding wave conditions is used (read Section B5 in Appendix B). In short, the estimate of erosion per year is calculated using this formula:

$$Erosion\ per\ year = modelled\ erosion \times 2 \times n(u) \times 365\ days \quad (11)$$

Where, $n(u)$ is number of events of the corresponding wind speed (thus wave conditions) per day (read Section B5)

By only focusing on how much erosion that can be mitigated by the FB, the cross-sectional erosion area in Table 5.7 without FB subtracts the erosion with FB. The estimation of cross-sectional area of erosion that can be mitigated by FB per year can be seen in Figure 6.4.

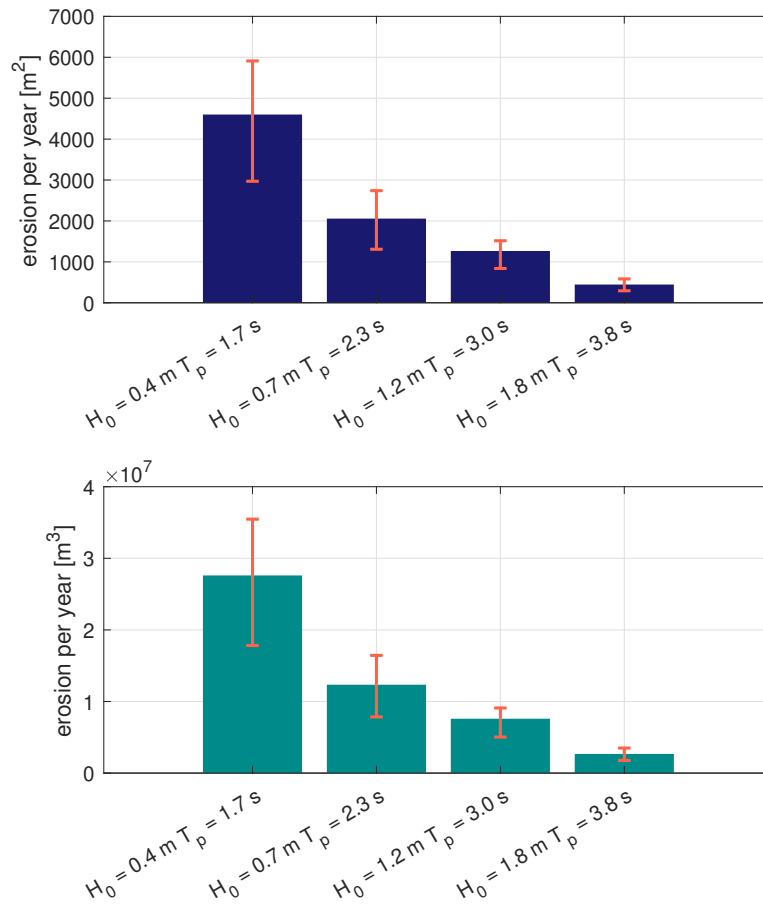


Figure 6.4. Estimated erosion per year that can be mitigated by FB; mitigated cross-sectional erosion by the FB (upper panel); mitigated volumetric erosion by the FB, assuming the length of the intertidal flat is 6000 m, which is approximately the length of Roggenplaat (lower panel); errors depicted in both panels are due to different water depth at FB positions, channel slopes and intertidal area slopes

As depicted by Figure 6.4, erosion that can be mitigated by FB is (overall) reaching a cross-sectional area of 4500 m^2 in mild wave condition ($H_0 = 0.4 \text{ m}$ and $T_p = 1.7 \text{ s}$). This amount is the highest because, this wave condition is most likely more frequent to occur compared to more extreme wave conditions i.e., higher incident wave heights and wave periods (read Section B5). Apart from that, in lower panel of Figure 6.4, estimation of erosion mitigated by FB in cubic meter was calculated. This was calculated based on the length of the Roggenplaat which is $\pm 6000 \text{ m}$, measured from the Roggenplaat which appears between -1.5 m NAP and 1.5 m NAP in the data depicted by Figure 3.7.

It is important to note that the erosion that can be mitigated by the FB is rough estimation and presumably overestimated. This is because as the intertidal area in the Eastern Scheldt erodes, the lowering rate (due to erosion) of the flats in the ES might eventually decrease when the intertidal areas approach an equilibrium height (de Vet et al., 2017). Hence, for instance, in a yearly basis, the

erosion rate that may occur in the intertidal area is not constant and becoming less. The calculation to obtain Figure 6.4 assumes that the rate of erosion is constant.

6.4.2 Effects of tide variation on erosion

To check the effects of tide variation, 16 additional simulations with a higher tide level (+1.00 m NAP) and lower tide level (-1.00 m NAP) are carried out. Hence, 16 simulations consist of 4 different wave conditions, 2 tide levels, 2 conditions: without and with FB ($h_{fb} = 10$ m). Cumulative erosion and sedimentation with different tides without FB from the mentioned simulations is depicted in Figure 6.5.

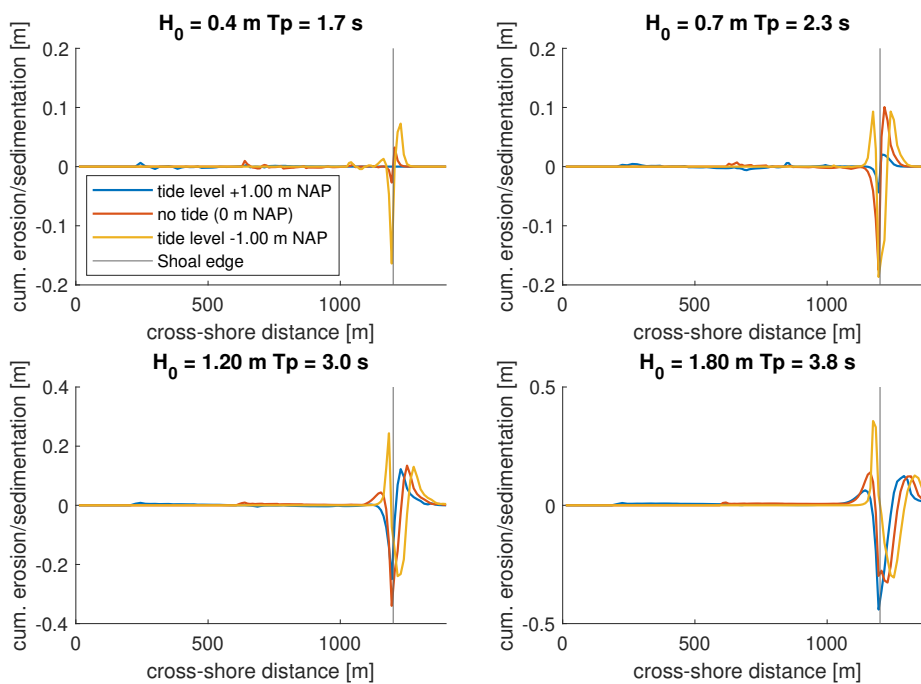


Figure 6.5. Cumulative erosion and sedimentation with different tide levels; simulations without FB on the channel slope 1:25 and intertidal area slope 1:400

Based on Figure 6.5, it can be seen that simulations with higher tide level resulted in bed level changes could reach until the upper part of the intertidal area. As the tide level was lowered, the positions in which the erosion or sedimentation occurred shifted to the lower part of the intertidal areas. Furthermore, from the same figure, it is apparent that the area of erosion differed with different tide level being imposed in the simulations. For instance, with a higher tide level (+1 m NAP), under mild wave condition (see upper panels in Figure 6.5), the depth of erosion is lesser compared to those with a lower tide level (0 m NAP, -1 m NAP).

Furthermore, to compare the effect of different tide levels on the annual erosion that could be mitigated by the FB, the same approach as explained in Section 6.4.1 is also executed. From Figure 6.6, it is seen that the cumulative area of erosion varied when the tide level is different. With a lower tide level (-1 m NAP), under mild wave conditions ($H_0 = 0.40$ m $T_p = 1.7$ s and $H_0 = 0.70$ m $T_p = 2.3$ s), the erosion is more prominent (14000 m^2 and 3000 m^2 respectively for both wave conditions) than erosion with higher tide level. This is presumably due to more intense wave breaking when the tide is low (-1.00 m NAP). Nevertheless, further study is needed to understand the causes better.

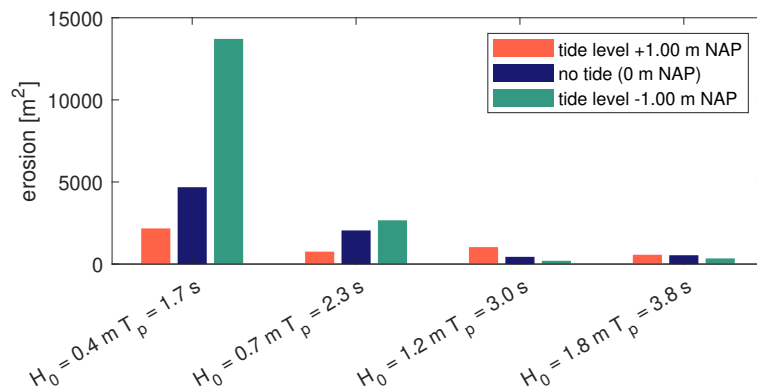


Figure 6.6. Annual erosion that could be mitigated by FB ($h_{fb} = 10 \text{ m}$) with different tide level under different wave conditions, simulated with a channel slope 1:25 and intertidal area slope 1:400

6.4.3 LIVING breakwater

In Section 1.1, we introduced LIVING breakwater developed by Zanden et al. (2022). It was planned to analyze the morphodynamic effects of this type of FB. Nonetheless, since no equation can be used to derive the transmission coefficient (of LIVING breakwater) associated with the wave conditions that were planned, the Macagno relation is used for the second research phase. Here, the Macagno relation formula that is used for the second research phase represents the box-type FB (see Figure 6.7).

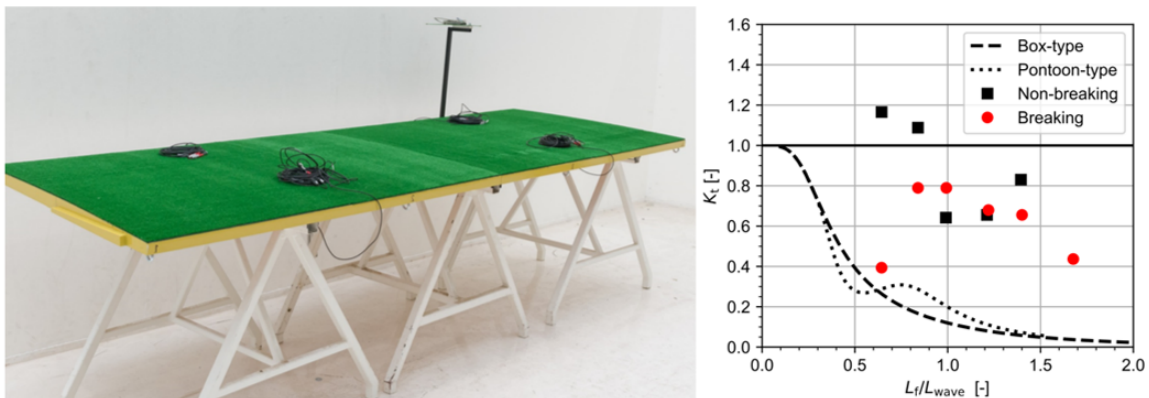


Figure 6.7. Novel floating (LIVING) breakwater (left) and the transmission coefficient of LIVING breakwater, represented by dots and square marks (right); L_f represents length of the floater, which is width (B_f) in this study, K_t is transmission coefficient (C_t) in the current study; retrieved from Zanden et al. (2022)

In this part, a small insight that relates to how the LIVING breakwater could reduce erosion based on the transmission coefficients that were observed by Zanden et al. (2022) is discussed, see right picture in Figure 6.7. Hence, the figure that exhibits erosion in relation to the transmission coefficient is provided (see Figure 6.8).

According to the transmission coefficient presented in the right picture in Figure 6.7, we can see that the transmission coefficient of LIVING breakwater ranges from 0.4 to 0.8. If we then see Figure 6.8, it can be witnessed that LIVING breakwater could reduce erosion from around 19 m^2 (without FB) to 6 - 15 m^2 (blue bars).

Comparing the performance of LIVING breakwater with box-type FB (current study), it can be seen that LIVING breakwater, with transmission coefficient = 0.40, could have almost similar effectiveness in reducing erosion with box-type FB (with reduced erosion of 5.90 m^2). Nevertheless, since LIVING breakwater was tested using mild wave conditions ($H_s = 0.027 - 0.160$ m, $T_p = 0.68 - 1.72$ s) (Zanden et al., 2022), it remains unknown whether the transmission coefficients presented in Figure 6.7 (right panel) is still valid for interpreting the amount of erosion with the prescribed wave condition ($H_0 = 1.8$ m, $T_p = 3.8$ s). Apart from that, based on Figure 6.7 (right panel), with the same transmission coefficient to box-type FB, LIVING breakwater may need larger dimension. With the mentioned conditions, the capability of LIVING breakwater in reducing erosion presented in the figure below might be flawed as well.

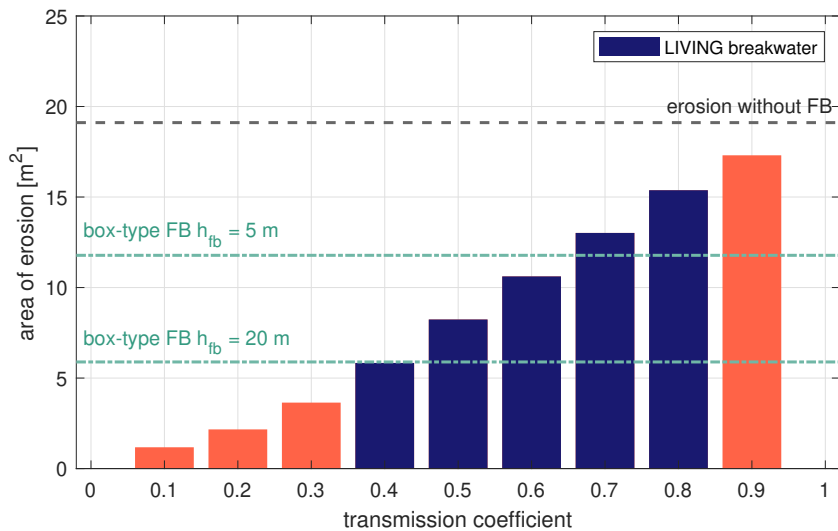


Figure 6.8. Erosion on different transmission coefficients; simulated using bathymetry with an intertidal area slope of 1:400 and channel slope of 1:25 (average); under wave condition 4: $H_0 = 1.8$ m, $T_p = 3.8$ s; box-type FB is the type of FB used in the current study; the simulations for this figure were derived by 12 hours simulation (morphology)

7 Conclusions and Recommendations

7.1 Conclusions

This research aims to assess the hydrodynamic and morphodynamic effects of a floating breakwater (FB) under varying wave conditions, FB positions, and slopes on the intertidal flats. In the conclusion, first research question related to the capability of the Delft3D model to reproduce the FB effects in the laboratory is answered, followed by the answer to the second research question related to the main objective: hydrodynamic and morphodynamic effects of FB. Furthermore, the key findings of the current study are elaborated following the answers of the second research phase.

Research question 1

How well does a numerical model Delft3D reproduce the FB effects yielded from the laboratory experiment of Shimoda et al. (1991)?

1a. How well does the numerical model Delft3D reproduce the cross-shore profiles observed in the laboratory experiment conducted by Shimoda et al. (1991)?

Three cross-sections with FB intervention observed in the laboratory experiment by Shimoda et al. (1991) were replicated using Delft3D numerical model: without FB, with landward FB (6.5 m from the shoreline), and seaward FB (8.0 m from the shoreline). There was no information regarding hydrodynamic parameters like wave height propagation or FB capacity to reduce wave height (i.e., transmission coefficient) by Shimoda et al. (1991) for model validation. Therefore, it was not possible to accurately reproduce the bed level pattern of the three cross-sections using Delft3D numerical model similar to those observed in the laboratory. Besides, imprecise digitization of the observed cross-shore profiles, sediment imbalance in the observed cross-sections (laboratory), not exploring all variables (e.g., multiplication factor of suspended sediment/bed load transport) and simplification of FB using transmission coefficient (C_t) feature in Delft3D are presumably also the causes of the inaccuracy.

Even though it was not possible to replicate the pattern of bed level of the mentioned cross-sections, the Delft3D was able to quantitatively reproduce the effects of FB in terms of reducing erosion and sedimentation in the lee-side of FB. Before, without FB, the cross-sectional area of erosion and sedimentation under laboratory experiment were 0.36 m^2 (erosion), 0.44 m^2 (sedimentation) whereas based on the selected results of Delft3D model, cross-sectional area of erosion was 0.32 m^2 and sedimentation was 0.32 m^2 . With landward FB, based on laboratory experiment, the mentioned erosion and sedimentation reduced to 0.02 m^2 and 0.07 m^2 , respectively. With landward FB intervention represented by C_t in Delft3D, from the closest result to the experiment, cross-sectional area of erosion reduced to 0.03 m^2 and sedimentation to 0.06 m^2 . For seaward FB, from the laboratory, it was reported that erosion reduced to 0.11 m^2 and sedimentation to 0.06 m^2 . The best Delft3D model with seaward FB predicted that erosion reduced to 0.06 m^2 and sedimentation to 0.08 m^2 . The reported cross-sectional area of erosion and sedimentation due to FB in laboratory and FB represented by C_t in Delft3D emphasized that FB in both methods (laboratory and Delft3D) exhibited a similar effect: reducing erosion and sedimentation (in the lee side of FB).

1b. How does the presence of FB impact the wave height based on the experiment and Delft3D model?

Based on the experiment by Shimoda et al. (1991), it was reported that the FB broke the incoming incident wave. However, in Delft3D numerical model, it seemed that the transmission coefficient only took away the wave energy, thus directly reduced the wave height after the waves passed the prescribed transmission coefficient in the model.

Furthermore, based on laboratory, it was reported that FB attenuated waves. The wave attenuation increased with the increase in FB's height (the side where the FB facing the incoming waves) and when FB was more exposed onto the water surface. Since in the Delft3D, FB was only represented by transmission coefficient (a ratio between transmitted wave height in the lee side of FB and incident wave height), increase or decrease in wave attenuation could be related to the changes in transmission coefficient (C_t). With a lower C_t , the wave attenuation increased. For example, based on Delft3D simulation, with a $C_t = 0.50$, an incident wave height (H_0) of 0.30 m was reduced to ± 0.15 m. For the simulations in Delft3D that resulted in closest cross-sectional area of erosion and sedimentation, the C_t was 0.10. Under $C_t=0.10$, with the imposed wave height of 0.30 m, the reduced wave height was ± 0.05 m. This highlights that the transmission coefficient could be slightly off from the prescribed transmission coefficient. Also, since there was no observed wave height based on laboratory experiment, the wave height propagation in the model could not be validated.

1c. How does the presence of FB impact the sediment transport according to the experiment and Delft3D model?

Based on the experiment of FB by Shimoda et al. (1991), it was reported that due to wave-breaking, sediment particle onshore of the FB is suspended and is transported toward offshore direction by the return flow. Regarding the direction of suspended load transport, results in Delft3D model with FB exhibited that the suspended load transport was directing offshore. This emphasized that, in terms of direction, both Delft3D model and laboratory experiment had a similar result. Nonetheless, Shimoda et al. (1991) did not report the direction of suspended load transport in the test without FB. Meanwhile, based on Delft3D simulation without FB, the suspended load transport was directing offshore. Thus, this information regarding the direction of suspended load transport without FB from Delft3D model could not be confirmed.

Furthermore, with the transmission coefficient representing FB in Delft3D, suspended load transport decreased when passing through the line of transmission coefficient. In this case, for instance a suspended load transport onshore of the FB (located seaward) in Delft3D with a magnitude of $4 \times 10^{-6} \text{ m}^3/\text{s}/\text{m}$ reduced to $0 \text{ m}^3/\text{s}/\text{m}$. This presumably the reason of accretion in the vicinity of FB modelled in Delft3D. In contrast to the results of Delft3D, the area below the FB in the laboratory experiment according to both cross-sections: with landward and seaward FB exhibited scouring. This denotes that sediment transport presumably increased in the vicinity of FB in the laboratory experiment, different with the Delft3D model result.

Research question 2

What are the hydrodynamic and morphodynamic effects of a floating breakwater (FB) under varying wave conditions, FB positions, and slopes representing the intertidal flats in the Eastern Scheldt?

2a. How do the transmission coefficients of the selected FB vary under different wave conditions and water depths at FB positions)?

The transmission coefficients (C_t) in the second research phase were calculated using Macagno relation, which relates to wave period, water depth at FB position, FB's width and FB's draft. Since FB width and FB draft in the current study was set to 8.00 m and 2.20 m respectively, which is the largest FB available in the market SF-Marina (2022), the C_t s were calculated only based on different wave periods ($T_p = [1.7 \ 2.3 \ 3.0 \ 3.8] \text{ s}$) and water depths at FB position ($h_{fb} = [5 \ 10 \ 15 \ 20] \text{ m}$). These wave periods and water depths at FB position were derived based on the condition in the Eastern Scheldt.

The results showed that the C_t increased more significantly with the increase of wave periods than water depths at FB position. With a wave period of 1.7 s the calculated C_t s were 0.0084 for all water depths at FB position. With the wave periods of 2.3 s, 3.0 s, and 3.8 s, the transmission coefficients were ranging from 0.0615 - 0.0623; 0.2046 - 0.2134; 0.4370 - 0.4584, respectively. The ranges emerged due to different water depths at FB position. Furthermore, with shallower water depth at FB position, the C_t became higher than the C_t in deeper water. For instance, with a wave period of 3.8 s, with a water depth of 5.0 m the C_t was 0.4584 whereas with a water depth 20.0 m the C_t was 0.4370.

The high C_t means that the FB is less effectively in attenuating wave and vice versa. Hence, from the previous paragraph, due to C_t increased with wave period and in shallower water. This implies that the FB is less effective to attenuate wave in longer wave period (thus longer wave length). In addition, the FB is also less effective in shallower water. Nevertheless, the difference of the effectiveness of FB in different water depths was less substantial compared to wave period.

2b. How do the hydrodynamic parameters (wave height, near-bed orbital velocity, and bed shear stress) vary under different wave conditions, floating breakwater (FB) positions, and slopes representing the intertidal flats environment?

Hydrodynamic parameters: wave height, near-bed orbital velocity and bed shear stress in general decreased due to the presence of FB. The reduction of the magnitude of hydrodynamic parameters were varying under different wave conditions, water depths at FB position (5 m, 10 m, 15 m, 20 m), intertidal area slopes (1:200, 1:400, 1:600), and channel slopes (1:15, 1:25, 1:55). Overall, different wave conditions affected the reduction capacity of FB on wave height, near-bed orbital velocity, and bed shear stress more significantly. Meanwhile, the effects of different water depths at FB position, intertidal area slopes, and channel slopes were less substantial than wave conditions.

Under mild wave conditions with $H_0 = 0.40 \text{ m}$ and $T_p = 1.7 \text{ s}$ (wave condition 1) and $H_0 = 0.70 \text{ m}$ and $T_p = 2.3 \text{ s}$ (wave condition 2), with the presence of FB, the transmitted wave height (observed on the shoal edges) were lowered with the reduction capacities of 99% (wave condition 1) and 94.3% - 94% (wave condition 2). This indicates that FB successfully reduced the wave height under these two wave conditions. Furthermore, based on the mean values, near-bed orbital velocity and bed shear stress were also significantly reduced for both wave conditions. Near-bed orbital velocity exhibited a reduction of 96.1% - 98.9% (for wave condition 1) and 86.2% - 89.0% (for wave condition 2). For bed shear stress, the reductions were ranging from 99.1% - 99.9% (for wave condition 1) and 96.3% - 96.7% (for wave condition 2). It is important to mention that the bed shear stress magnitudes with the presence of FB for wave conditions 1 and 2 were below the critical bed shear stress ($\tau_b = 0.15 \text{ N/m}^2$)

regardless of different water depths at FB position, intertidal area slopes, and channel slopes. This indicated that there was no sediment motion due to the FB intervention for wave conditions 1 and 2.

Under more extreme wave conditions, with $H_0 = 1.20\text{ m}$ and $T_p = 3.0\text{ s}$ (wave condition 3) and $H_0 = 1.80\text{ m}$ and $T_p = 3.8\text{ s}$ (wave condition 4), the reductions of transmitted wave height, near-bed orbital velocity, and bed shear stress were less favorable compared to wave conditions 1 and 2. In this case, the presence of FB could reduce the wave height (observed on the shoal edges) by 80.7% - 81.2% (wave condition 3), and 57.4% - 60.7% (wave condition 4). Under FB intervention, the near-bed orbital velocity and bed shear stress also declined. In this context, near-bed orbital velocity demonstrated reductions that ranged from 45.2% - 50.3% (wave condition 3) and 14.4% - 16.3% (wave condition 4). For the bed shear stress, the mean values after the presence of FB ranged from 0.16 - 0.24 N/m^2 (wave condition 3) and 0.62 - 0.78 N/m^2 (wave condition 4), these ranges of values were above the critical bed shear stress ($\tau_b = 0.15\text{ N/m}^2$), indicating that even FBs were imposed (in wave conditions 3 and 4), the sediment transport was apparently still occurring.

Furthermore, different water depths at FB position insignificantly affected wave height, near-bed orbital velocity, and bed shear stress (under wave conditions 3 and 4). Regarding FB positions, it was found that FB located in shallower water was slightly less effective than those with FB in deeper water. For example, the difference in $H1$ was approximately $\pm 0.04\text{ m}$ for water depths at FB positions of 5 m and 20 m.

Next, with different channel and intertidal area slopes, under wave conditions 3 and 4, the reduction of magnitudes of wave height, near-bed orbital velocity, and bed shear stress were insignificant. For example, with FB intervention, different channel slopes exhibited a small difference in bed shear stress, which was $\pm 0.1\text{ N/m}^2$ between the steepest channel slope (1:15) and mildest channel slope (1:55). Also, with FB, the small difference of magnitudes was also demonstrated by different intertidal slopes. For example, the mean bed shear stress with the steepest intertidal area slope (1:200) ranged from 0.7 - 0.9 N/m^2 while with the most gentle slope (1:600) ranged from 0.6 - 0.8 N/m^2 . Nonetheless, the gentle channel slope (1:55) or gentle intertidal area slope (1:600) were slightly more effective in lowering the overall magnitudes of wave height, near-bed orbital velocity, and bed shear stress compared to the steeper channel (1:15, 1:25) and steeper intertidal area slopes (1:200, 1:400).

Lastly, the peaks of near-bed orbital velocity and bed shear stress appeared on different locations with different transmitted wave heights ($H1$). Under (mild) wave condition 1 without FB ($H1: 0.38\text{ m}$), or wave condition 3 with FB intervention ($H1: 0.22 - 0.23\text{ m}$), the peaks of near-bed orbital velocity and bed shear stress appeared landward of the shoal edges (on the intertidal area). Meanwhile, with higher $H1$ (e.g., wave condition 2 without FB $H1=0.60\text{ m}$, or transmitted wave condition 4 $H1: 0.71 - 0.77\text{ m}$), the peaks of near-bed orbital velocity and bed shear stress were starting to be more prominent in the vicinity of the shoal edge. This suggested that the presence of FB could reduce wave height, thus shifting the peak of near-bed orbital velocity and bed shear stress, depending on $H1$.

2c. How does the presence of FBs in the intertidal flats, under varying wave conditions, FB positions, and slopes, impact the amount of sediment transported (bed load and suspended load) and cross-sectional erosion area?

In general, morphodynamic parameters: bed load, suspended load transport and erosion were reduced with the presence of FB. The impact of wave conditions (under FB intervention) on reductions of bed load, suspended load transport and erosion were more considerable compared to different water depths at FB position, intertidal area slopes and channel slopes.

Under mild wave conditions, $H_0 = 0.40 \text{ m}$ and $T_p = 1.7 \text{ s}$ (wave condition 1) and $H_0 = 0.70 \text{ m}$ and $T_p = 2.3 \text{ s}$ (wave condition 2), the presence of FB could fully reduce the bed load and suspended load transport as well as erosion (100%). Hence, there was no sediment transport with the presence of FB under wave conditions 1 and 2. Also, for wave conditions 1 and 2, regardless of variations in water depths at the FB's position, different channel slopes, and intertidal area slopes, the presence of FB could fully mitigate erosion at the intertidal area.

Under more extreme wave conditions, $H_0 = 1.20 \text{ m}$ and $T_p = 3.0 \text{ s}$ (wave condition 3) and $H_0 = 1.80 \text{ m}$ and $T_p = 3.8 \text{ s}$ (wave condition 4), the FB was able to reduce bed load, suspended load transport and thus erosion even though they were not fully reduced like in wave conditions 1 and 2. Under wave condition 3 with FB intervention, bed load transports were reduced by 83.9% - 100% and suspended load transport were reduced by 88.4% - 96.6%. Along with the reduction of bed load and suspended load transport, cross-sectional erosion decreased by 92.7% - 96.4% (reduced from 5.68 - 12.0 m^2 to 0.21 - 0.88 m^2). Under more energetic wave condition 4, bed load transport decreased with the reduction ranging from 33.6% - 34.9%. Meanwhile for suspended load transport, the reduction was ranging between 55.6% - 68.9%. Reflecting from the reduced bed load and suspended load transport, the FB was able to reduce cross-sectional erosion from around 11.55 - 24.08 m^2 to 4.92 - 9.01 m^2 .

For wave conditions 3 and 4, different water depths at FB position affects the bed load, suspended load transport and erosion. In this context, FB located in shallower water (5.0 m) was less effective in reducing the magnitudes of bed load, suspended load transport and erosion compared to those in deeper water. Based on erosion with the FB interventions in different water depths, FB in deeper water (10.0 m, 15.0 m, 20.0 m) on average diminished erosion two times lesser than FB in shallower water (5.0 m) for both wave conditions 3 and 4.

Under FB intervention, bed load transport, suspended load transport and erosion were slightly differing with different channel slopes and intertidal area slopes. The trend showed that the steep channel slopes (1:15) and intertidal area slopes (1:200) were resulting in higher magnitudes (of bed and suspended load transport) than those on the gentler channel slopes (1:25, 1:55) and gentler intertidal area slopes (1:400, 1:600). However, for different channel slopes, the difference of erosion on the steepest channel slope (1:15) and the most gentle channel slope (1:55) is only obvious yet relatively small on wave condition 4 (difference = $\pm 3 \text{ m}^2$). For intertidal area slope, there was almost no difference in erosion after the FBs were implemented.

Regarding direction of the sediment transport, bed load transport was mostly directed onshore (to the intertidal area) whereas suspended load transport was predominantly directed offshore (to the channel). When the transmitted wave height (H_1) is relatively small (e.g., wave condition 3 with FB intervention, H_1 : 0.22 - 0.23 m), suspended sediment transport predominantly appeared on the intertidal area, resulting erosion on intertidal area too. With relatively high transmitted wave height (e.g., wave condition 4 with FB, H_1 : 0.71 - 0.77 m), suspended sediment transport predominantly appeared near the shoal edge. Thus erosion mostly occurred in the vicinity of the shoal edge.

2d. What inferences can be made from the hydrodynamic and morphodynamic effects of FB under different wave conditions, floating breakwater positions, and slopes, particularly with regard to erosion?

It can be inferred that FB is reliable in reducing erosion on the intertidal area under mild wave conditions: $H_0 = 0.40\text{ m}$ and $T_p = 1.7\text{ s}$ and $H_0 = 0.70\text{ m}$ and $T_p = 2.3\text{ s}$. Next to that, the FB started to be less effective in reducing erosion when more extreme wave conditions were imposed: $H_0 = 1.20\text{ m}$ and $T_p = 3.0\text{ s}$ and $H_0 = 1.80\text{ m}$ and $T_p = 3.8\text{ s}$. Hence, extra protections (e.g., brushwood dams, two parallel FBs) might be needed to fully protect the intertidal area against erosion in these more extreme wave conditions.

Regarding the water depths at FB position, the difference of magnitudes of hydrodynamic parameters (wave height, near-bed orbital velocity and bed shear stress) may not be significant. Yet, the difference in erosion due to different water depths at FB position could be substantial: FB in deeper water (10 m, 15 m, 20 m) could be resulting in two times lesser erosion compared to FB in shallow water (5 m). This highlighted that placing FB in deeper water is favorable.

The channel and intertidal area slopes could affect the amount of erosion. In this case, erosion could be less on gentler channel slope (1:55) and gentler intertidal area slopes (1:600). Yet, the differences in erosion due to different channel slopes and intertidal area slopes after implementing FB were not prominent. Therefore, channel slope and intertidal slope may not be the first priority to consider when placing the FB in the field. This also considers the real bathymetry that is not linear, which makes it difficult to judge the channel and intertidal area slopes.

Key findings

According to the results we discussed, three key findings could be drawn such as:

1. Wave conditions determine the effectiveness of FB in reducing the magnitudes of erosion in the intertidal area. In this case, the FB is effective in reducing erosion under mild wave conditions and less effective in more extreme wave conditions.
2. Water depths at FB position affect the magnitudes of erosion. FB located in shallow water depth may reduce erosion insignificantly compared to FB located in deep water.
3. With the FB intervention, different channel slopes and intertidal area slopes do not affect erosion much.

7.2 Recommendations

Further research can improve the current study's findings to increase the comprehension of the intertidal flats environment's behavior when subjected to the FB intervention. To do that, several recommendations are provided

1. With the limitations of the 1D model in the current study, the assessment of floating breakwater could be carried out in 2DH (depth-averaged) to assess the hydrodynamic and morphodynamic effects of FB with the oblique incident waves. By doing this, the effects of FB on the sediment behavior, location of the accumulation, and sediment patterns could also be understood.
2. Another suggestion is undertaking the floating breakwater assessment in 2DV. In this case, since [Koftis et al. \(2006\)](#) only carried out simulations to assess the hydrodynamic characteristics of FB. Further study could also explore the morphodynamic study of FB in 2DV. Thereby, the effects, like jet-type flow patterns, could be captured by the model. This may change the sediment transport and, thus, erosion pattern with floating breakwater intervention.
3. Next, to understand the effects of FB on the sediment behavior, location of the accumulation, and sediment patterns that could not be explained in a 1D model without compromising the actual effects of FB on hydrodynamics (e.g., jet-type flow pattern), the 3D model could be considered.
4. To understand the effects of wave growth due to wind on hydrodynamic and morphodynamic, the effects of wind could be included in the model.
5. Considering a single grain size that is used in the current study, the sensitivity analysis with different grain sizes could be carried out to understand the effects of grain size variation on morphodynamic.
6. A Study about the difference between the model with the real bathymetry and schematized bathymetry could also be undertaken. By doing this, we can relate whether the conceptual knowledge we derived from this study represents the model undertaken with real bathymetry.
7. Furthermore, we could also try to explore the study case, which involves the FB as explained in Section 6.3.2. Hence, we can evaluate whether double FB onshore and offshore could effectively dissipate waves or how the effects of erosion when we include brushwood dam near the edge under calm wave conditions.

References

- Anonymous. (2020). *The breugem and holthuijsen (2006) shallow water formulation*. Retrieved from http://weatherclasses.com/uploads/3/6/2/3/36231461/bh_formulation.pdf
- Beiboer, L. (2020). *Update erosion eastern scheldt* (Master's Thesis). Hanze University of Applied Sciences.
- Biesheuvel, A. C. (2013). *Effectiveness of floating breakwaters: Wave attenuating floating structures* (Master's Thesis). TU Delft.
- Bosboom, J., & Stive, M. J. (2021). *Coastal dynamics*. Delft University of Technology.
- Bouwmeester, E., & Breggen, H. v. d. (1984, Mar). Floating breakwater, literature review. *Floating breakwater*.
- Brand, E., Ramaekers, G., & Lodder, Q. (2022). Dutch experience with sand nourishments for dynamic coastline conservation – an operational overview. *Ocean and Coastal Management*, 217, 106008. doi: 10.1016/j.ocecoaman.2021.106008
- Breugem, W. A., & Holthuijsen, L. H. (2007). Generalized shallow water wave growth from lake george. *Journal of Waterway, Port, Coastal, and Ocean Engineering*, 133(3), 173–182. doi: 10.1061/(asce)0733-950x(2007)133:3(173)
- Daly, C., Roelvink, D., van Dongeren, A., van Thiel de Vries, J., & McCall, R. (2012). Validation of an advective-deterministic approach to short wave breaking in a surf-beat model. *Coastal Engineering*, 60, 69–83. doi: 10.1016/j.coastaleng.2011.08.001
- Deltares. (2022). *Manual and documentation - delft3d*. Retrieved from <https://oss.deltares.nl/web/delft3d/manuals>
- Deltares. (2023a). *Delft3d-wave user manual*. Author.
- Deltares. (2023b). *Delft3d-flow user manual*. Author.
- de Vet, P. L., van Prooijen, B., & Wang, Z. (2017). The differences in morphological development between the intertidal flats of the eastern and western scheldt. *Geomorphology*, 281, 31–42. doi: 10.1016/j.geomorph.2016.12.031
- de Vet, P. L., van Prooijen, B. C., Schrijvershof, R. A., van der Werf, J. J., Ysebaert, T., Schrijver, M. C., & Wang, Z. B. (2018). The importance of combined tidal and meteorological forces for the flow and sediment transport on intertidal shoals. *Journal of Geophysical Research, Earth Surface*, 123(10), 2464–2480. doi: 10.1029/2018jf004605
- de Vries, M. (2007). *Morphological modelling of the haringvlietmonding using delft3d* (Master's Thesis). University of Twente.
- Drieman. (2011). *Feasibility study on the use of a floating breakwater to protect a new artificial beach in balchik, bulgaria* (Unpublished master's thesis). TU Delft.
- EcoShape. (2020, Sep). *Channel-shoal interaction*. Retrieved from <https://www.ecoshape.org/en/knowledge-articles/interaction-between-tidal-basins-and-ebb-tidal-deltas/channel-shoal-interaction/>

Eelkema, M. (2013). *Eastern scheldt inlet morphodynamics* (Unpublished doctoral dissertation). Technische Universiteit Delft.

Giardino, A., Werf, J. v. d., & Ormondt, M. v. (2010). *Simulating coastal morphodynamics with delфт3d: Case study egmond aan zee*. Retrieved from https://www.researchgate.net/profile/Alessio-Giardino/publication/266143896_Simulating_Coastal_Morphodynamics_with_Delft3D_case_study_Egmond_aan_Zee/links/5427dc0e0cf238c6ea7ae495/Simulating-Coastal-Morphodynamics-with-Delft3D-case-study-Egmond-aan-Zee.pdf

Guo, W., Zou, J., He, M., Mao, H., & Liu, Y. (2022). Comparison of hydrodynamic performance of floating breakwater with taut, slack, and hybrid mooring systems: An sph-based preliminary investigation. *Ocean Engineering*, 258, 111818. doi: 10.1016/j.oceaneng.2022.111818

Hydraulics, W. D. (2003, Nov). *Modelling of sand transport in delфт3d*. DelftHydraulics.

Knook, P. (2013). *Sediment transport on various depth contours of the 'holland coast' shoreface* (Master's Thesis). TU Delft.

Koftis, T., Prinos, P., & Koutandos, E. (2006). 2d-v hydrodynamics of wave–floating breakwater interaction. *Journal of Hydraulic Research*, 44(4), 451–469. doi: 10.1080/00221686.2006.9521697

Lesser, G., Roelvink, J., van Kester, J., & Stelling, G. (2004). Development and validation of a three-dimensional morphological model. *Coastal Engineering*, 51(8-9), 883–915. doi: 10.1016/j.coastaleng.2004.07.014

Li, H., Chen, J., Bao, L., & Jiang, C. (2021). Research on wave attenuation performance of floating breakwater. *Energies*, 14(24), 8316. doi: 10.3390/en14248316

Liang, J.-m., Liu, Y., Chen, Y.-k., & Li, A.-j. (2022). Experimental study on hydrodynamic characteristics of the box-type floating breakwater with different mooring configurations. *Ocean Engineering*, 254, 111296. doi: 10.1016/j.oceaneng.2022.111296

Maas, B. (2020). *Feasibility of using sand nourishments to increase water safety in the eastern scheldt* (Unpublished master's thesis). Utrecht University.

Mojabi, S. M., Oumeraci, H., & Cappietti, L. (2018). *Effect of porosity and submergence of detached homogeneous rubble mound breakwaters on wave transmission and short term coastal erosion, a numerical study*. (PhD thesis). Technische Universitat Braunschweig.

Pezij, M. (2015). *Understanding the morphological development of the oesterdam nourishment* (Unpublished master's thesis). University of Twente.

Ranasinghe, R., Larson, M., & Savioli, J. (2010). Shoreline response to a single shore-parallel submerged breakwater. *Coastal Engineering*, 57(11-12), 1006–1017. doi: 10.1016/j.coastaleng.2010.06.002

Roelvink, Reniers, A., van Dongeren, A., van Thiel de Vries, J., McCall, R., & Lescinski, J. (2009). Modelling storm impacts on beaches, dunes and barrier islands. *Coastal Engineering*, 56(11-12), 1133–1152. doi: 10.1016/j.coastaleng.2009.08.006

Ruol, P., Martinelli, L., & Pezzutto, P. (2012). Limits of the new transmission formula for pi-type floating breakwaters. *Coastal Engineering Proceedings*, 1(33), 47. doi: 10.9753/icce.v33.structures.47

-
- Ruol, P., Martinelli, L., & Pezzutto, P. (2013). Formula to predict transmission for π -type floating breakwaters. *Journal of Waterway, Port, Coastal, and Ocean Engineering*, 139(1), 1–8. doi: 10.1061/(asce)ww.1943-5460.0000153
- Sabrina, M., & Karjadi, E. A. (2022). Numerical study of hydrodynamic and sedimentation for sustainable marine floating cage aquaculture in indonesia: A case study in situbondo, east java. *IOP Conference Series: Earth and Environmental Science*, 1065(1), 012027. doi: 10.1088/1755-1315/1065/1/012027
- SF-Marina. (2022, Sep). *Floating breakwater products*. Retrieved from <https://sfmarina.com/solutions/breakwaters/>
- Shimoda, N., Murakami, N., & Iwata, K. (1991). Beach erosion control by submerged floating structure. *Coastal Engineering 1990*. doi: 10.1061/9780872627765.210
- Siemes, R. W., Borsje, B. W., Daggenvoorde, R. J., & Hulscher, S. J. (2020). Artificial structures steer morphological development of salt marshes: A model study. *Journal of Marine Science and Engineering*, 8(5), 326. doi: 10.3390/jmse8050326
- Theol, S. A. A. A. (2020). *The use of delft3d to simulate the deposition of cohesive and non-cohesive sediments in irrigation systems* (PhD thesis). Wageningen University.
- Tsai, C.-P., Chen, H.-B., Hwung, H.-H., & Huang, M.-J. (2005). Examination of empirical formulas for wave shoaling and breaking on steep slopes. *Ocean Engineering*, 32(3–4), 469–483. doi: 10.1016/j.oceaneng.2004.05.010
- van der Werf, J. (2021). *Syllabus wave-dominated coastal dynamics*. University of Twente.
- van der Werf, J., de Vet, P., Boersema, M., Bouma, T., Nolte, A., Schrijvershof, R., . . . et al. (2019). An integral approach to design the roggenplaat intertidal shoal nourishment. *Ocean and Coastal Management*, 172, 30–40. doi: 10.1016/j.ocecoaman.2019.01.023
- van der Werf, J., Reinders, J., van Rooijen, A., Holzhauer, H., & Ysebaert, T. (2015). Evaluation of a tidal flat sediment nourishment as estuarine management measure. *Ocean and Coastal Management*, 114, 77–87. doi: 10.1016/j.ocecoaman.2015.06.006
- van der Werf, J., Schrijvershof, R. A., Brakenhoff, L. B., & Grasmeyer, B. T. (2022). Observations of near-bed orbital velocities and small-scale bedforms on the dutch lower shoreface. *Ocean and Coastal Management*, 218, 106012. doi: 10.1016/j.ocecoaman.2021.106012
- van de Wardt, W. (2018). *Modelling cross-shore transport of graded sediments under waves* (Master thesis). University of Twente.
- van Noortwijk, J., & Klatter, H. (1999). Optimal inspection decisions for the block mats of the eastern-schedt barrier. *Reliability Engineering and System Safety*, 65(3), 203–211. doi: 10.1016/s0951-8320(98)00097-0
- van Rijn, L., Walstra, D., Grasmeyer, B., Sutherland, J., Pan, S., & Sierra, J. (2003). The predictability of cross-shore bed evolution of sandy beaches at the time scale of storms and seasons using process-based profile models. *Coastal Engineering*, 47(3), 295–327. doi: 10.1016/s0378-3839(02)00120-5

-
- Vieira, B. F., Pinho, J. L., Barros, J. A., & Antunes do Carmo, J. S. (2020). Hydrodynamics and morphodynamics performance assessment of three coastal protection structures. *Journal of Marine Science and Engineering*, 8(3), 175. doi: 10.3390/jmse8030175
- Vlijm, R. (2011). *Process-based modelling of morphological response to submerged breakwater* (Master's Thesis). TU Delft.
- Vona, I., Gray, M., & Nardin, W. (2020). The impact of submerged breakwaters on sediment distribution along marsh boundaries. *Water*, 12(4), 1016. doi: 10.3390/w12041016
- Wiberg, P., & Sherwood, C. (2008, 10). Calculating wave-generated bottom orbital velocities from surface-wave parameters. *Computers and Geosciences*, 34, 1243-1262. doi: 10.1016/j.cageo.2008.02.010
- Wright, J., Colling, A., & Park, D. (2008). *Waves, tides, and shallow-water processes*. Butterworth-Heinemann, in association with the Open University.
- Xiong, J., Wang, Y. P., Gao, S., Du, J., Yang, Y., Tang, J., & Gao, J. (2018). On estimation of coastal wave parameters and wave-induced shear stresses. *Limnology and Oceanography: Methods*, 16(9), 594–606. doi: 10.1002/lom3.10271
- Zanden, J. V. D., Hout, A. V. D., Otto, W., Walles, B., & Wilde, J. D. (2022). Experimental study on a breaking-enforcing floating break-water. *Journal of coastal and hydraulic structure*, 2, 18. Retrieved from <https://doi.org/10.48438/JCHS.2022.0018>
- Zanuttigh, B., & Nicholls, R. (2015). *Coastal risk management in a changing climate*. Butterworth-Heinemann.
- Zhang, H., Ding, X., Zhou, B., Zhang, L., & Yuan, Z. (2019). Hydrodynamic performance study of wave energy-type floating breakwaters. *Journal of Marine Science and Application*, 18(1), 64–71. doi: 10.1007/s11804-019-00064-y

Appendix A - Physical and Numerical Aspects of Delft3D

Two Delft3D modules, Delft3D-FLOW and Delft3D-WAVE, are used to perform the numerical simulations in the current study. Delft3D-FLOW resolves the hydrodynamic simulation, including morphological simulation, whereas Delft3D-WAVE performs wave simulation. An additional explanation about the transmission coefficient is also included in this part.

A1. Governing Equations in Delft3D-FLOW Module

Hydrodynamic

Delft3D-FLOW module solves the Navier-Stokes equations for an incompressible fluid under shallow water (i.e., hydrostatic pressure) and the Boussinesq assumptions (The effect of variable density is only taken into account in the pressure term). The vertical accelerations are neglected by assuming that they are small compared to the gravitational acceleration. This reduces the vertical momentum equation to the hydrostatic pressure equation. The system equations consist of:

- Continuity equation
- Horizontal equation of motion

The continuity equation is given by,

$$\frac{\partial \zeta}{\partial t} + \frac{\partial(d + \zeta)u}{\partial x} + \frac{\partial(d + \zeta)v}{\partial y} + \frac{\partial \omega}{\partial z} = 0 \quad (\text{A.1})$$

Next, the momentum equation in the x-direction is expressed by,

$$\frac{\partial u}{\partial t} + u \frac{\partial u}{\partial x} + v \frac{\partial u}{\partial y} + \frac{\omega}{h} \frac{\partial u}{\partial z} = -g \frac{\partial \zeta}{\partial x} + fv + v_H \left(\frac{\partial^2 u}{\partial x^2} + \frac{\partial^2 u}{\partial y^2} \right) + \frac{1}{h^2} \frac{\partial}{\partial z} \left(v_v \frac{\partial u}{\partial z} \right) - \frac{gu\sqrt{u^2 + v^2}}{hC^2} \quad (\text{A.2})$$

And momentum equation in the y-direction is expressed by,

$$\frac{\partial v}{\partial t} + u \frac{\partial v}{\partial x} + v \frac{\partial v}{\partial y} + \frac{\omega}{h} \frac{\partial v}{\partial z} = -g \frac{\partial \zeta}{\partial y} + fu + v_H \left(\frac{\partial^2 v}{\partial x^2} + \frac{\partial^2 v}{\partial y^2} \right) + \frac{1}{h^2} \frac{\partial}{\partial z} \left(v_v \frac{\partial v}{\partial z} \right) - \frac{gv\sqrt{u^2 + v^2}}{hC^2} \quad (\text{A.3})$$

In which ζ is the water level according to a reference level [m], d is the water depth [m], h is the total water depth ($h = d + \zeta$) [m], u is flow velocity in x-direction [m/s], v is flow velocity in y-direction [m/s], ω is flow velocity in z-direction [m/s], f is Coriolis parameter [1/s], v_H is horizontal eddy viscosity [m^2/s], v_v is vertical eddy viscosity [m^2/s], and C is Chezy-coefficient [$m^{1/2}/s$].

When considering the 3D approach, no vertical momentum equation is solved. This is because the assumption is made that the vertical accelerations are smaller compared to the gravitation acceleration. The vertical velocity is calculated from the continuity equation. In the 2DH approach, the terms containing the vertical coordinate (z), the vertical flow velocity (w), and the vertical eddy

viscosity (ν_V) are not taken into consideration. These terms only affect the vertical distribution of momentum. Thus, the same set of equations are solved in the 2DH approach as in the 3D. Nevertheless, the vertical distribution of momentum is not computed in the 2DH approach. In this study, the model simulations were conducted using the 2DH approach. Since this study was aimed to see the results of the cross-sectional view, we selected a cross-section from the midpoint of the alongshore distance of the FLOW grids to visualize the results (1 layer in the middle). More information can be read in [Hydraulics \(2003\)](#)

Morphodynamic

For the transport of non-cohesive sediment, the sediment formulation of van Rijn (1993, 2000) is applied by default in Delft3D ([Hydraulics, 2003](#)). In this study, apart from using the default formulation, van Rijn (1993, 2000), we also used van Rijn (2007) sediment formulation, especially in the first research phase. In all mentioned formulations, both are distinguished into bed load and suspended load transport. Bed load and suspended load transport have a wave-related and current-related contribution as presented below:

$$q_s = q_{s,c} + q_{s,w} \quad (\text{A.4})$$

$$q_b = q_{b,c} + q_{b,w} \quad (\text{A.5})$$

In which, q_s is suspended load transport, $q_{s,c}$ is current-related suspended load transport, and $q_{s,w}$ is wave-related suspended load transport. Meanwhile, q_b is bed load transport, $q_{b,c}$ represents current-related bed load transport, and $q_{b,w}$ is wave-related bed load transport.

The change of bed level is a result of gradients in sediment transport. This can be expressed by following the mass balance principle:

$$(1 - n) \frac{\partial z_b}{\partial t} - \frac{\partial (q_{b,x} + q_{s,x})}{\partial x} - \frac{\partial (q_{b,y} + q_{s,y})}{\partial y} = 0 \quad (\text{A.6})$$

In which, n is porosity, $q_{b,x}$ is bed load transport in the x-direction, $q_{s,x}$ is suspended load transport in the x-direction, $q_{b,y}$ is bed load transport in the y-direction, and $q_{s,y}$ is suspended load transport in the y-direction. More information can be read in Delft3D-FLOW manual [Deltares \(2023b\)](#) and [Hydraulics \(2003\)](#)

A2. Governing Equations in Delft3D-WAVE Module

Delft3D-WAVE is also known as the SWAN model - SWAN is an acronym for Simulating WAVes Nearshore. This SWAN model is able to simulate the evolution of random, short-crested wind-generated waves in estuaries, tidal inlets, lakes etc. In SWAN, even when nonlinear phenomena are dominant (e.g., in the surf zone), the representation of waves employs a two-dimensional wave action density spectrum. Next, the considered spectrum in SWAN is on the action density spectrum $N(\sigma, \theta)$ rather than the energy density spectrum $E(\sigma, \theta)$. The independent variables are the relative frequency σ (as observed in a frame of reference moving with the current velocity) and the wave direction θ (the direction normal to the wave crest of each spectral component). The action density is equal to the energy density divided by the relative frequency: $N(\sigma, \theta) = \frac{E(\sigma, \theta)}{\sigma}$. In SWAN this spectrum may vary in time and space.

From the Delft3D-WAVE manual (Deltares, 2023a), it is stated that the evolution of the wave spectrum is described by the spectral action balance in SWAN, which for Cartesian coordinates is:

$$\frac{\partial}{\partial t}N + \frac{\partial}{\partial x}c_xN + \frac{\partial}{\partial y}c_yN + \frac{\partial}{\partial \sigma}c_\sigma N + \frac{\partial}{\partial \theta}c_\theta N = \frac{S}{\sigma} \quad (\text{A.7})$$

The first term on the left-hand side in the action balance equation or Equation A.7 represents the local rate of change of action density in time, the second and third terms represent the propagation of action in geographical space (with propagation velocities c_x and c_y in x- and y-space, respectively). Next, the fourth term represents the shifting of the relative frequency due to variations in depths and currents (with propagation velocity c_σ in σ -space). Afterward, the fifth term represents depth-induced and current-induced refraction (with propagation velocity c_θ in θ -space). The expressions for these propagation speeds are taken from linear wave theory. The term $S(= S(\sigma, \theta))$ at the right-hand side of the action balance equation (Equation A.7) is the source term in terms of energy density representing the effects of generation, dissipation, and non-linear wave-wave interactions. More information can be read in the Delft3D-WAVE manual by Deltares (2023a).

A3. Obstacle representing FB (transmission coefficient)

In the current study, floating breakwater is represented by the transmission coefficient which is inputted in SWAN as an obstacle. Since obstacles usually have a transversal area that is too small to be resolved by the bathymetry grid in SWAN, an obstacle is modelled as a line (Deltares, 2023a). The transmission coefficient can reduce the wave height locally all along the prescribed length of the transmission coefficient line (Deltares, 2023a). In this case, the ratio of the transmitted wave height at the landward side of the obstacle over the incident wave height at the seaward side of the obstacle is equal to the wave transmission coefficient (C_t) of the obstacle (floating breakwater). By using this approach, it might be adequate to predict the wave field leeward of the (floating) breakwater (Mojabi et al., 2018). To clarify, Figure A.1 illustrates how the transmission coefficient representing FB affects the wave.

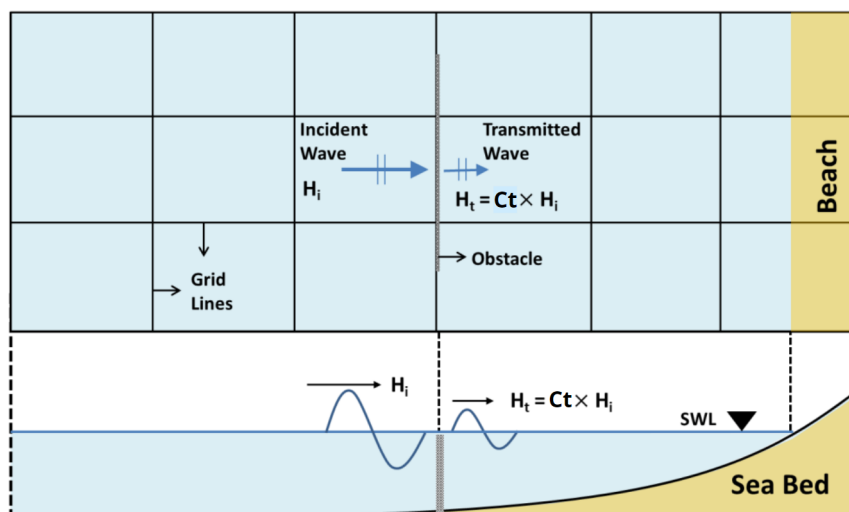


Figure A.1. Incident and transmitted wave with the application of the transmission coefficient in Delft3D; Bigger arrow/curve represents the greater wave height and smaller for the smaller wave height, retrieved from Mojabi et al. (2018)

Appendix B - Methods and data derivation

B1. Error statistics

Four error statistics are used in this study, especially in the first research phase, such as determination coefficient R^2 , Relative Bias, SCI Index, and Brier Skill Score. All these four parameters were used by Roelvink et al. (2009) to assess the performance of the computed erosion/sedimentation pattern. Nevertheless, Roelvink et al. (2009) emphasized that the Brier Skill Score is a parameter mainly to judge the skill of the sedimentation/erosion patterns. The equations of the mentioned parameters are provided below (Roelvink et al., 2009):

$$R^2 = \frac{Cov(m, c)}{\sigma_m \sigma_c} \quad (B.1)$$

$$SCI = \frac{rms_{c-m}}{\max(rms_m, |m|)} \quad (B.2)$$

$$Relative\ Bias = \frac{c - m}{\max(rms_m, |m|)} \quad (B.3)$$

$$Brier\ Skill\ Score = 1 - \frac{var(c - m)}{var(m)} \quad (B.4)$$

In these equations, σ is standard deviation, Cov is covariance, rms is root mean square, var is variance. c and m are computed and measured data respectively.

Interpretation of the results of error statistics

- If R^2 is equal to 1 (a perfect fit), it means that there is no scatter. Nevertheless, the tendency may still be wrong, which means that R^2 does not guarantee that the underlying relationship between the variables is correctly captured by the model (Roelvink et al., 2009),
- For relative bias and SCI Index, results with the least bias and scatter are the most favorable (Daly et al., 2012),
- For the Brier Skill Score van Rijn et al. (2003) summarized the qualification of the error to determine model's skill. This can be seen in Table B.1.

Table B.1. Qualification of error ranges of process parameters (brier skill score) based on van Rijn et al. (2003)

Qualification	Morphology (Brier Skill Score)
Excellent	1.0 - 0.8
Good	0.8 - 0.6
Reasonable/fair	0.6 - 0.3
Poor	0.3 - 0
Bad	<0

B2. Shoreface slope map of the Galgeplaat

Apart from analyzing the shoreface slopes of Roggenplaat mentioned in Section 3.3.2. We also analyzed the shoreface slopes of Galgeplaat using QGIS. From analyzing these two biggest shoals in the Eastern Scheldt, it is hoped that the derived shoreface slopes for Delft3D simulations already represent the shoals or intertidal flats in the Eastern Scheldt, even the intertidal flats in general.

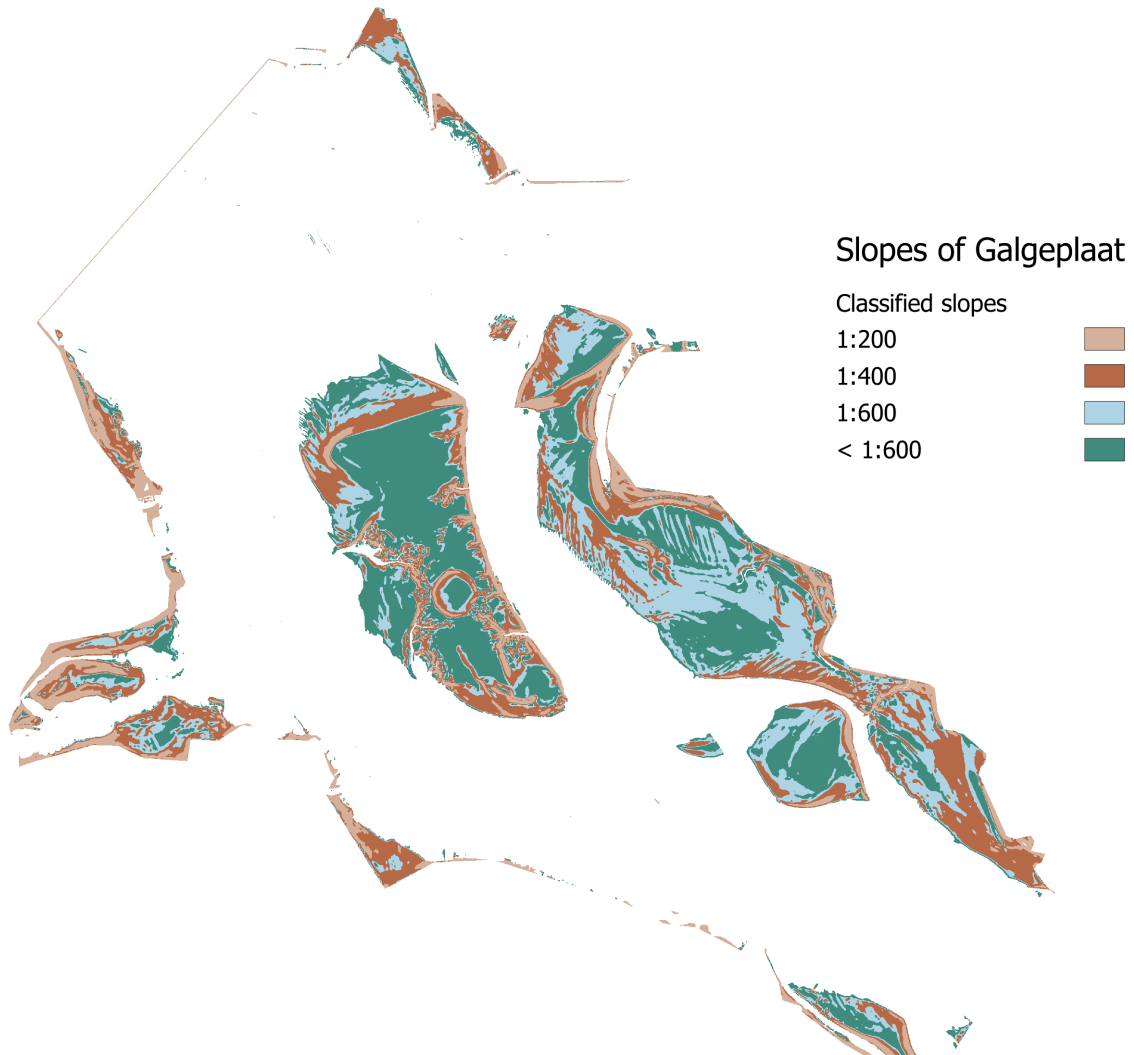


Figure B.1. Slope of Galgeplaat as another reference of shoreface slope derivation

B3. Cross-sections to derive channel slopes

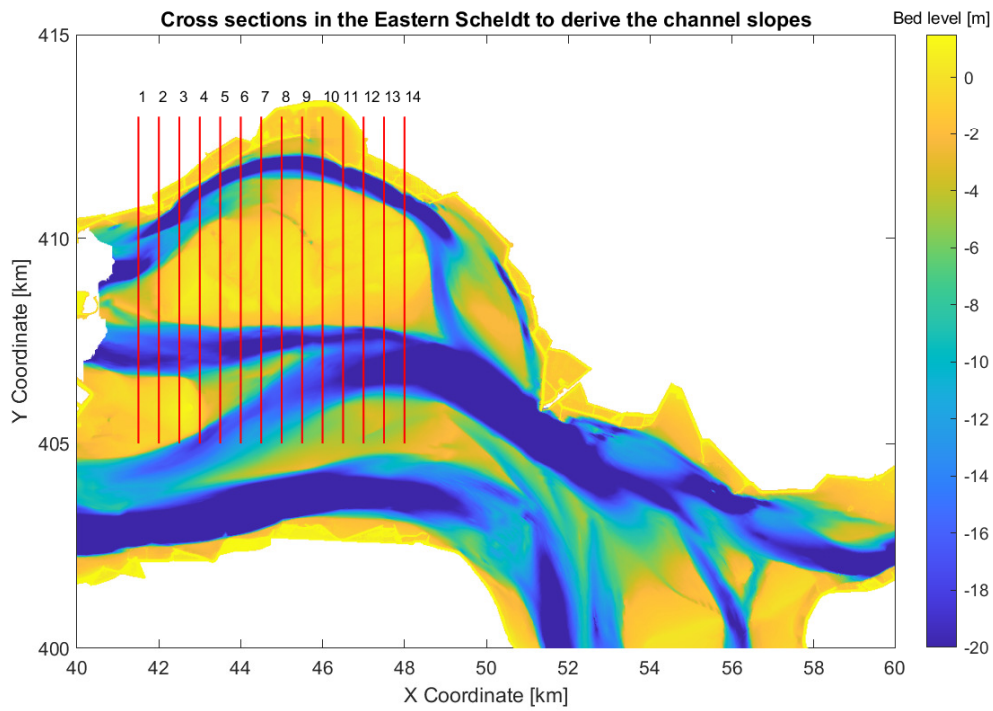


Figure B.2. Plan view of Roggenplaat representing the cross-sections to derive channel slopes

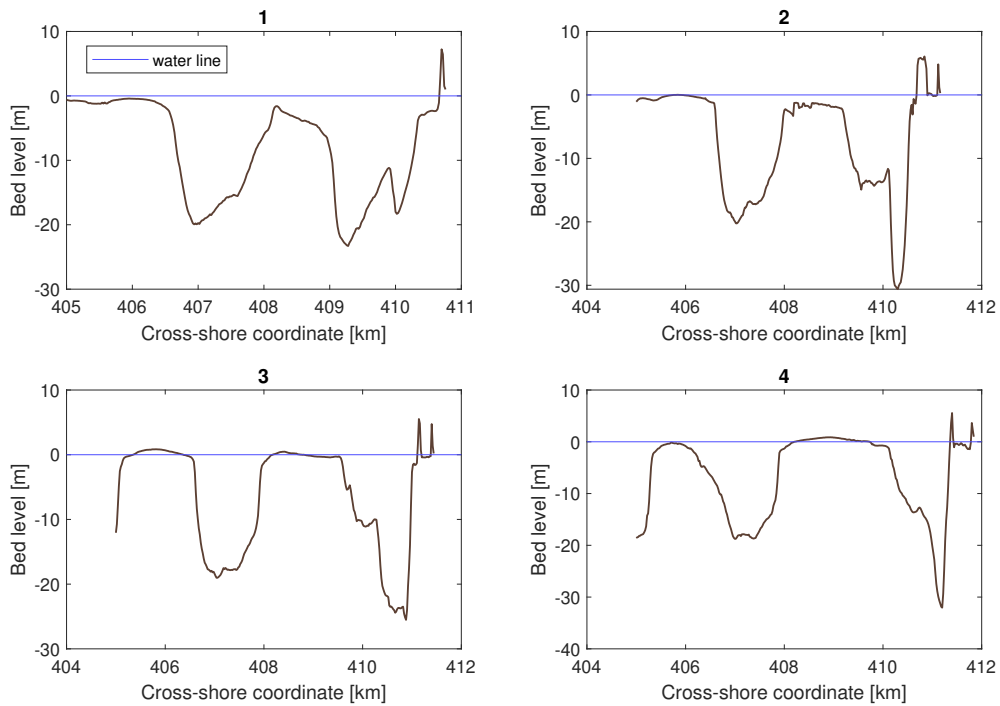


Figure B.3. Cross-sections of Roggenplaat 1-4

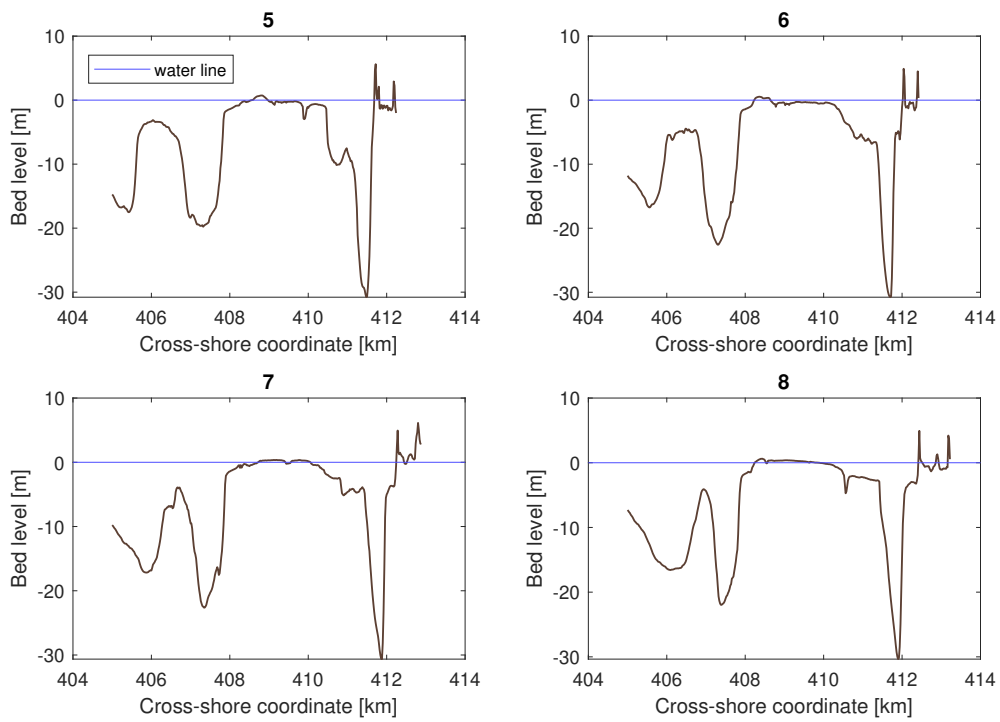


Figure B.4. Cross-sections of Roggenplaat 5-8

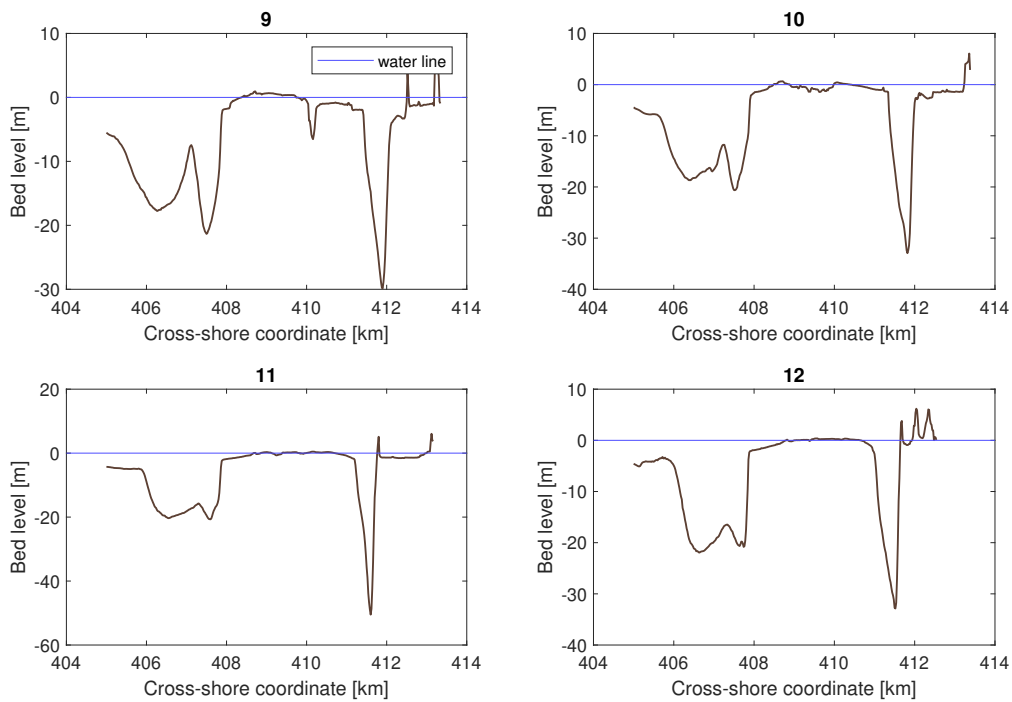


Figure B.5. Cross-sections of Roggenplaat 9-12

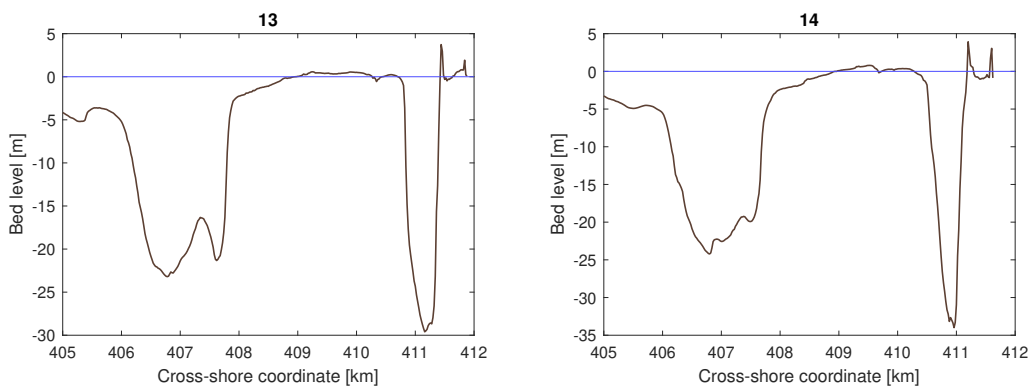


Figure B.6. Cross-sections of Roggenplaat 13-14

B4. A detailed derivation of the wave conditions

In this study, the derivation of wave conditions is basically synthesized from wind data and fetch measured at the Eastern Scheldt. After that, we use a nomogram presented in Figure B.11 to read the wind data and fetch distance to translate them into wave conditions: wave height and wave period. For wind data, we refer to the magnitude of wind speed of STAV (Figure B.8) and ZBWI station (Figure B.9), two nearest stations in the Eastern Scheldt (see Figure B.7 for the location). These two wind stations are located near the Eastern Scheldt.



Figure B.7. Location of two wind stations: STAV and ZBWI in the Eastern Scheldt, the upper right panel shows the overview position where the stations are located

From wind roses in Figure B.8 and Figure B.9, we can see that the wind speeds' magnitude varies from 0 - 25 m/s. Matching the magnitudes presented in Figure B.8 and Figure B.9 with the magnitude of wind speed that can be read in nomogram (Figure B.11), we take multiple magnitudes that correspond to both (wind roses and nomogram) to derive the wave conditions: 5 m/s, 7.5 m/s, 10.0 m/s, 12.5 m/s, 15.0 m/s, 17.5 m/s, and 20.0 m/s.

As mentioned before, we use wind speed (in m/s) and fetch (in km) to derive wave conditions (wave height and wave period). We take multiple lines from the Roggenplaat and Galgeeploot to calculate the fetch distance (see Figure B.10). The fetch distance derivation can be seen in Figure B.10, where the distances from the Roggenplaat and Galgeeploot to the southern land are determined, considering the wind direction indicated by the windroses. We obtain 5, 6, and 7 km for the fetch distance at the Roggenplaat. For the Galgeeploot, we obtain 2 and 3 km. We also add a distance of 10 km to obtain a more extreme wave condition.

We already defined the wind speed and fetch distance. Then, we use the considered wind speed and fetch distances for deriving the wave height and wave period. From Figure B.11, we can see the nomogram used to derive wave height (on the left x-axis) and wave period (curvy dashed line).

Windroos STAV Periode 01.10.1990 - 31.12.2022

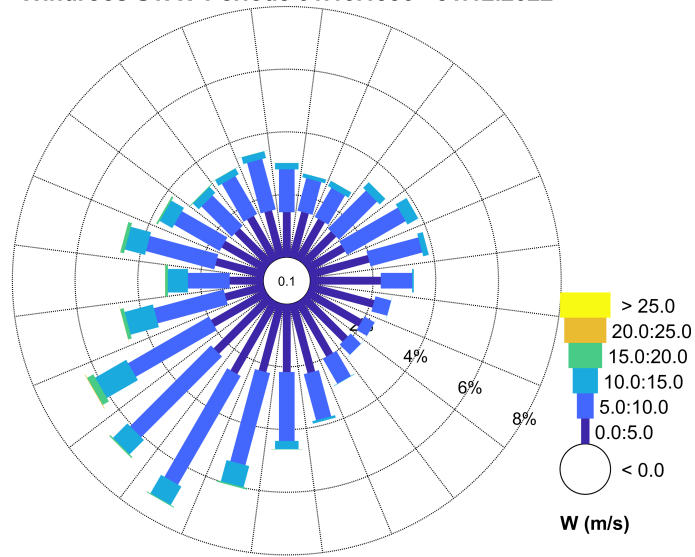


Figure B.8. Wind rose for STAV station, data recorded from 1990 to 2022

Windroos ZBWI Periode 01.01.2010 - 31.12.2022

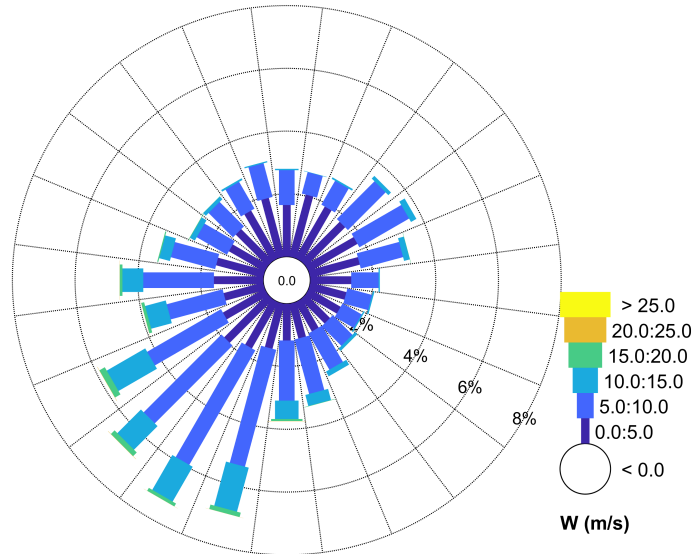


Figure B.9. Wind rose for ZBWI station, data recorded from 2010 to 2022

The way to derive the wave height and wave period from the nomogram (see Figure B.11) starts by selecting the considered wind speed (right y-axis of Figure B.11) and the fetch distance at the upper bold lines in Figure B.11.

Figure B.12 shows an example of the derivation of wave conditions (wave height and wave period). This Figure shows the derivation of wave conditions based on the wind speeds of 5.0, 7.5, 10.0, 12.5, 15.0, 17.5, and 20.0 m/s, and fetch of 2 km. For the wave height, the fetch of 2 km is marked. Next,

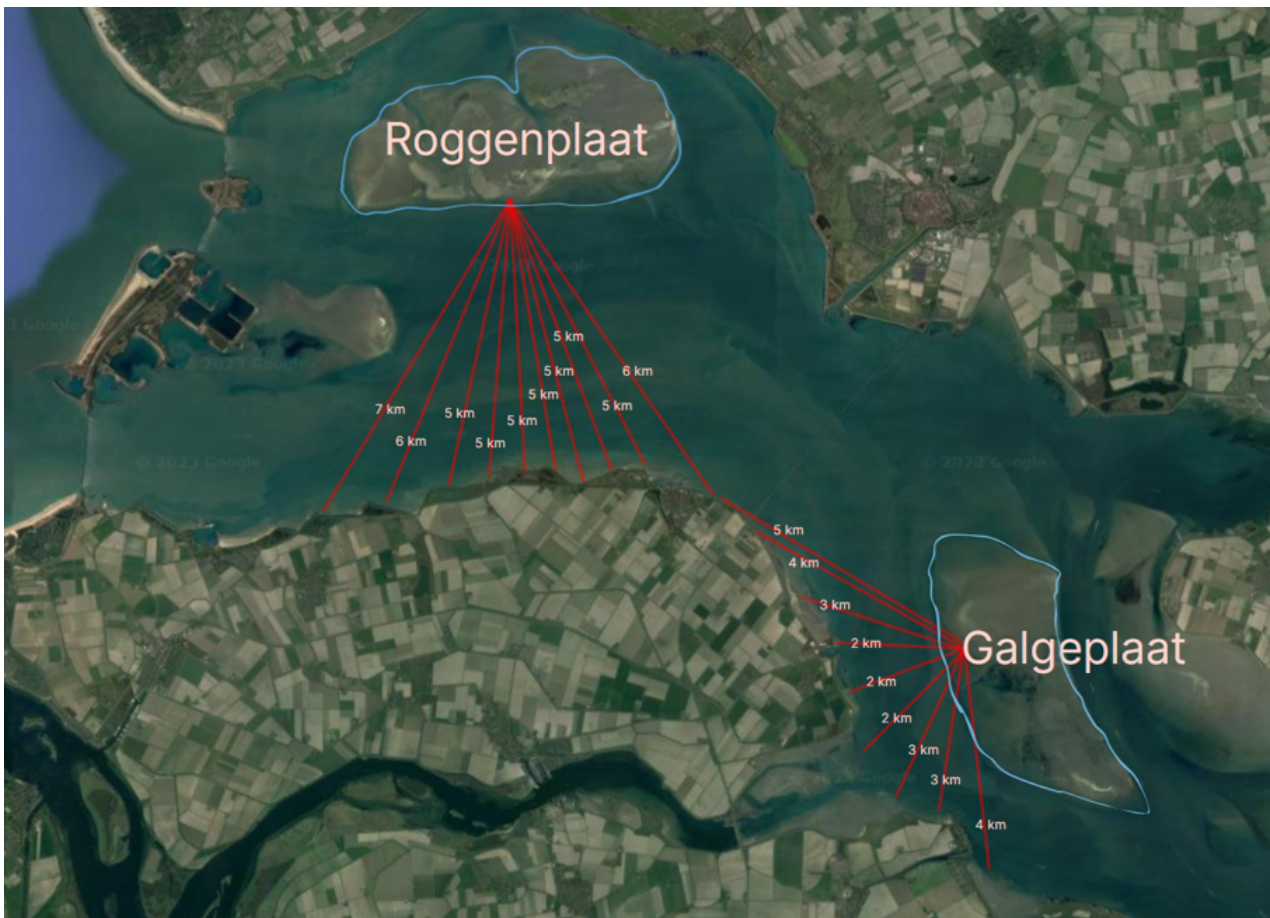


Figure B.10. Fetch distance measurement near the Roggenplaat and Galgeplaat in the Eastern Scheldt

the wind magnitudes follow the wind speed lines on the right y-axis. As the fetch and wind magnitudes lines meet, we can further take the horizontal lines for getting the wave height magnitudes (see Figure B.12 on the left panel).

Furthermore, the wave period was executed almost similarly to the wave height derivation. Until the lines of fetch and wind velocities are met, the intersection points are used to approximate the wave period. The highlighted red lines in Figure B.12 indicate the wave period of 2 s and 3 s. For the intersection points in between or below 2 s, we approximated the value of the wave periods. To see the derived values for all wind speeds and fetch distances, we can see Table B.2. The wave conditions remarked by bold texts mean that they are the selected wave conditions in this study.

According to Table B.2, it can be witnessed that we select four-wave conditions that were presented in Section 3.3.3. The wave conditions were selected by ensuring that the selected wave conditions were from different fetch distances (see Table B.2) and within the range of the wave condition presented by the wave roses (Figure B.13 and Figure B.14). This selection process aimed to ensure a diverse representation of wave conditions for the analysis in research phase two.

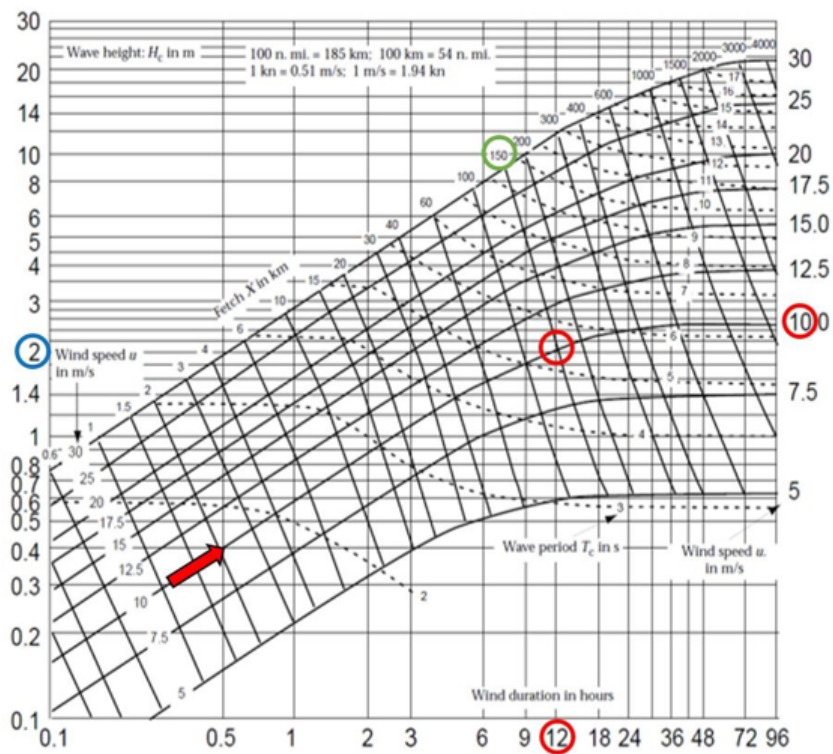


Figure B.11. Wave nomogram, retrieved from Breugem and Holthuijsen (2007)

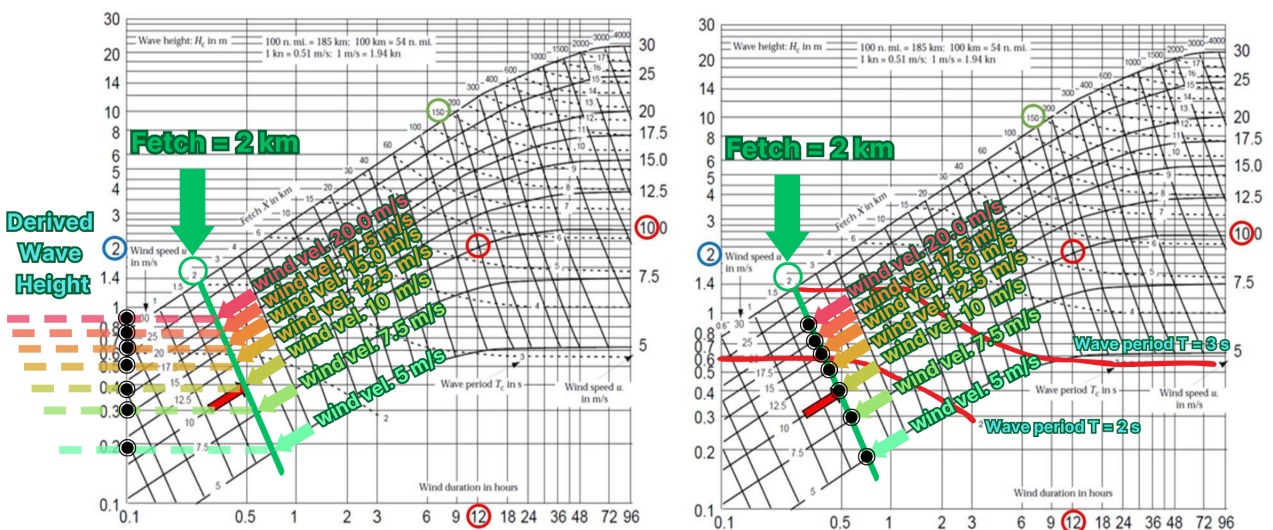


Figure B.12. Wave derivation with the wind speeds of 5, 7.5, 10, 12.5, 15, 17.5, and 20 m/s and fetch of 2 km

Table B.2. Derived wave conditions from different fetch length and wind velocity, derived data in bold is the used wave conditions for the second research phase

Wind velocity u_{10}	fetch = 2 km		fetch = 3 km		fetch = 6 km		fetch = 7 km		fetch = 10 km	
	Hs	Tp	Hs	Tp	Hs	Tp	Hs	Tp	Hs	Tp
	m	s	m	s	m	s	m	s	m	s
5 m/s	0.19	1.20	0.21	1.50	0.29	1.70	0.32	1.90	0.35	2.00
7.5 m/s	0.30	1.50	0.32	1.70	0.45	2.00	0.51	2.20	0.60	2.40
10.0 m/s	0.40	1.70	0.50	1.90	0.65	2.30	0.70	2.50	0.8	2.80
12.5 m/s	0.50	1.90	0.60	2.10	0.80	2.50	0.90	2.80	1.10	2.90
15.0 m/s	0.60	2.00	0.70	2.30	1.00	2.80	1.10	2.90	1.30	3.10
17.5 m/s	0.70	2.20	0.90	2.50	1.20	3.00	1.30	3.00	1.50	3.40
20.0 m/s	0.90	2.50	1.10	2.80	1.40	3.10	1.60	3.20	1.80	3.80

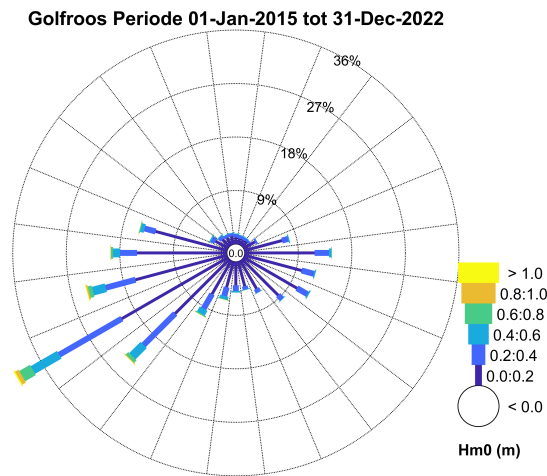


Figure B.13. Wave rose for the wave height recorded from 01 January 2015 to 31 December 2022

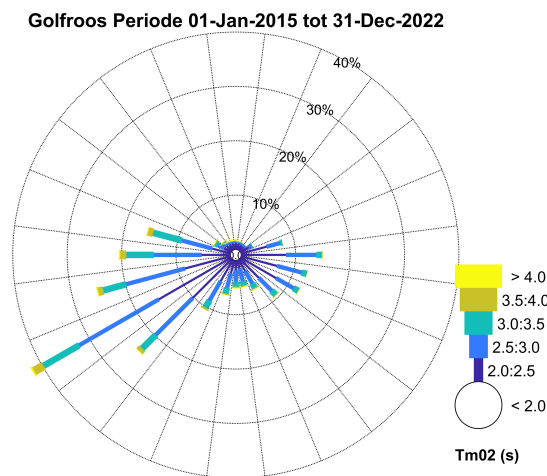


Figure B.14. Wave rose for the wave period recorded from 01 January 2015 to 31 December 2022

B5. Probability of the wind speeds from the selected wave conditions

We also computed the probability of occurrence of the windspeeds used for deriving the wave conditions: 10.0 m/s, 15.0 m/s, 17.5 m/s, and 20.0 m/s. To calculate the probability of occurrence, we used wind data from the ZBWI station with 4012 data points (wind data every 10 minutes) recorded from 11 June 2023 to 09 July 2023. After that, these data points from the biggest and the smallest values are arranged. We also computed the mean and standard deviation values of these data points, resulting in an average wind velocity of 5.32 m/s with a standard deviation of 2.623 m/s. After that, we also computed the method of moments estimators of the Gumbel (maximum) distribution, represented by two variables $\tilde{\beta}$ and $\tilde{\mu}$. These parameters can be calculated using the equation below:

$$\tilde{\beta} = \frac{s\sqrt{6}}{\pi} \quad (\text{B.5})$$

Where s equals standard deviation $\left(\sqrt{\frac{(X-\bar{X})^2}{n-1}}\right)$, and $\pi = 3.14$. Meanwhile, for $\tilde{\mu}$, we can calculate using the equation below:

$$\tilde{\mu} = \bar{X} - 0.5772\tilde{\beta} \quad (\text{B.6})$$

Where \bar{X} is the mean value of the wind.

Calculating these two variables, $\tilde{\beta}$ and $\tilde{\mu}$, allow us to calculate the probability of occurrence of a wind velocity. We can calculate the probability of occurrence of the wind by employing this equation below:

$$P = 1 - \exp\left(-\exp\left(-\left(\frac{X - \tilde{\mu}}{\tilde{\beta}}\right)\right)\right) \quad (\text{B.7})$$

Using the equation above, we calculate the probability of wind data from the ZBWI station and the probability of wind data representative of those selected wave conditions presented by Table B.2. Figure B.15 visualizes the whole data's wind probability and highlights the wind data that are representative of the selected wave conditions.

Number of events in a year

The calculated probability using every 10-minute data results in different probabilities of occurrence for different wind speeds. To calculate the number of events based on the calculated probability, the formula below is used:

$$P = \frac{n(u)}{n(S)} \quad (\text{B.8})$$

In which P is the probability, $n(u)$ is the number of events of the corresponding wind speed, $n(S)$ is the total number occurring in a sample space.

With the known probability for every wind speed, a total number of events can be known by re-arranging Equation B.8. Since the probability was derived using 10-minute data, the number of events per day with the interval of 10 minutes is $n(S) = 144$ data sample. To calculate the number of events of the corresponding wind speed, $n(S)$ is multiplied by the probability P . Thereby, we obtain:

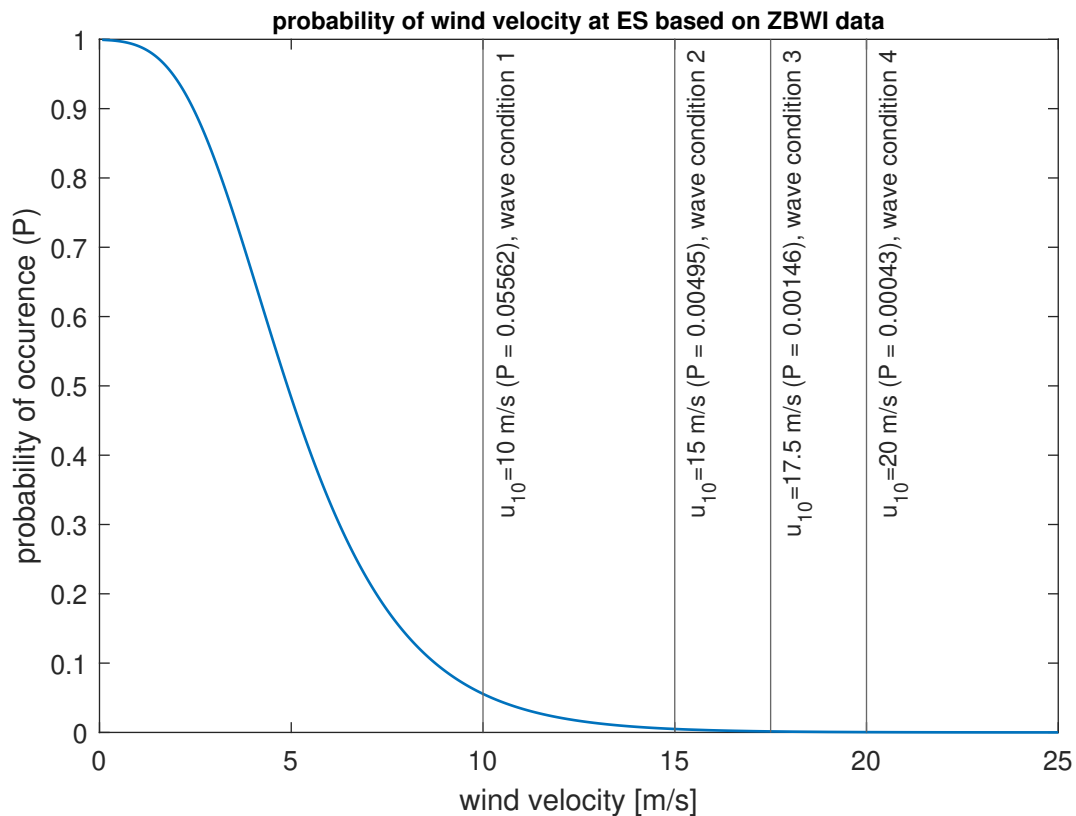


Figure B.15. Probability of occurrence of the wind for deriving wave conditions in the second research phase, ES means Eastern Scheldt

- $n(S) = 0.05562 \times 144 = \mathbf{8.01 \text{ events}}$ in a day for wind speed with $u_{10} = 10.0 \text{ m/s}$, (corresponds to wave condition 1: $H_0 = 0.40 \text{ m}$ $T_p = 1.7 \text{ s}$)
- $n(S) = 0.00495 \times 144 = \mathbf{0.71 \text{ events}}$ in a day for wind speed with $u_{10} = 15.0 \text{ m/s}$, (corresponds to wave condition 2: $H_0 = 0.70 \text{ m}$ $T_p = 2.3 \text{ s}$)
- $n(S) = 0.00146 \times 144 = \mathbf{0.21 \text{ events}}$ in a day, for wind speed with $u_{10} = 17.5 \text{ m/s}$, (corresponds to wave condition 3: $H_0 = 1.20 \text{ m}$ $T_p = 3.0 \text{ s}$)
- $n(S) = 0.00043 \times 144 = \mathbf{0.06 \text{ events}}$ in a day, for wind speed with $u_{10} = 20.0 \text{ m/s}$ (corresponds to wave condition 4: $H_0 = 1.80 \text{ m}$ $T_p = 3.8 \text{ s}$)

B6. Calculation of critical bed shear stress

The calculation of critical bed shear stress (τ_{cr}) is done by employing this formula (Deltares, 2023b):

$$\tau_{cr} = (\rho_s - \rho_w)gD_{50}\theta_{cr} \quad (\text{B.9})$$

Where ρ_s is sediment density = 2650 kg/m^3 , ρ_w is fluid density = 1000 kg/m^3 , g is the acceleration of gravity = 9.81 m/s^2 , D_{50} is sediment particle size = $150 \text{ }\mu\text{m}$ (sediment particle used in the current study), θ_{cr} is dimensionless critical shear stress that can be calculated by using the equation below (Deltares, 2023b):

$$\theta_{cr} = \begin{cases} 0.24D_*^{-1} & 1 < D_* \leq 4 \\ 0.14D_*^{-0.64} & 4 < D_* \leq 10 \\ 0.04D_*^{-0.1} & 10 < D_* \leq 20 \\ 0.013D_*^{0.29} & 20 < D_* \leq 150 \\ 0.055 & 150 < D_* \end{cases} \quad (\text{B.10})$$

As dimensionless grain size (D_*) has not been known, we need to calculate it using the equation below:

$$D_* = D_{50} \left(\frac{\Delta g}{\nu^2} \right)^{1/3} \quad (\text{B.11})$$

Calculation of D_*

we then calculate D_* by first calculating:

- $\Delta = \frac{\rho_s}{\rho_w} - 1 = \frac{2650}{1000} - 1 = 1.65$
- then, with kinematic viscosity coefficient $\nu = 0.000001 \text{ m}^2/\text{s}$, we can calculate D_*
- by plugging in the known values (D_{50}, Δ, g, ν) for Equation B.11, we obtain $D_* = 3.79$

Calculation of θ_{cr}

With the known D_* we shift to Equation B.10. Here since D_* is lie within this range $1 < D_* \leq 4$, we use $0.24D_*^{-1}$ to calculate θ_{cr} . This results in $\theta_{cr} = 0.0632$

Calculation of bed shear stress τ_{cr}

As θ_{cr} (=0.0632) is known, we can calculate the critical bed shear stress (τ_{cr}). Using Equation B.9, we obtain a critical bed shear stress (τ_{cr}) = 0.153 N/m^2 . This value is used to interpret bed shear stress in Section 5.2.3.

Appendix C - Calibration in Delft3D

C1. Grid size effects and wave spectra

In the Delft3D setting for the first research phase, the WAVE grid and wave spectra were adjusted to avoid unexpected wave decline across the model domain. This was because we considered a more gradual decrease in wave height, which is more reasonable (de Vries, 2007). Concerning that, we found strange wave height declines in the first try of the Delft3D model for the first research. In this case, the wave suddenly dropped just after propagating from the open boundary (offshore). To diminish this effect, we tried to increase the size of the Delft3D-WAVE grid in the alongshore distance. As seen in Figure C.1, when the alongshore grid size increases, the wave height across the shore becomes normal (no sudden drop). Furthermore, there was still a wave height drop when we set the alongshore grid size to 60 m, 75 m, and 100 m. Nevertheless, we presumed this is no longer due to the grid effects.

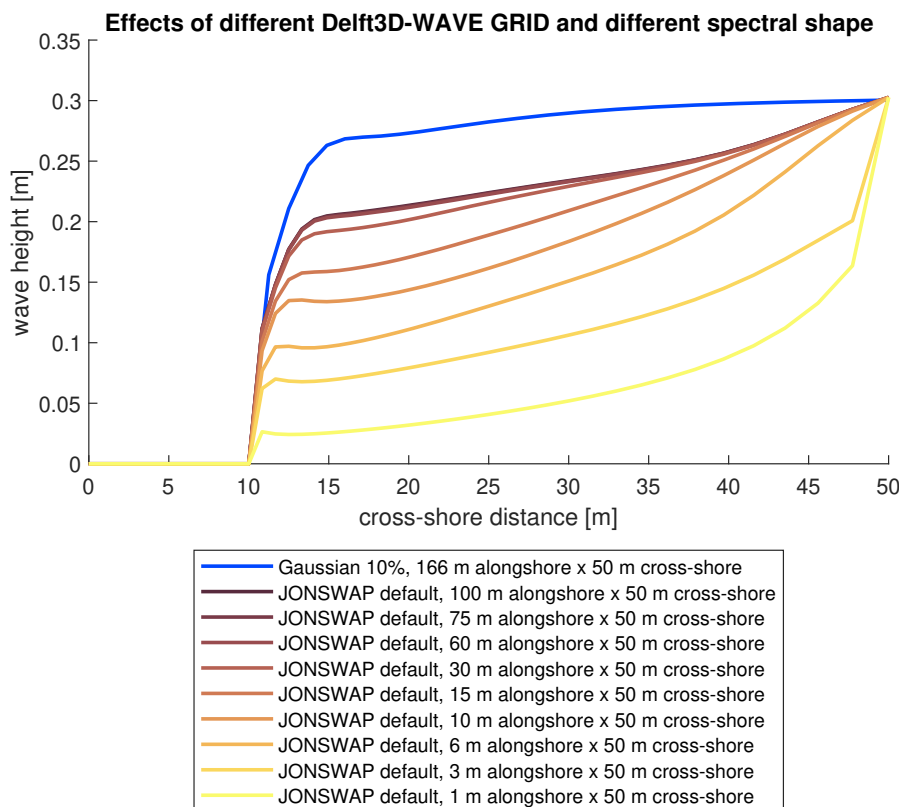


Figure C.1. Different wave grid size to avoid unexpected wave height decline across the boundary (cross-shore profile), simulated using wave condition phase 1 (Shimoda), $H_0 = 0.30$ m $T_p = 1.8$ s

Because the intention for the first phase was to reproduce the wave under a laboratory setting, the JONSWAP spectrum would not be representative. Regarding this, we needed a stationary wave condition (there is no change of the imposed wave from the open boundary). A stationary wave condition was set to address this by adjusting the wave spectra from the JONSWAP spectrum to Gaussian with a spreading of 10% (0.1) and a sufficiently wide Delft3D-WAVE grid.

C2. Wave spectra, bottom friction, and white capping

To avoid the sudden drop in wave height, we implemented the same approach for the second research phase as what we explained for the first research phase: set the Gaussian distribution shape to 10% and define a sufficiently wide Delft3D-WAVE grid. However, we found that the sudden drop in wave height still occurred.

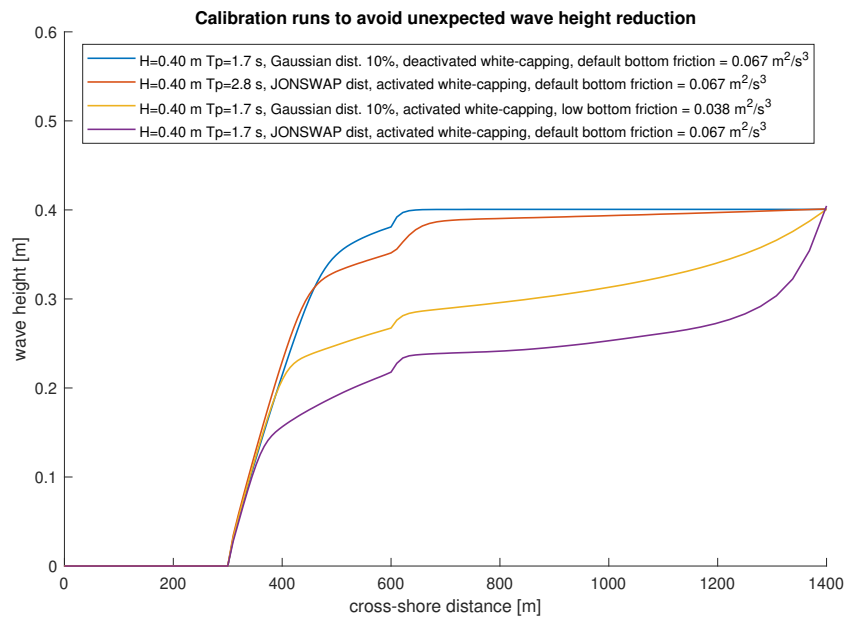


Figure C.2. Calibration runs to avoid unexpected wave height decline across the boundary (cross-shore profile), simulated using wave condition 1 (research phase 2): $H_0 = 0.40$ m $T_p = 1.7$ s, except for one case (orange line)

To tackle this issue, we ran four simulations and altered some parameters. In this case, we followed the calibration attempts advised by [de Vries \(2007\)](#). The changes in Delft3D were related to bottom friction, wave period, and white-capping. By focusing on those parameters, alterations in Delft3D were made. First, we reduced the value of bottom friction to diminish the effect of wave reduction due to bottom friction. As seen in [Figure C.2](#), the sudden decrease in wave height still occurred. Next, we adjusted the wave period from 1.7 s to 2.8 s. The adjustment of the wave period was intended to decrease the wave steepness, resulting in a lower possibility of white-capping to occur. In this case, white-capping means the wave breaking in deep water due to a very steep wave during storm conditions ([de Vries, 2007](#)). After adjusting the wave period, we obtained the gradually decreasing wave height. However, since it was not the wave period that we derived during our data collection, we tried to implement another solution to avoid this sudden wave height decline. Hence, we further tried to deactivate white-capping in our Delft3D-WAVE setting. Afterward, we obtained the straight propagating wave height, which decreased after being influenced by the bottom friction. It is important to note that the physical processes are not better represented without white-capping, and therefore, deactivation of white-capping is not a desirable option ([de Vries, 2007](#)). Nevertheless, this way was also implemented for matching the wave height with the measurement by [Dingemans \(1983\)](#), ([de Vries, 2007](#)). To deduce, we found that the deactivation of white-capping is useful to avoid the sudden drop in wave height while keeping the data we derived for the simulation in the second research phase. We also acknowledge from this issue that the data we derived for the second research might be flawed.

Appendix D - Complementing information for the results in research phase 1 and 2

D1. Reproduced cross-sections with different adjustments of basic settings

Model settings 1

This cross-section and wave height were derived from the model setting with adjustment (model settings) 1. Based on this setting, the wave height suddenly dropped, starting from below 0.2 m instead of 0.3 m (see lower panel on cross-shore distance 40 m) as it was supposed to be, according to the experimental data.

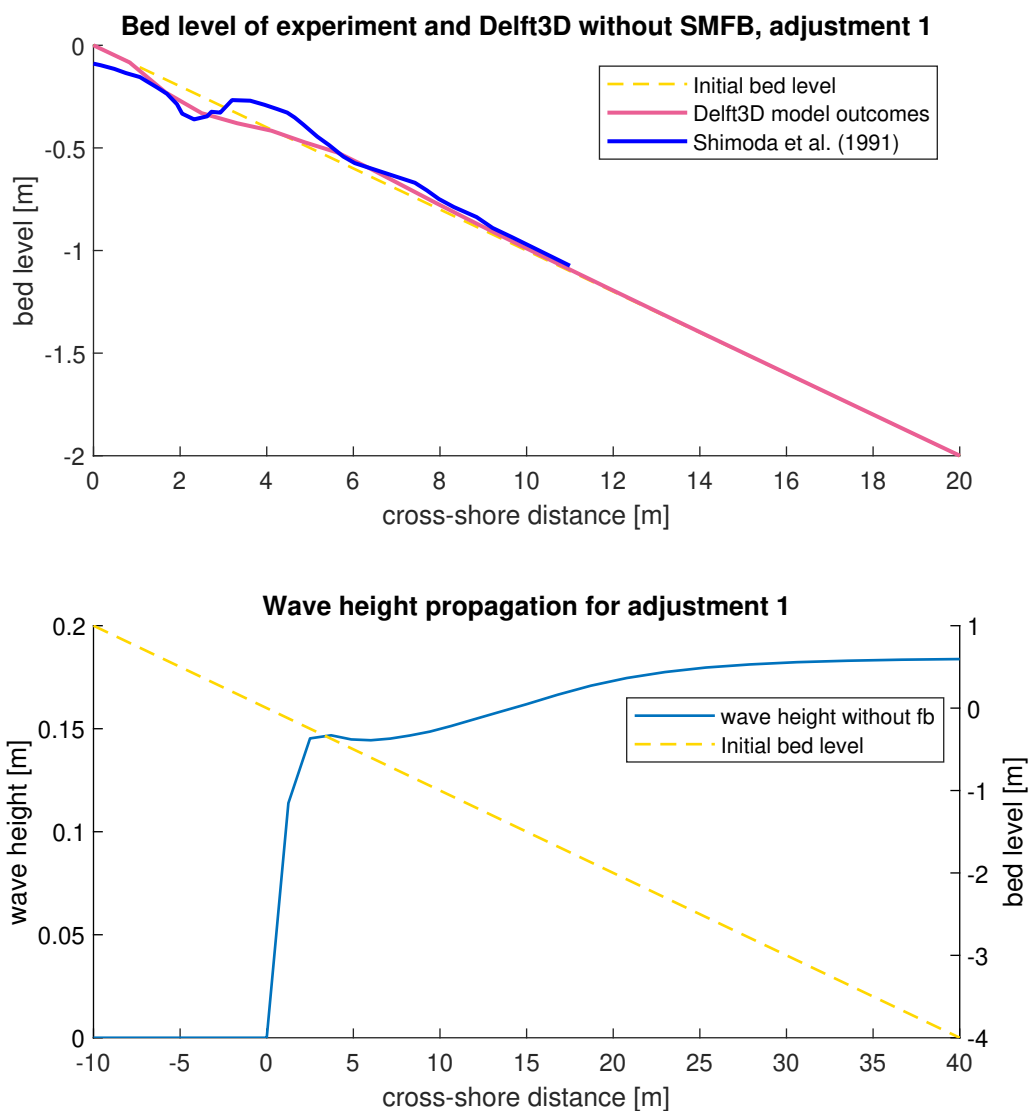


Figure D.1. Cross-section and wave height based on model settings 1

Model settings 2

This cross-section and wave height were derived from the model setting with adjustment (model settings) 2. Based on this setting, the wave height suddenly dropped, starting from below 0.2 m instead of 0.3 m (see lower panel on cross-shore distance 40 m) as it was supposed to be, according to the experimental data.

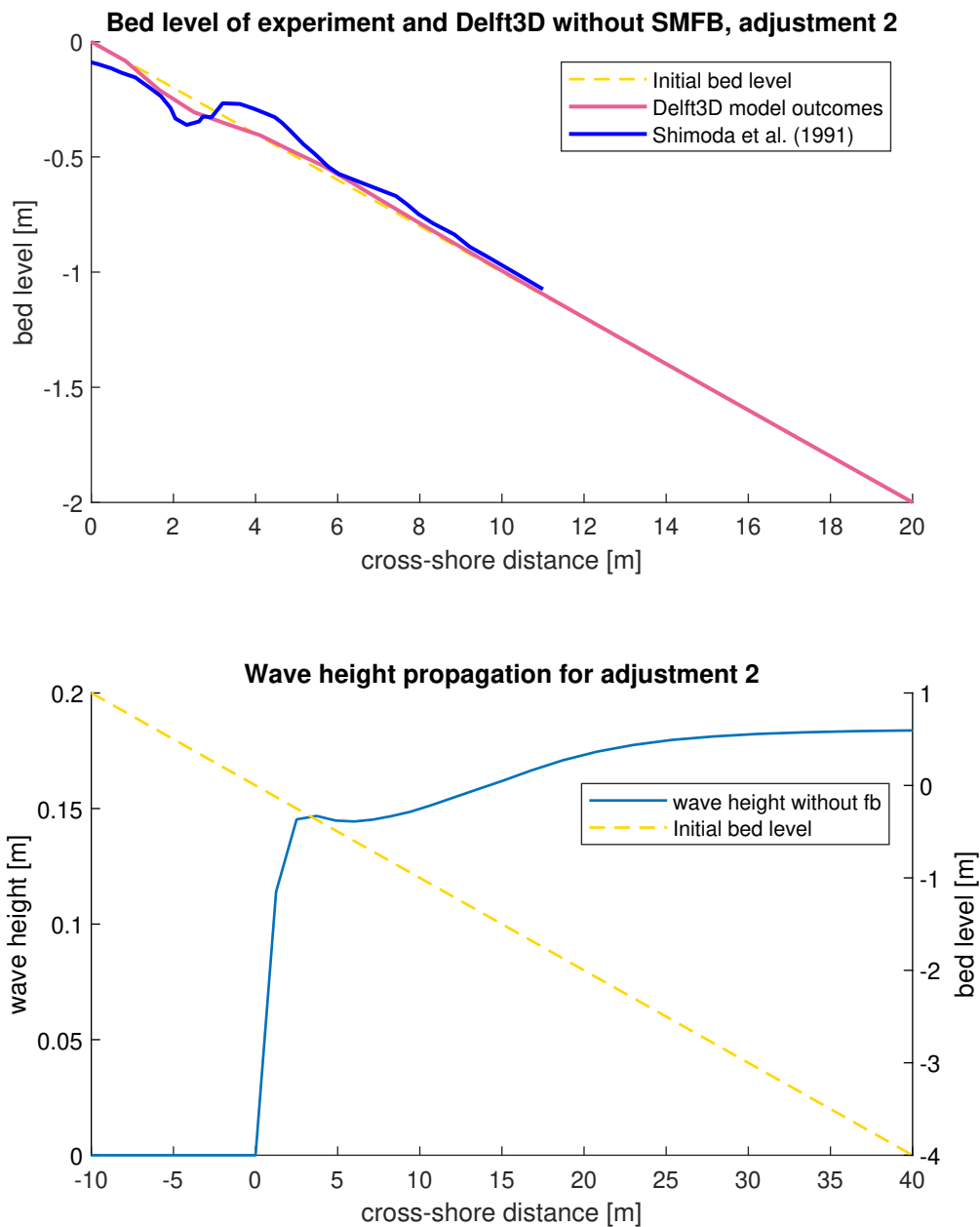


Figure D.2. Cross-section and wave height based on model settings 2

Model settings 3

This cross-section and wave height were derived from the model setting with adjustment (model settings) 3. Based on this setting, the wave height suddenly dropped, starting from below 0.2 m instead of 0.3 m (see lower panel on cross-shore distance 40 m) as it was supposed to be, according to the experimental data.

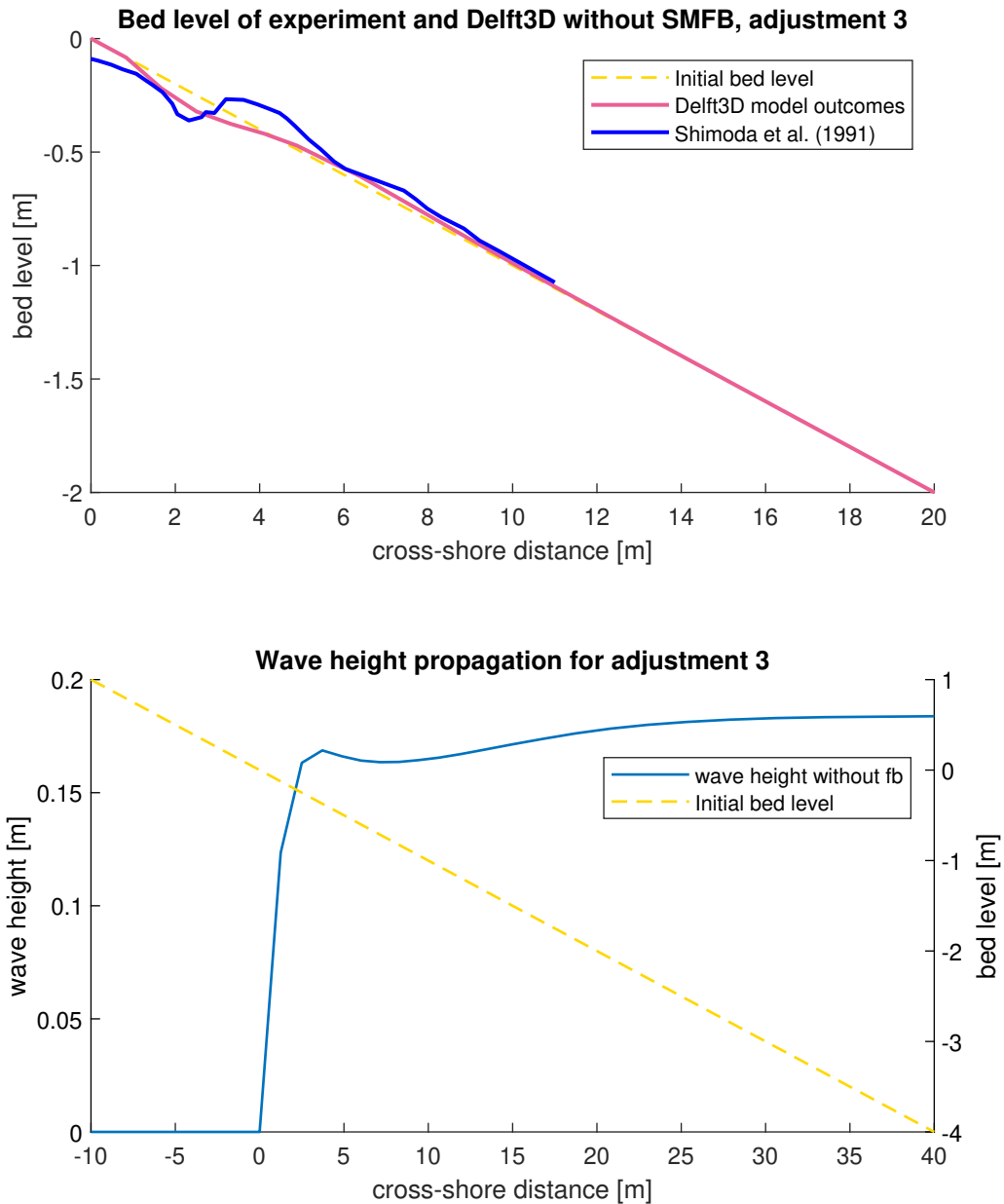


Figure D.3. Cross-section and wave height based on model settings 3

Model settings 4

This cross-section and wave height were derived from the model setting with adjustment (model settings) 4. This was the setting we selected because this setting showed the most significant value according to error statistics (R^2 , sci, relbias, bss), and the wave height did not drop significantly in the open boundary (cross-shore distance 40 m).

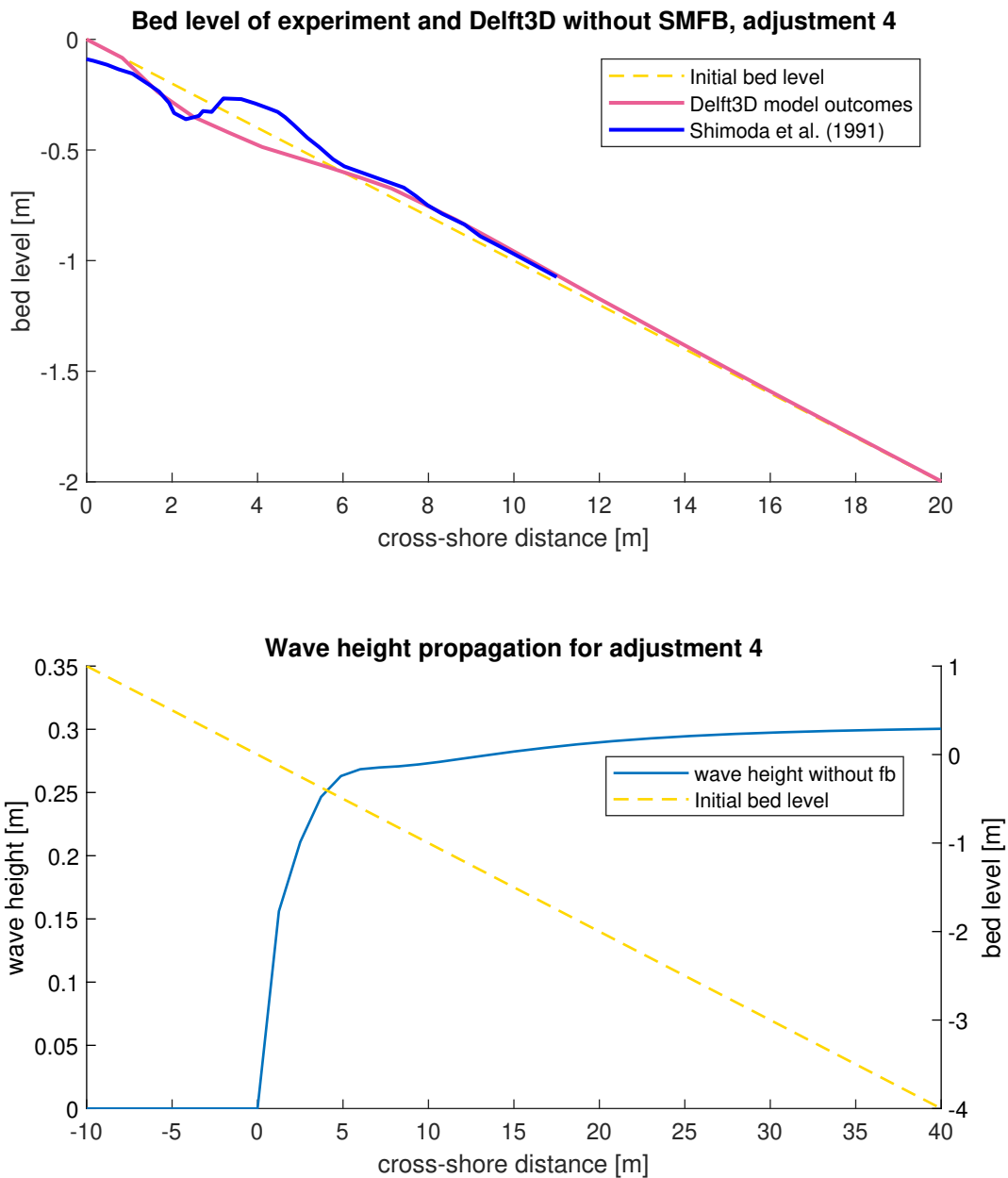


Figure D.4. Cross-section and wave height based on model settings 4

Model settings 5

This cross-section and wave height were derived from the model setting with adjustment (model settings) 5. This was not selected because, according to error statistics (R^2 , sci, relbias, bss), the values were slightly below adjustment 4. In this adjustment, the wave height did not drop significantly in the open boundary (cross-shore distance 40 m).

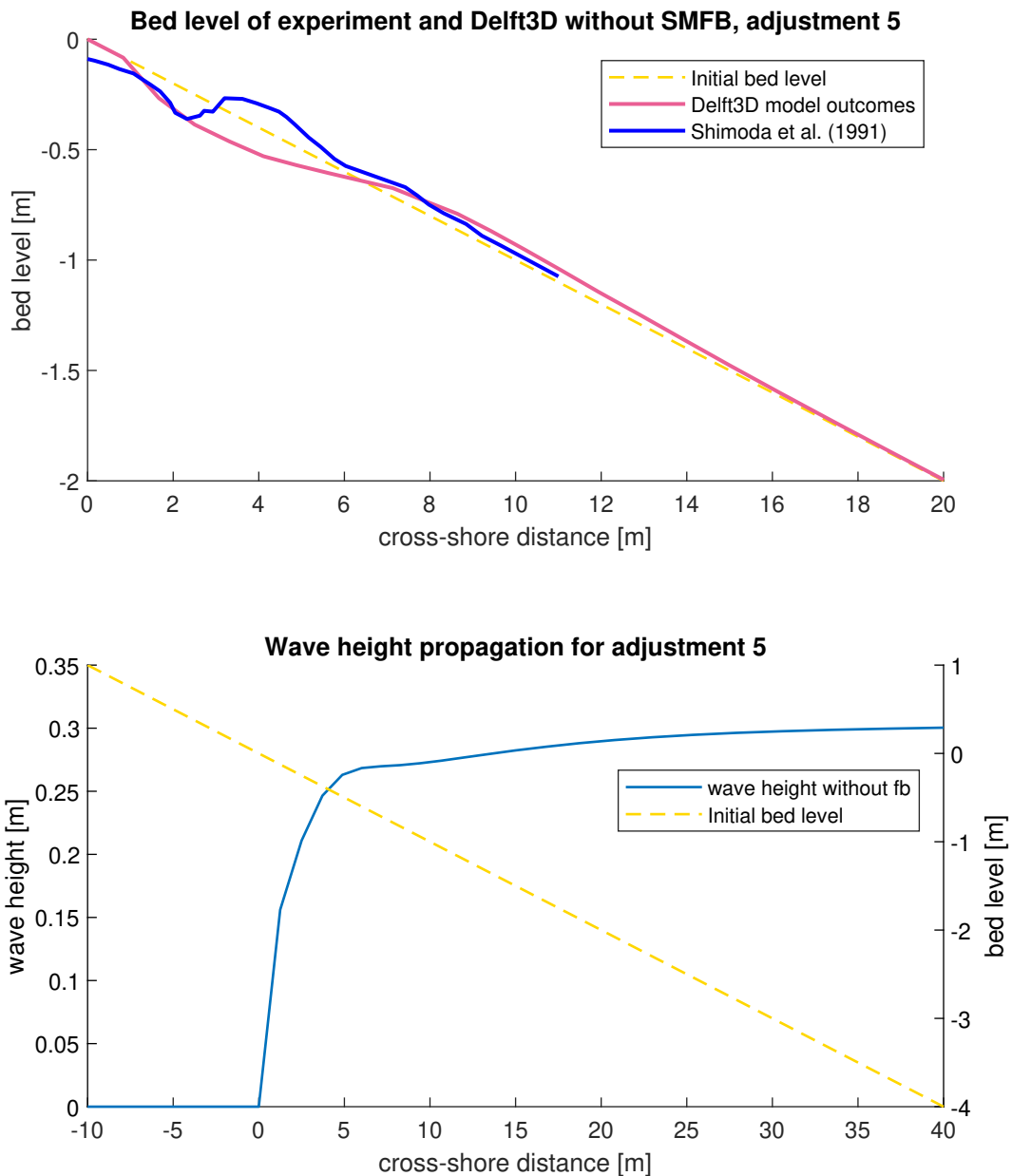


Figure D.5. Cross-section and wave height based on model settings 5

Model settings 6

This cross-section and wave height were derived from the model setting with adjustment (model settings) 6. The difference from all previous cross-sections is the sediment transport formulation. Here, we use van Rijn (2007) sediment transport formulation. We did not select this setting because there was no significant difference in cross-shore evolution when the FB was imposed.

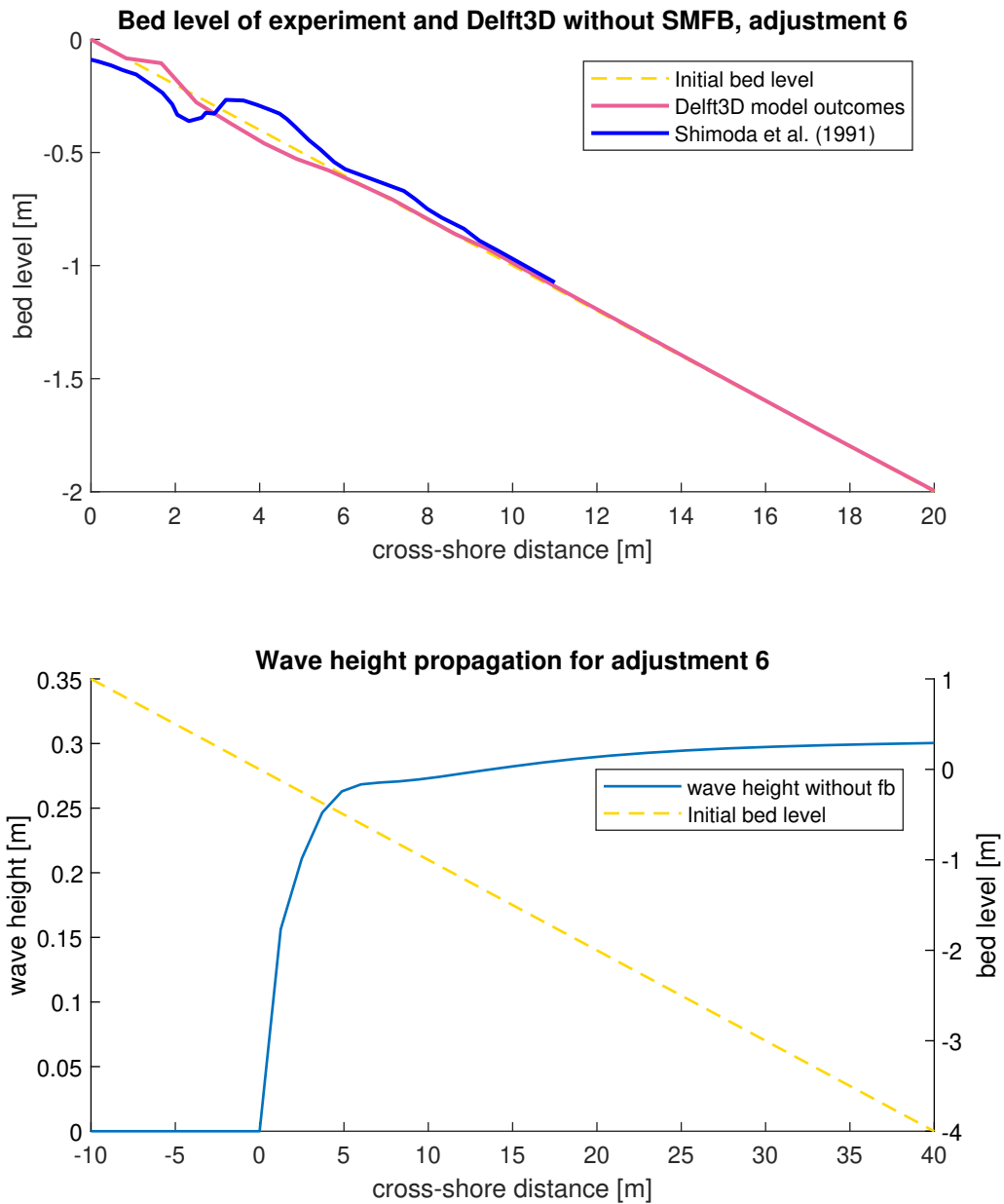


Figure D.6. Cross-section and wave height based on model settings 6

D2. Near-bed orbital velocity, bed shear stress, and depth-averaged velocity without and with FB in the first research phase

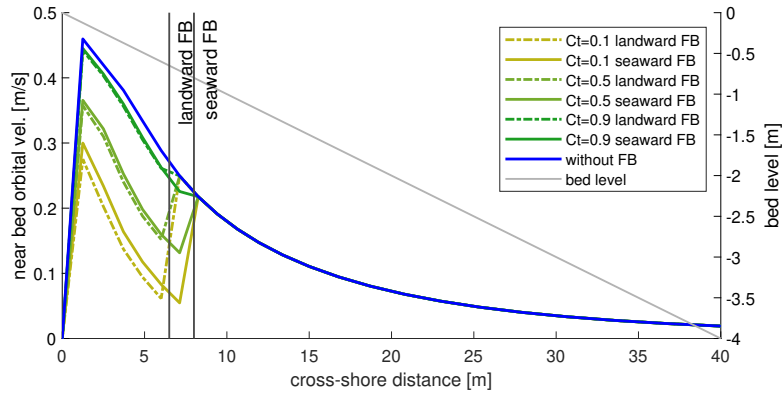


Figure D.7. Near bed orbital velocity without and with FB, see the peak and reduced peaks near the shoreline for seeing the FB effects

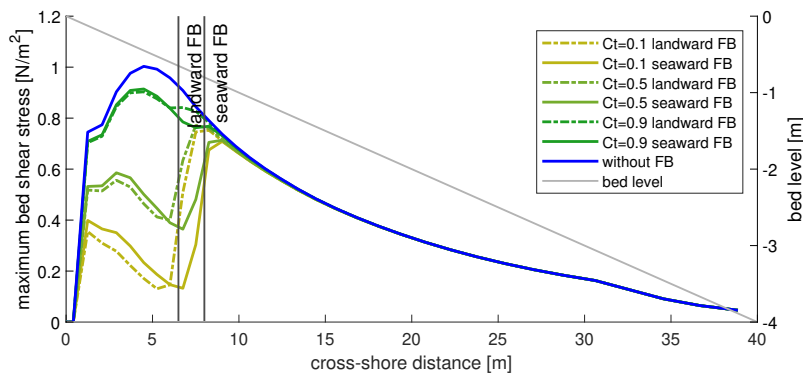


Figure D.8. Bed shear stress without and with FB, see the peak and reduced peaks near the shoreline for seeing the FB effects

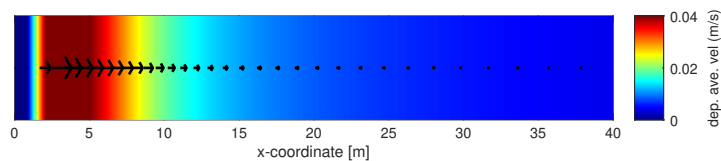


Figure D.9. Depth averaged velocity without submerged moored floating breakwater (SMFB) in the first research phase

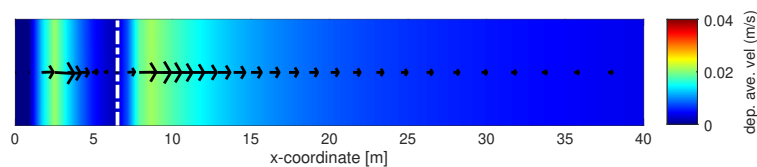


Figure D.10. Depth averaged velocity with submerged moored floating breakwater (SMFB), $C_t = 0.1$, in the first research phase, white dashed line represents FB

D3. Wave transformations in the second research phase

Shoaling effects

Here, we present the shoaling effect, mainly under milder wave conditions. Therefore, we did not include wave conditions 3 and 4 in the figure below.

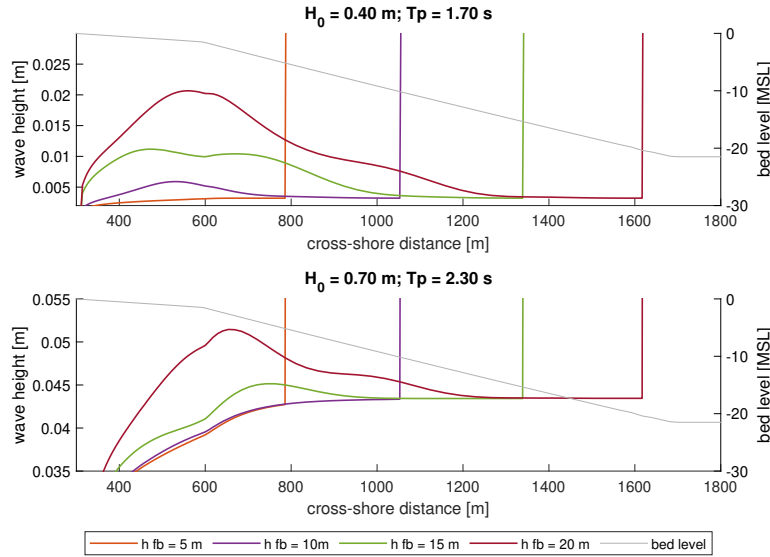


Figure D.11. Shoaling effects with different positions of FB, derived from the simulations with a shoreface slope of 1:200 and channel slope of 1:55

Wave dissipation due to bottom friction on the channel slopes

To understand the effect of bed friction we performed 6 simulations with the bed friction coefficient deactivated and activated (with coefficient = $0.067 \text{ m}^2 \text{ s}^{-3}$) under the JONSWAP type.

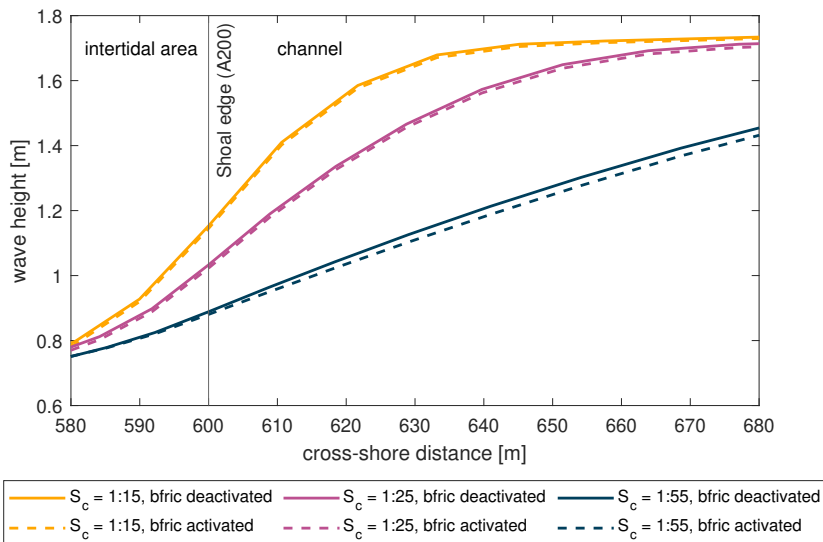


Figure D.12. Wave dissipation due to bottom friction (bfric) on different channel slopes; the same intertidal area slopes = 1:200; incident wave $H_0 = 1.80 \text{ m}$ and $T_p = 3.80 \text{ s}$; simulations without FB

D4. Profile of magnitudes of near-bed orbital velocity and bed shear stress on different channel slopes and intertidal area slopes

Near-bed orbital velocity on different channel slopes

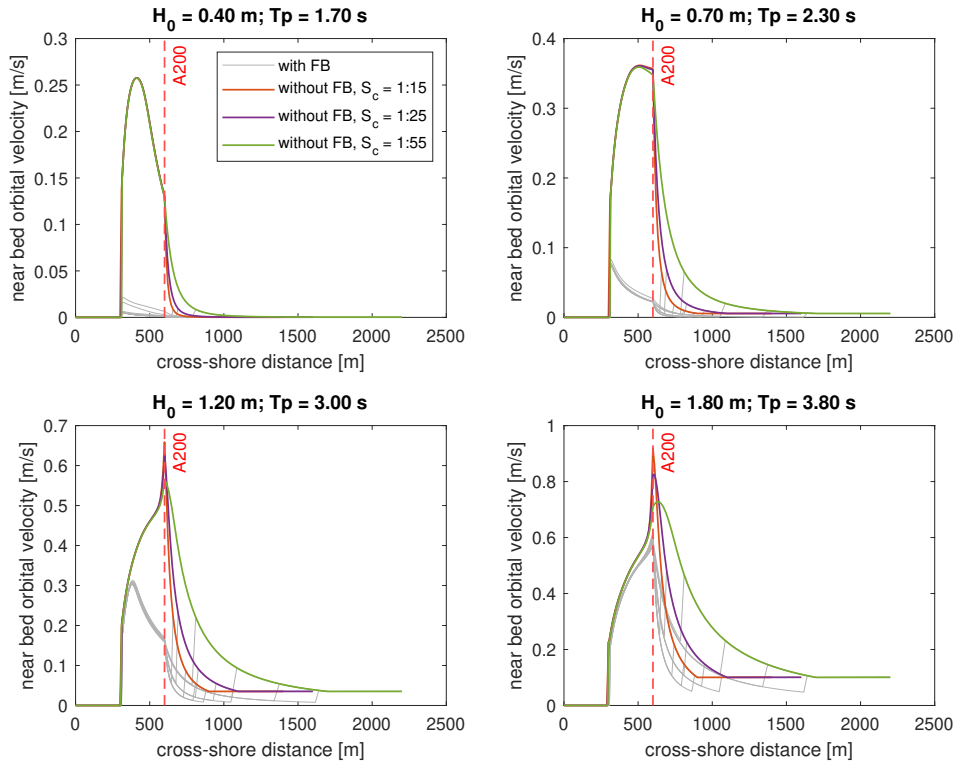


Figure D.13. Effects of different channel slopes on near bed-orbital velocity (u_b) without FB; derived from the simulations with shoreface slopes of 1:200, different channel slopes: 1:15, 1:25 and 1:55

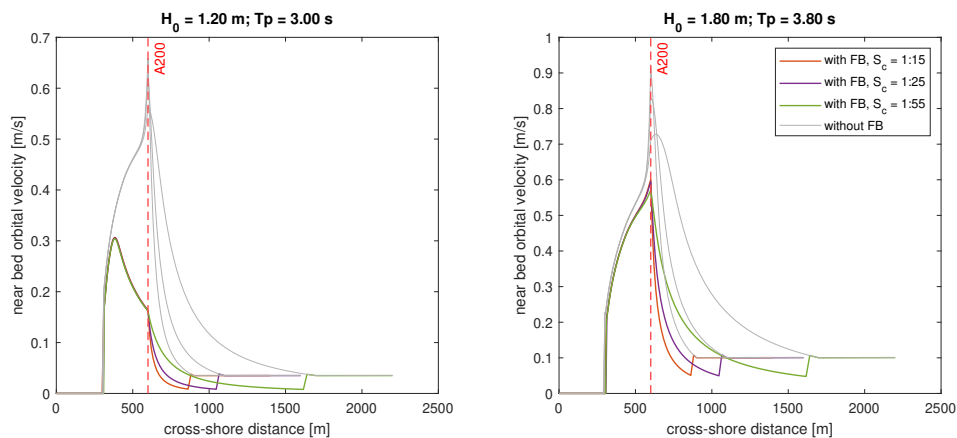


Figure D.14. Effects of different channel slopes on near bed-orbital velocity (u_b) with FB ($h_{fb} = 20$ m); derived from the simulations with shoreface slopes of 1:200, different channel slopes: 1:15, 1:25 and 1:55 under wave condition 3 (left panel) and 4 (right panel)

Near-bed orbital velocity on different intertidal area slopes

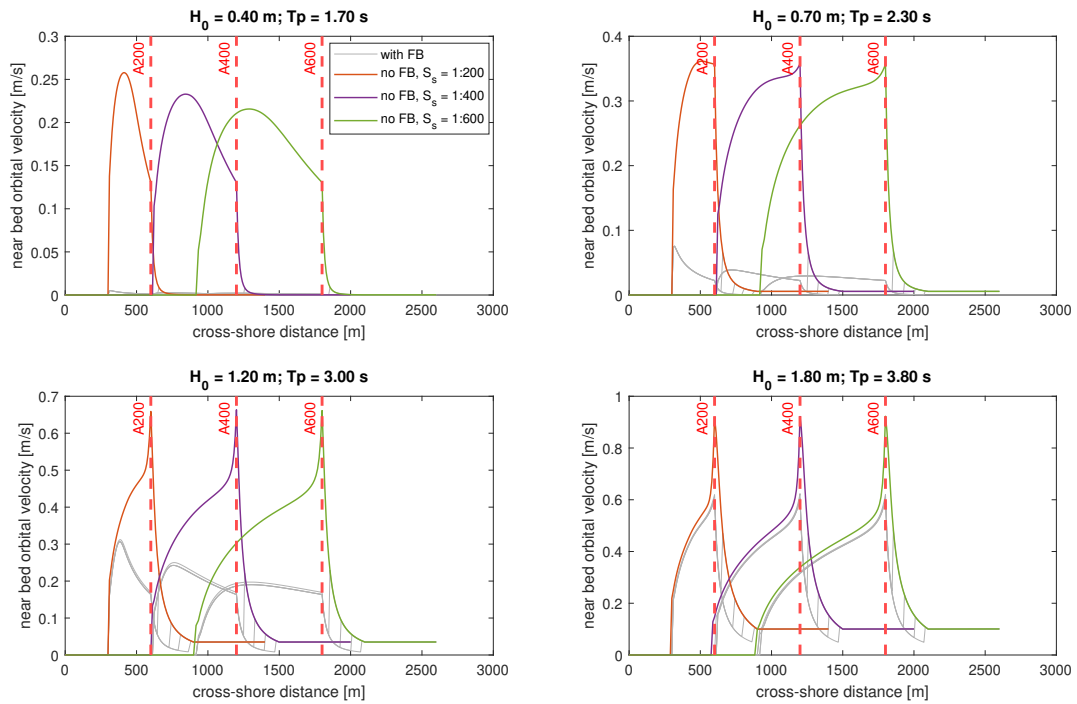


Figure D.15. Effects of different intertidal area slopes on near bed-orbital velocity (u_b) without FB under all wave conditions; A200, A400, A600 represent the locations of the edges separating the intertidal flats and channel (shoal edge)

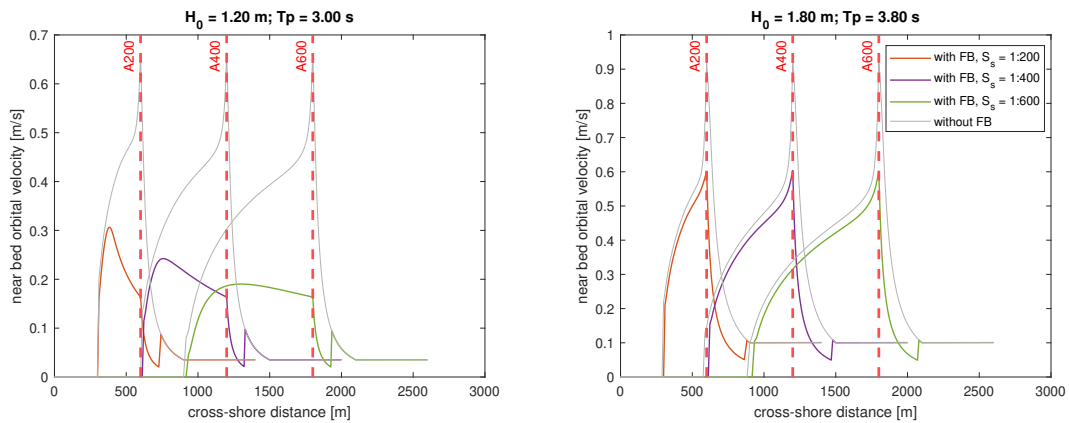


Figure D.16. Effects of different intertidal area slopes on near bed-orbital velocity (u_b) with FB ($h_{fb} = 20$ m); derived from the simulations with channel slopes of 1:15, under wave condition 3 (left panel) and 4 (right panel)

Bed shear stress on different channel slopes

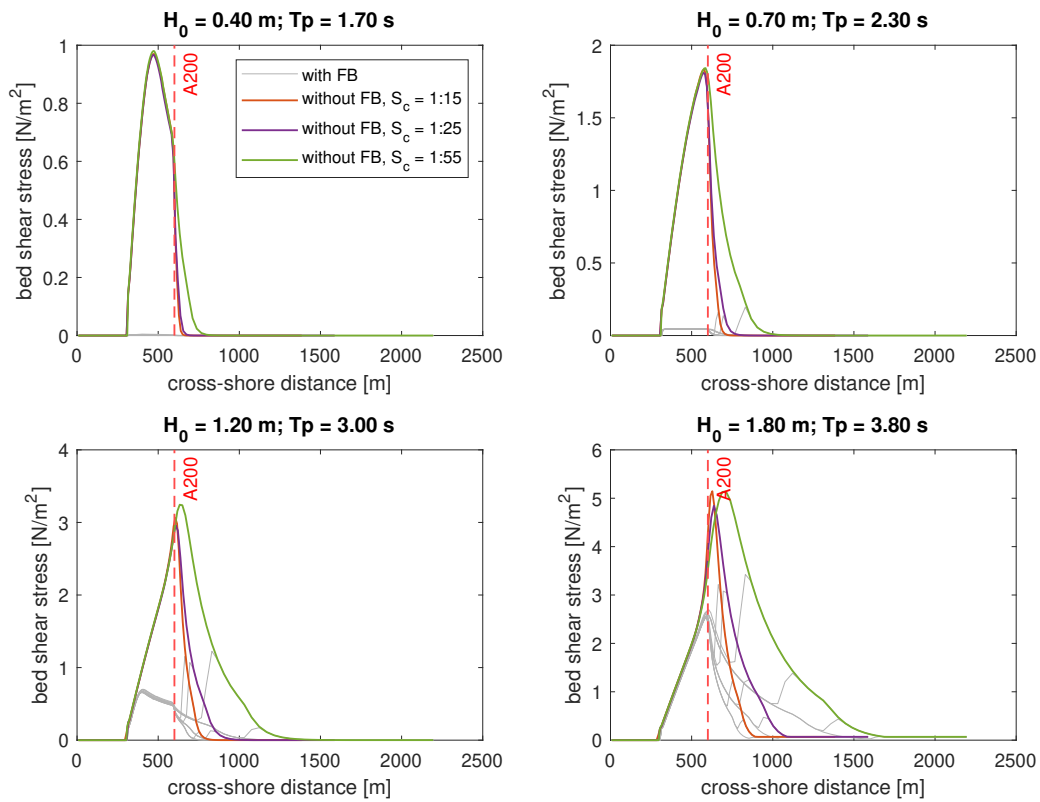


Figure D.17. Effects of different channel slopes on bed shear stress without FB; derived from the simulations with intertidal area slopes of 1:200, different channel slopes: 1:15, 1:25 and 1:55

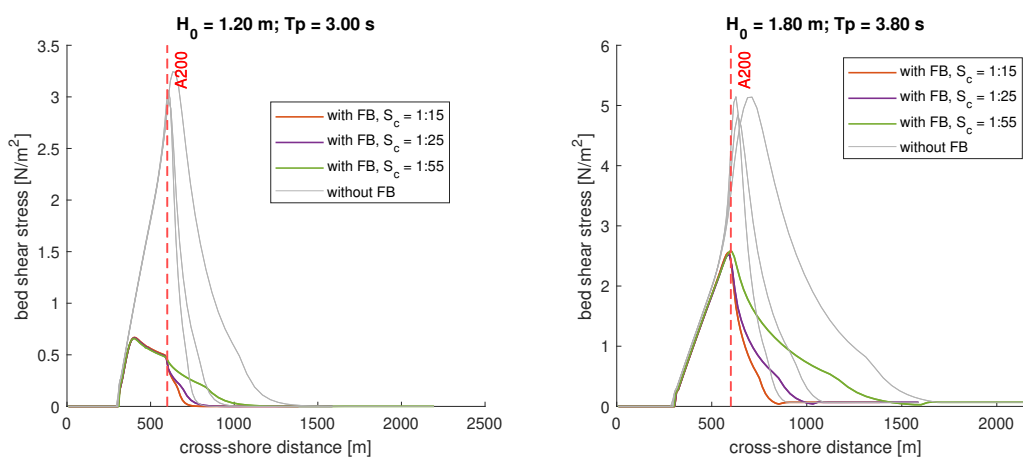


Figure D.18. Effects of different channel slopes on bed shear stress with FB ($h_{fb} = 20$ m), wave conditions 3 (left panel) and 4 (right panel); derived from the simulations with intertidal area slopes of 1:200, different channel slopes: 1:15, 1:25 and 1:55

Bed shear stress on different intertidal area slopes

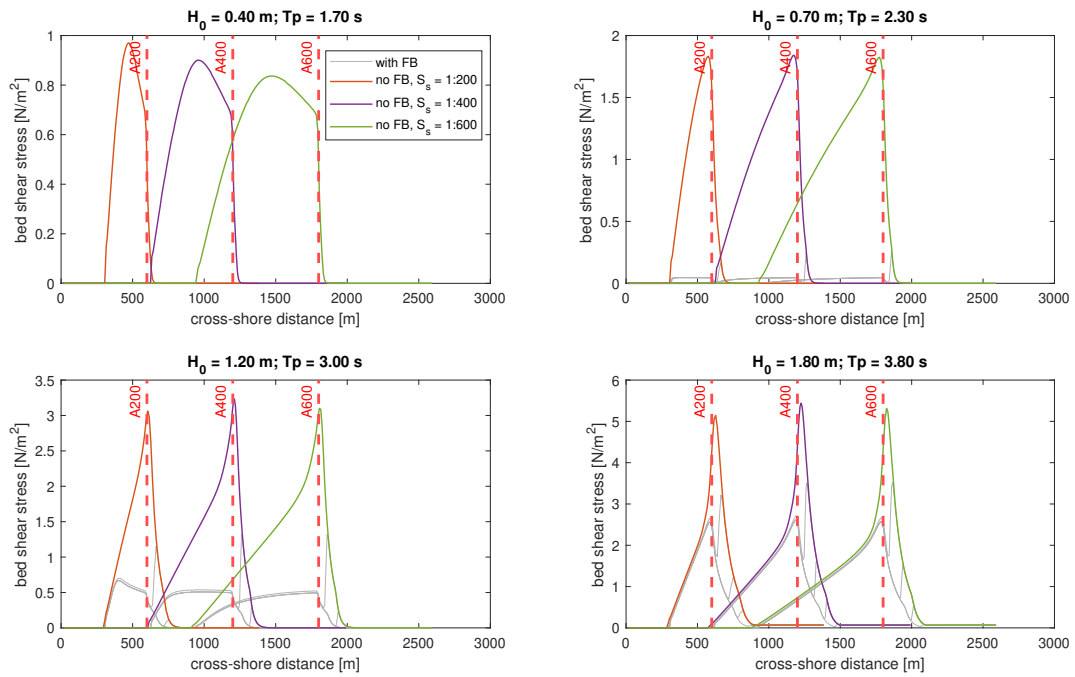


Figure D.19. Effects of different intertidal area slopes on bed shear stress without FB; derived from the simulations with channel slopes of 1:15, different intertidal area slopes: 1:200, 1:400 and 1:600

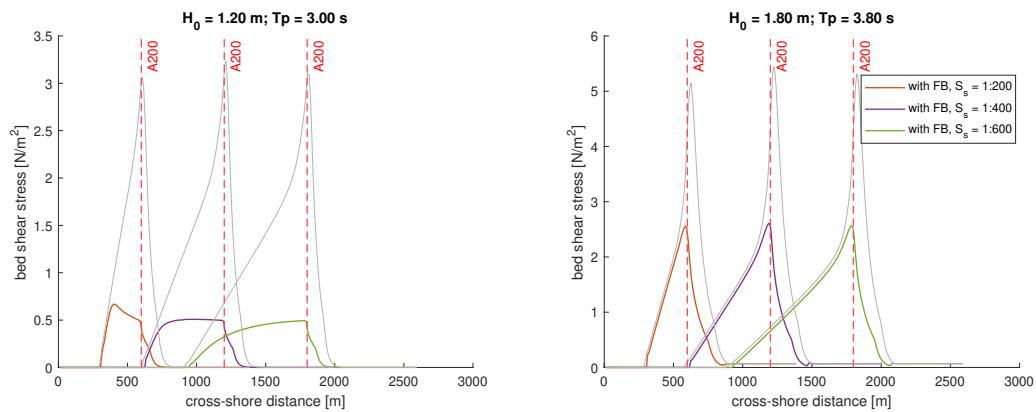


Figure D.20. Effects of different intertidal area slopes on bed shear stress with FB ($h_{fb} = 20$ m); derived from the simulations with channel slopes of 1:15, different intertidal area slopes: 1:200, 1:400 and 1:600; wave condition 3 (left panel) and wave condition 4 (right panel)

D5. Profile of magnitudes of bed load transport and suspended load transport on different channel slopes and intertidal area slopes

Bed load transport on different channel slopes

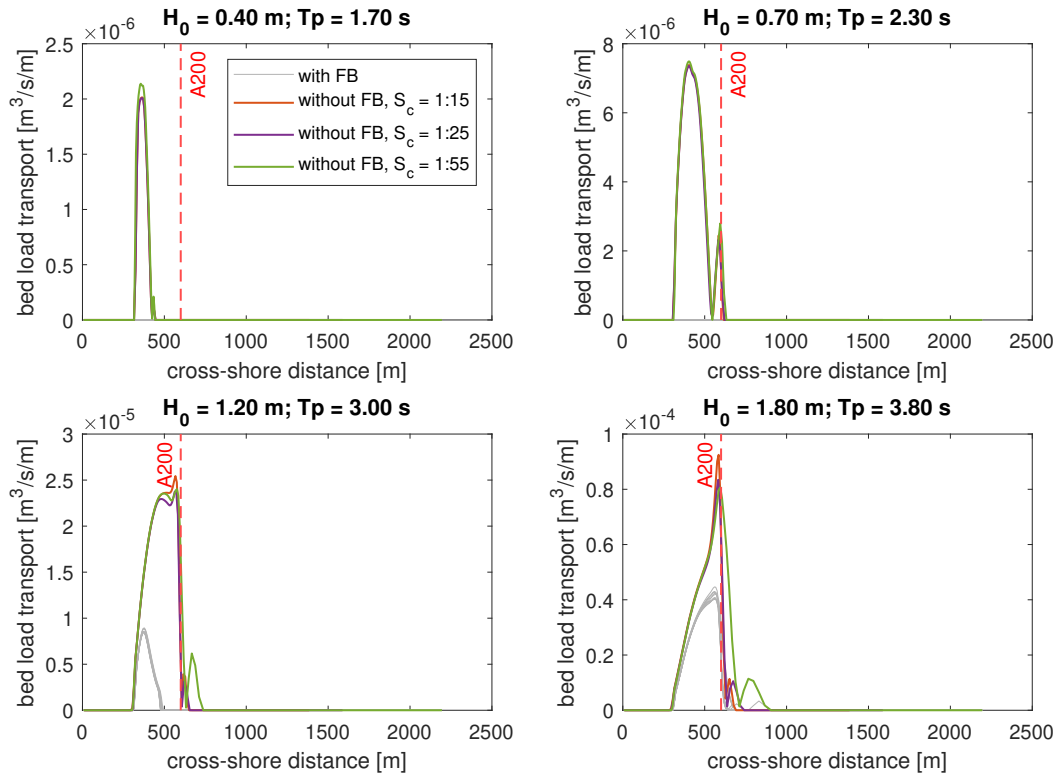


Figure D.21. Effects of different channel area slopes on bed load transport without FB; derived from the simulations with intertidal area slopes of 1:200, different channel slopes: 1:15, 1:25 and 1:55

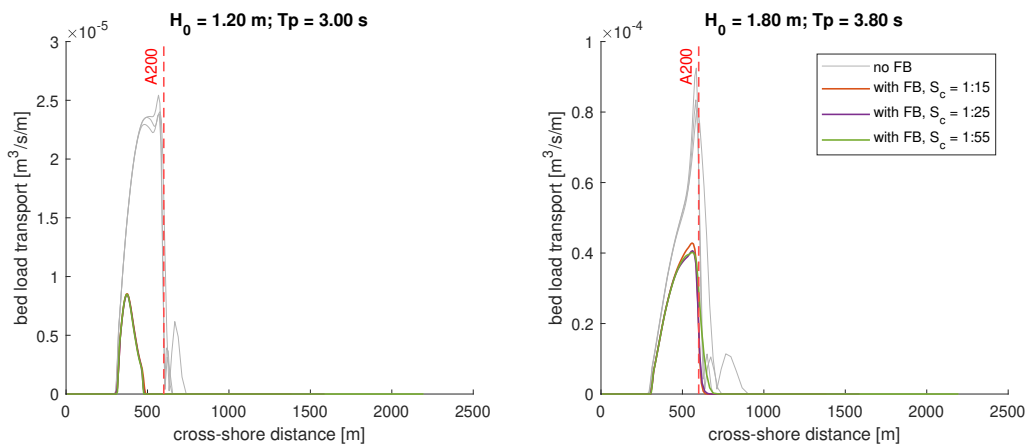


Figure D.22. Effects of different channel slopes on bed load transport with FB ($h_{fb} = 20$ m), wave conditions 3 (left panel) and 4 (right panel); derived from the simulations with intertidal area slopes of 1:200, different channel slopes: 1:15, 1:25 and 1:55

Suspended load transport on different channel slopes

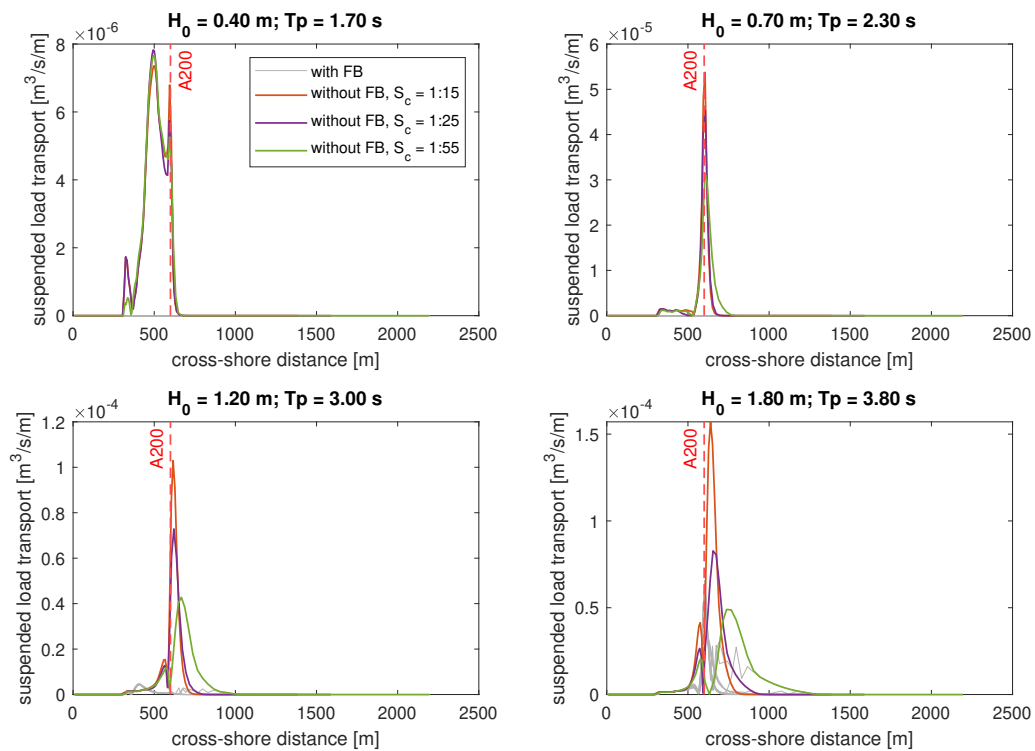


Figure D.23. Effects of different channel slopes on suspended load transport without FB; derived from the simulations with intertidal area slopes of 1:200, different channel slopes: 1:15, 1:25 and 1:55

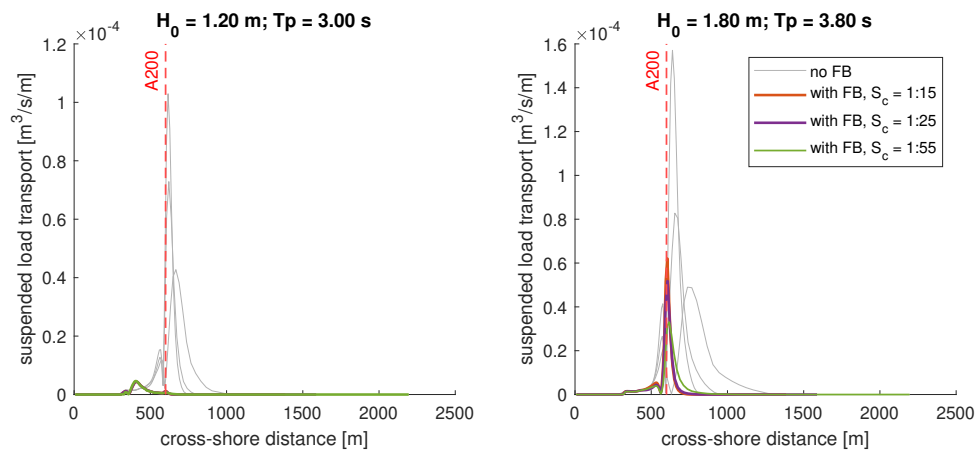


Figure D.24. Effects of different channel slopes on suspended load transport with FB ($h_{fb} = 20$ m), wave conditions 3 (left panel) and 4 (right panel); derived from the simulations with intertidal area slopes of 1:200, different channel slopes: 1:15, 1:25 and 1:55

Bed load transport on different intertidal area slopes

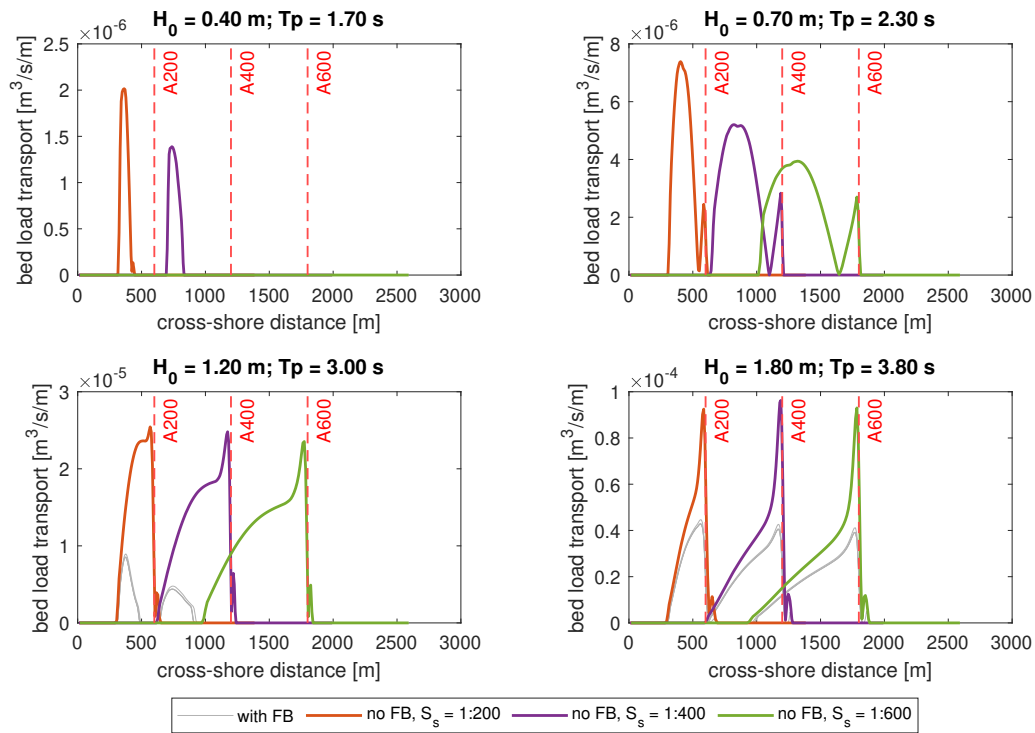


Figure D.25. Effects of different intertidal area slopes on bed load transport without FB; derived from the simulations with channel slopes of 1:15, different intertidal area slopes: 1:200, 1:400, and 1:600

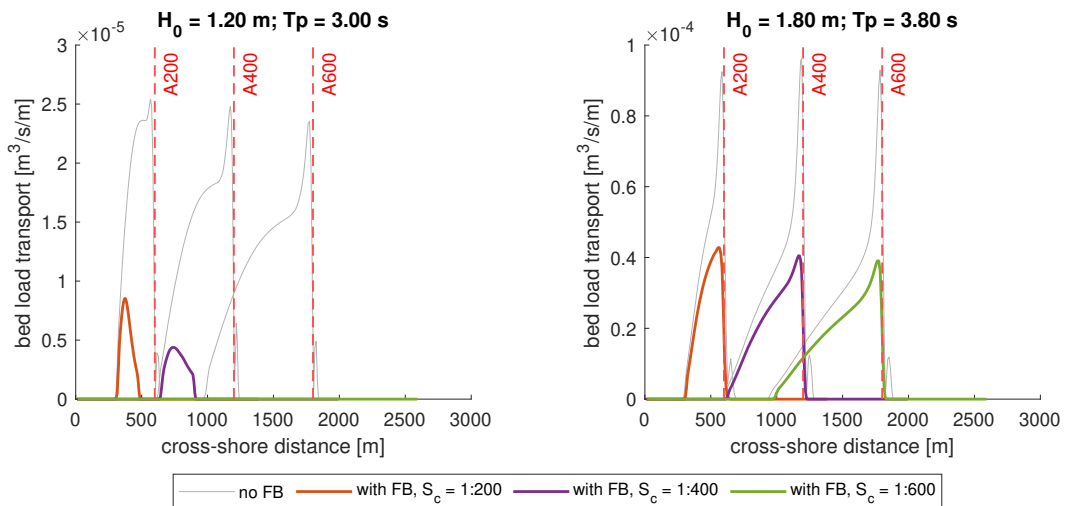


Figure D.26. Effects of different intertidal area slopes on bed load transport with FB ($h_{fb} = 20$ m), wave conditions 3 (left panel) and 4 (right panel); derived from the simulations with channel slopes of 1:15, different intertidal area slopes: 1:200, 1:400, and 1:600

Suspended load transport on different intertidal area slopes

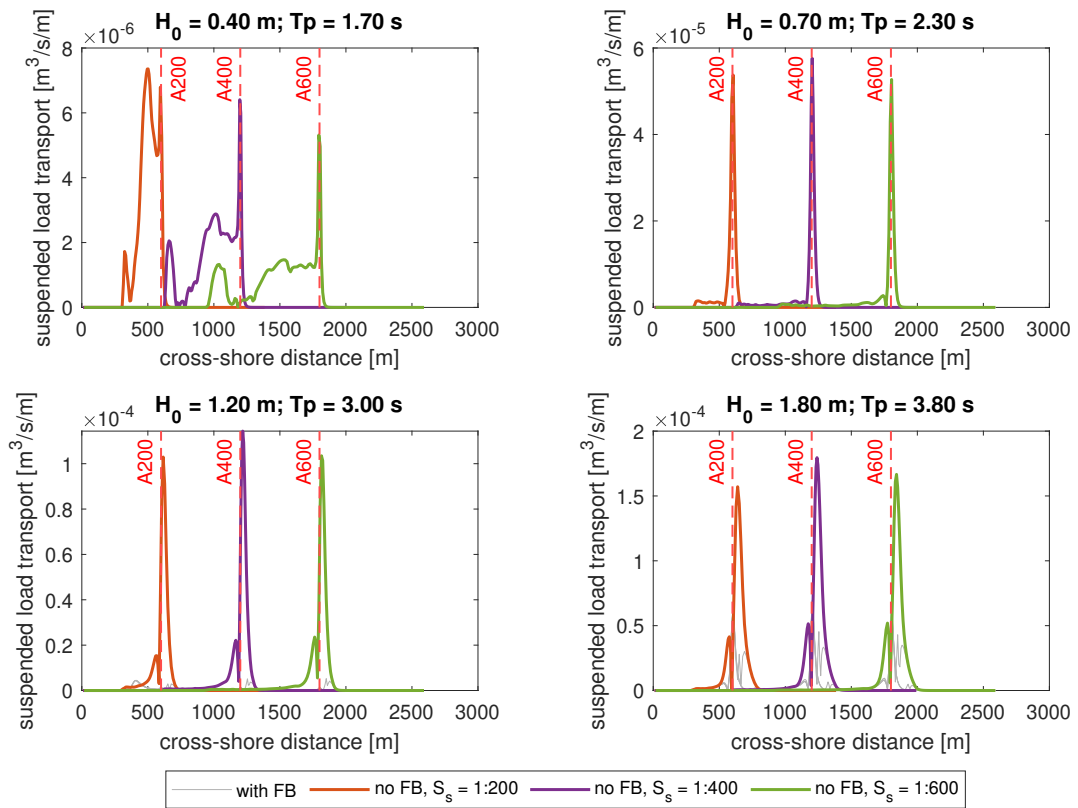


Figure D.27. Effects of different intertidal area slopes on suspended load transport without FB; derived from the simulations with channel slopes of 1:15, different intertidal area slopes: 1:200, 1:400, and 1:600

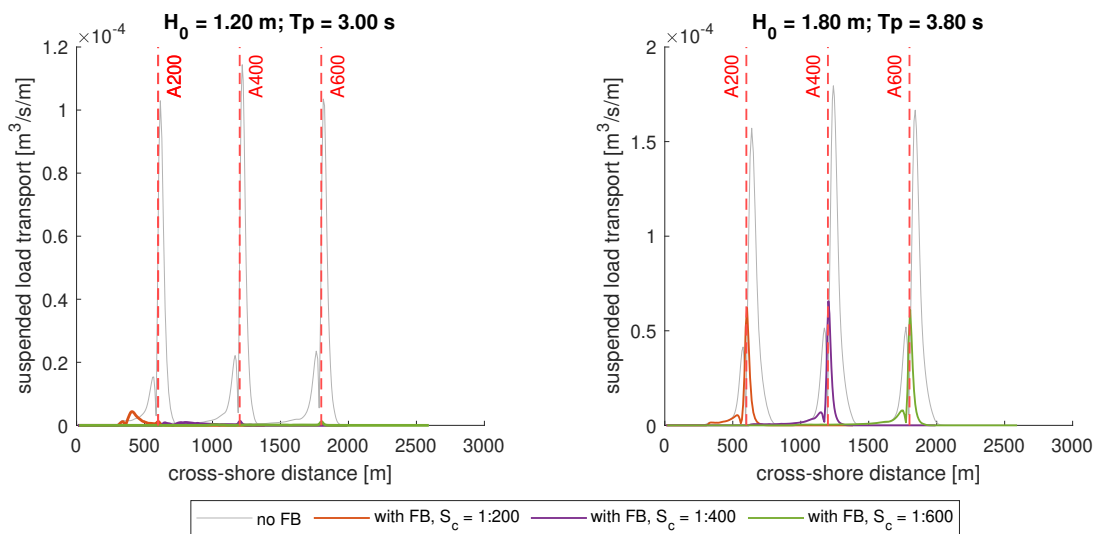


Figure D.28. Effects of different intertidal area slopes on suspended load transport with FB ($h_{fb} = 20$ m), wave conditions 3 (left panel) and 4 (right panel); derived from the simulations with channel slopes of 1:15, different intertidal area slopes: 1:200, 1:400, and 1:600

D6. Erosion on different channel slopes and intertidal area slopes

Erosion on different channel slopes

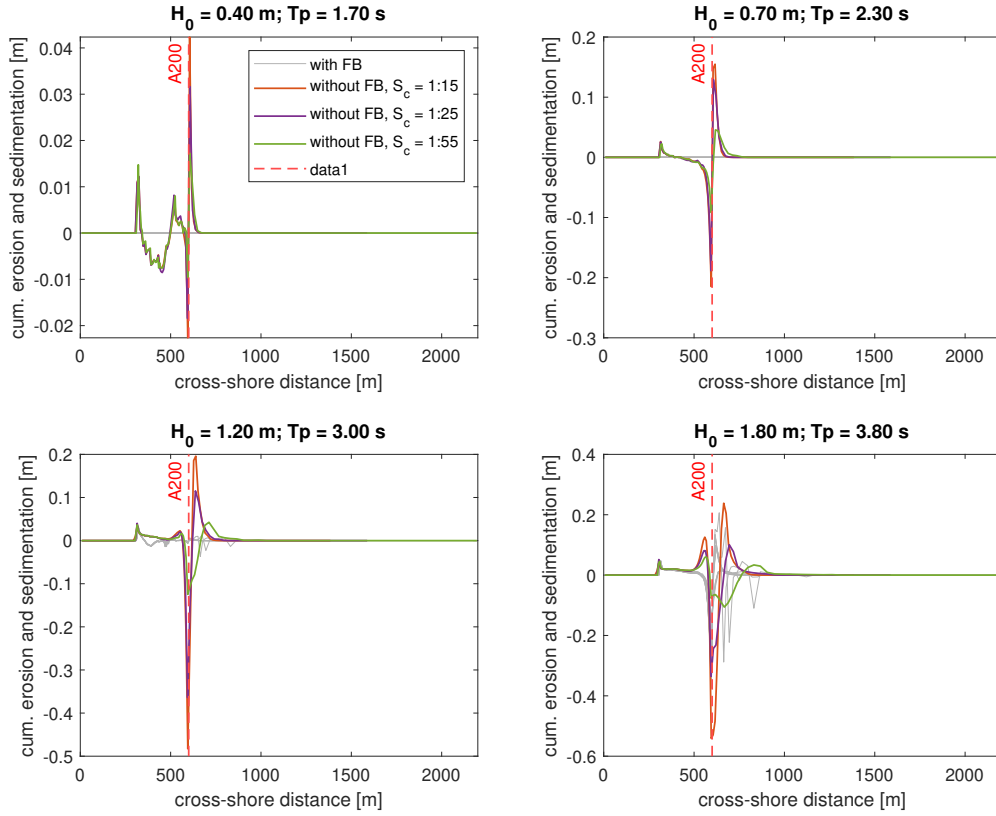


Figure D.29. Erosion on different channel slope without FB; derived from the simulations with channel slopes of 1:15, 1:25 and 1:55 with an intertidal area slope of 1:200

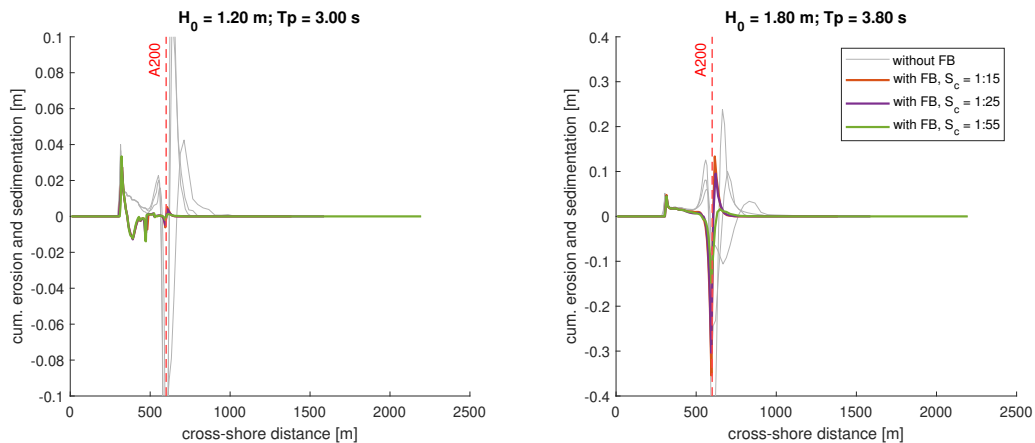


Figure D.30. Erosion on different channel slope with FB ($h_{fb} = 20$ m); wave conditions 3 (left panel) and 4 (right panel); derived from the simulations with intertidal area slopes of 1:200, different channel slopes: 1:15, 1:25 and 1:55

Erosion on different intertidal area slopes

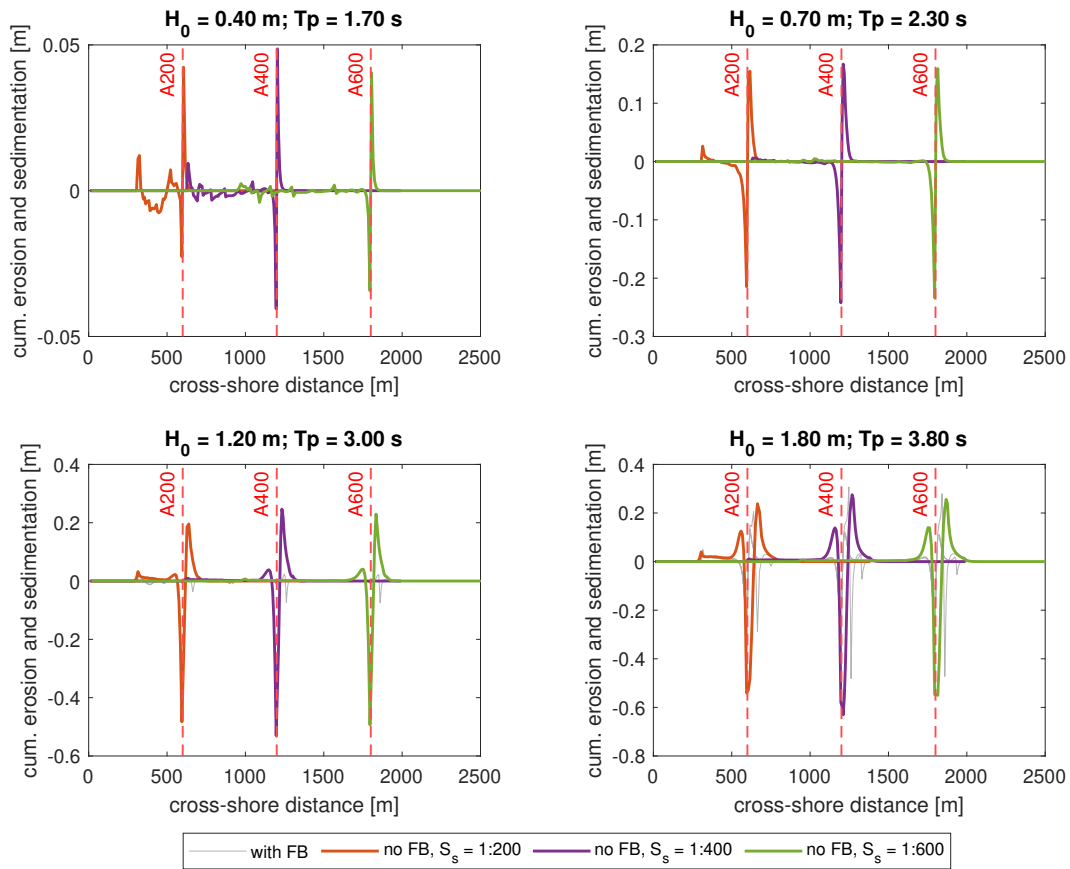


Figure D.31. Erosion profile on different intertidal area slope without FB; derived from the simulations with the intertidal area slopes of 1:200, 1:400, and 1:600 with a channel slope of 1:15

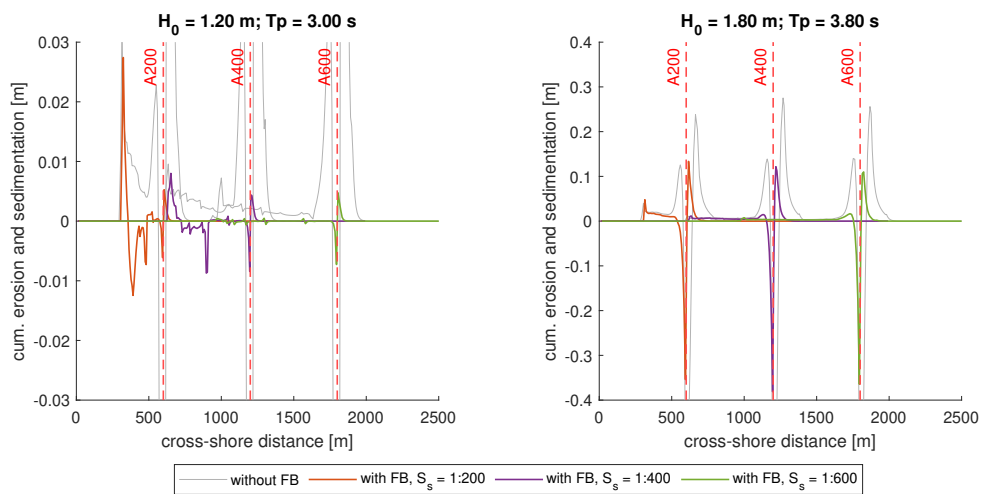


Figure D.32. Erosion on different intertidal area slope with FB ($h_{fb} = 20$ m); wave conditions 3 (left panel) and 4 (right panel); derived from the simulations with the intertidal area slopes of 1:200, 1:400, 1:600 with a channel slope of 1:15

